NASA CONTRACTOR REPORT

NASA CR-1053

PROCEDURES FOR ESTIMATING THE EFFECTS OF DESIGN AND OPERATIONAL CHARACTERISTICS OF JET AIRCRAFT ON GROUND NOISE

by Robert Lee, James Farrell, George Henry, and Albert Lowe

Prepared by
CONESCO DIVISION, FLOW CORPORATION
Watertown, Mass.
for Langley Research Center

NATIONAL AERONAUTICS AND SPACE ADMINISTRATION • WASHINGTON, D. C. • JUNE 1968

PROCEDURES FOR ESTIMATING THE EFFECTS OF DESIGN AND OPERATIONAL CHARACTERISTICS OF JET AIRCRAFT ON GROUND NOISE

By Robert Lee, James Farrell, George Henry, and Albert Lowe

Prepared under Contract No. NAS 1-5724 by
CONESCO DIVISION, FLOW CORPORATION
Watertown, Mass.

for Langley Research Center

NATIONAL AERONAUTICS AND SPACE ADMINISTRATION

For sale by the Clearinghouse for Federal Scientific and Technical Information
Springfield, Virginia 22151 – CFSTI price $3.00

TABLE OF CONTENTS

TABLE OF CONTENTS
(Continued)

TABLE OF CONTENTS
(Continued)

TABLE OF CONTENTS
(Continued)

LIST OF FIGURES

LIST OF FIGURES
(Continued)

LIST OF FIGURES
(Continued)

LIST OF FIGURES
(Continued)

PROCEDURES FOR ESTIMATING THE EFFECTS OF DESIGN AND OPERATIONAL CHARACTERISTICS OF JET AIRCRAFT ON GROUND NOISE

By Robert Lee, James Farrell, George Henry, and Albert Lowe
Conesco Division of Flow Corporation

SUMMARY

Procedures have been developed for estimating the effects of design and operational characteristics of jet aircraft on ground noise; this has been done for various engine-cycle parameters, aircraft-design characteristics, and aircraft-flight characteristics; parametric plots have been prepared to show how these different inter-related factors influence noise; and, when possible, assessments have been made of the accuracies and limitations of the graphs, nomographs, and equations that have been developed. One important general conclusion that can be drawn from all this effort is that it is feasible to develop simplified analytic procedures for relating aircraft design and flight characteristics to ground noise, and that such techniques can be extremely useful for providing design guidance and for showing how various flight paths influence ground noise. The report includes the following:

1. Noise-prediction procedures for jets and compressors including a direct method for estimating jet PNdb, a procedure for calculating the $PNdb_o$ of combined jets in fan engines, and the modification of several suggested compressor noise-prediction methods into one unified method.

2. An analytical investigation of noise as a function of engine-cycle parameters for jet and fan engines, and parametric plots that show how jet and fan noise vary as these different parameters are changed.

3. Several simplified calculational methods for determining PNdb including (a) jet and compressor noise PNdb from overall sound-pressure level, (b) PNdb of the combined jet and compressor noise from individual PNdb values, and (c) variation of PNdb with distance for jet, compressor, and jet combined with compressor noise.

4. An analytical study of ground noise as a function of design and flight characteristics. Parametric plots are presented that relate such parameters as wing loading, drag-to-weight ratio, power loading, and maximum lift coefficient to ground noise.

5. Graphical and analytical procedures for establishing ground noise at specific locations when an aircraft is in flight. Also, PNdb contours, magnitudes of ground areas as a function of PNdb, and annoyance levels have been calculated for several flight paths and the results for the different paths have been compared.

Some of the conclusions that can be drawn from the work are:

1. For a constant climb gradient, the ground contours of constant PNdb and effective PNdb will be in the form of ellipses.

2. The area experiencing a given PNdb level will be reduced by increasing the climb-out or landing-approach angle.

3. In high by-pass ratio designs of turbofan engines, both the compressor noise per unit flow and the jet noise Q, tend to be minimized; thus, on an "equal thrust" basis, high by-pass designs are desirable for minimum noise.

4. Ground noise levels under the aircraft during a second segment climb-out may be reduced markedly as a result of increased power loading of the aircraft. Increased power loading may result in a shortened take-off roll, a steep initial climb angle, and a greater power reduction during cutback. For example, increasing the power loading from .25 to .35 can result in a noise reduction of from 5 to 7 PNdb for both jet and compressor noise under the second segment.

1. INTRODUCTION

In recent years, with the increasing demand for rapid air transportation coupled with the development of larger and more powerful aircraft, the problem of aircraft noise has become very important. Advances in the design of jet aircraft and their powerplants has made the noise problem and its control quite complex. Two aspects of the noise-control problem are particularly significant:

1. It must be recognized that the noise problem is essentially a system problem and noise reduction, if it is to be taken at the early design stage, requires knowledge of how various design and operation factors of the engine/aircraft system are combined to influence the noise level on the ground.

2. Because of its increasing complexity, the noise problem can no longer be viewed as one belong only to the "acoustic experts". Planners, mission analysts, designers, and operators must share in the technical responsibility for its solution. Each of them has, in fact, an opportunity to influence the final noise level of the engine/aircraft system under design. To fully exploit this opportunity, these people must be equipped with certain minimum tools which will permit them to relate noise to what they do in their normal technical functions.

The program reported here was organized with these two important considerations in mind. Specifically, it is concerned with the study of how various factors inherent in the design and operation of any engine/aircraft system are combined to influence the noise level on the ground. The aim of the program was to identify the various factors of importance and to develop quantitative descriptions of how they are related to noise. A further aim of the program was to develop and present simplified and easy-to-use parametric charts, nomographs, and formulae that will enable designers and others to quickly relate important engine and airplane design parameters directly to noise.

It is expected that results of the program will be largely used to facilitate the prediction of noise from jet aircraft and their operation so that the noise effect of various design decisions can be known. Emphasis has been given to the development and presentation of prediction methods in a form that can be used at the earliest design stage.

How design and operating factors in an engine/aircraft system influence the noise level received on the ground during take-off and landing operations is studied. In general, three groups of factors have been considered; engine-design factors, airplane-design or performance factors, and factors related to airplane operational procedures. The physical factors considered are those having significant influences on the noise-source characteristics (compressor and jet) or on the flight-path characteristics at take-off and landing. Analysis has

been limited to the noise in the vicinity of the airport and at the airport proper due to jet aircraft operation.

The study first examines how design and operating factors directly influence the engine-noise sources and the flight-path characteristics of the plane. This leads to the development of relations linking these factors to the noise level on the ground. Noise parameters of interest are overall sound pressure, spectrum shape, loudness level (phon and annoyance level (PNdb)). While the factors initially selected are those quantities that are directly related to noise source or path characteristics, the final form of some of the developed relations employs parameters that are more useful during the preliminary design of an engine or aircraft.

The extent to which detailed design and operational factors have been considered has been limited by the state-of-the-art information relating noise to design, and by the practical considerations of the accuracy requirement of the prediction methods. On the latter point, factors whose maximum variation (within practical design limits) do not cause an overall noise change greater than $\pm$ 2db have been considered as relatively unimportant and are treated as constants.

The work reported in the following sections includes:

1. Development of procedures for predicting combined spectra noise from jet exhaust and compressor noise.

2. Investigation of the effect of jet and fan engine cycle parameters on noise and presentation of parametric plots of the effects of these variables on noise.

3. Investigation of the effects of airframe design and operational factors on ground noise from the viewpoint that as design and operational factors influence flight path, they influence the distance between the noise source and a ground observer and, hence, they influence the ground noise.

4. Preparation of parametric plots showing how these various parameters influence ground noise.

5. Demonstration of the use of the procedures and charts for determining and comparing the ground noise produced by aircraft using various take-off and landing flight paths and procedures.

2. JET ENGINE DESIGN AND NOISE

2.1 Introduction

A jet engine is a fluid propulsion device which continuously draws air from the atmosphere, compresses it, adds energy to it in the form of heat, and then expends it through the nozzle — thereby converting part of the added energy to jet kinetic energy. The imparting of momentum to the working fluid (air) between the engine inlet and the exhaust results in propulsive thrust. Changes of state of the fluid flow across the various engine components involve irreversible thermodynamic processes and are accompanied by frictional and unsteady flow effects, and inherent to these processes is the production of acoustic energy. The compression process across the compressor or fan, and the turbulent mixing process of the expanded jet are well known sources of acoustic energy in aircraft jet engines.

In this section of the report noise from jet engines is considered and methods are developed and summarized for making noise calculations using salient design parameters of the powerplant. Both jet exhaust and compressor noise are considered. No attempt is made to improve existing methods of noise prediction in the sense of attempting to add to the understanding of the physics of the problem. The principle effort is given to extending and modifying existing prediction methods into forms that are readily and easily usable by aircraft and powerplant designers. With the aid of digital computers a series of design charts have been developed and are presented.

In order to facilitate a systems approach to the engine/aircraft/airport noise problem it is important that parameters selected to describe the noise behavior in one part of the system be also meaningful when viewed from another part of the system. For example, relating a powerplant design to PWL (sound power level) is not as meaningful as relating the design directly to PNdb since the latter is the preferred measure for judging acceptability with respect to airport noise planning. With this in mind, effort has been made to develop and present calculational methods, charts, and graphs in terms of parameters that are directly usable by aircraft, powerplant, or airport designers.

The noise to be calculated or predicted for engines of various designs will be maximum pass-by levels referred to the standard sideline distance of 200 feet. This is called the engines' reference noise level and is denoted by the subscript o added to the bottom right of the noise level symbol (e.g., $PNdb_o$, SPL_o). The reason for standardizing the noise level of an engine as being the maximum level observed along a line parallel to and 200 feet away from the engine axis is that this leads to a relatively simple procedure for estimating the maximum noise level observed on the ground during aircraft fly-by. Thus, if $PNdb_o$ is the engine reference level, and the change in PNdb due to distance, say $\triangle$PNdb, is expressed as some function of the ratio of distance to the standard distance of 200 feet, the maximum noise level observed on the ground during an aircraft fly-by would be

$$PNdb_{max} = PNdb_o - \triangle PNdb$$

where $\triangle PNdb = f\left(\frac{d}{200}\right)$, with d as the slant range distance (or closest approach distance) between the flight path and the observer. Development of $\triangle PNdb$ functions in terms of distance ratio for jet and compressor noise is discussed in Section 3.

2.2 Jet Exhaust Noise

2.2.1 Review of the "SAE" method.- The noise associated with the turbulent-mixing process of the expanded jet issuing from a standard conical jet engine nozzle has been thoroughly studied and reported. The most important parameter affecting the noise power generation is the exhaust velocity of the jet, while the jet density and nozzle area play secondary roles. A commonly accepted method for calculating standard jet engine exhaust noise is the SAE method. In this method the engine reference noise level (i.e., maximum noise level at the sideline distance of 200 feet) is given by the relation,

$$SPL_o = 20 \log \rho + 10 \log A + 10 \log f(V_R) \qquad (1)$$

where SPL_o is the reference overall SPL of the jet, ρ is the exhaust jet density, A is the exhaust nozzle area, V_R is the relative velocity between the jet exit velocity and the airplane speed, thus,

$$V_R = V_j - v_o \qquad (2)$$

The empirically determined function 10 log $f(V_R)$ is plotted in figure 1. The curve of 10 log $f(V_R)$ as a function of V_R for the range of V_R between 800 ft/sec and 4000 ft/sec may be fitted by the following 4th order equation

$$10 \log f(V_R) = 62.7 + 8.95 \times 10^{-2} V_R - 3.15 \times 10^{-5} V_R^2 + 5.49 \times 10^{-9} V_R^{-3} - 3.8 \times 10^{-13} V_R^4 \qquad (3)$$

Figure 1 - Normalized Jet Noise Versus Velocity

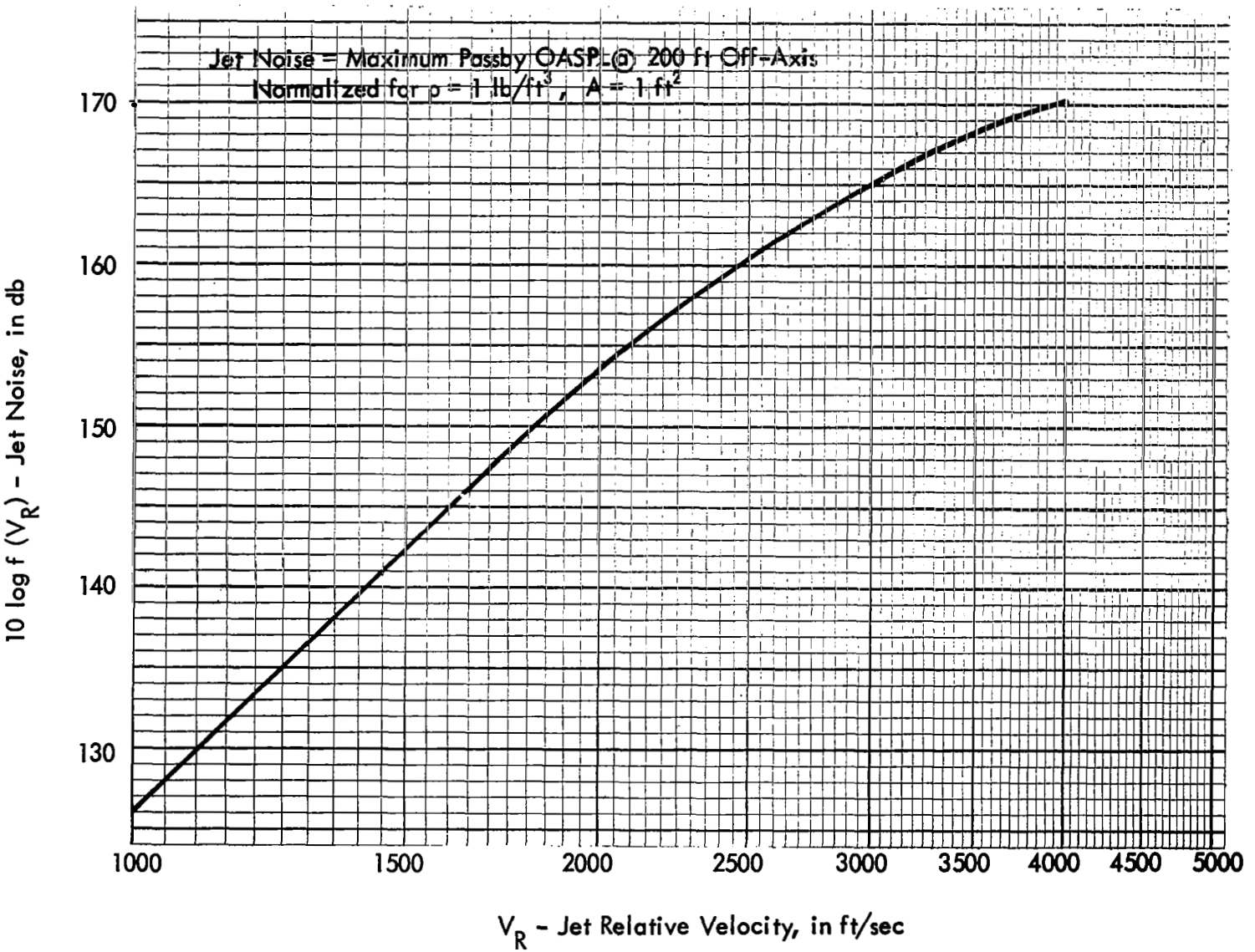

There is negligible error in using the equation rather than the curve, and the equation is convenient for performing calculations on a computer.

Equation (1) applies to both the case of an engine stationary on the ground and the case of an engine on a flying aircraft. In the latter case, SPL_o is simply the maximum SPL experienced by an observer on the ground when the aircraft flies a straight course whose slant range distance (or closest approach distance) is 200 feet.

Inspection of Eqs. (1) and (2) indicate that the engine reference sound pressure SPL_o for jet noise depends only on four independent variables, jet exit velocity V_j, jet exit density ρ, nozzle area A, and aircraft speed v_o. This set of independent variables is complete, but not unique. Another set of four variables could equally well be considered. For example, since ρ and V_j of the jet are directly related to the nozzle pressure ratio p_r, and nozzle total temperature T_t, either ρ or V_j could be replaced by T_t or p_r as independent variables (in conjunction with A and v_o) in determining SPL_o. In a similar fashion it will be seen later that the engine reference SPL_o as well as the reference $PNdb_o$ for the jet noise can be described by a set of four independent variables associated with the engine cycle; *namely, overall engine pressure ratio, turbine inlet temperature, engine size* (represented by either area, thrust, or weight flow), and aircraft speed. For a fan engine, two additional independent variables are required, fan pressure ratio, and bypass ratio.

For easy reference, the relationship between ρ, V_j (fully expanded isentropic velocity), T_t, and p_r are given below:

$$\rho = \frac{140}{T_t} \; p_r^{0.23} \tag{4}$$

and

$$V_j = 122 \sqrt{T_t \left(1 - \frac{1}{p_r}\right)^{0.23}} \tag{5}$$

In arriving at the above two relations, simplification has been made by taking $\gamma = 1.3$, $R = 53.3$ ft lb/lb$^{\circ}$R and $p_s = 2116$ 16/ft^2. The error introduced by this simplification is less than 1/2 db over the entire range of application.

Figure 2 is a plot relating SPL_o to ρ, V_j, p_r, and T_t for a unit area ($A = 1$ ft^2) stationary circular nozzle ($v_o = 0$). Figure 2 has another use. Given any two of the set of four variables ρ, V_j, T_t, p_r, the remaining two are directly determined by inspection and interpolation of the curves in the figure.

The SAE method for estimating the noise level of stationary engines on the ground is very good; however, the relative velocity effects associated with the aircraft motion in the manner described by equation (1) has not been completely verified by flight test data.

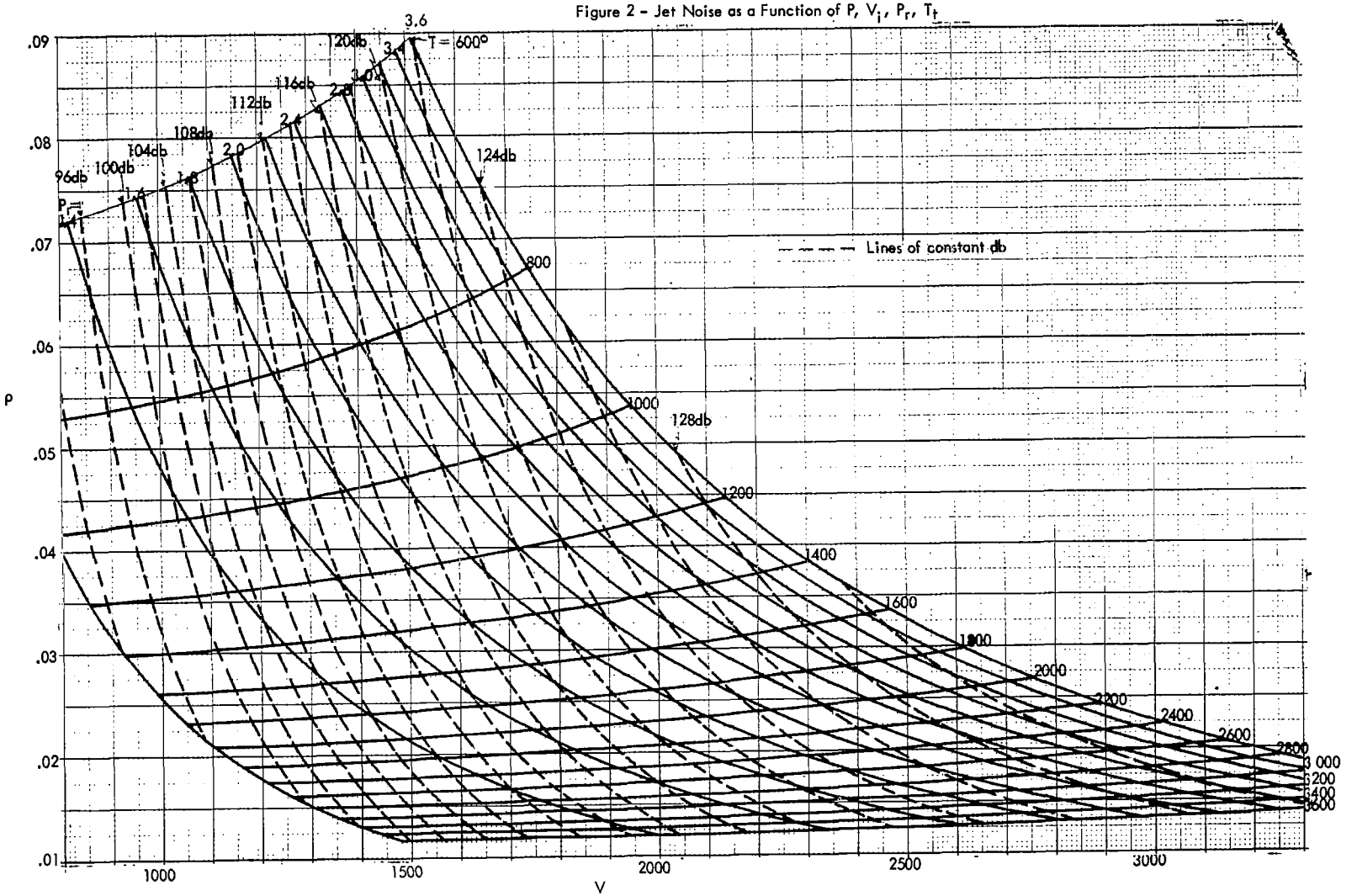
Figure 2 – Jet Noise as a Function of P, V_j, P_r, T_t
Lines of constant db
T = 600°
3.6
3.4
3.0
2.8
2.4
2.0
1.8
1.4
120db
116db
112db
108db
104db
100db
96db
124db
128db
800
1000
1200
1400
1600
1800
2000
2200
2400
2600
2800
3 000
3200
3400
3600
P
V
.09
.08
.07
.06
.05
.04
.03
.02
.01
1000
1500
2000
2500
3000

In the absence of any information to the contrary, the basic SAE method for estimating jet noise for aircraft in flight is the best available.

2.2.2 Direct method for estimating jet noise PNdb. - A procedure has been developed for calculating from the overall SPL for jet engine exhaust noise without having to go through any manipulation of the jet noise spectrum. We will define $PNdb_o$ as the reference perceived noise level of the engine associated with the jet exhaust. The numerical difference between $PNdb_o$ and SPL_o is determined by the spectrum shape of the jet noise. The SAE method suggests two standard spectrum shapes (one for the ground and one for flight) with the Strouhal number fD/V_R as the normalizing parameter. These are shown in figure 3. It can be seen that depending on the design parameter V_R/D, the noise spectrum will shift left or right on the actual frequency scale, giving rise to differences in the quantity $PNdb_o - SPL_o$ because of the basic relationship between subjective noise and frequency. Thus, when V_R/D is large, the jet peak frequency as well as the entire spectrum will move to the right. This in turn gives rise to a large high frequency content in the total noise, and hence a large difference between $PNdb_o$ and SPL_o. On the other hand, the shifting of the spectrum to the left (associated with a lower V_R/D parameter) will decrease the difference between $PNdb_o$ and SPL_o.

By using the SAE recommended spectrum shape and calculating the quantity $PNdb_o - SPL_o$ for varying V_R/D over the range of interest, the following empirical rule can be obtained which is within $\pm$ 0.5 db of exact calculations,

$$PNdb_o - SPL_o = 8 \log \frac{V_R}{D} - 15 \qquad (6)$$

The above equation holds true for jet noise peak frequency ($0.35 \times V_R/D$) lies anywhere between the first and fifth octave band and whose spectrum shape is in accordance with the SAE flight spectrum shape. For ground run-up conditions with the aircraft velocity equal to zero, the constant in Eq. (6) should be 17 instead of 15, since according to the SAE method, the ground spectrum contains less high frequency noise than the flight spectrum.

Equations (1) through (6) permits one to calculate the engine reference $PNdb_o$ in terms of four independent variables A, v_o, ρ and V_j (or p_r, and T_t) directly. Thus,

$$PNdb_o = 20 \log \rho + 6 \log A + 10 \log f(V_R) + 8 \log V_R - 15.5 \qquad (7)$$

Figure 3 - Standard SAE Jet Spectrum

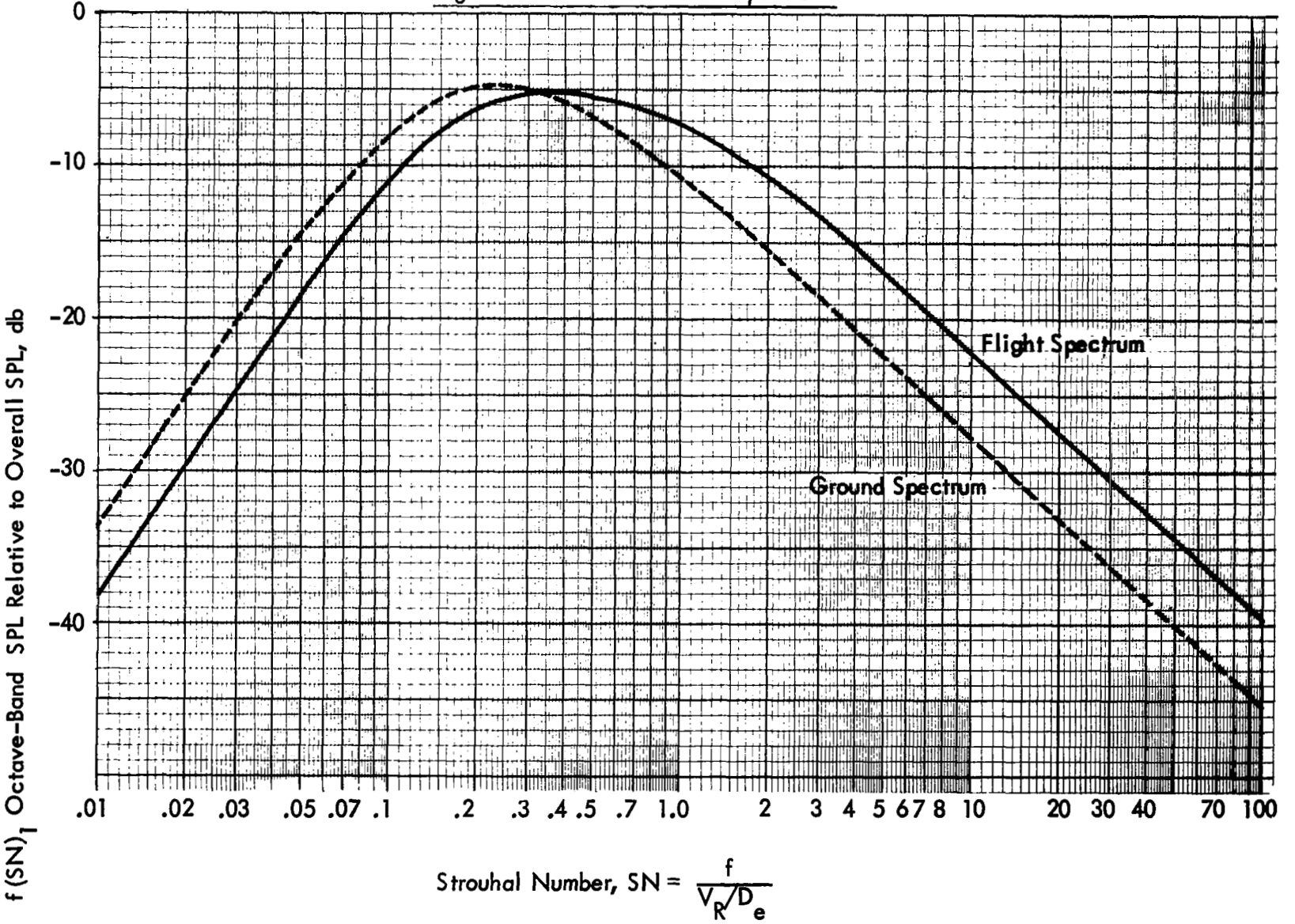

where 10 log $f(V_R)$ as a function of V_R is given by Eq. (3) or figure 1. To facilitate use by designers we have employed Eqs. (2) (3) (4) (5) and (7), and computed values of $PNdb_o$ for various combinations of p_r, T_t, A and v_o. The results are presented in the form of parametric charts in figure 4. Nozzle pressure ratio, p_r, and total temperature, T_t, have been selected as basic variables in constructing the design charts (instead of ρ and V_j) since they are more commonly used in calculations by nozzle designers.

The net thrust of the engine at aircraft speed v_o is given by,

$$F_n = \frac{1}{g} \rho A V_j (V_j - v_o) \tag{8}$$

For purposes of design which will become apparent later, it is useful to define a quantity Q as being

$$Q = PNdb_o - 10 \log F_n \tag{9}$$

This quantity relates PNdb to thrust and can be considered as the log of the ratio of perceived noise to thrust. It is an expression of the amount of perceived noise per pound of thrust.

Q is of course again a function of the four independent variables p_r, T_t, A and v_o. Computed results of Q in terms of these variables are also included in figure 4.

2.2.3 Approximate method for jet noise calculation.- Sometimes it is useful to present design calculation methods in the simplest analytic form, even at the loss of some accuracy, so that the designer can quickly see the relative importance of the design parameters involved. A set of simplified calculation methods applicable to exhaust jet noise have been developed for this purpose.

Starting with the basic SAE method of Eq. (1), the function 10 log $f(V_R)$ is approximated by two straight line functions — one for the high velocity region, and one for the low velocity region thus,

Figure 4a - $PNdb_o$ as a Function of P_r, T_t, A, and V

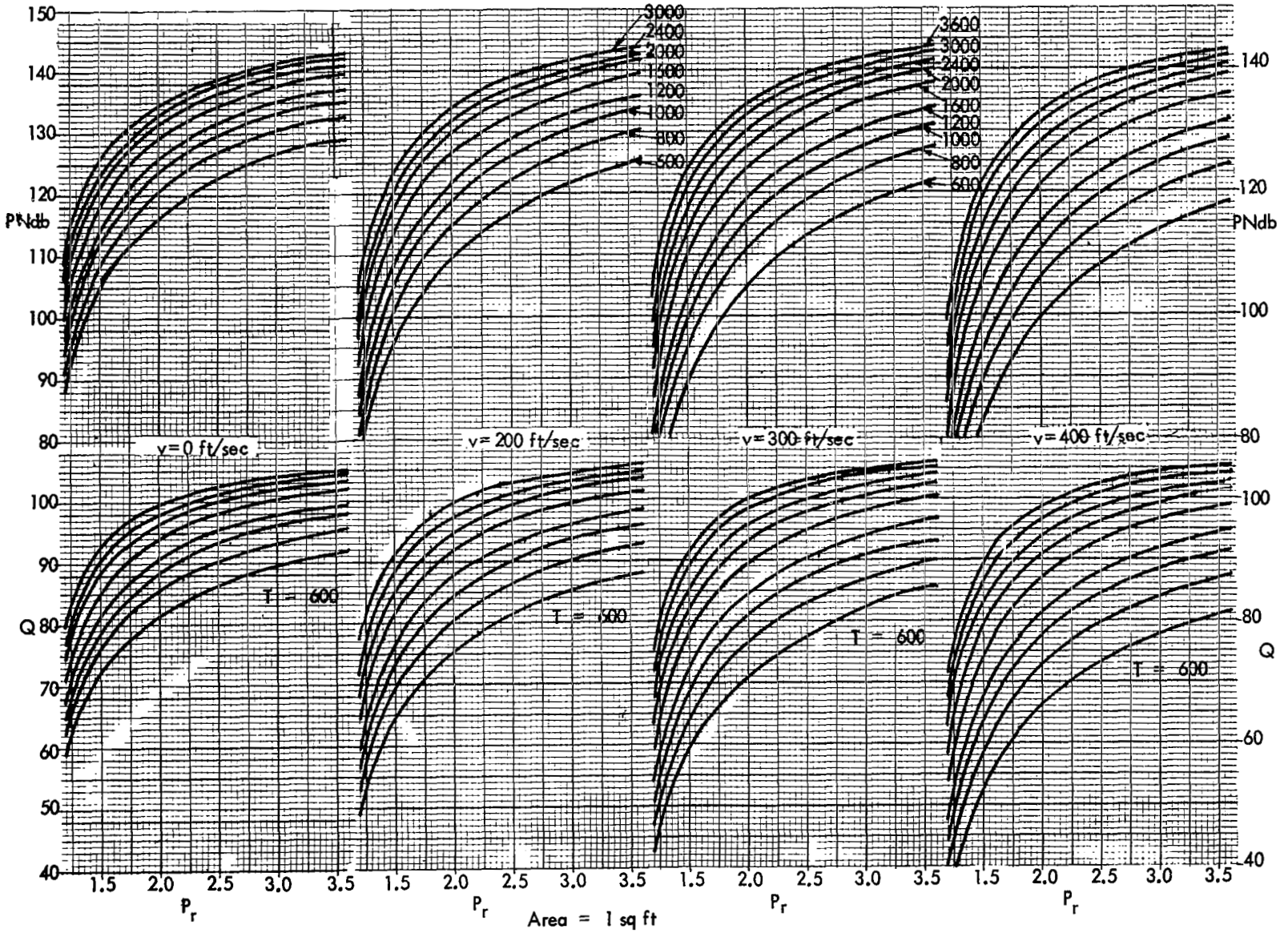

Figure 4b - $PNdb_o$ as a Function of P_r, T_t, A, and V

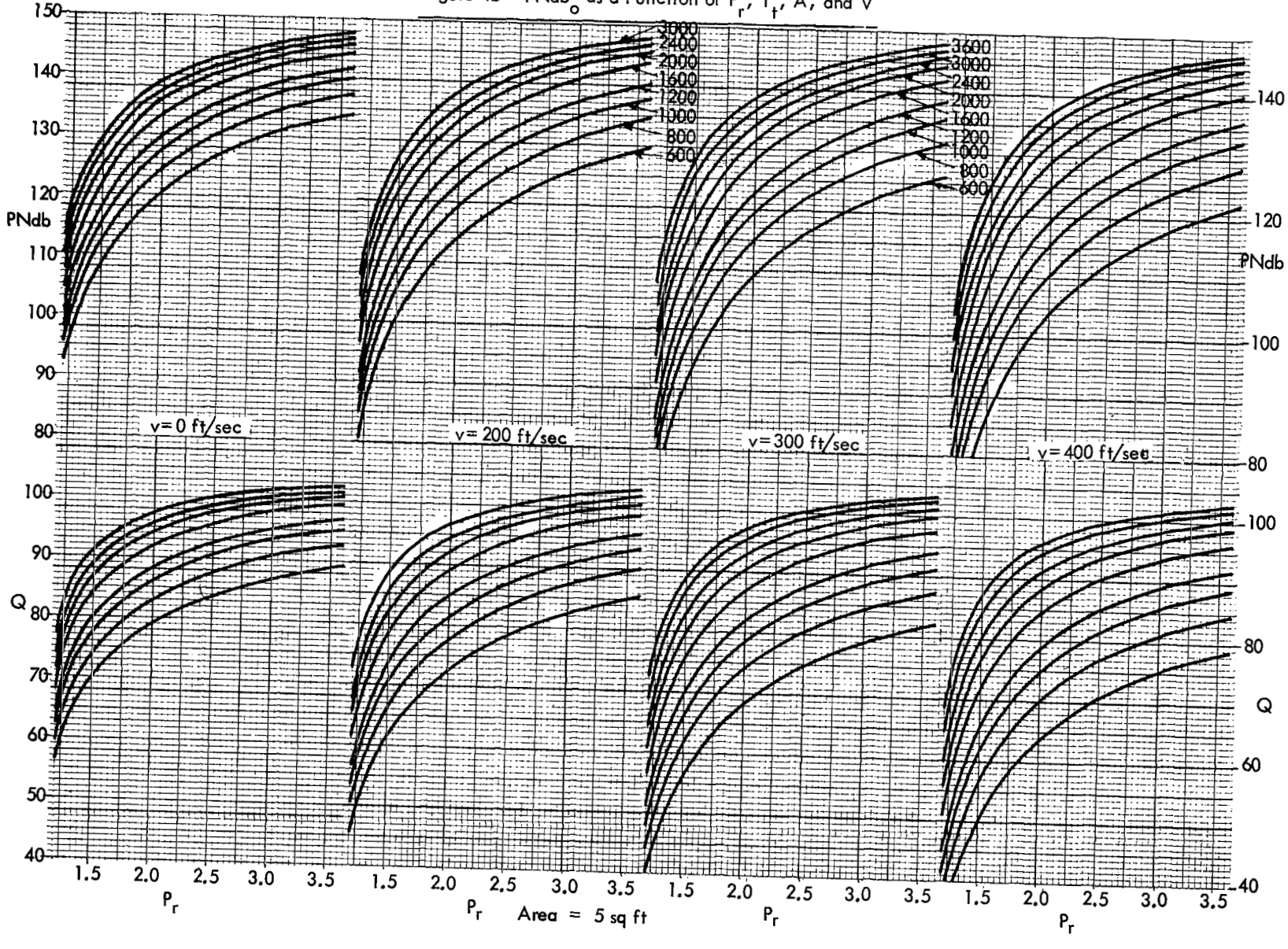

Figure 4c - $PNdb_o$ as a Function of P_r, T_t, A, and V

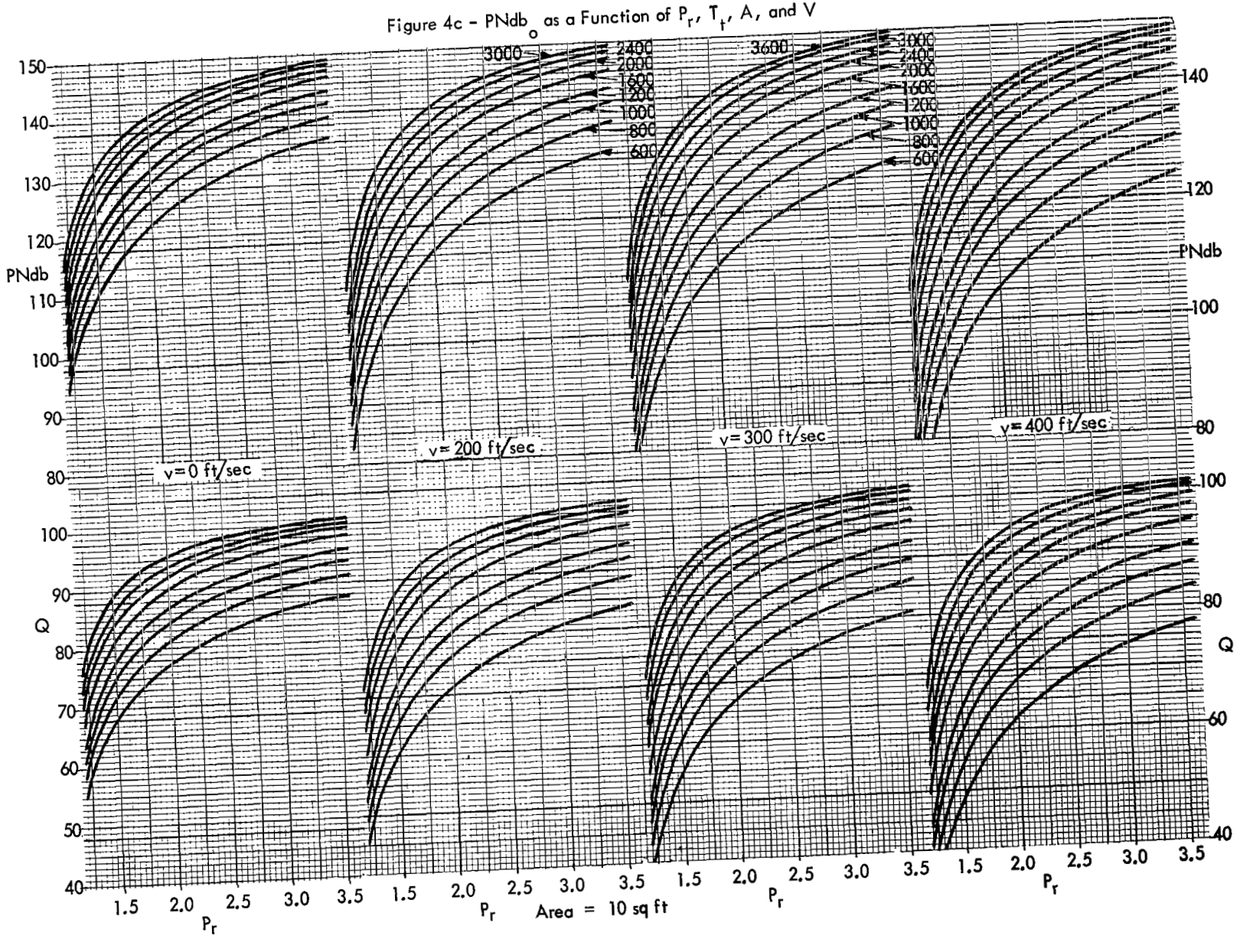

Figure 4d - $PNdb_o$ as a Function of P_r, T_t, A, and V

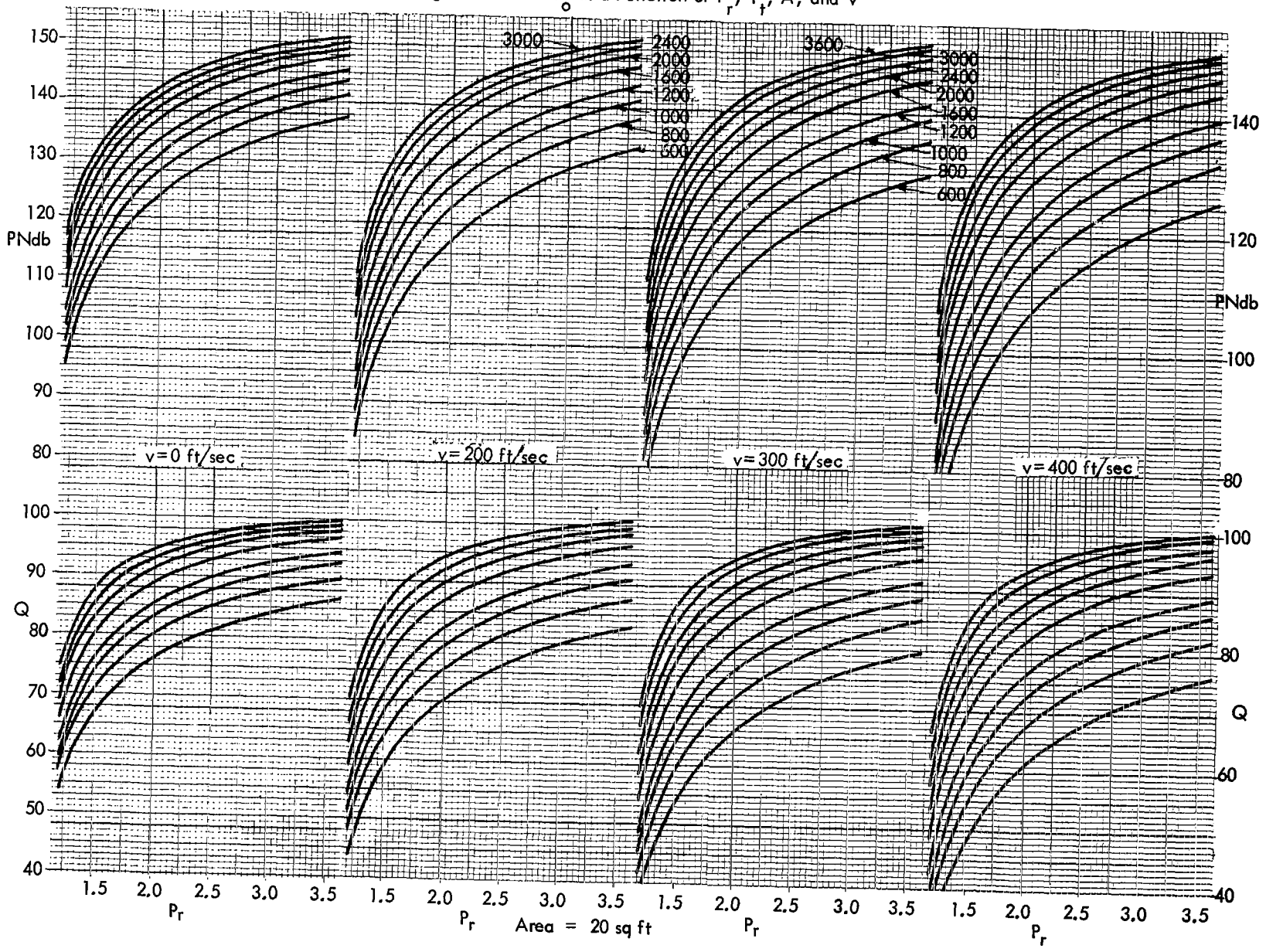

Case 1: $1500 \text{ ft/sec} \leq V_R \leq 3500 \text{ ft/sec}$

$$10 \log f(V_R) = 70 \log V_R - 78 \tag{10}$$

and

Case 2: $800 \text{ ft/sec} \leq V_R \leq 2500 \text{ ft/sec}$

$$10 \log f(V_R) = 80 \log V_R - 112 \tag{11}$$

Within an accuracy of about ± 1 db, Case 1 and 2 equations are suitable for representing the relative velocity functions for afterburning and non-afterburning jets respectively. With these simplifications, equations (2) (4) (5) (7) and (8) can be used to obtain relatively simple expressions for the engine reference PNdb in terms of F_n, ρ, V_j, A and v_o, or $PNdb_o$ in terms of F_n, p_r, T_t, A and v_o. The results are presented below:

Case 1: $1500 \text{ ft/sec} \leq V_R \leq 3500 \text{ ft/sec}$, applicable to AB engines,

$$PNdb_o - 10 \log F_n = 10 \log \rho + 58 \log V_j - 4 \log A + 68 \log \left[1 - \frac{v_o}{V_j}\right] - 78.5 \tag{12}$$

or

$$PNdb_o - 10 \log F_n = 19 \log T_t + 38.5 \log p_r - 4 \log A + 68 \log \left[1 - \frac{v_o}{V_j}\right] + 23 \tag{13}$$

Case 2: $800 \text{ ft/sec} \leq V_R \leq 2500 \text{ ft/sec}$, applicable to non AB engines

$$PNdb_o - 10 \log F_n = 10 \log \rho - 4 \log A + 68 \log V_j + 78 \log \left[1 - \frac{v_o}{V_j}\right] - 112.5 \tag{14}$$

or

$$PNdb_o - 10 \log F_n = 24 \log T_t + 62 \log p_r - 4 \log A + 78 \log \left[1 - \frac{v_o}{V_j}\right] - 1.5 \tag{15}$$

Remembering that $Q = PNdb_o - 10 \log F$, Eqs. (12) and (14) have been reduced to the form of the nomograph which is presented in figure 5. For any given values of ρ, V_j, A and v_o, Q can be determined directly from the chart. The accuracy of the chart is estimated to be about $\pm$ 1.5 db of the exact value.

A more concise representation of the above equations may be written if the following operational definition is made:

$$PN_o = \log^{-1} \frac{PNdb_o}{10} \tag{16}$$

The quantity $\overline{PN_o}$ is related to the perceived noise and its meaning is as defined by Eq. (16). For convenience $\overline{PN_o}$ will be called the perceived noise. The modified equations are now,

Case 1: $1500 \text{ ft/sec} \leq V_R \leq 3500 \text{ ft/sec}$, applicable to AB engines

$$\frac{\overline{PN_o}}{F_n} = 1.4 \times 10^{-8} \frac{\rho V_j^{5.8}}{A^{.4}} \left(1 - \frac{v_o}{V_j}\right)^{6.8} \tag{17}$$

$$\frac{\overline{PN_o}}{F_n} = 2 \times 10^2 \frac{T_t^{1.9} p_r^{3.85}}{A^{.4}} \left(1 - \frac{v_o}{V_j}\right)^{6.8} \tag{18}$$

Case 2: $800 \text{ ft/sec} \leq V_R \leq 2500 \text{ ft/sec}$ applicable to non AB engines

$$\frac{\overline{PN_o}}{F_n} = 5.64 \times 10^{-12} \frac{\rho V_j^{6.8}}{A^{.4}} \left(1 - \frac{v_o}{V_j}\right)^{7.8} \tag{19}$$

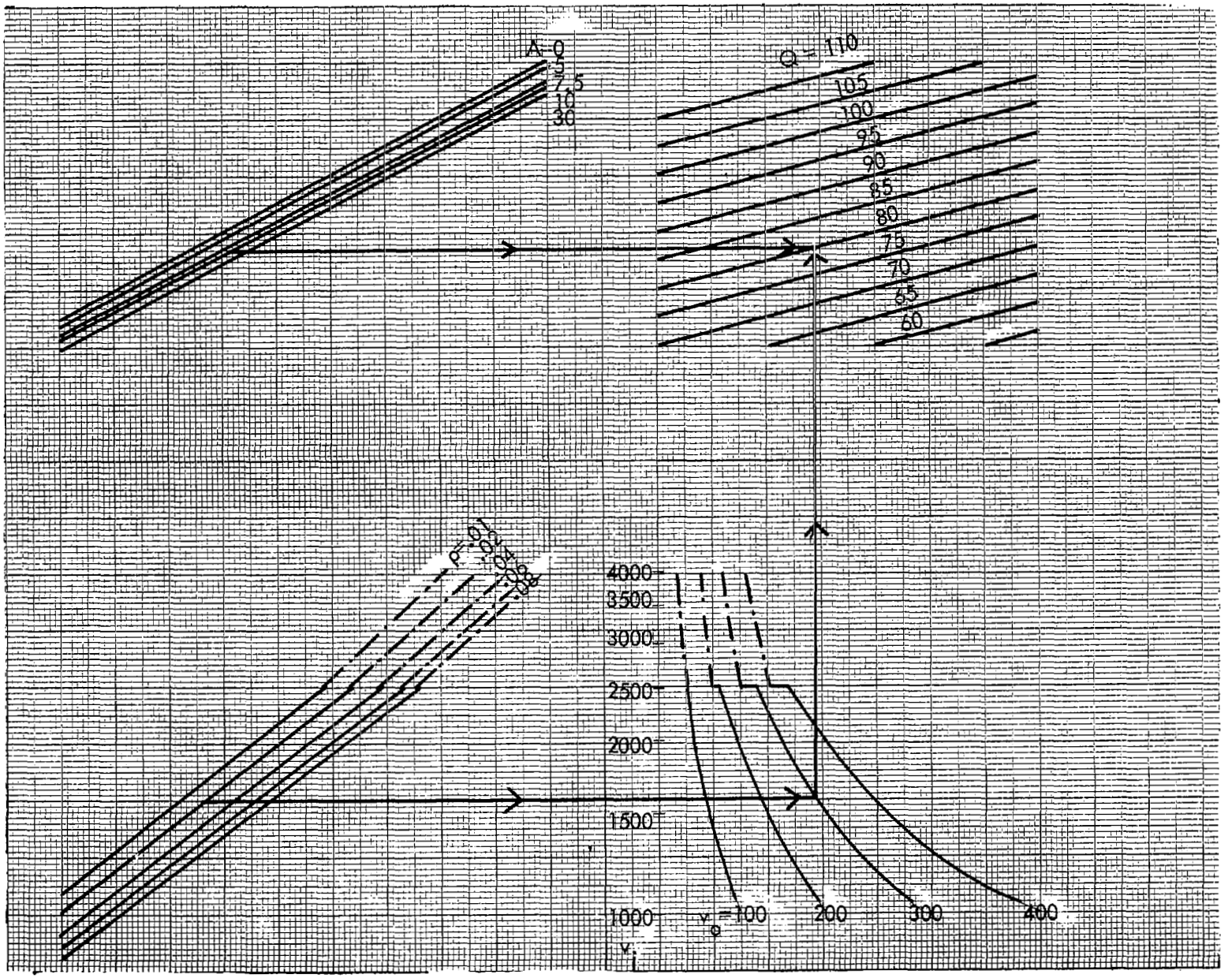

Figure 5 - Nomograph for Q

$$\frac{\overline{PN_o}}{F_n} = 7.1 \times 10^{-1} \frac{T_t^{2.4} p_r^{6.2}}{A^{.4}} \left(1 - \frac{V_o}{V_j}\right)^{7.8} \qquad (20)$$

It should be pointed out that $\overline{PN_o}$ per unit thrust is not independent of the size of the engine. Once the nozzle design pressure ratio and temperature are fixed, it is not precisely correct to assume that $\overline{PN_o}$ will be directly proportional to the engine thrust, since the area of the nozzle, though not a very strong parameter, will influence $\overline{PN_o}$. Generally if F_n, ρ, V_j (or T_t and p_r) and V_o are specified, A can be calculated (see Eq. (8).

The effect of nozzle area, and ratio of aircraft speed to exhaust jet velocity on the normalized reference $PNdb_o$ (i.e., Q) are shown in figures 6 and 7 respectively. It is noted that the normalized reference $PNdb_o$ decrease slowly with increase in nozzle area. This is associated with the shifting of the noise spectrum to the left due to nozzle area increase.

The effect of aircraft velocity on Q is strong when the exhaust velocity V_j of the jet is relatively low. This suggests that any operational procedures adopted by a pilot to accelerate an aircraft after take-off (say from V_2 + 10 knots to say V_2 + 50 knots and accompanied by flap retraction) is probably beneficial for low-velocity turbofan engines, and not beneficial for higher-velocity turbojets. The point to be made is that possible benefits associated with aircraft operational procedures depend on the engine design to some degree.

It should be pointed out also that in Eqs. (12) to (20) the quantities related to the perceived noise (either $\overline{PN}$ or PNdb) are expressed as functions of five variables (F_n, ρ, V_j, V_o, A). Of course, consistent with what has already been mentioned, only four independent variables are needed to calculate $\overline{PN_o}$ or $PNdb_o$ since the term F_n and A are interchangeable once ρ, V_j and V_o are specified. The five-variable equations are employed in order to develop the parameter $\overline{PN_o}/F_n$ or Q which are useful parameters for design purposes.

2.2.4 Calculation of $PNdb_o$ for combined jets in fan engines.- The SAE method suggests that in estimating jet noise produced by unmixed jet exhausts of fan engines, the total noise (SPL) be calculated as the sum of the individual contributions, octave by octave. Conversion to PNdb is then made based on the combined spectrum. In this section we have developed a short cut method that eliminates the need for combining the spectra from the two jets before converting to PNdb.

The question is if the PNdb value of each of two individual jets is known, is there a simple rule for combining the two PNdb values to obtain the same total PNdb as would be obtained using the SAE procedure. A series of calculations have been performed involving

Figure 6

$\triangle$PNdb and $\triangle$Q as a Function of A_r

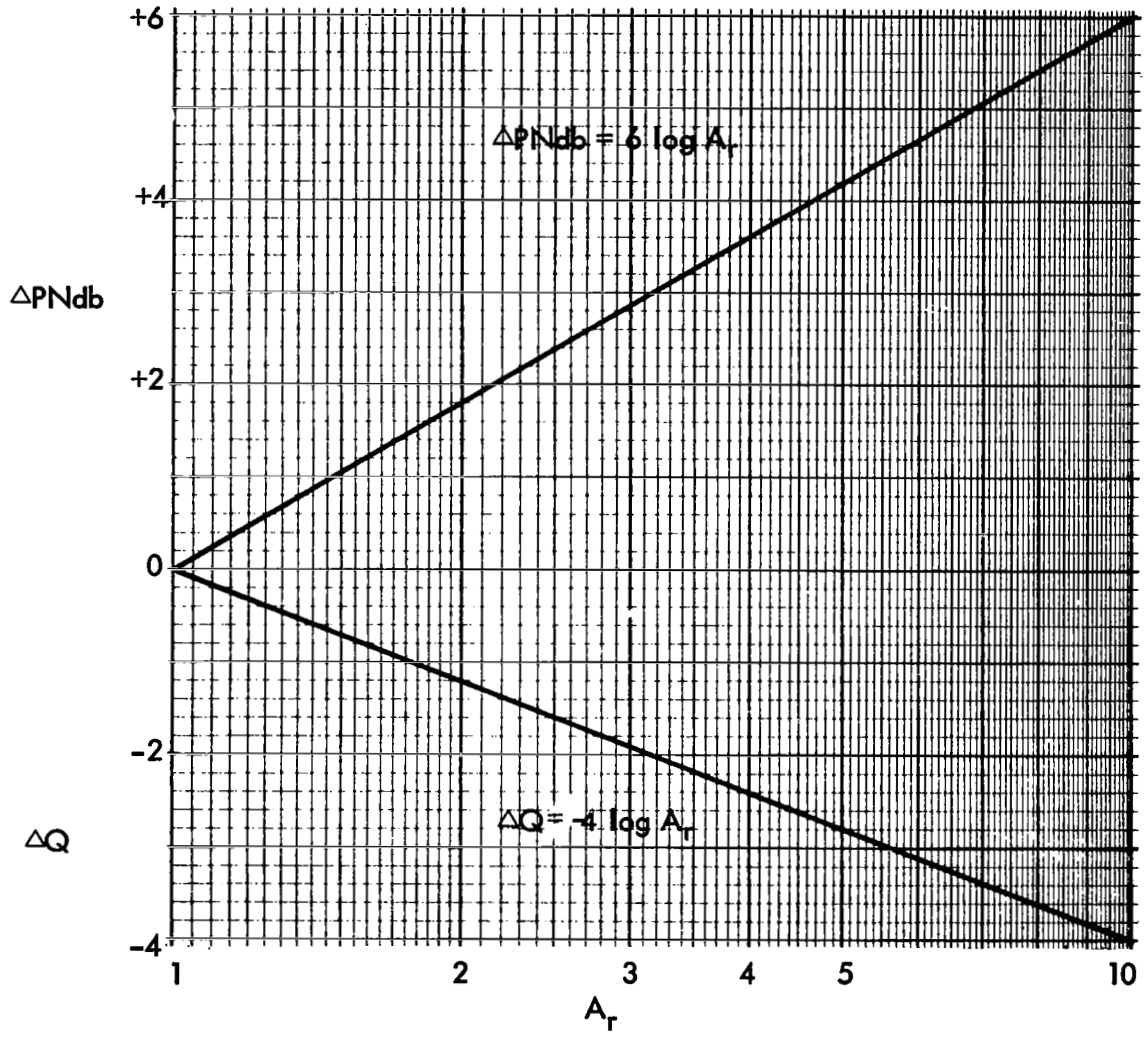

Figure 7

ΔPN_{db} Versus V_i

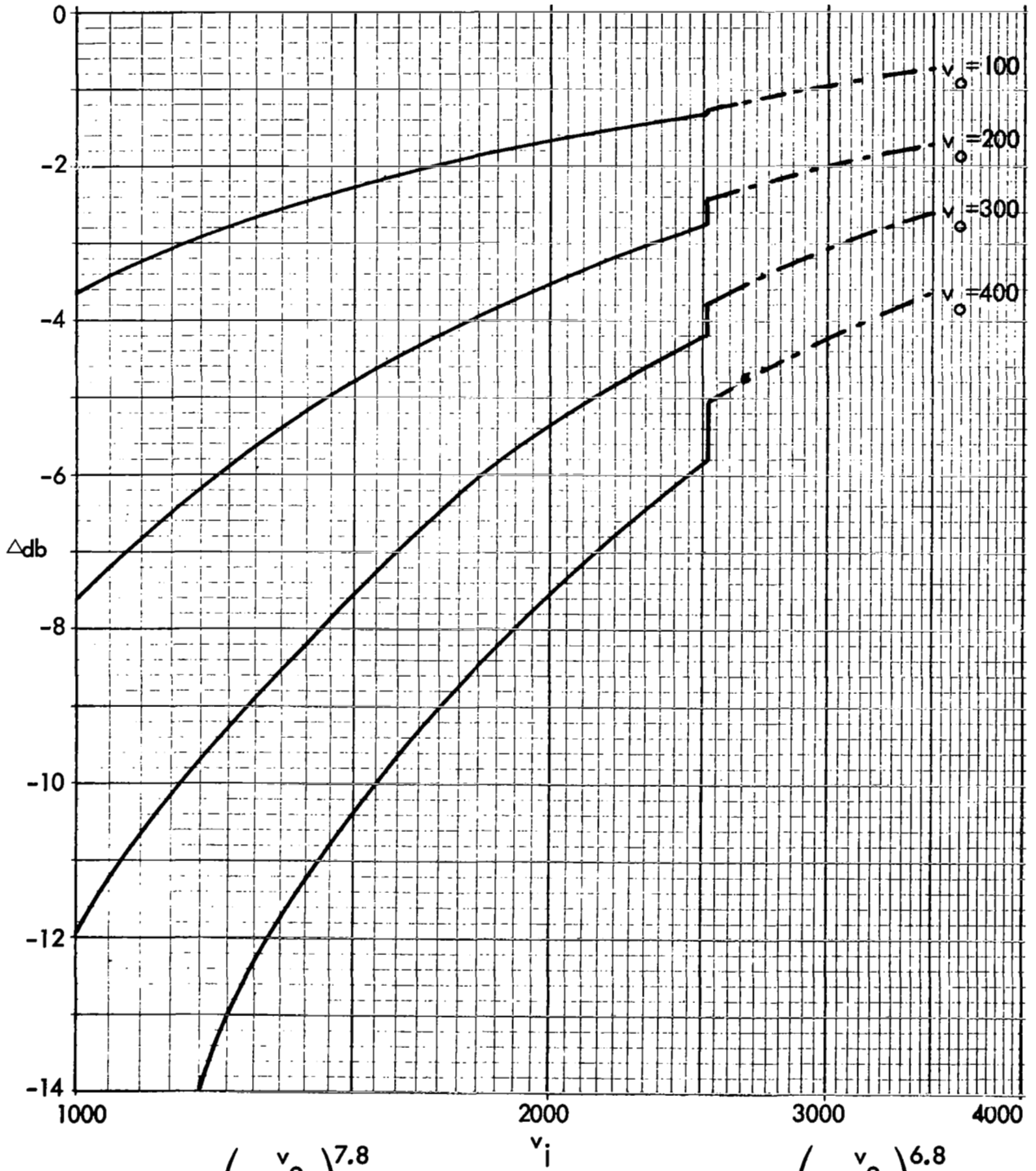

——— $\Delta db = \left(1 - \frac{v_o}{v_i}\right)^{7.8}$ -.-.-. $\Delta db = \left(1 - \frac{v_o}{v_i}\right)^{6.8}$

variations of the overall SPL and location on the frequency axis of two jet noise spectra. Each of the two spectra had the basic SAE recommended spectrum shape and the frequency peak of each never exceeded the fifth octave band. For each set of level and spectrum location variations, the PNdb of each spectrum, and the combined PNdb (by the SAE method) were obtained. Examination of the individual jet PNdb and the combined PNdb for various possible combinations indicate that within an accuracy of $\pm$ 0.5 db, the total combined PNdb may be related to the individual PNdb by the rule analogous to that used for adding sound power level.

$$PNdb_o(\text{total}) = 10 \log \left[\log^{-1} \frac{PNdb}{10} + \log^{-1} \frac{PNdb_o}{10} \right] \quad (21)$$

Remembering the operational definition

$$\overline{PN}_o = \log^{-1} \frac{PNdb_o}{10} \quad (16)$$

Eq. (21) may be written as

$$\overline{PN}_o(\text{total}) = \overline{PN}_{01} + \overline{PN}_{02} \quad (22)$$

The above equation states the approximate rule that the total perceived noise ($\overline{PN}$ (total)) is the algebraic sum of the perceived noise from each jet so long as the individual spectra follows the SAE recommended spectrum shape for jet noise and neither of the two frequency peaks lie outside the range between the first and fifth octave band. A method for combining PNdb for compressor noise will be given later in Section 3.

As the result of the above rule, the procedure for calculating the engine reference jet noise for a fan engine becomes clear. If the nozzle design parameters A, ρ, V_j of both the gas generator and fan jets are known and the aircraft velocity v_o is known, Eq. (7) or figure 4 may be used to obtain the $PNdb_o$ for each jet and these can be summed according to Eq. (21).

For approximate calculations Eqs. (12) to (20) may be combined with the rule set above to obtain analytic expressions for total $\overline{PN_o}$, $\overline{PN_o}/F_n$, total $PNdb_o$, and total Q for the non-AB turbofan engines. The results are presented below:

$$\overline{PN_o}\,(\text{total}) = \left[1.78 \times 10^{-13}\ \rho_1^{-2}\ A_1^{0.6}\ V_{j1}^{8.8}\ M_1^{8.8}\right] \times \left[1 + \omega_r u_r^{7.8}\ \rho_r\ A_r^{-.4}\ \left(\frac{M_2}{M_1}\right)^{8.8}\right] \tag{23}$$

where, $M = \left(1 - \frac{v_o}{V_j}\right)$, $\rho_r = \frac{\rho_2}{\rho_1}$ for density ratio, $\omega_r = \frac{\rho_2 A_2 V_{j2}}{\rho_1 A_2 V_{j1}}$, or by pass ratio, $u_r = \frac{V_{j2}}{V_{j1}}$ exit velocity ratio, and $A_r = \frac{A_2}{A_1}$ area ratio, and subscripts 2 and 1 refer to the fan and primary jets respectively.

$$PNdb_o\,(\text{total}) = 20 \log \rho_1 + 6 \log A_1 + 88 \log V_{j1} + 88 \log M_1 + 10 \log\left[1 + \omega_r u_r^{7.8}\ \rho_r A_r^{-.4}\ \left(\frac{M_2}{M_1}\right)^{8.8}\right] - 127.5 \tag{24}$$

$$\frac{\overline{PN}(\text{total})}{F_n\,(\text{total})} = \left[5.64 \times 10^{-12}\ \rho_1 A_1^{-.4}\ V_{j1}^{6.8}\ M_1^{7.8}\right]\left[\frac{1 + \omega_r u_r^{7.8}\ \rho_r A_r^{-.4}\left(\frac{M_2}{M_1}\right)^{8.8}}{1 + \omega_r u_r\left(\frac{M_2}{M_1}\right)^2}\right] \tag{25}$$

$$PNdb_o(\text{total}) - 10 \log F_n(\text{total}) = 10 \log \rho_1 - 4 \log A_1 + 68 \log V_{j1} + 78 \log M_1$$

$$+ 10 \log \left[\frac{1 + \omega_r u_r^{7.8} A_r^{-.4} \left(\frac{M_2}{M_1} \right)^{8.8}}{1 + \omega_r u_r \left(\frac{M_2}{M_1} \right)^2} \right] \qquad (26)$$

It should be noted that the first bracket term on the right hand side of Eq. (23) represents $\overline{PN_o}$ and in Eq. (25) the bracket represents $\overline{PN_o}/F_n$, also the first four terms on the right of Eq. (24) represents $PNdb_o$ and the first four terms on the right of Eq. (26) represents Q (these are all with respect to the primary jet).

It is of interest to note that in Eq. (26), if the parameters of secondary importance (ρ, A, M) are neglected, the following expression is obtained.

$$\frac{\overline{PN_o}(\text{total})}{F_n(\text{total})} \propto V_{j1}^{6.8} \left[\frac{1 + \omega_r u_r^{7.8}}{1 + \omega_r u_r} \right] \qquad (27)$$

From Eq. (27) it is apparent that both primary and secondary jet velocities are important in influencing the perceived noise per unit thrust for the fan engine. Plot of the parameter $\left[\frac{1 + \omega_r u_r^{7.8}}{1 + \omega_r u_r} \right]$ is given in figure 8.

2.3 Compressor or Fan Noise

At the present time, there is no completely satisfactory method for predicting compressor noise. Many different factors in the design of the axial compressor or fan have been observed to have direct influence on the noise output. However, no quantitative relationship linking these design factors to noise generation has been established. The complexity of turbo-machinery design make even the prediction of aerodynamic performance sometimes

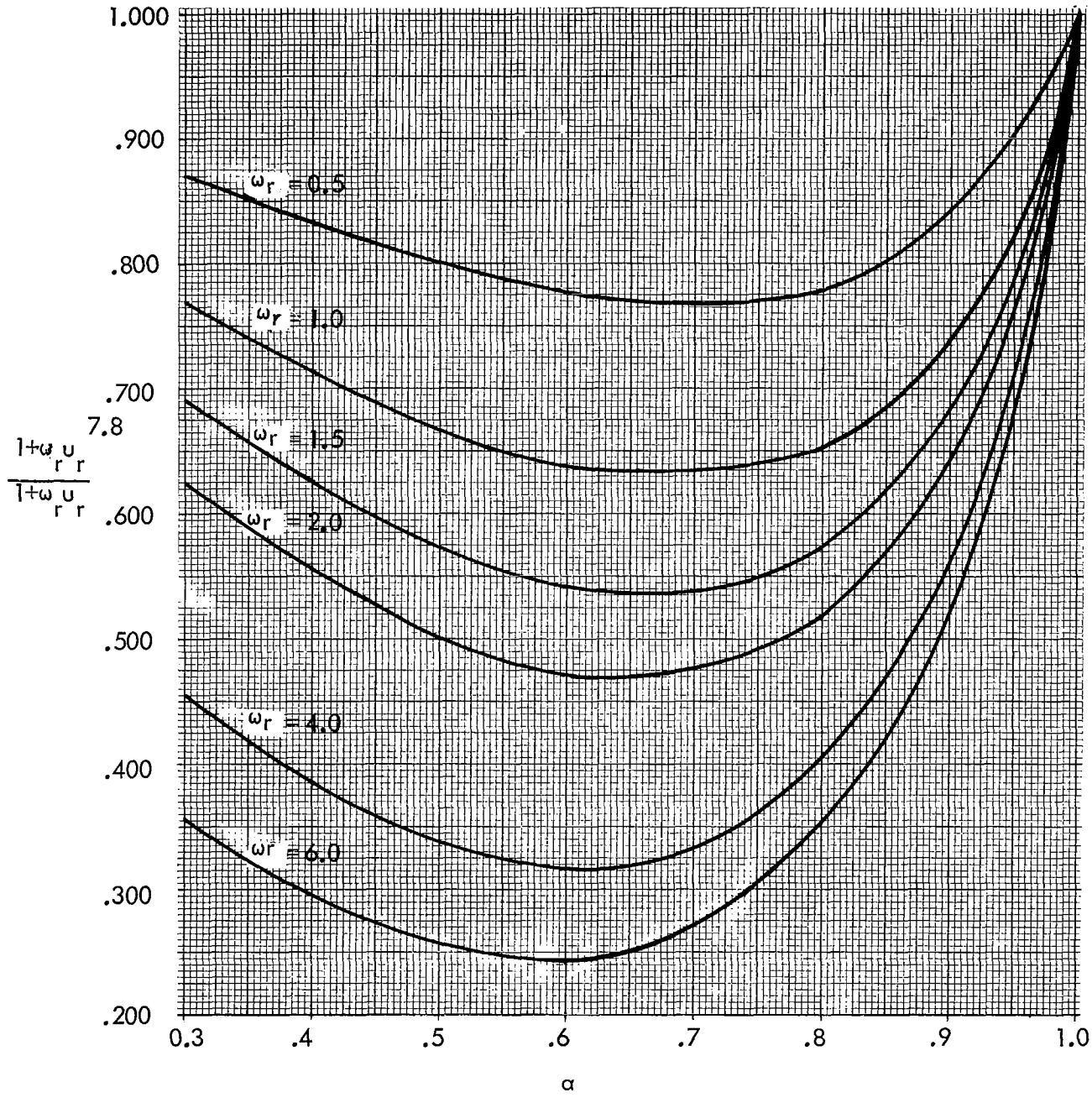

Figure 8

$\frac{1-\omega_r u_r}{1-\omega_r u_r}^{7.8}$ Versus u_r and ω_r

difficult, and it is not anticipated that methods for the accurate prediction of acoustic performance of compressors or fans will be developed in the near future. For preliminary design and airport noise planning purposes it would be very useful to have a procedure that would provide even a gross estimation of the compressor or fan sound and to this end, three tentative prediction methods that have been suggested by experienced workers in the field have been reviewed. From these three methods an "average" method has been developed that is consistent with the empirical data which forms the basis of the three prediction methods.

The three compressor noise prediction methods, which we will call A, B, and C, are described in detail in References 2, 3, and 4. Method A considers relative blade tip velocity, stator-rotor spacing, and size to be the most important parameters. The relative velocity (and not the tip velocity alone) effect was demonstrated quite well by experimental data. Method A suggests the following formulation,

$$SPL_A = 85 + 50 \log \frac{u_{rel}}{1000} + 10 \log w - 10 \log\left(\frac{s}{c}\right)^2 + \triangle F \qquad (28)$$

where SPL_A refers to the maximum sideline (100 foot) level associated with the fundamental discrete frequency tone alone (not including any compressor generated white noise, or pure tone harmonics), u_{rel} is the relative blade tip velocity, s/c is the ratio of rotor-stator spacing to rotor chord, w is the weight flow, and $\triangle F$ is the flow correction factor for forward arc radiation (i.e., a correction for the apparent fact that as inlet velocity increases, the ratio of forward to backward radiation (in the case of a fan) decreases.

Method B is the simplest in that it involves only two parameters, the tip speed and tip diameter. It was pointed out in reference 3 that the method is intended only to give a gross estimation and is not expected to have an accuracy better than $\pm$ 10 db. Method B suggests the following relation,

$$SPL_B = 20 \log D - 44 + 46 \log u_t \qquad (29)$$

where SPL_B refers to the maximum sideline (200') SPL associated with the fundamental discrete tone only, u_t is the tip speed, and D is the tip diameter (in feet).

Method C uses the energy flux (proportional to ρu) across the compressor and several other design parameters such as hub-tip ratio, blade number, and size as the basis for

prediction. Method C is said to be consistent with test data from a large variety of compressor and fans, and it gives the following relation for predicting the acoustic power output of the compressor

$$PWL_C = 10 \log\left[\frac{A_n}{N_R}\left(\frac{D_h}{D_t}\right)^2 \frac{D_t}{3.4}\right] + 10 \log f[E] \qquad (30)$$

where PWL_C refers to the sound power associated with the fundamental and various harmonics of the discrete compressor tones, but does not include any compressor broad band noise. A is the compressor flow area, n is the RPM, N_R is the number of rotor blades, D_h/D_t is the hub tip ratio, and E is the energy flux, which may be written an $E = 125\ w/A$. w/A is the weight flow per unit compressor face area. The function $10 \log f(E)$ was shown as a smooth curve in reference 4, but has been approximated by us as

$$10 \log f(E) = \quad 43 \log E - 22 \quad \text{for } 500 < E < 3500 \qquad (31)$$

$$10 \log f(E) = \quad 13.2 \log E + 83.5 \quad \text{for } 3500 < E < 10{,}000 \qquad (32)$$

All the above methods have in common some characteristic speed as the most important parameter affecting the noise level. For example, method C in the parameter E ($25\rho_o U_z$) implies that the axial speed U_z is the characteristic speed. Method A employs the relative tip speed u_{rel}, while method B uses the tip speed u_t. For any given compressor design, these velocities are related in terms of the design flow coefficient and air inlet angle (see air velocity diagram in figure 9). While u_{rel} appears to be probably the most meaningful choice, either one of the other two U_z and u_t, are acceptable for gross estimating purposes. Since u_t is the most easily obtained parameter, it will be selected later as the velocity parameter for the "average" method.

It is desirable to estimate a maximum overall SPL at the 200' sideline that will include not only contributions from all the fundamental and harmonic discrete tones of the compressor (associated with blade passage) but also the broad band random noise that accompany the discrete tones. References 2, 3, and 4, include specific details for estimating the white noise, although they differ somewhat in procedures. From these procedures, it appears that the amount to be added to the SPL levels shown in Eqs. (28) (29) and (30) to obtain the maximum overall SPL at 200 feet sideline is approximately 2 to 4 db. This fact is used later in developing the average method.

In order to put the various prediction methods into a form where comparisons could be made, it was necessary to eliminate certain non-common parameters by substituting into

Figure 9

Air Velocity Diagram

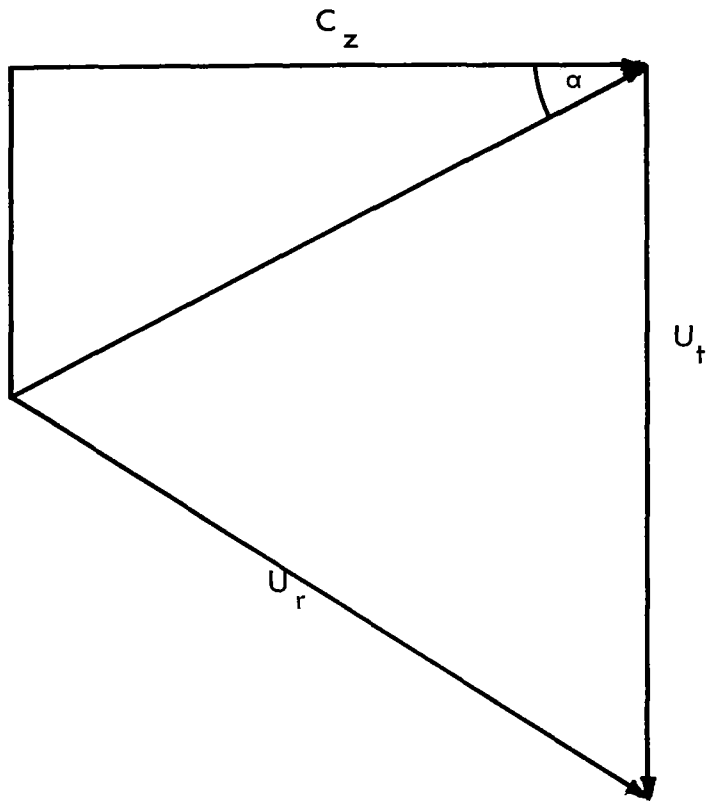

their places typical design values. Simplifying assumptions were also made when necessary. Using this approach, method A was simplified by making the following modifications:

1. let $\frac{s}{c} \approx 0.25$
2. let $u_{rel} \approx 0.90\ u_t$ to represent a typical design
3. let $\triangle F \approx 0$ (since we would accept either forward or backward radiation, whichever is greater)
4. correction for going from the fundamental tone to the overall SPL = 2 db.

Eq. (28) then becomes,

$$SPL_{0A} = 50\ u_t + 10 \log w - 60 \tag{33}$$

Similarly, method B was simplified by making the following modifications:

1. D in Eq. (29) may be written as

$$D^2 = \frac{4}{\pi} \frac{A}{(1 - e^2)} = \frac{4}{\pi} \frac{\omega}{(1 - e^2)\rho_o u_z} = \frac{4}{\pi} \frac{\omega}{(1 - e^2)(\rho_o \phi u_z)}$$

2. let e (hub-tip ratio) ≈ 0.70
3. let ϕ (flow coefficient) ≈ 0.50
4. ρ_o (air inlet density) ≈ 0.075
5. Correction for going from the fundamental tone to the overall SPL = 4 db

Thus, Eq. (29) for method B may be written as,

$$SPL_{0B} = 36 \log u_t + 10 \log w - 38.5 \tag{34}$$

Finally, Method C was simplified by making the following modifications:

1. PWL is converted to SPL by assuming the angle of maximum radiation to be at either 60° or 120° from the inlet, and the directivity index to be 7 db.

2. The form $\frac{A_n}{N_R} l^2 \frac{D_t}{3.4}$ is rewritten as $\frac{\omega}{\phi} \frac{e^2 - e^3}{AR\ \sigma}$

3. let hub-tip ratio $e \approx 0.70$

4. let ϕ flow coefficient, ≈ 0.50

5. let solidity $\sigma = 1.0$

6. let blade aspect ratio $AR \approx 2.5$

7. the term E is rewritten as $125 \frac{w}{A} = 125\ \rho_o\ \phi\ u_t$, and can be written as $E = 4.70\ u_t$ after letting $\phi = 0.50$.

8. Correction to include white noise = add 2 db. Thus, Method C may be written as

$$SPL_{0c} = 10 \log w - 49 + 10 \log f \left[4.70\ u_t\right] \tag{35}$$

To calculate $10 \log f \left[4.70\ u_t\right]$, use Eqs. (31) and (32), after letting $4.70\ u_t = E$).

The three simplified prediction methods given in Eqs. (33) (34) and (35) are plotted in figure 10 for $SPL_o - 10 \log w$ versus u_t. It can be seen that the three curves intercept one another and within a broad band of $\pm$ 6 db generally agree with one another. A straight line drawn across the overlapping curves to provide the best fit yields the final relation,

$$SPL_o = 10 \log w + 40 \log u_t - 34 \tag{36}$$

Figure 10

SPL_o -10 log Versus U_t

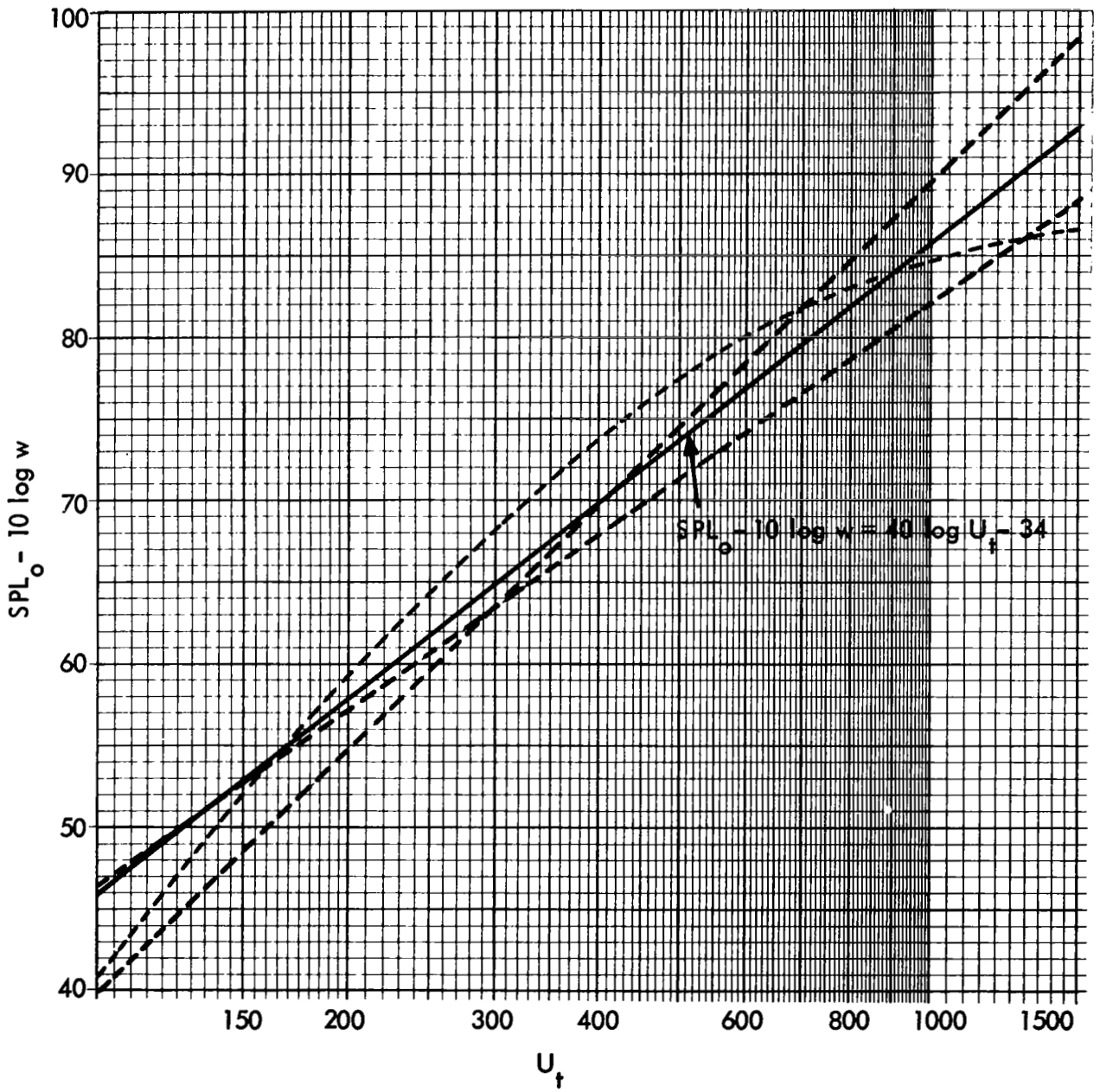

where SPL_o is the 200-ft sideline maximum overall sound pressure level which includes both discrete tones and white noise, ω is the weight flow, and u_t is the tip speed of the single-stage compressor. It is not possible to assign an accuracy limit to this "average" method of compressor noise prediction without having to examine in detail a great deal of data.

As will be developed later, there exists an approximate relationship between the compressor overall SPL and the PNdb. This relationship may be written as follows:

$$PNdb_o = SPL_o - 4 + 5 \log f \tag{37}$$

where f is the frequency of the pure tone fundamental. $PNdb_o$ consists of both the compressor discrete tone and white noise associated with the compressor.

Frequency f is related to the tip speed, number of blades, and diameter of the compressor. These parameters are in turn functions of other design quantities and f may be written as

$$f = \frac{2\sigma AR}{(1-1)} \quad \frac{\pi}{4} \rho_o (1 - e^2)\, \phi \quad 1/4 \; \frac{u_t^{0.75}}{\omega^{0.25}} \tag{38}$$

For a typical design, $\sigma = 1$, $AR = 2.5$, $e = 0.70$, $\phi = 0.5$, and when f is substituted into Eq. (35) the final expression for the reference $PNdb_o$ of the compressor sound is obtained.

$$PNdb_o = -36.5 + 7.5 \log \omega + 47.5 \log u_t \tag{39}$$

Figure 11 is a plot of $PNdb_o$ as a function of engine tip speed and weight flow. It applies only to a single-stage axial compressor.

2.4 Noise and Engine Cycle Parameters

2.4.1 Jet noise and cycle variables.- For a turbofan* engine, the basic engine cycle is defined at any point of operation when the following independent variables are established:

*The equations shown in this section also apply to turbojet (non-after-burning) engines if the by-pass ratio β is set equal to zero wherever it appears.

Figure 11

PNdb$_o$ Versus Tip Speed and Weight Flow

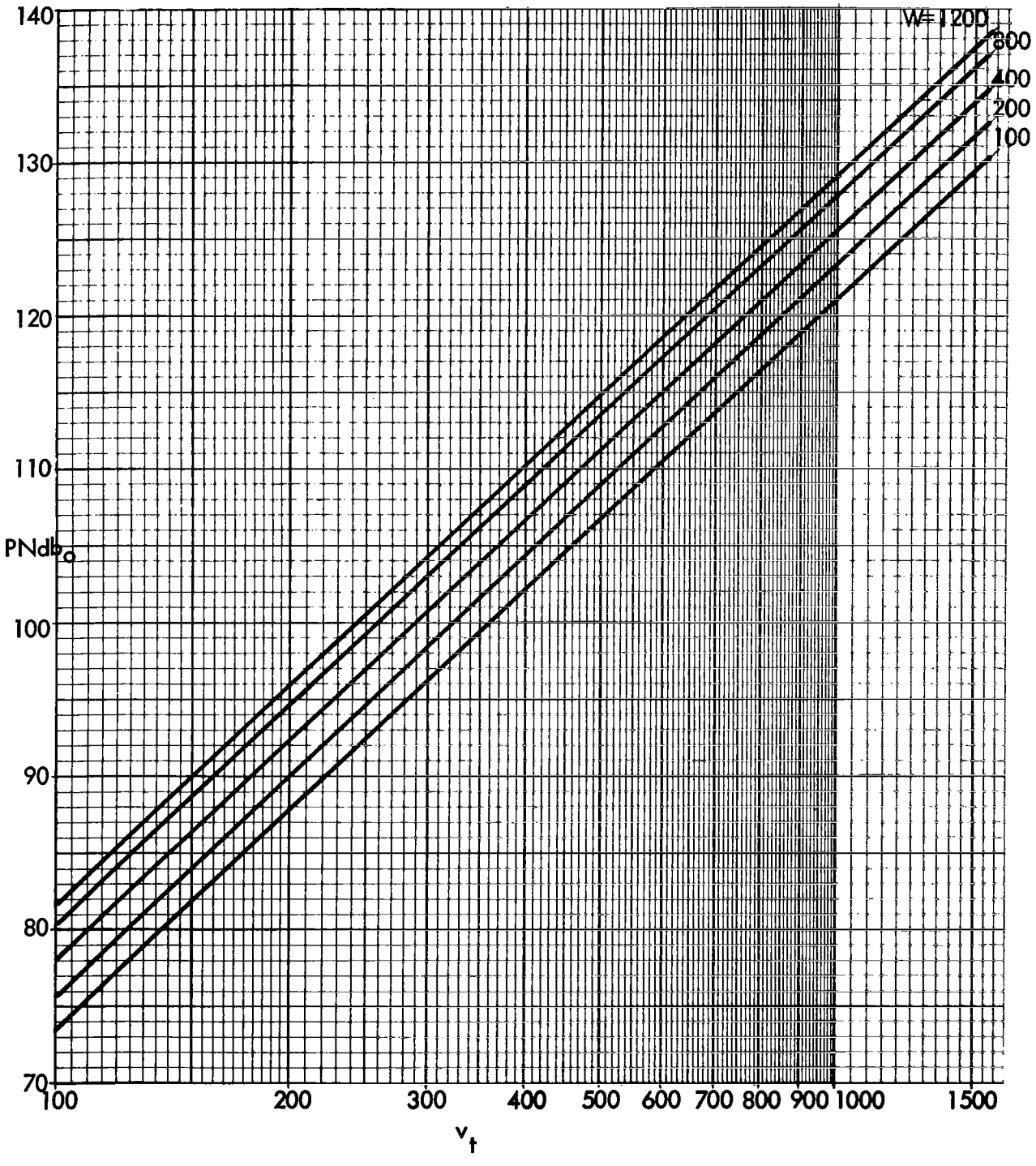

$\overline{CPR}$ - overall cycle pressure ratio

$\overline{FPR}$ - fan pressure ratio

β - by-pass ratio

T_4 - turbine inlet temperature

v - aircraft speed

η_c, η_{fc}, η_b, η_t, η_n, - component efficiencies for the main compressor, fan, burner, turbine, and nozzle, respectively.

Engine size is established when total net thrust, total weight flow or total nozzle area is given. As already developed in Section 2, the total exhause jet $PNdb_o$ of a turbofan engine is the logarithmic sum of the individual PNdb of the two streams, and can be calculated by means of Eqs. 7 and 21. In general,

$$PNdb_o \text{ (total jet noise)} = f\ (\rho, v, A)\ \text{jet},\ (\rho, V, A)\ \text{fan},\ v \tag{40}$$

Thus, it can be seen that $PNdb_o$ may be related to the cycle variables if we can first establish the relationship between nozzle design variables (ρ, V, A) and cycle variables. These necessary relations between nozzle and cycle variables are now summarized. For the primary jet stream,

$$\rho_j = \frac{40(\eta_b \overline{CPR})^{0.23}}{T_4} \frac{1 - \frac{1}{\eta_t} \frac{T_o A}{T_4}}{1 - \frac{T_o B}{T_4}}, \tag{41}$$

$$v_j = \frac{\eta_n T_4}{(\eta_b \overline{CPR})^{.23}} \left(1 - \frac{T_o B}{T_4}\right) \frac{1}{1 - \frac{1}{\eta_n} \frac{T_o A}{T_4}} (\eta_b \overline{CPR})^{.23} \left(1 - \frac{1}{\eta_t} \frac{T_o A^*}{T_4}\right) - 1 \tag{42}$$

*The equations shown in this section also apply to turbojet (non-after-burning) engines if the by-pass ratio β is set equal to zero wherever it appears.

where

$$A^* = 0.8 \quad \frac{\overline{CPR}^{.286}-1}{\eta_c} - \frac{\overline{FPR}^{.286}-1}{\eta_{fc}}$$

$$B = 0.8 \quad \frac{\overline{CPR}^{.286}-1}{\eta_c} + \frac{\overline{FPR}^{.286}-1}{\eta_{fc}}$$

The fan stream, exhaust velocity and jet density are given by the following equations:

$$\rho_f = \rho_o = 0.075 \tag{43}$$

$$v_f = 110 \quad \eta_n T_o \, \overline{FPR}^{.286}-1 \tag{44}$$

The jet and fan nozzle areas (A_j, A_f) can be determined if the engine size is specified either in terms of total thrust or total nozzle area (A_t); thus,

$$A_j = \frac{0.075 \, V_f A_t}{0.075 \, V_f + \beta \rho_j v_j} \tag{45}$$

or

$$A_j = \frac{32.2 F_n \text{(total)}}{\rho_j V_j \, (V_j - v_o) + \beta (V_f - v_o)} \tag{46}$$

and

$$A_f = A_t - A_j \tag{47}$$

For an aircraft fligh Mach number less than 0.30 (which covers about all take-off and landing situations of interest in noise analysis) the inlet ram pressure and temperature rise associated with speed has a negligible effect on jet exit density and velocity and need not be considered.

Because of the complexities of the equations involved, it is not possible to derive simple explicit relations between the total jet $PNdb_o$ and the cycle variables; however, there are calculation procedures for determining $PNdb_o$ for specific values of variables and these procedures can be used to see what effect cycle variables have on total jet $PNdb_o$. The following steps are involved:

1) Given cycle variables, together with component efficiencies and size, calculate the nozzle exit velocity and density for the two jet streams according to Eqs. 41, 42, 43, and 44.

2) Based on calculated values of ρ and V for the two streams and the given engine size and airplane velocity, calculate jet and fan nozzle areas (Eqs. 45, 46, and 47).

3) Use Eq. 7 in Section 2.2.2 to obtain the $PNdb_o$ for each stream and sum the PNdb according to Eq. 21.

4) Relate the total $PNdb_o$ to the given cycle variables, repeat the same process for several sets of cycle variables, and plot the results. The effect of cycle variables on $PNdb_o$ can then be established by inspection of these plots.

The above procedures have been carried out with the aid of a digital computer and the results using this approach will be given in Section 2.4.3 after the relationship between fan compressor noise and cycle variables has been considered.

2.4.2 Fan noise and cycle variables.- The following discussion applies only to the single-stage fan of the turbofan engine. Eq. 39 has been developed for the $PNdb_o$ of the fan noise in terms of weight flow through the fan and its tip speed. Since the tip speed is related to the fan-pressure ratio, $\overline{FPR}$, by a compressor design parameter ψ (called the temperature rise coefficient) defined as

$$\psi = \frac{2\gamma R}{\gamma - 1} \frac{T_o (\overline{FPR}^{.286} - 1)}{(u_t)^2} \tag{48}$$

the $PNdb_o$ of the fan can be related to the fan-pressure ratio by combining Eqs. 39 and 48 to obtain

$$PNdb_o \text{ (fan)} = 125 + 7.5 \log \omega - 23.8 \log \psi + 23.8 \log \overline{FPR}^{.286} - 1 \tag{49}$$

The fan weight flow, $\omega = \rho_o A_f V_f$, may be obtained by Eqs. 44, 46, and 47 when cycle parameters are given. A typical design value of ψ is 0.8.

The exhaust jet noise on the fan side may be related also to the fan-pressure ratio $\overline{FPR}$ by the use of Eqs. 8, 19, and 44. Since the ratio of fan stream jet noise to fan compressor noise as a function of $\overline{FPR}$ and ψ is of interest, this ratio has been derived and is (for an airplane velocity v = o),

$$\frac{PN_o \text{ (fan stream jet noise)}}{PN_o \text{ (fan compressor noise)}} \approx 4.0 \ (\overline{FPR}^{.286} - 1)^{1.65} \psi^{2.38} \tag{50}$$

Eq. 50 is plotted in Fig. 12. It can be seen that in the design range of interest, the fan compressor noise is generally exceeded by the fan jet noise. However, when the aircraft is in motion, this difference should become smaller because of the relative velocity effect on jet noise generation.

2.4.3 Parametric graphs of fan and jet noise in terms of cycle variables.- With the aid of digital computers each of the four basic cycle parameters have been systematically varied over a practical range and the noise parameters have been calculated. The component efficiencies were assumed as

$$\eta_c = 0.85,\ \eta_{fc} = 0.90,\ \eta_b = 0.95,\ \eta_t = 0.90,\ \eta_n = 0.95,$$

and the total nozzle area was fixed at $A = 10\ ft^2$. The principal results are shown in Fig. 13, with Q (for jet noise) plotted against by-pass ratio β and fan-pressure ratio $\overline{FPR}$ for different sets of T_4 and engine cycle pressure ratio, $\overline{CPR}$. Four different airplane velocities are covered. Q is defined here as

$$Q = PNdb_o - 10 \log F_n - 4 \log \frac{A_t}{10} \qquad (51)$$

where F_n and A_t are the total net thrust and total nozzle area of the engine.

With Fig. 13, and the equation 51, the total reference jet noise $PNdb_o$ may be obtained whenever the following engine cycle parameters are specified: F_n, A_t, v, $\overline{FPR}$, $\overline{CPR}$, β, T_4. It can be seen from Fig. 13 that reductions in T_4 and $\overline{CPR}$, and increases in the by-pass ratio and fan-pressure ratio all tend to reduce Q. These cycle effects on noise are, of course, directly related to their effects on the exit velocities of the two streams. It should be noted that for any given set of β, T_4, and $\overline{CPR}$ there exists an optimum fan-pressure ratio $\overline{FPR}$ (generally fairly high, and therefore not shown in all the plots in Fig. 13) that corresponds to a minimum Q. This is the condition at which both the jet and fan exit velocities are equal. These curves in Fig. 13 may be used for preliminary design purposes if the assumed component efficiencies are not too far from actual cases.

Attempts to minimize the jet noise Q by cycle selection generally lead to high flow, and high fan noise in turbofan engines. The difference in $PNdb_o$ between total jet noise and fan-compressor noise is plotted in Fig. 14 for several design variables (since the effect of cycle-pressure ratio $\overline{CPR}$ on this difference was found to be small, it is not included as a variable). As would be expected, an increase in by-pass and fan-pressure ratios and a reduction in T_4 (e.g., partial power) all tend to emphasize the compressor PNdb with respect to the total jet PNdb. For a given T_4 there exist unique sets of β and $\overline{FPR}$ for which the total jet noise is equal to the fan noise, which might be of interest in design. However, because of the approximate nature of the compressor noise prediction method from which these curves are derived, Fig. 14 should be considered mainly as an approximate guide and precise noise calculations for specific cycle parameter values should be treated with caution.

Figure 12 - PN_i/PN_f Versus FPR for Various ψ

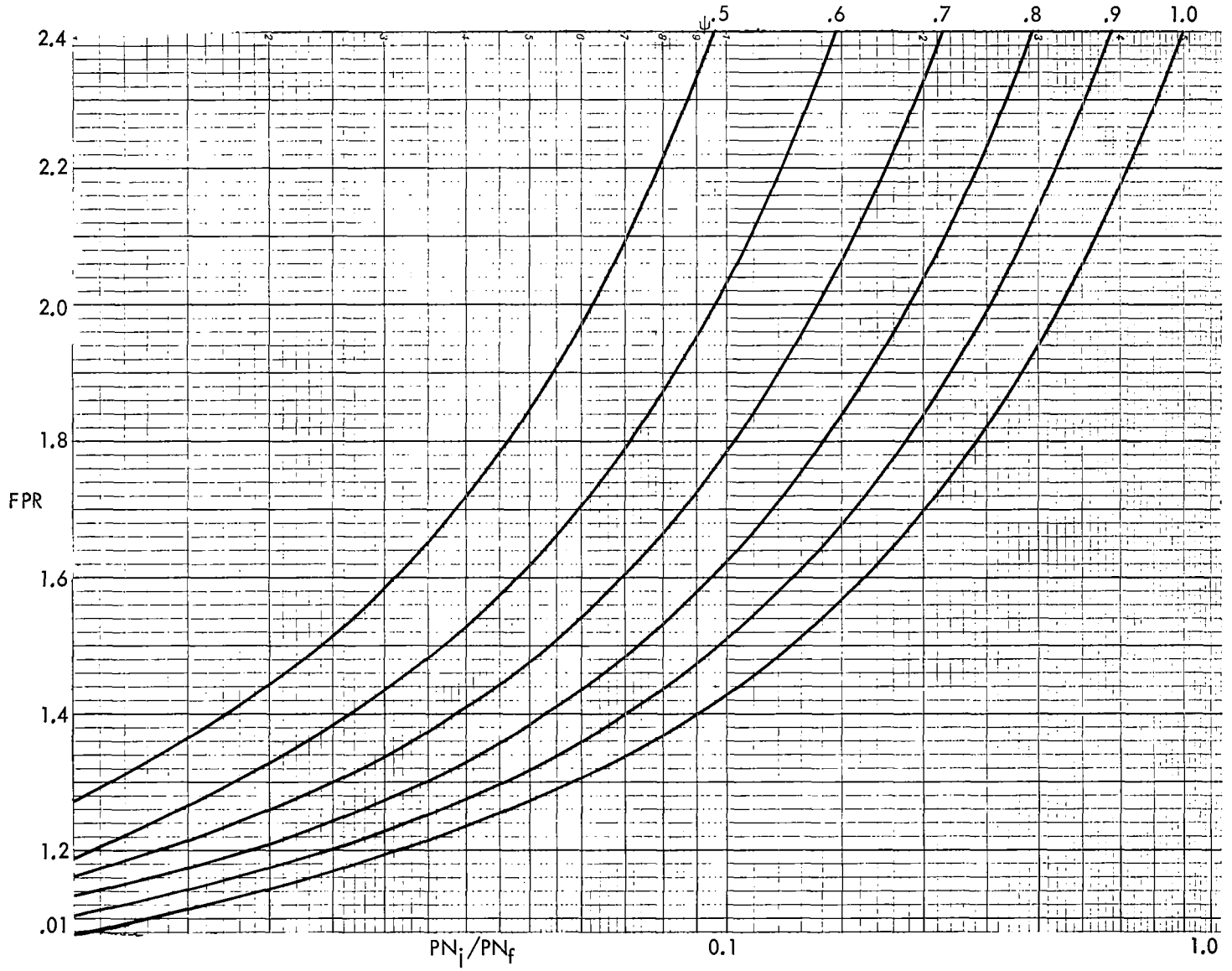

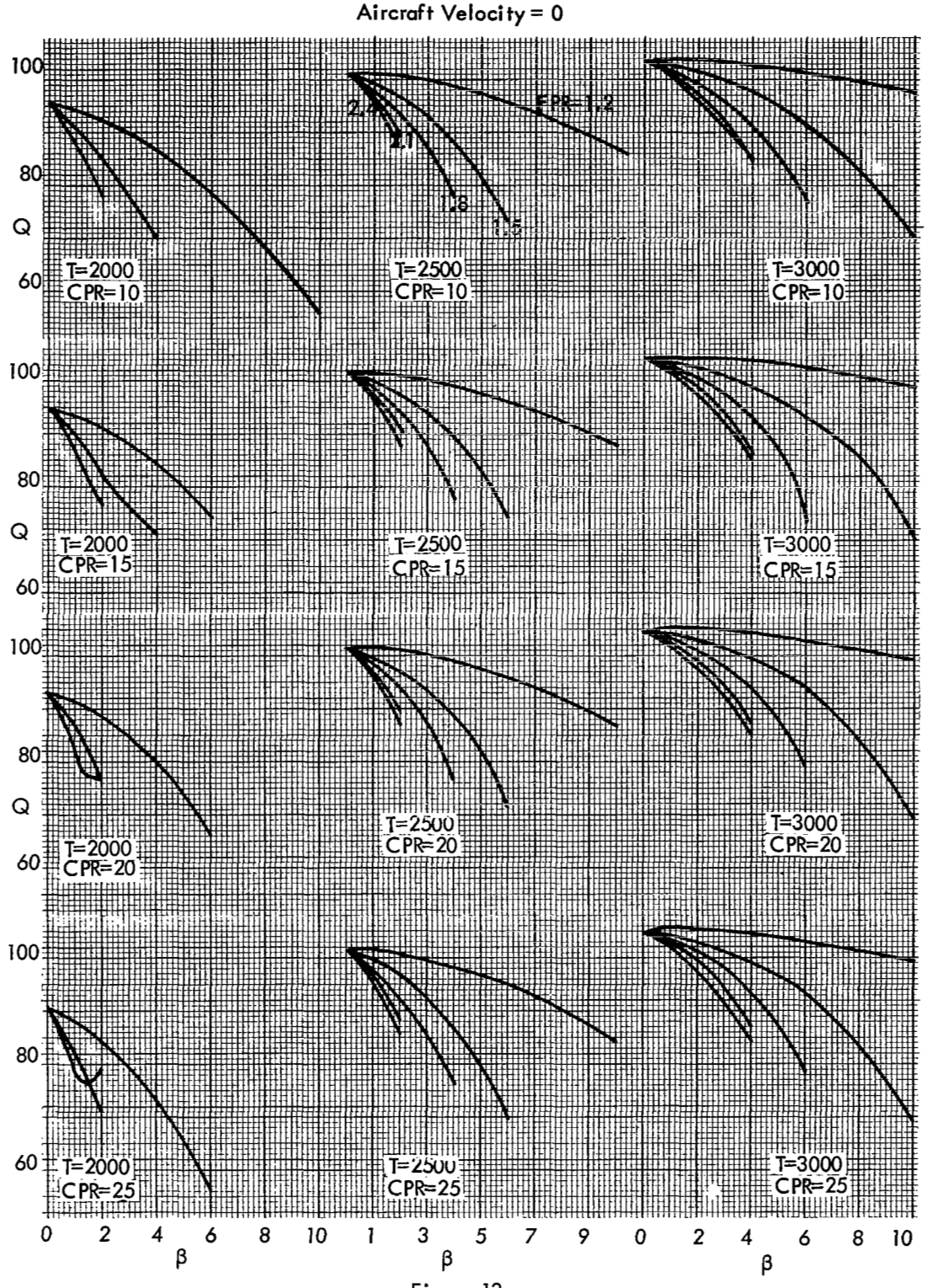

Figure 13a

Q as a Function of B, FPR, T4, CPR for Various Aircraft Velocities

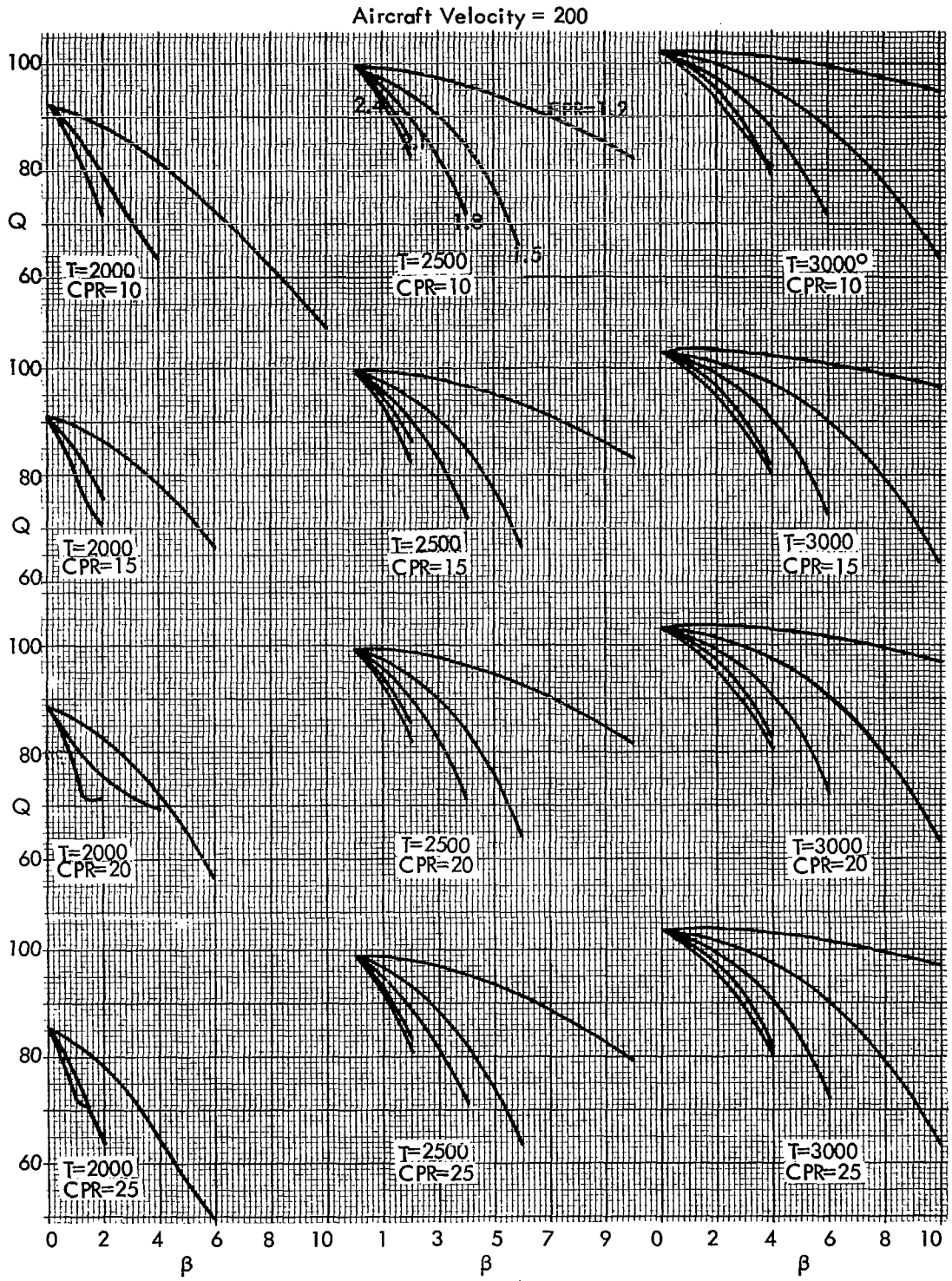

Figure 13b

Q as a Function of B, FPR, T4, CPR for Various Aircraft Velocities

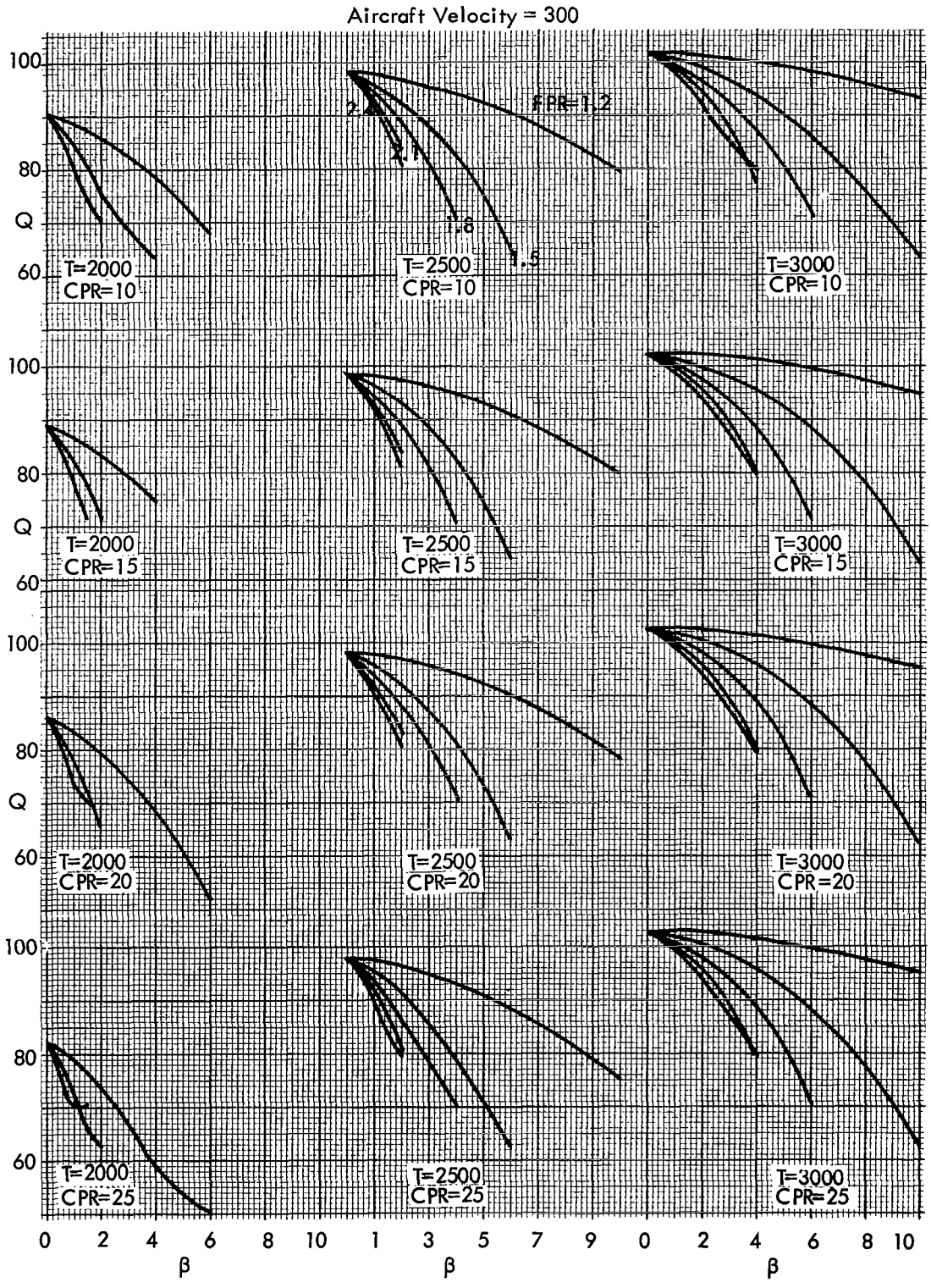

Figure 13c

Q as a Function of B, FPR, T4, CPR for Various Aircraft Velocities

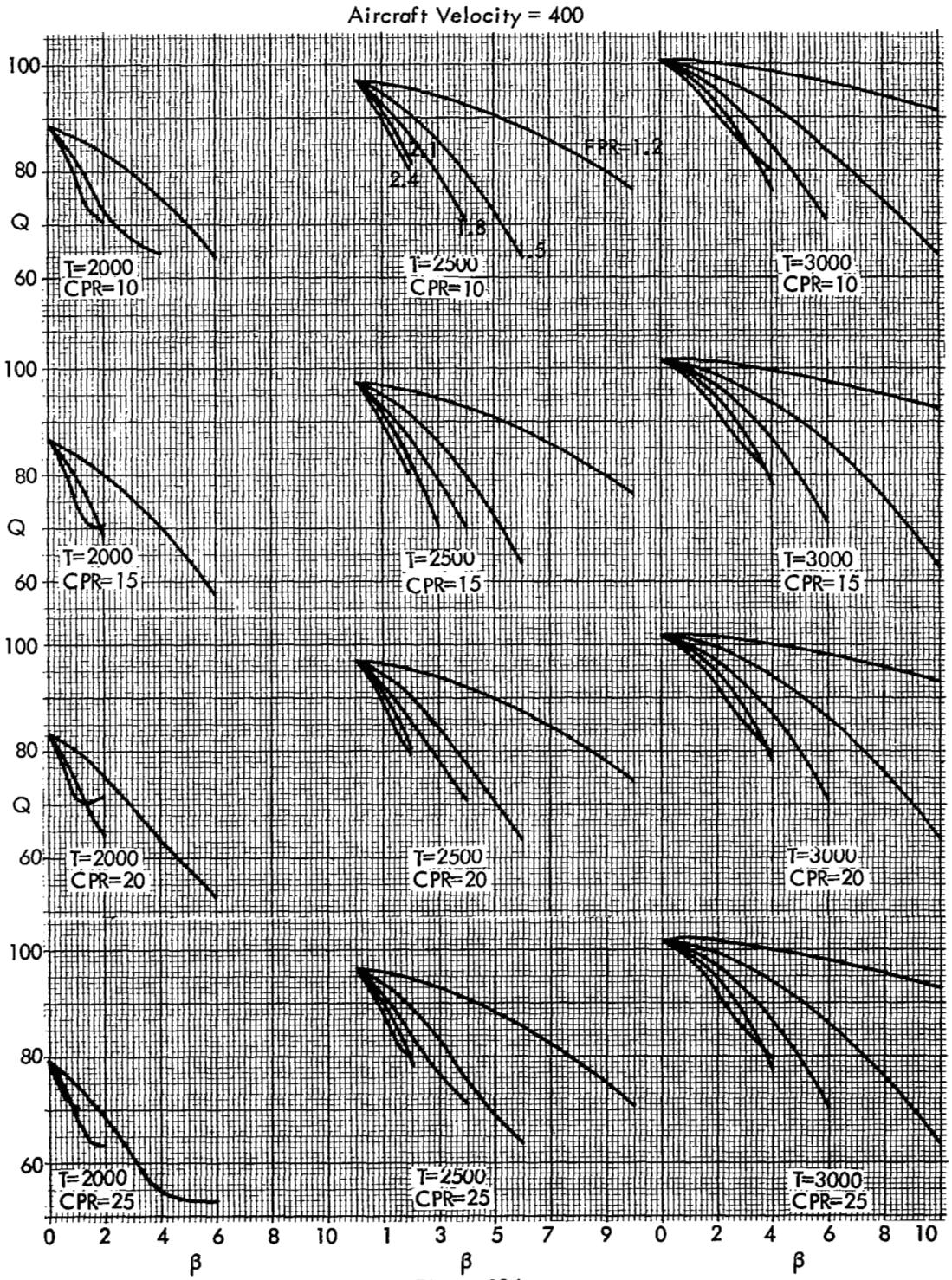

Figure 13d

Q as a Function of B, FPR, T4, CPR for Various Aircraft Velocities

Figure 14 - Total PNdb - PNdb Fan Versus B, FPR, and Temperature

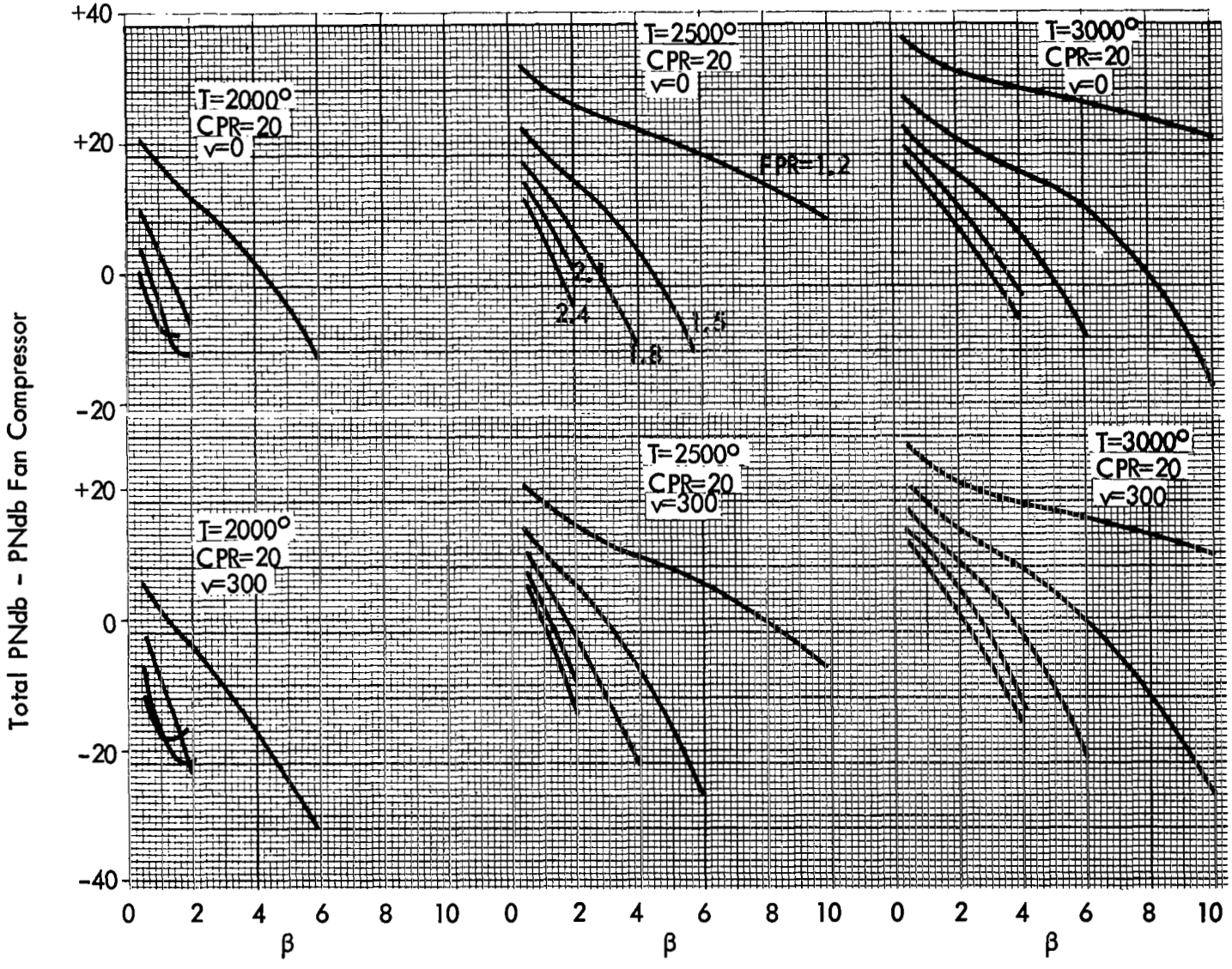

Not all the cycle designs represented in Fig. 13 are necessarily realistic. Two factors more important than noise must be considered: fuel economy in terms of SFC (specific full consumption), and engine size relative to the thrust produced. These parameters, like noise, are direct functions of cycle variables, and calculations have been made of these parameters as a function of cycle variables. Fig. 15 shows plots of Q versus SFC for various combinations of $\overline{CPR}$, $\overline{FPR}$, β, and T_4. It can be seen that a low Q is generally associated with a low SFC. For an ideal engine of given cycle pressure ratio and turbine inlet temperature, the minimum SFC and minimum jet noise (per unit thrust) tend to occur together at those $\overline{FPR}$ and β values where the exit velocities of the fan streams are equal. As the by-pass ratio increases, fan pressure needed to yield most efficient operation (low SFC) goes down, and there is less fan compressor noise. Thus, it can be seen that in optimum high by-pass ratio designs, both the compressor noise per unit flow and the jet noise Q, as well as the engine SFC, tend to be minimized. On an equal thrust basis, therefore, high by-pass designs are favorable on both counts of total noise and economy.

2.5 Part-Power Operation and Noise

2.5.1 Jet noise.- An approximate method is developed in this section for determining the amount of noise reduction associated with the part-power operation of the engine. This is useful for calculating the noise level during power cut-back and landing operations in those cases when detailed nozzle design or the cycle design parameters are not available for the part-power conditions. For more exact calculations, the engine design data corresponding to these reduced-power points must be used.

Consider first the exhaust jet noise under static conditions with the nozzle area fixed. The perceived noise, according to Eq. 19 for a non-afterburning engine, is

$$PN_o\,(jet) \propto F_n\, \rho\, V_j^{6.8} \tag{52}$$

and remembering that,

$$F \propto \rho\, V_j^2 \tag{53}$$

Eq. 52 may be reduced to the following form after some algebraic manipulation,

$$PN_o\,(jet) \propto \frac{1}{\rho^{2.4}}\ (F_n)^{4.4} \tag{54}$$

For simplicity, it is desirable to remove the density term from Eq. 54. During engine operation, any thrust reduction is accompanied by a density increase of the primary jet stream. The exact relationship between density change due to thrust change is somewhat complex and depends on the basic engine cycle, but it can be represented as being approximately

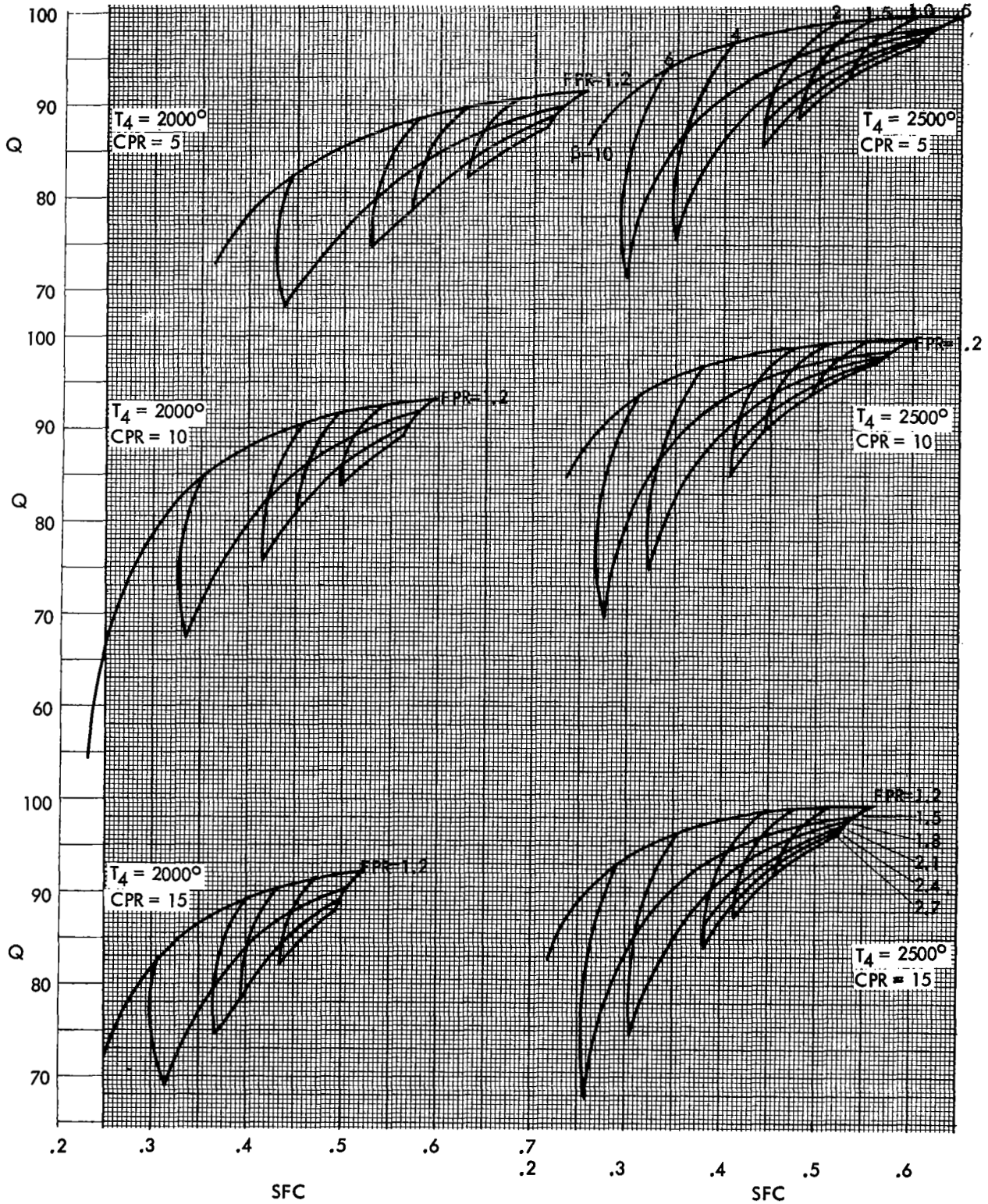

Figure 15a - Q Versus SFC for Various CPR, FPR, B, and T4

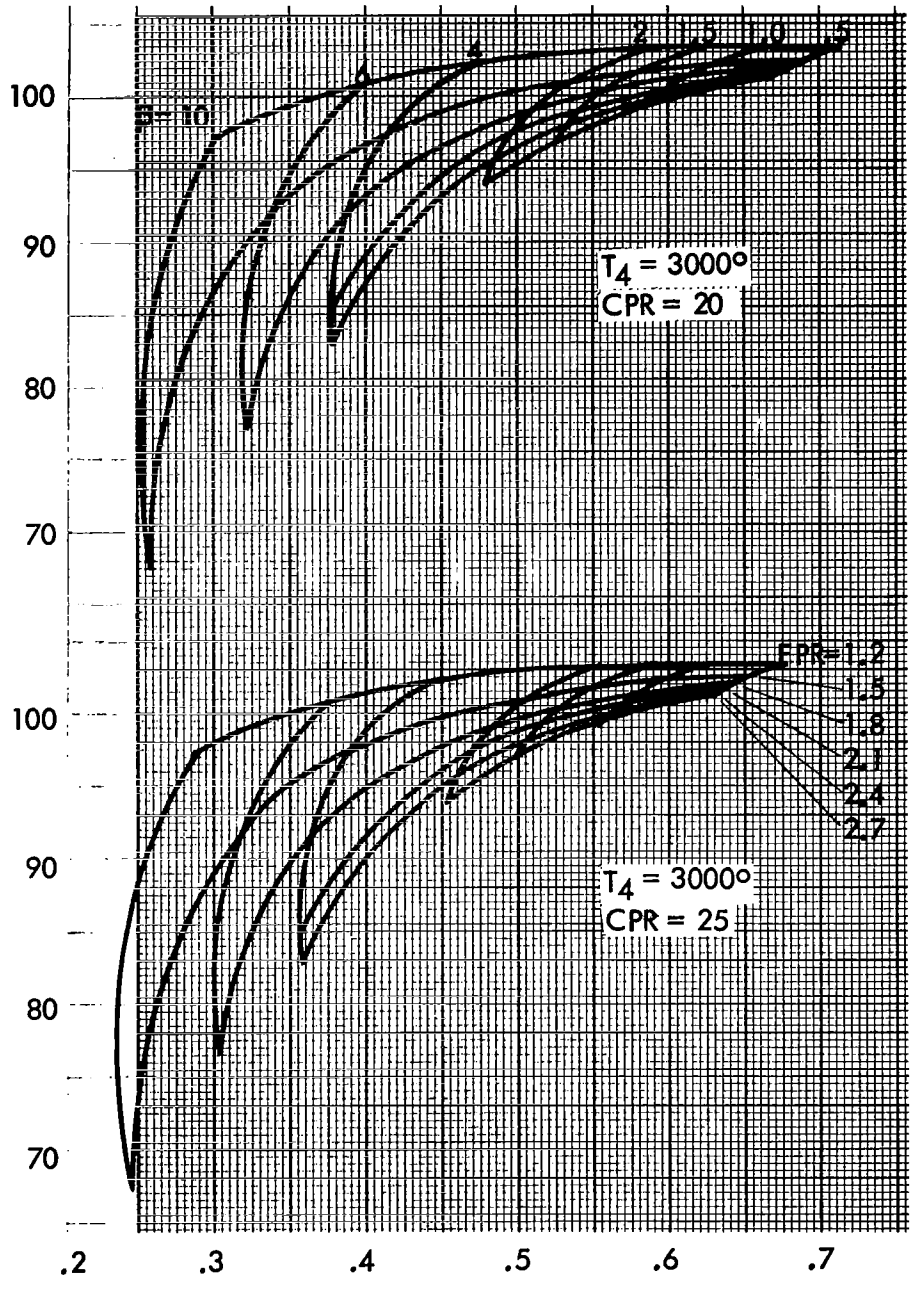

Figure 15b

Q Versus SFC for Various CPR, FPR, B, and T4

$$\rho \propto \left(\frac{1}{F}\right)^{\lambda} \tag{55}$$

Eq. 54 may thus be simplified to

$$PN_o\,(jet) \propto F_n^{\,(4.4 + 2.4\,\lambda)} \tag{56}$$

where λ is estimated from some typical engine cycle data as being between 0.2 and 0.4 . If a value of $\lambda = 0.25$ is assumed, a very simple relationship is obtained for estimating the noise change due to part-power operation for a given engine,

$$PN_o\,(jet) \propto F_n^{\,5} \tag{57}$$

or

$$\Delta PNdb_o\,(jet\ PR.) = 50 \log\left(\frac{F_n}{F_{n_o}}\right) \tag{58}$$

where F is the reduced thrust, F_{no} is the maximum thrust, and PR denotes power reduction.

Because of the uncertainty associated with the selection of λ , another approach can be taken to determine the power function that directly relates PN_o and thrust. This involves taking the density and exhaust velocity data at various thrust levels for four typical engine cycles and then calculating the perceived noise levels using the SAE method outlined in Section 2.2.1. For this analysis the following cycles were selected:

(a) A typical commercial 11,000-lb thrust turbojet engine,

(b) A typical 16,000-lb thrust commercial turbofan engine with a by-pass ratio of about 1.5,

(c) A typical 40,000-lb thrust high by-pass turbofan engine with a by-pass ratio of about 6, and

(d) A typical 65,000-lb thrust SST turbojet engine (non-AB operation).

The calculated data are plotted in Fig. 16 for relative $PNdb_o$ versus percent of maximum engine thrust. The best-fit straight line with data scatter of less than 2db is found to obey the following form,

$$PN_o\,(jet) \propto F_n^{\,5} \tag{59}$$

or

$$\Delta PNdb_o\,(jet,\ PR) = 50 \log\left(\frac{F_n}{F_o}\right) \tag{60}$$

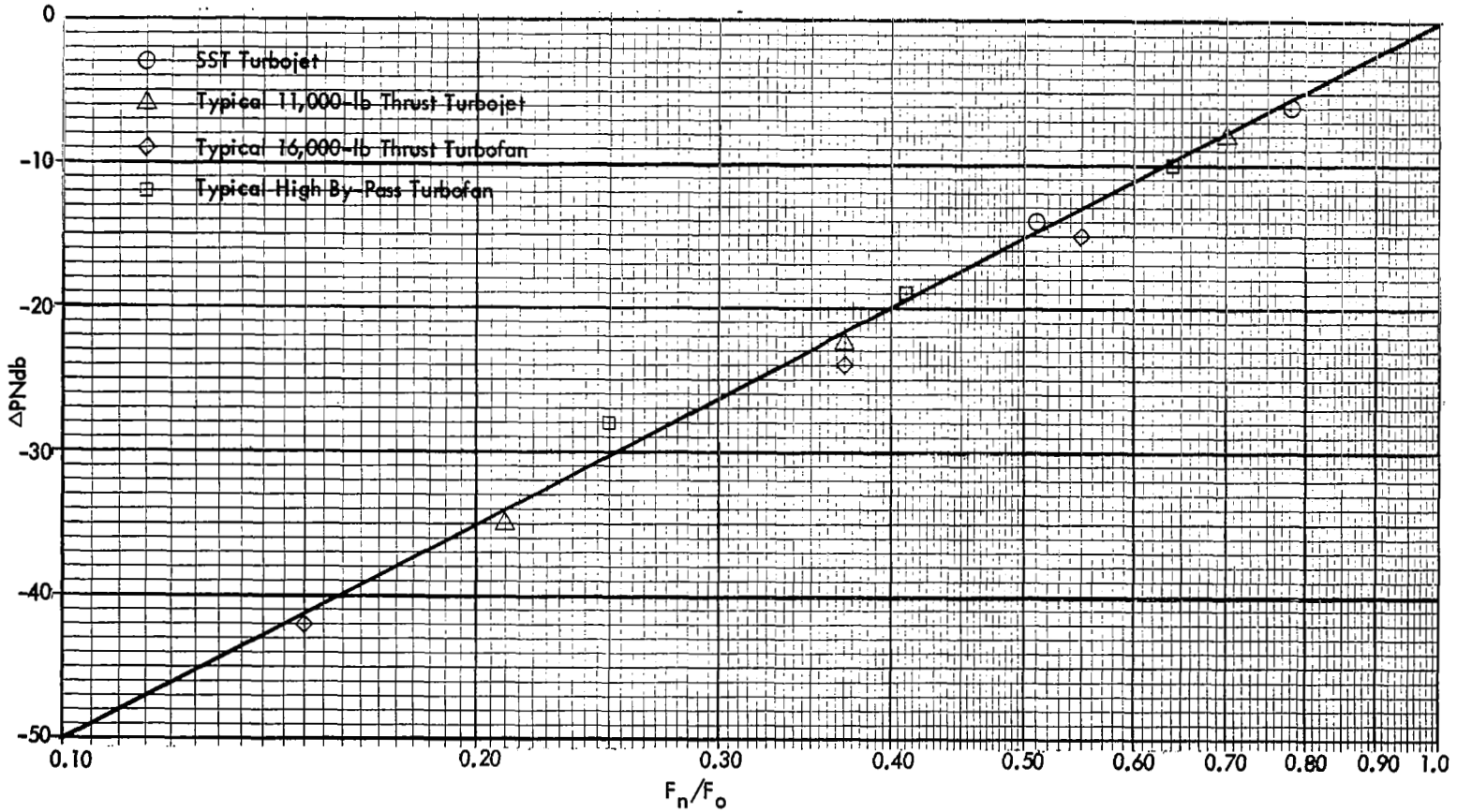

Figure 16 - PNdb Reduction Due to Part-Power Operation

The fifth-power relation between engine reference perceived noise and the percent of maximum thrust for both turbojet and turbofan cycles is noteworthy. It is to be remembered, however, that this relation holds mainly for static, fixed-nozzle area operation. It is probably not applicable to engines with jet noise suppressors, since the jet noise behavior of suppressor-nozzles (as a function of exit velocity) is known to be different from that estimated by the SAE method. For very high by-pass ratio fans, where the jet noise is due mainly to the fan stream, the 4.4th power role (Eq. 54) is expected to hold, since the jet density of the fan stream is independent of power setting. Although not exact, the above equations are believed to be applicable when power reduction takes place during flight if the aircraft velocity is not significantly altered as the result of power reduction.

For engines involving nozzle-area variation (e.g., afterburning engines), the perceived noise versus thrust relationship must take into account the area variation. By using Eq. 19 and not neglecting the area terms (and assuming again that $\lambda = 0.25$), the following equation is obtained:

$$PN_o\,(jet) \propto F^{5.0}\left(\frac{1}{A}\right)^{3.8} \tag{61}$$

or

$$\Delta PNdb\,(jet, PR) = 50 \log\left(\frac{F}{F_o}\right) + 38 \log\left(\frac{A_o}{A}\right) \tag{62}$$

where F and A are for part power, and F_o and A_o are for maximum power conditions. Eq. 62 is plotted in Fig. 17 for ΔPNdb versus $\frac{F}{F_o}$ for various ratios of A_o/A. It can be clearly seen that thrust reduction accompanied by $\frac{F}{F_o}$ area reduction, as in the case of AB to non-AB operation, gives a smaller amount of noise reduction than the case where the area is fixed. For part-power operation at a certain thrust level, if the nozzle area is allowed to increase, the net result is extra noise reduction, since the exit velocity is reduced. This form of noise control by nozzle-area variation is essentially engine-cycle control, although it is not always practical to provide variable-nozzle capability in an engine.

2.5.2 Compressor noise.- Consider first the compressor noise associated with the fan in a turbofan engine. In almost all situations the compressor noise of the gas generators is small and can be neglected. The perceived noise of the fan is related to the weight flow through the fan and to the fan tip speed by Eq. 39, which may be written in the following form:

$$PN_o\,(fan) \propto \omega^{0.75}\, u_t^{4.75} \tag{63}$$

The weight flow w is proportional to axial inlet speed u_z, and is proportional to u_t if it is assumed that the flow coefficient $= \frac{u_z}{u_t}$ of the fan remains constant for a given machine. Fan tip speed is proportional to fan rpm denoted by N, and thus

$$PN_o\,(fan) \propto N_f^{5.5} \tag{64}$$

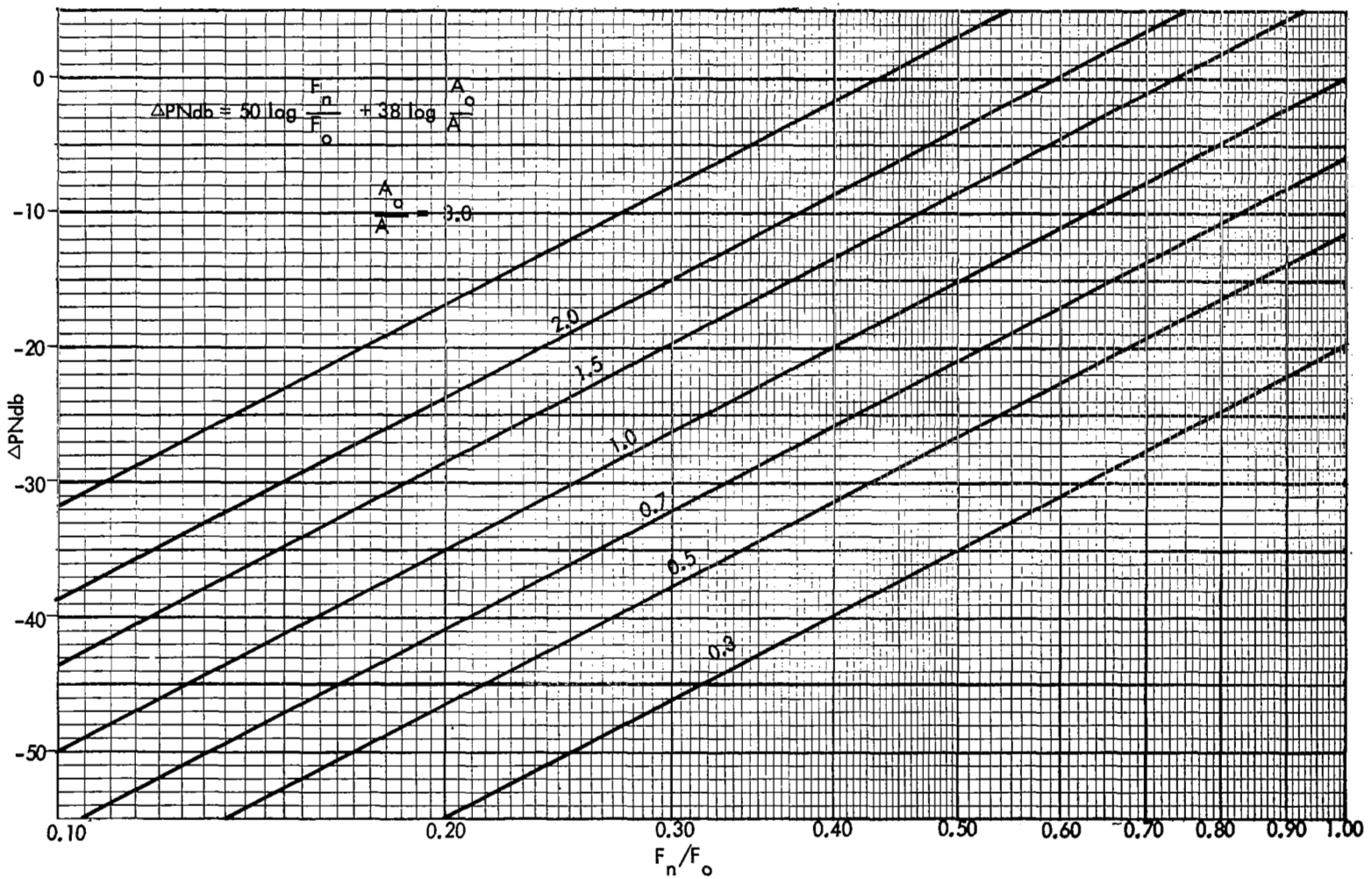

Figure 17 - Cutback ΔPNdb as a Function of Nozzle Area

The percent maximum engine thrust is related to the percent maximum fan rpm for typical turbofan engines by the approximate proportionality,

$$F \propto N_f \tag{65}$$

From an examination of cycle data for gypical fans, it appears that "b" has a value somewhere between 2 and 2.5 depending on the fan design details. If a value of b= 2.2 is assumed, and Eqs. 64 and 65 are combined, the result is

$$PN_o \text{ (fan compressor)} \propto F^{2.5} \tag{66}$$

or

$$\Delta PNdb \text{ (fan, PR)} = 25 \log\left(\frac{F}{F_o}\right) \tag{67}$$

where F/F_o is the ratio of part-power thrust to maximum sea level static thrust of the engine. Comparing Dqs. 60 and 67, it is interesting to note that for a given amount of engine power reduction, the drop in jet $PNdb_o$ is exactly twice the drop in fan compressor PNdb. The part-power point, $\frac{F}{F_o}$, at which the fan noise equals the jet noise is dependent only on the $PNdb_o$ differences between the two sources at full thrust. Fig. 18 is a plot showing this relationship. For example, if the jet $PNdb_o$ is greater than the fan compressor $PNdb_o$ at maximum power by 10db, the percent maximum thrust point at which the two are equal is 40 percent. Below this thrust, the fan noise will dominate.

Although the compressor noise associated with turbojet engines is generally not very high compared with that generated by fans, there is som difference in the compressor noise versus thrust relationships between the two cases. For turbojet engines, because of the energy addition by the burner, the index "b" in Eq. 65 is approximately 3.3 which results in the following equations,

$$PN_o \text{ (turbojet compressor)} \propto \left(\frac{F}{F_o}\right)^{1.65} \tag{68}$$

or

$$\Delta PNdb_o \text{ (turbojet PR)} = 16.5 \log\left(\frac{F}{F_o}\right) \tag{69}$$

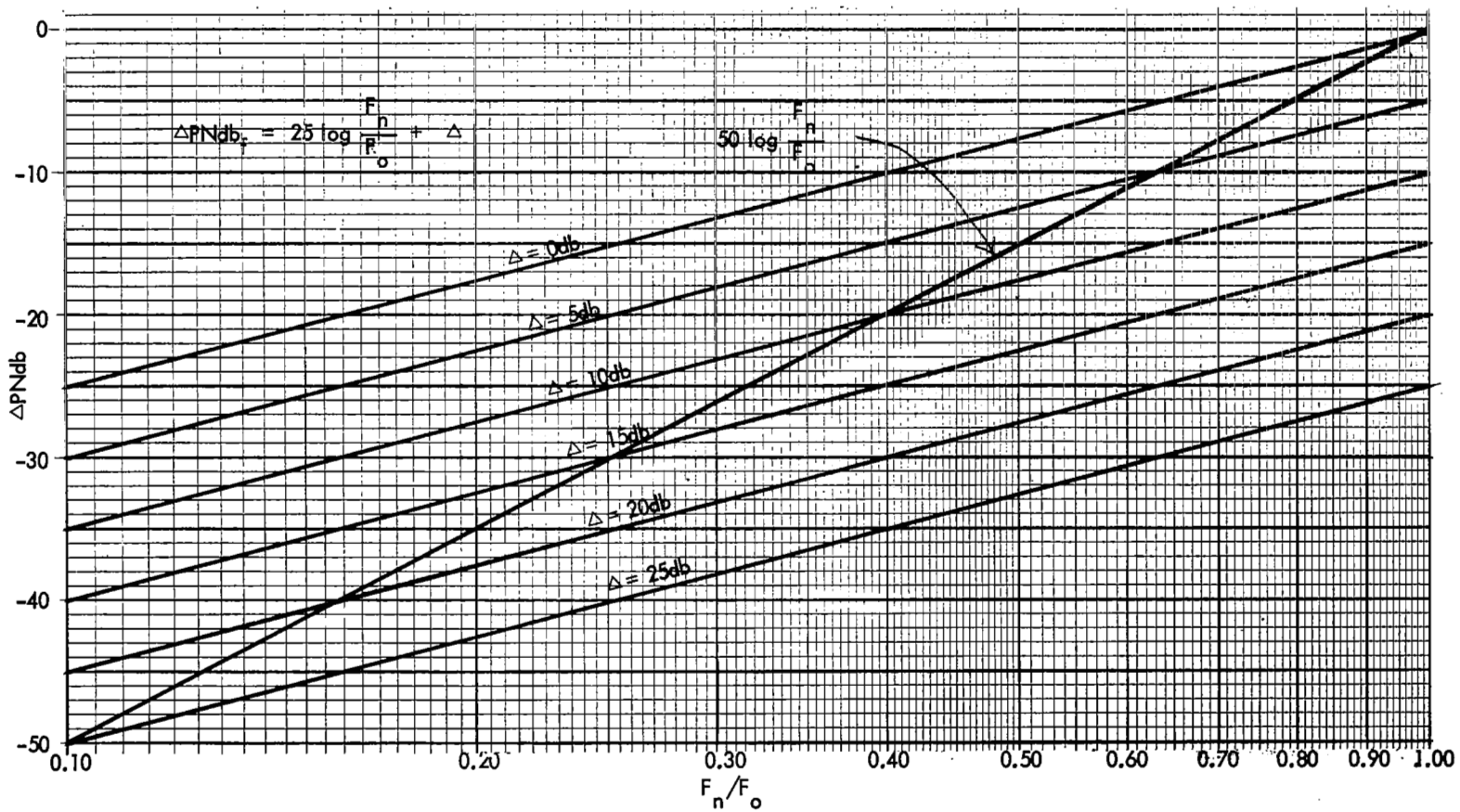

Figure 18 - Jet Cutback ΔPNdb Versus Fan Cutback ΔPNdb

3. SIMPLIFIED CALCULATION METHODS INVOLVING PNdb

3.1 Summary

This section gives methods of calculating (1) jet and compressor noise PNdb from overall sound pressure level, (2) PNdb of the combination of jet and compressor noise from the individual PNdb values, and (3) prediction of the variation of PNdb with distance for jet, compressor, and jet combined with compressor noise.

Calculating jet and compressor noise PNdb from overall sound pressure level is done with Figures 19 and 20. To use these graphs, simply calculate the overall sound pressure level for the jet or compressor noise and add the amount shown on the graph to give the PNdb. Note that the pertinent frequency for the jet is the frequency of the sound pressure level peak. The pertinent compressor frequency is the lowest blade passing frequency (RPS x blade number).

To combine jet and compressor PNdb, subtract the compressor PNdb from the jet PNdb and look up the increment on the solid curve of Figure 21. The increment is added to the higher of the PNdb and gives the PNdb of the combined noise. This is accurate to within $\pm$1.5db; however, by following the rules given in Section 3.3, the accuracy can be improved to $\pm$0.25 PNdb.

To predict the change in PNdb with distance, it is first necessary to determine the appropriate α and β from Figures 23, 24, 25, 26, 27, and 28, and calculate the change in PNdb for the distance using the equation

$$\triangle PNdb = \alpha \log R + \beta \frac{200}{\sin\theta} (R-1) \qquad (70)$$

where R is the ratio of the sideline or passby distance (referred to as H in Section 4) to 200 feet; thus,

$$R = \frac{H}{200} = \frac{H}{H_o} \quad \text{(for the general case)} \qquad (71)$$

θ is the angle of sound radiation of interest as determined along the 200-foot sideline. Again, the pertinent frequencies are the jet noise peak SPL frequency and the lowest blade passing frequency.

The following sections present the methods in detail and a discussion of their derivation.

3.2 PNdb from Overall Sound-Pressure Level

The following is a description of the method for determining PNdb from OA SPL with a discussion of its accuracy. Figures 19 and 20 give the db to be added to jet and compressor OA SPL to give the PNdb of the noise. To use the jet noise curve in Figure 19, determine the frequency of the peak SPL and find the db rise of the PNdb above the OA SPL. Add this to the OA SPL to determine the PNdb of the jet noise. As an example, for a jet spectra with an OA SPL of 120db and a peak frequency at 500 cps, the increase would be 10.2db, giving a PNdb of 130.2 PNdb. The method for finding the compressor PNdb is the same, with the difference that the lowest frequency of the blade whine is the determining frequency.

These graphs are limited to sideline distances of 200 feet and have an accuracy of $\pm 1/2$db for the jet and ± 1.5db for the compressor noise. The computer investigation showed that the PNdb was found to depend upon the jet peak frequency and the compressor fundamental pure tone. The variation in compressor PNdb was due to the variation of compressor broadband components (the extreme values are plotted upon the graph as crosses). These results are otherwise independent of any other parameters such as absolute OA SPL levels, etc. On each graph the equation of the curve is given for convenience in computer applications.

3.3 PNdb of Jet and Compressor Noise in Combination

Figure 21 can be used to determine the combined PNdb of jet and compressor noise from the individual PNdb values. The graph uses only the difference between the respective PNdb of the two noise sources and elininates the necessity of determining the combined sound pressure level spectrum and the subsequent PNdb calculations. The abscissa is determined by subtracting the compressor PNdb from the jet PNdb. Negative values indicate that the compressor PNdb is higher than the jet PNdb. The ordinate to the solid curve gives the amount to be added to the higher of the two PNdb to determine the combined PNdb. The solid curve gives the average increase and can be used for most applications since it gives the combined PNdb to within ± 1.5 PNdb.

For greater accuracy, the dotted curves can be used as will be described. The PNdb increase was found to depend upon the compressor pure tone fundamental frequency and the level of the broadband noise. The higher the pure tone frequency and broadband noise level, the greater the increase. In Figure 21 the upper dotted curve gives the increase for a compressor noise with a pure tone fundamental of 4000 cps and broadband noise level 5db below the level of the fundamental. Similarly, the lower curve gives the increase for a pure tone frequency of 500 cps and broadband level 15db below the fundamental level. This is illustrated in Figure 22 where typical data is shown. As can be seen, there is an increase of 0.5db in level between the -15 and -5db data.

To use the two dotted curves to determine the increase in PNdb the following rules are used:

Fig. 19 - Jet Noise PNdb - OASPL Difference

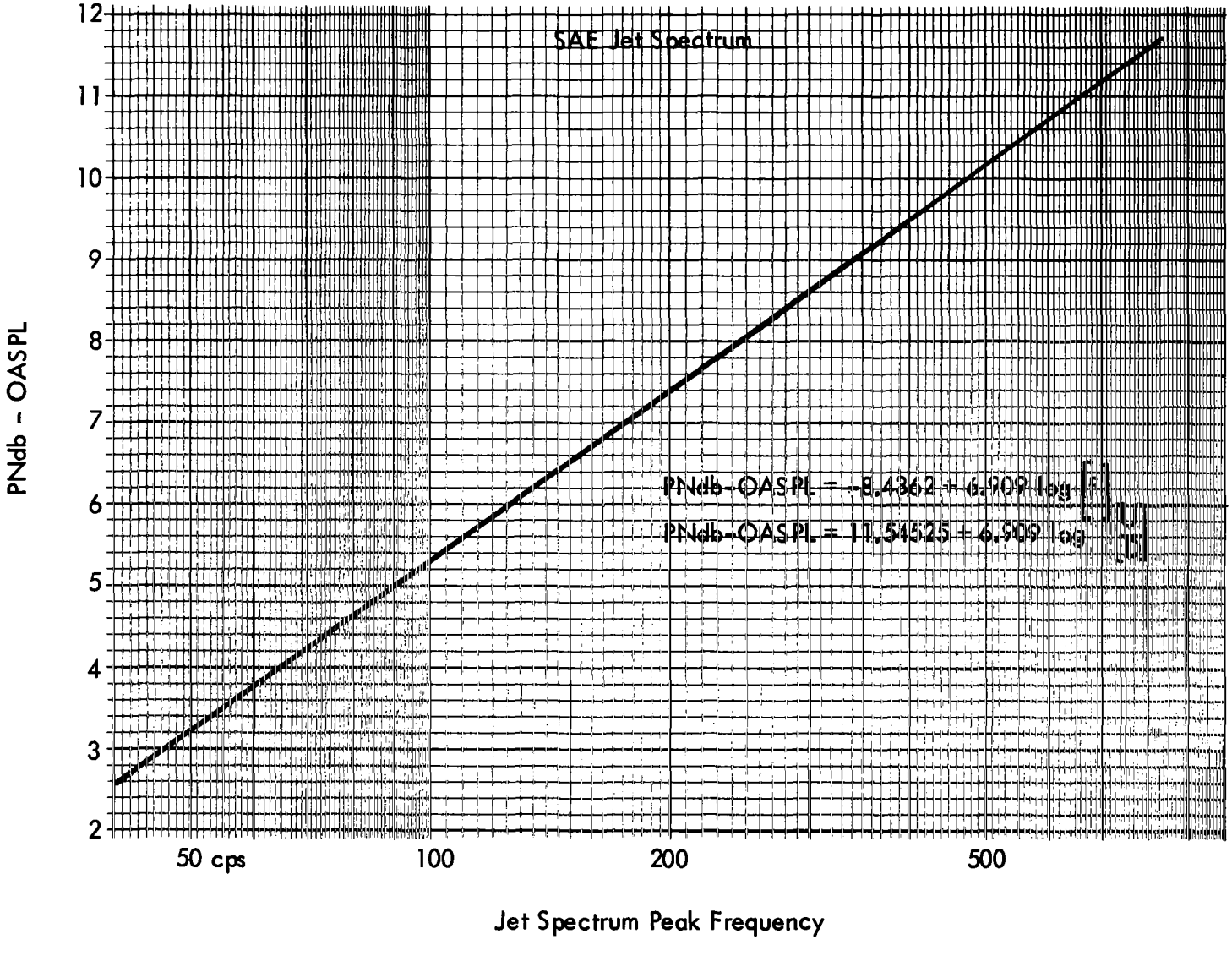

Fig. 20 - Compressor Noise PNdb - OASPL Difference

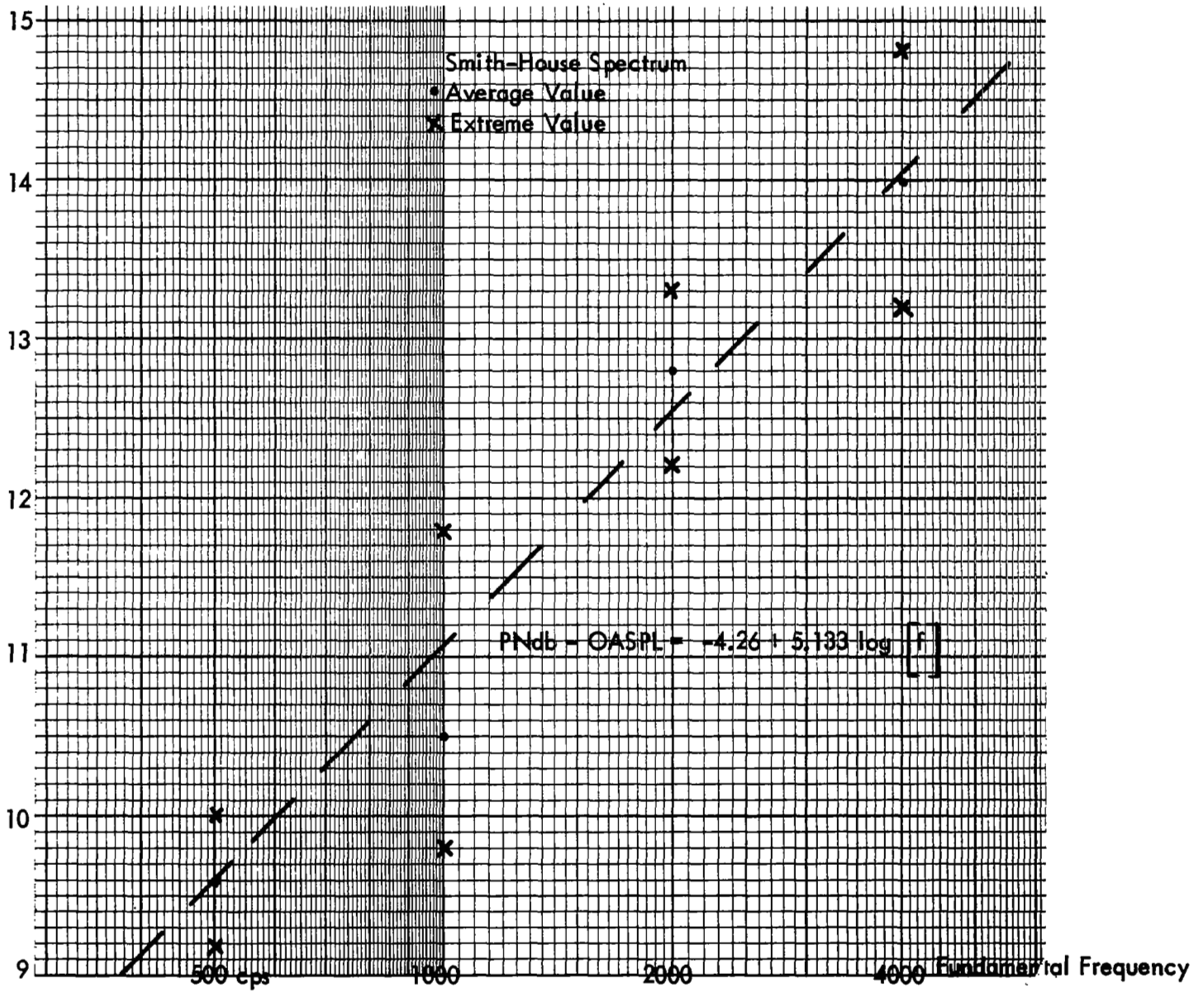

Fig. 21 - Combining PNdb

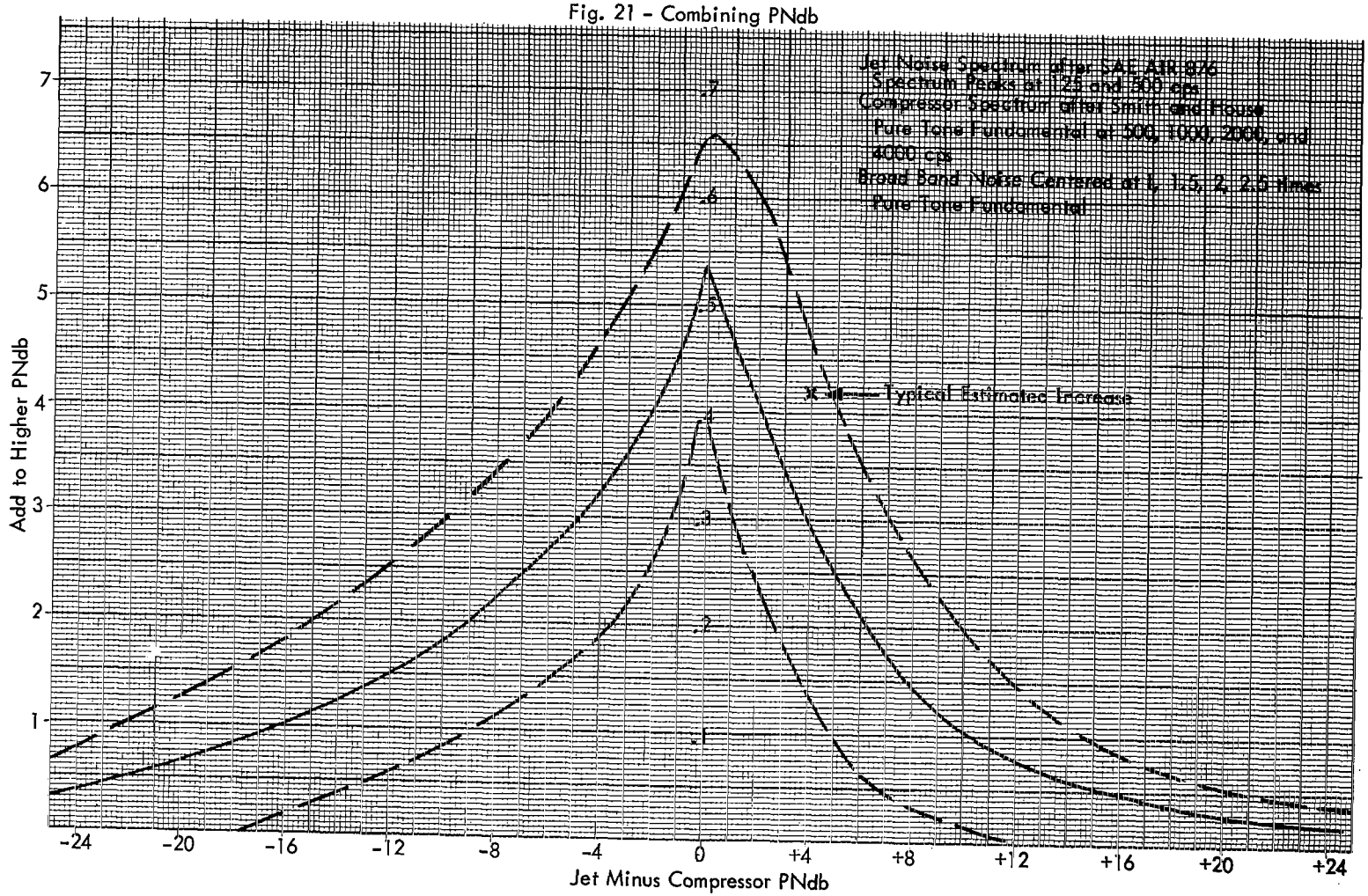

Fig. 22 - Sample Data

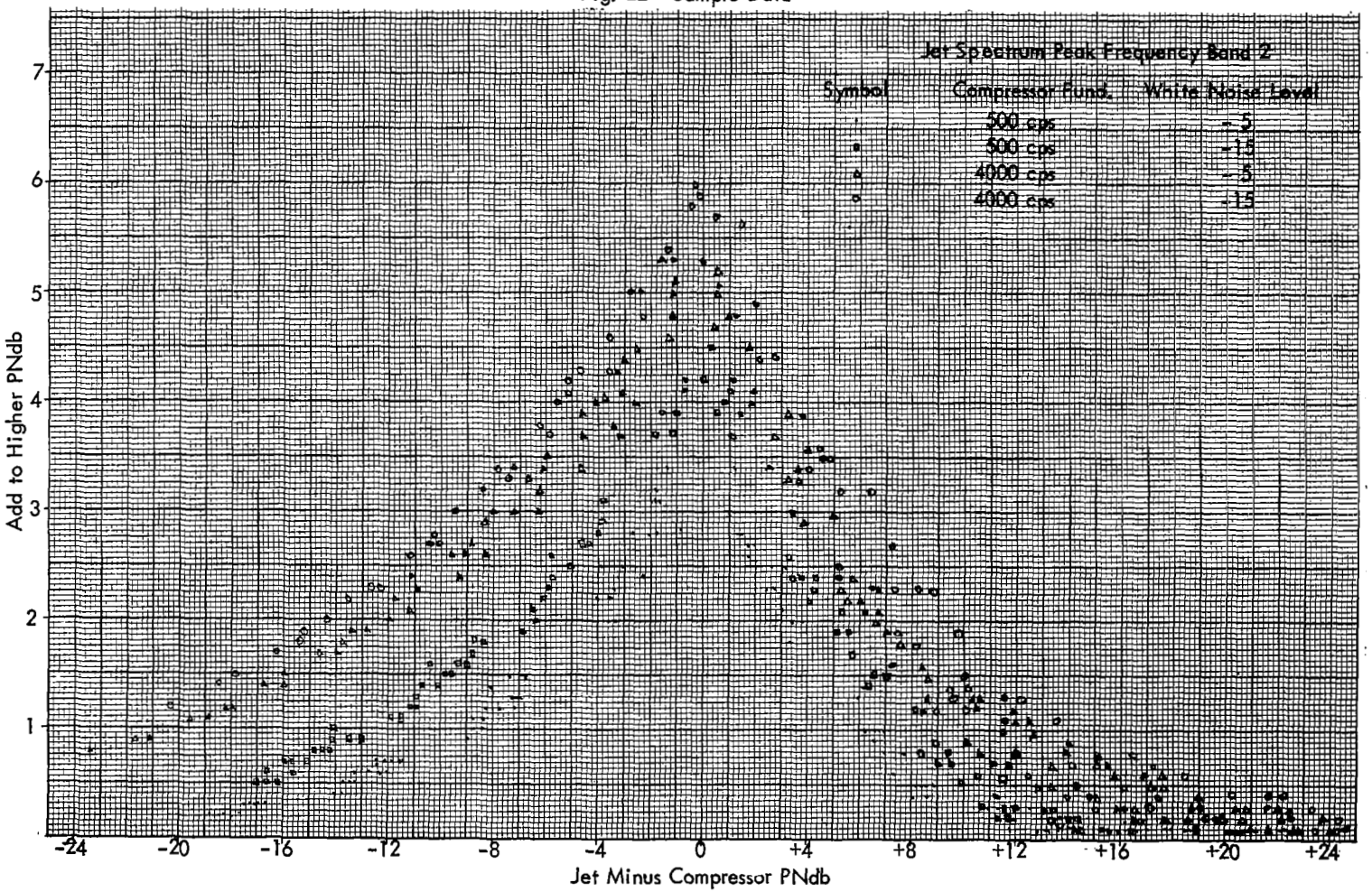

(1) If the compressor frequency is between 500 and 4000 cps, reckon that the PNdb increases by one-third of the distance between dotted curves for each octave above 500 cps (i.e., 1000 cps is one-third the distance and 2000 cps is two-thirds the distance between curves).

(2) The following table lists the corrections to be added to (1) for various compressor frequency and broadband level combinations.

TABLE 1

	Compressor Frequency		
Broadband Level	500-1500	1500-3000	3000-4000
-5 db	+ .5 db	.25 db	0
-10 db	+.25db	0	- .25 db
-15 db	0	-.25 db	-.5 db

As an illustration of this method assume a jet noise with a typical SAE-type spectrum and a PNdb of 124.5 and a compressor noise with a pure tone fundamental at 4000 cps and a broadband noise level 15db below the pure tone, the compressor PNdb being 120.5. The difference in PNdb would be +4 (compressor PNdb being subtracted from the jet PNdb). Since the pure tone frequency is 4000 cps and the broadband noise level is -15db, we estimate the PNdb increase to be given by a point 0.5db below the upper dotted curve. This point is noted on the graph and gives an increase of 4.2 PNdb. Thus, the PNdb of the combination would be 128.7 PNdb. This is accurate to within about +0.25 PNdb. Using the solid average curve would give a value of 127.4 PNdb. This would be accurate to within 1.5db.

The data used in compiling Figure 21 consisted of the individual PNdb increases for various sideline distances and as can be seen from Figure 22, the individual increase was also independent of the compressor broadband peak frequency and jet frequency. Thus, the solid curve can be used to predict the PNdb increase within $\pm$1.5 PNdb regardless of distance and these particular frequencies.

3.4 PNdb versus Distance

This section deals with the prediction of PNdb as a function of distance. The first part explains the method of noise field description and the second part outlines the method and discusses its accuracy.

To facilitate PNdb contour prediction (See Section 6), a simple alternative to the usual description of the noise field was adopted. Instead of the description of a noise field in terms of noise strength versus polar angles at a fixed radius, a description in terms of a reference sideline distance to the axis of the jet and the angle from the exhaust is used.

Two quantities are required for this technique. The first is a reference distance in the far field, and the second is the angle of maximum noise corresponding to the angle between the point of maximum noise on a line parallel to the jet axis at the reference distance and the jet engine. This angle will be close to but not equal to the angle of maximum directivity (DI), specified by normal methods. Since the distance to the sideline increases as the angle decreases, spreading loss and humidity absorption will cause the noise levels to change more rapidly with angle than in a polar specification; thus, the angle of maximum noise will be larger than the polar angle of maximum DI. Specification of a jet noise field with this method would involve a reference sideline distance and a "sideline DI" consisting of the DI as measured along the sideline referred to the angle from the jet. This method has the disadvantage that at small and large angles, such as 10° and 160° the measurement of the DI will be difficult, but has the advantage that the levels at these angles will be low enough so that their contribution can be ignored. Assuming that a sideline DI and a referenced distance have been provided, their use can be shown with the following diagram.

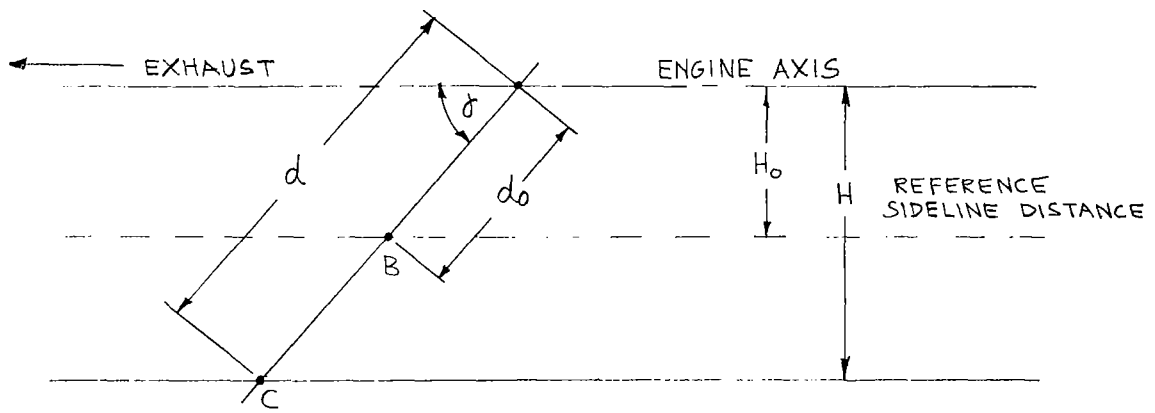

Sideline DI Schematic

In the diagram, γ is the angle of maximum noise at the sideline, H_o is the reference sideline distance, H is the sideline distance to the point C, d is the slant range to the point C, and d_o is the slant range to the sideline. In polar notation, the SPL at a given frequency at the point of interest would be given by

$$SPL_c = SPL_o - 20 \log \frac{d_c}{d_o} - A \left[d_c - d_o \right] \tag{72}$$

where SPL_o and SPL_c are the sound-pressure levels at the referenced base point B and point C, respectively, d_c and d_o are the distances to the point C and the base distance respectively, and A is the humidity-absorption coefficient.

This can be expressed in terms of sideline distances and radiation angle γ

$$SPL_c = SPL_o - 20 \log \frac{H}{H_o} - A \left[\frac{H}{\sin \gamma} - \frac{H}{\sin \gamma} \right] \tag{73}$$

which can be reduced to

$$SPL_c = SPL_o - 20 \log R - A \frac{H_o}{\sin \gamma} \left[R - 1 \right] \tag{74}$$

where R is H/H_o.

With the equation in this form, the noise analysis can be carried out in a simple manner of predicting PNdb versus distance that would be compatible with the above specification technique. An examination of the available curves of PNdb versus distance (based on computer outputs) showed that the prediction formula took the following simple form,

$$\triangle PNdb(DA) = PNdb_o - PNdb_c = \alpha \log R + \frac{\beta H_o}{\sin \gamma} \left[R - 1 \right] \tag{75}$$

where DA denotes distance attenuation, $PNdb_c$ is the PNdb at the desired point, $PNdb_o$ is the PNdb at the sideline reference distance, α and β are constants determined by the character of the noise. It is to be noted that this form is analogous to Eq. 74 with a term for the ratio of distance and a term equivalent to the humidity absorption. This is expected, since the PNdb is directly proportional to SPL over most SPL levels.

Figures 23 through 36 give the constants α and β to be used for predicting jet, compressor, and combined jet and compressor noise for in-flight and on-ground conditions.

Figures 23 through 26 give the β's for compressor and combined noise for in-flight and on-ground. The α's are constant and are given at the tops of the graphs. β is also given in equation form on the graphs to allow computer calculations or greater accuracy. The pertinent frequency is again the lowest compressor blade whine frequency or the compressor fundamental pure tone. For convenience, the following two tables give values for important octave bands.

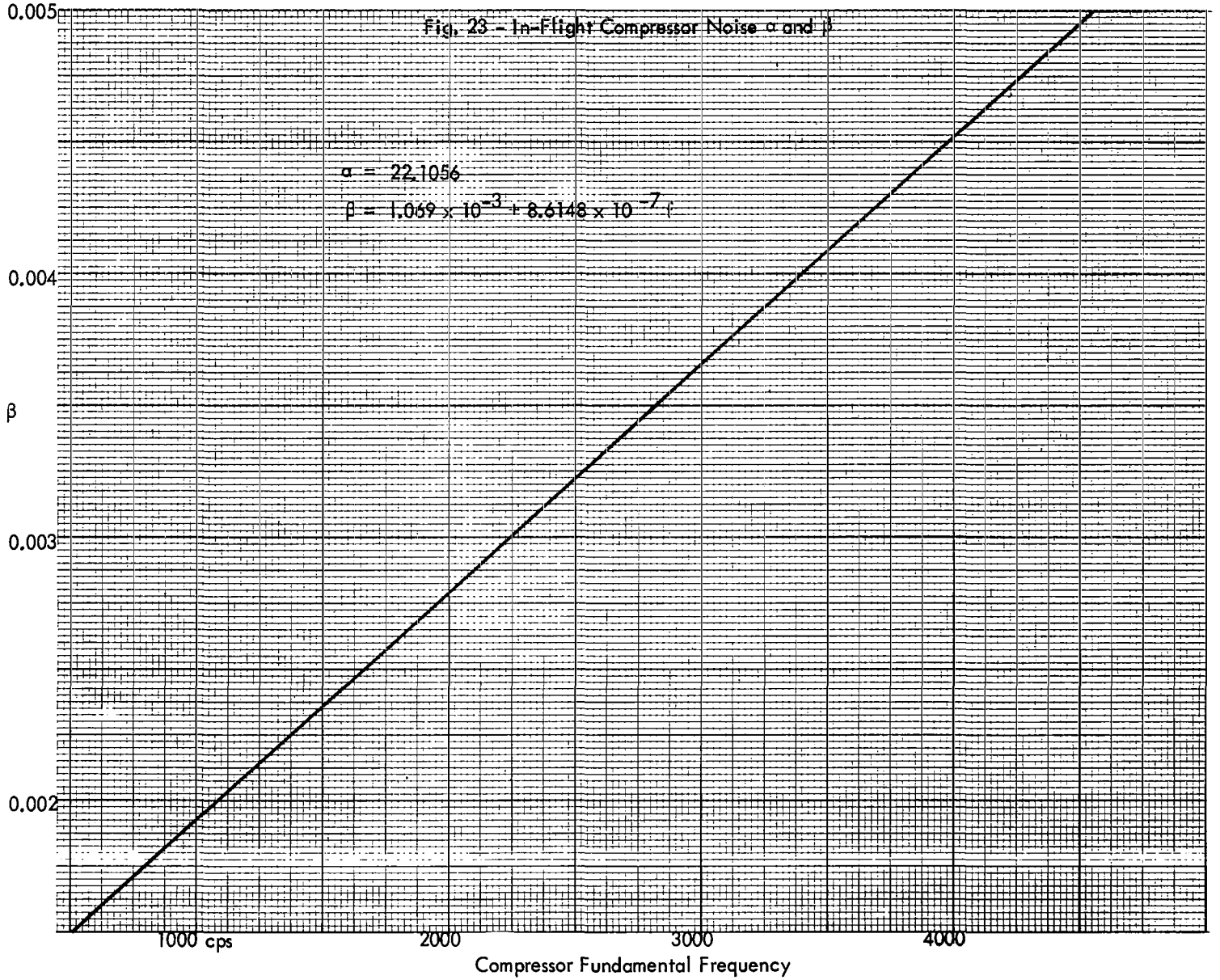
Fig. 23 - In-Flight Compressor Noise α and β
α = 22.1056
β = 1.059 x 10^-3 + 8.6148 x 10^-7 f
0.005
0.004
β
0.003
0.002
1000 cps
2000
3000
4000
Compressor Fundamental Frequency

Fig. 24 - In-Flight Combined Jet and Compressor Noise α and β

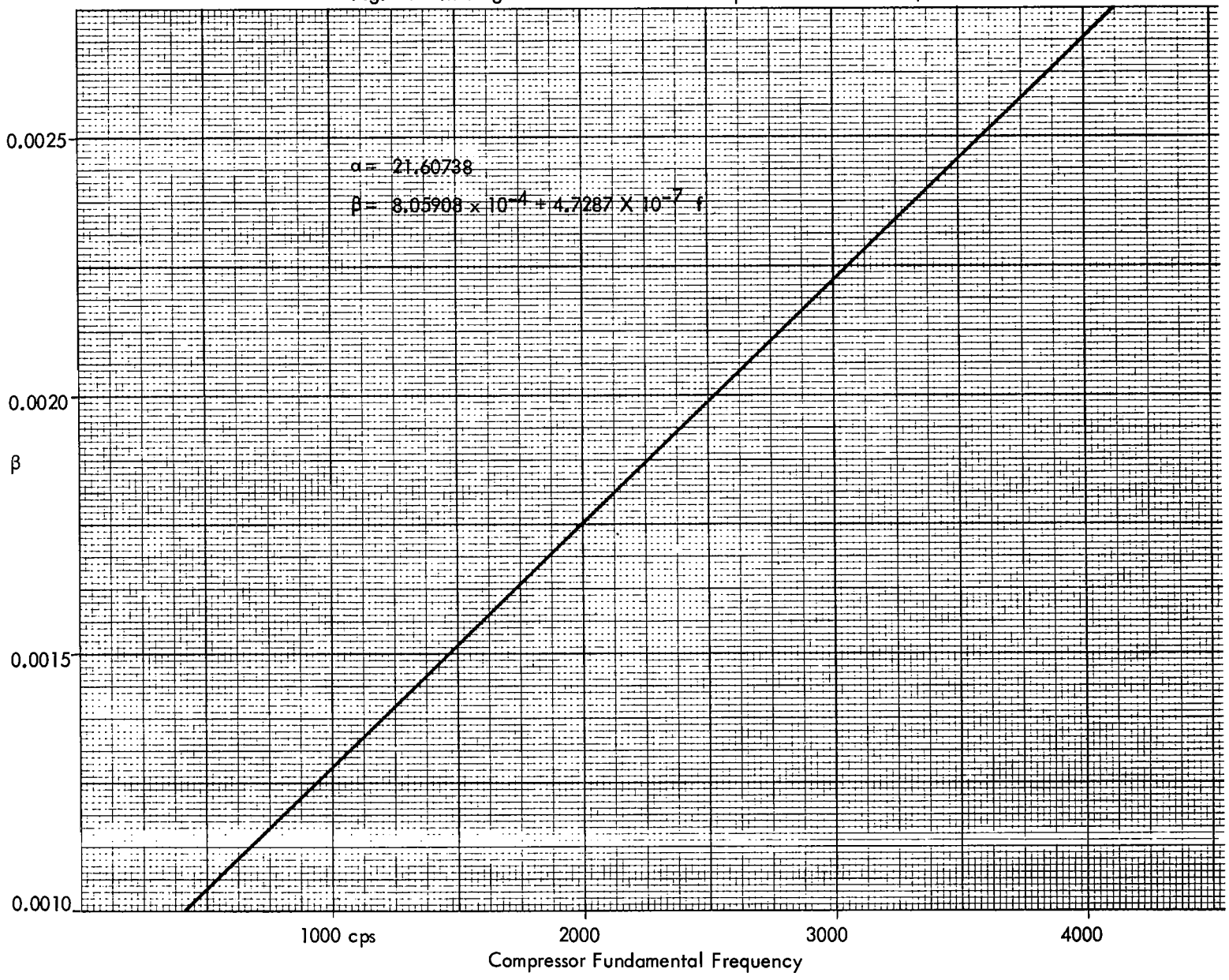

Fig. 25 - On-Ground Compressor Noise α and β

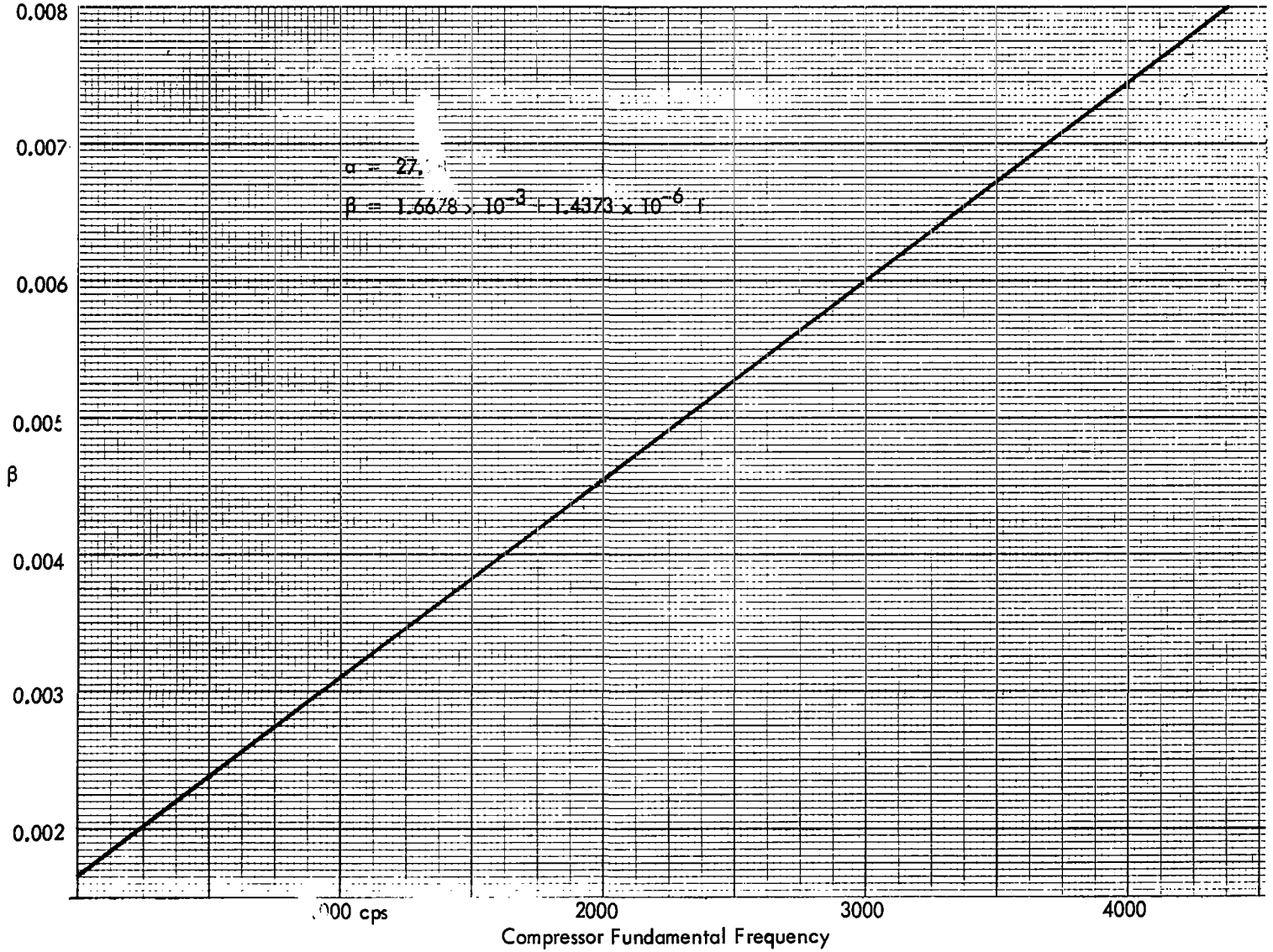

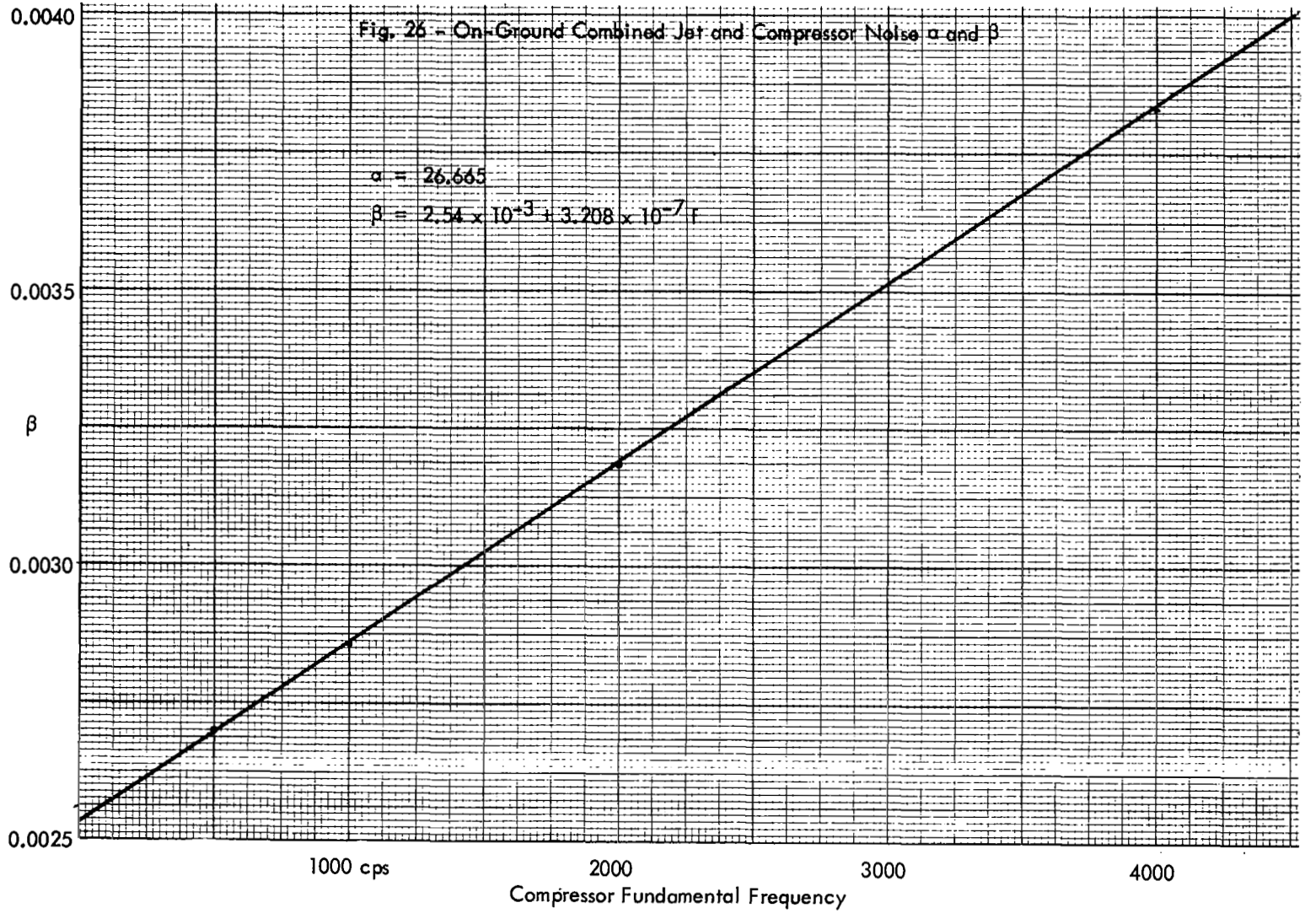
Fig. 26 - On-Ground Combined Jet and Compressor Noise α and β
α = 26.665
β = 2.54 x 10^-3 + 3.208 x 10^-7 f
0.0040
0.0035
β
0.0030
0.0025
1000 cps
2000
3000
4000
Compressor Fundamental Frequency

TABLE 2
In-Flight α and β
(See Eq. 75)

Source	α	β Band 4	β Band 5	β Band 6	β Band 7
Jet	21.95	0.0008375		Constant	
Compressor	22.1056	0.001499	0.0019305	0.002792	0.004515
Combined	21.607	0.001042	0.001278	0.001752	0.002697

TABLE 3
On-Ground α and β

Source	α	β Band 4	β Band 5	β Band 6	β Band 7
Jet	27.11	1.769×10^{-3}		Constant	
Compressor	27.98	2.386×10^{-3}	3.105×10^{-3}	4.542×10^{-3}	7.417×10^{-3}
Combined	26.67	2.700×10^{-3}	2.861×10^{-3}	3.182×10^{-3}	3.823×10^{-3}

Note that the α and β for jet noise are constant in both cases. It was found that the spread in △PNdb for jet noise was small enough (see graphs 35 and 36) to allow representation with constant values for all jet peak frequencies. The maximum error will be ±3db at the limit of 6400 ft in-flight and 4000 ft on the ground.

Figures 27 through 34 show the △PNdb plotted using the α and β from TABLES 1 and 2. The angles of maximum radiation of 30, 45, and 60 degrees were chosen as being the ones most likely to be encountered in practice. Note the α's and β's can be used with any angle and are not limited to the angle of maximum radiation. The distance to which the predictions extend decreases as the angle becomes smaller. This is due to the nature of the equations, and is discussed later. Also, the higher frequency content noise decreases most rapidly, which would be expected since the humidity and ground absorption are highest for the high frequencies. Standard humidity and ground-absorption rates are based on Reference

Figures 35 through 40 show plots of the predicted △PNdb along with the data used in their formulation. Plots such as these were used to determine the accuracy of fit of the α's and β's. In checking the accuracy, the worst case was chosen so as to establish the maximum error to be encountered. In our case this was 30 degrees, the smallest angle likely to be encountered. Figures 41 and 42 show the effect of angle on the accuracy. The shaded area on the jet noise plots represents all of the data for jet noise and covers all cases likely to be encountered. As can be seen, the spread is not great and the maximum error is +3 PNdb at the extreme range representing an absolute distance of 6400 feet in flight and 4000 feet on ground. At any lesser range, the accuracy is greatly improved. Figures 37

Fig. 27 - In-Flight Jet and Compressor ΔPNdb

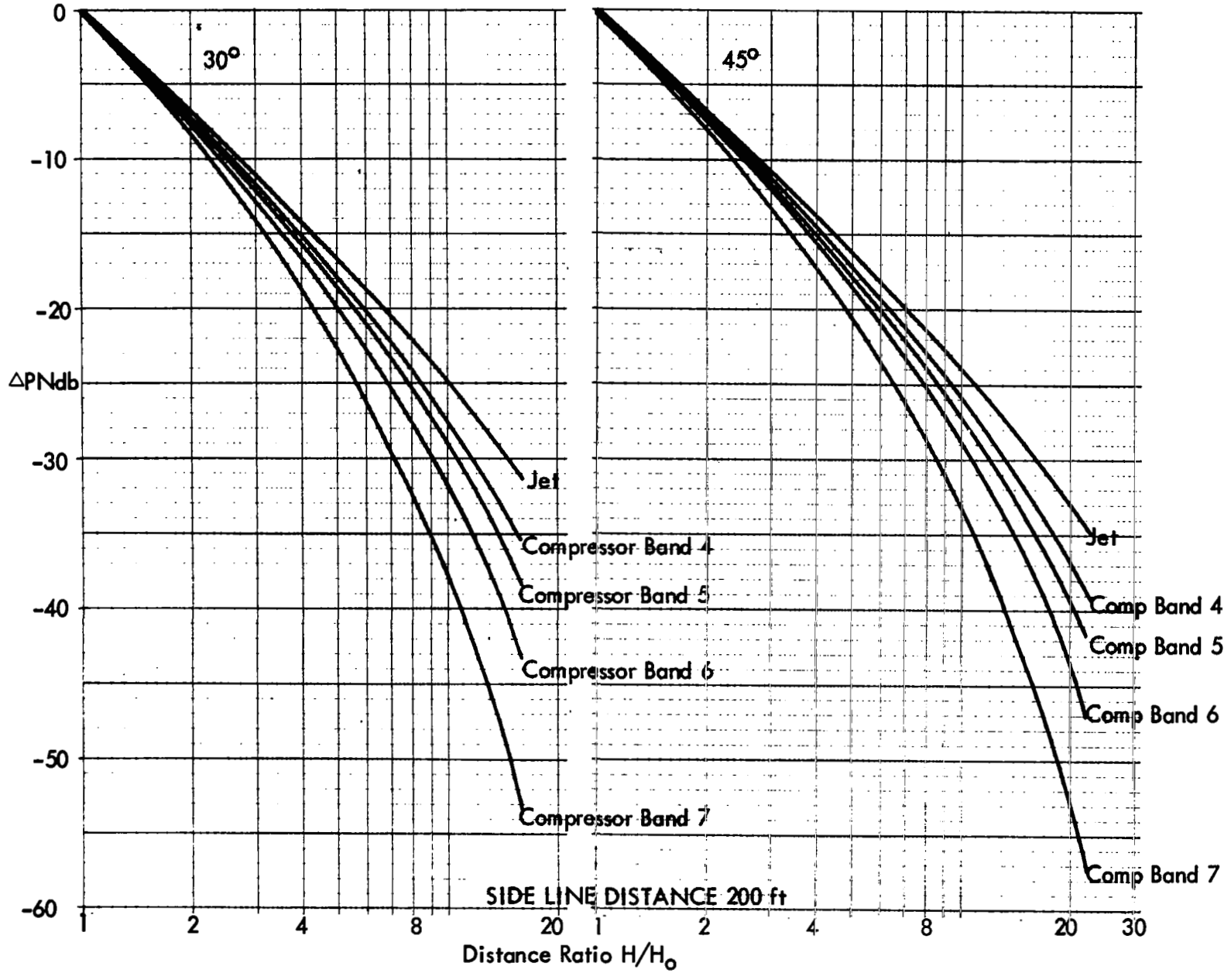

Fig. 28 – In-Flight Jet and Compressor △PNdb

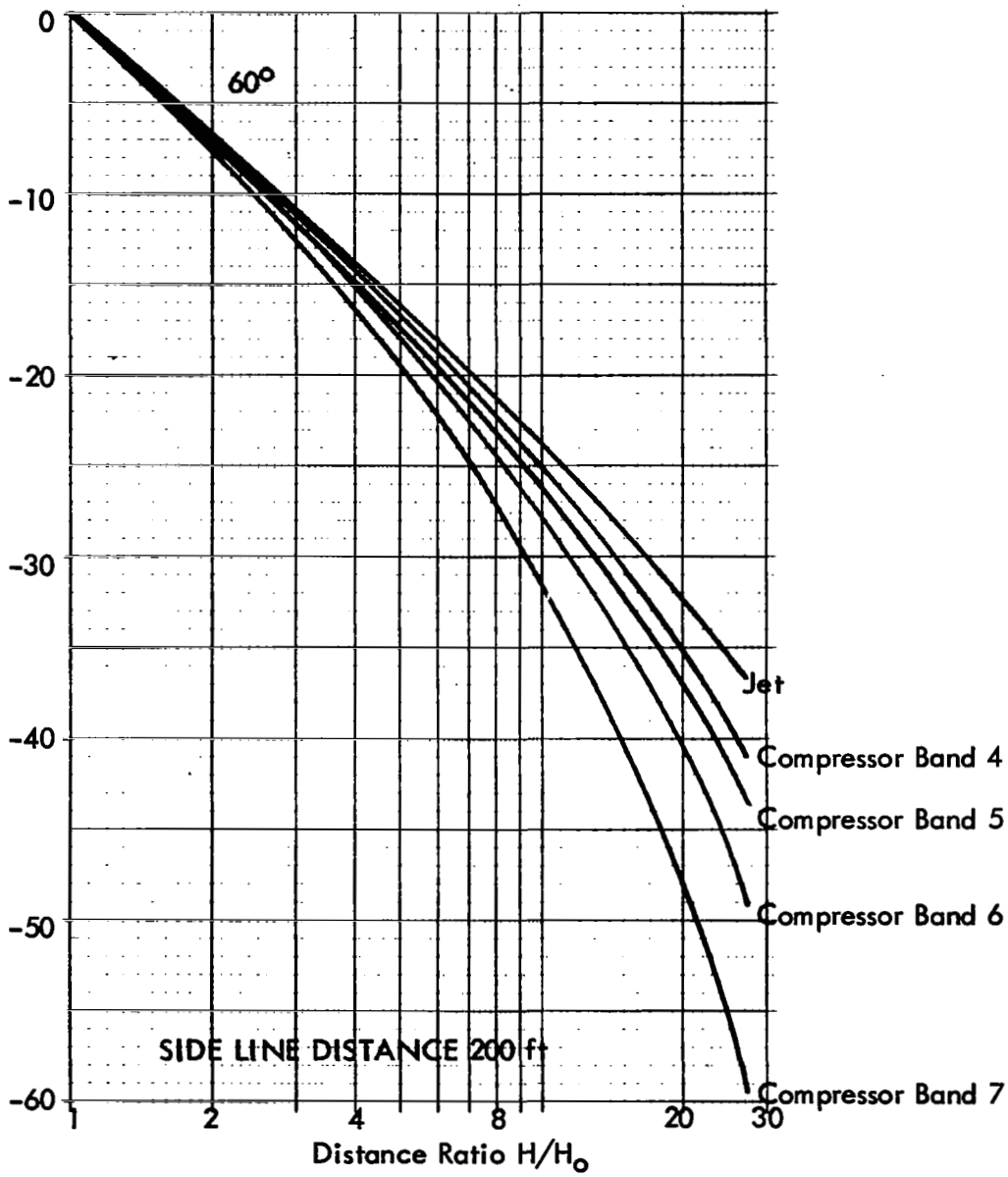

Fig. 29 - In-Flight Combined Jet and Compressor △PNdb

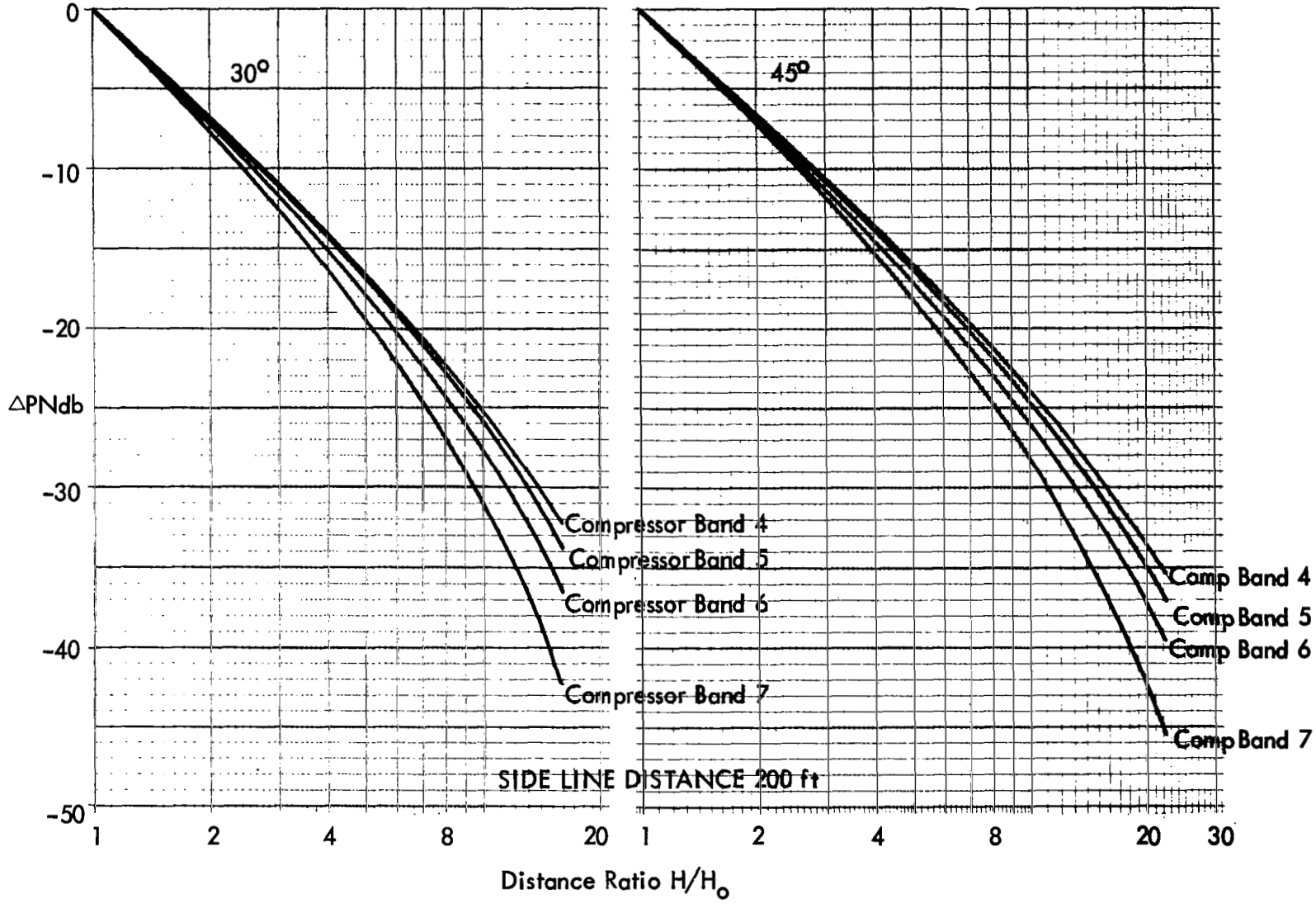

Fig. 30 - In-Flight Combined Jet and Compressor ΔPNdb

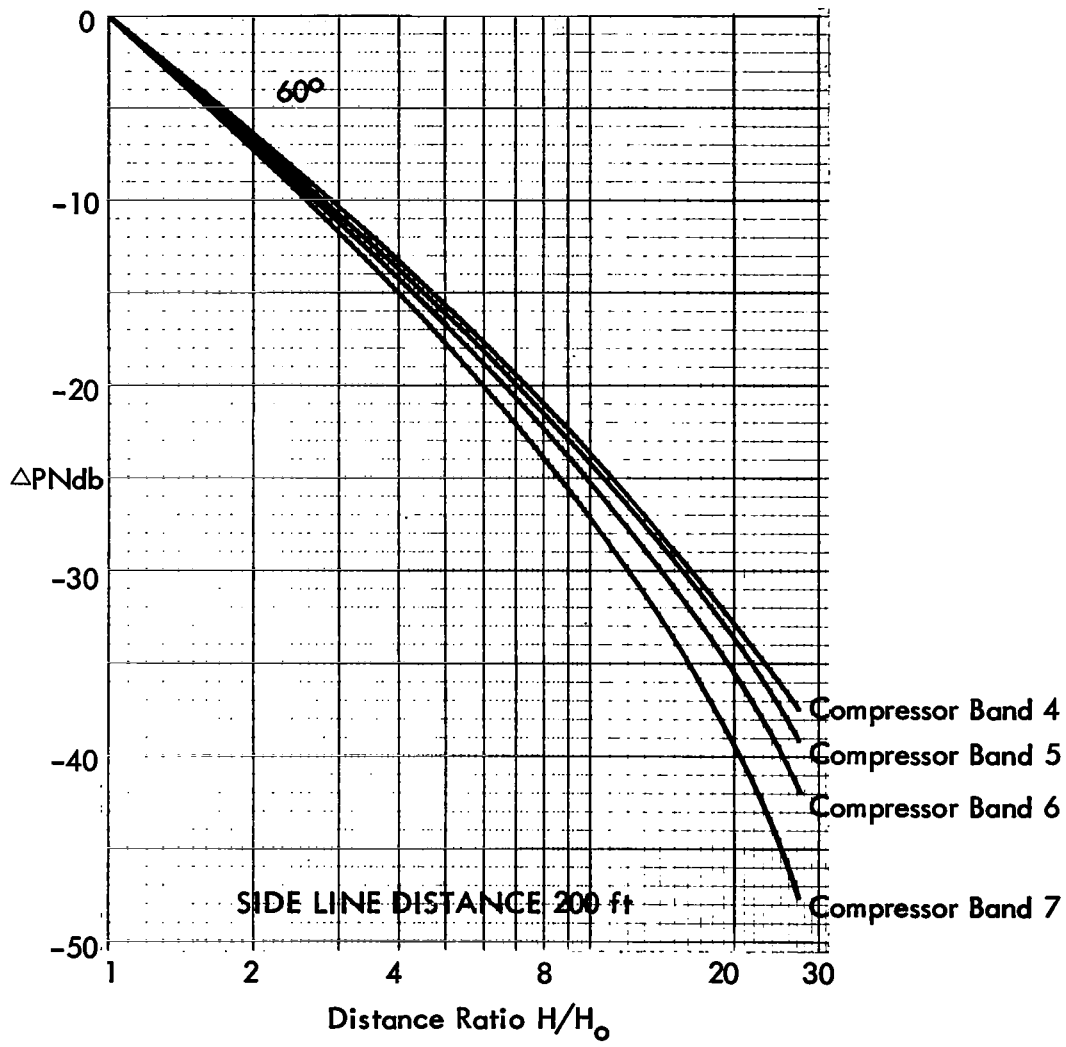

Fig. 31 - On-Ground Jet and Compressor ΔPNdb

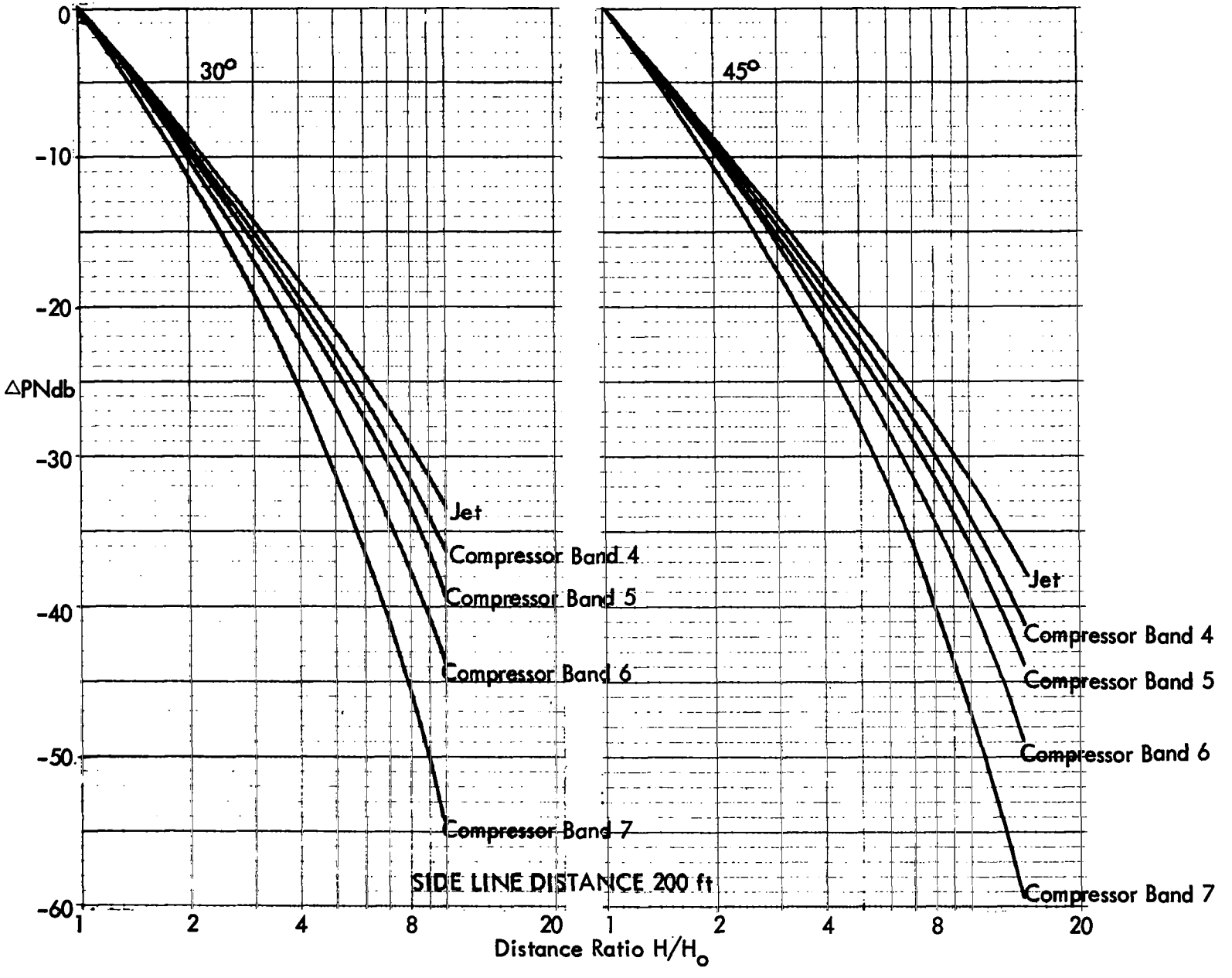

Fig. 32 - On-Ground Jet and Compressor ΔPNdb

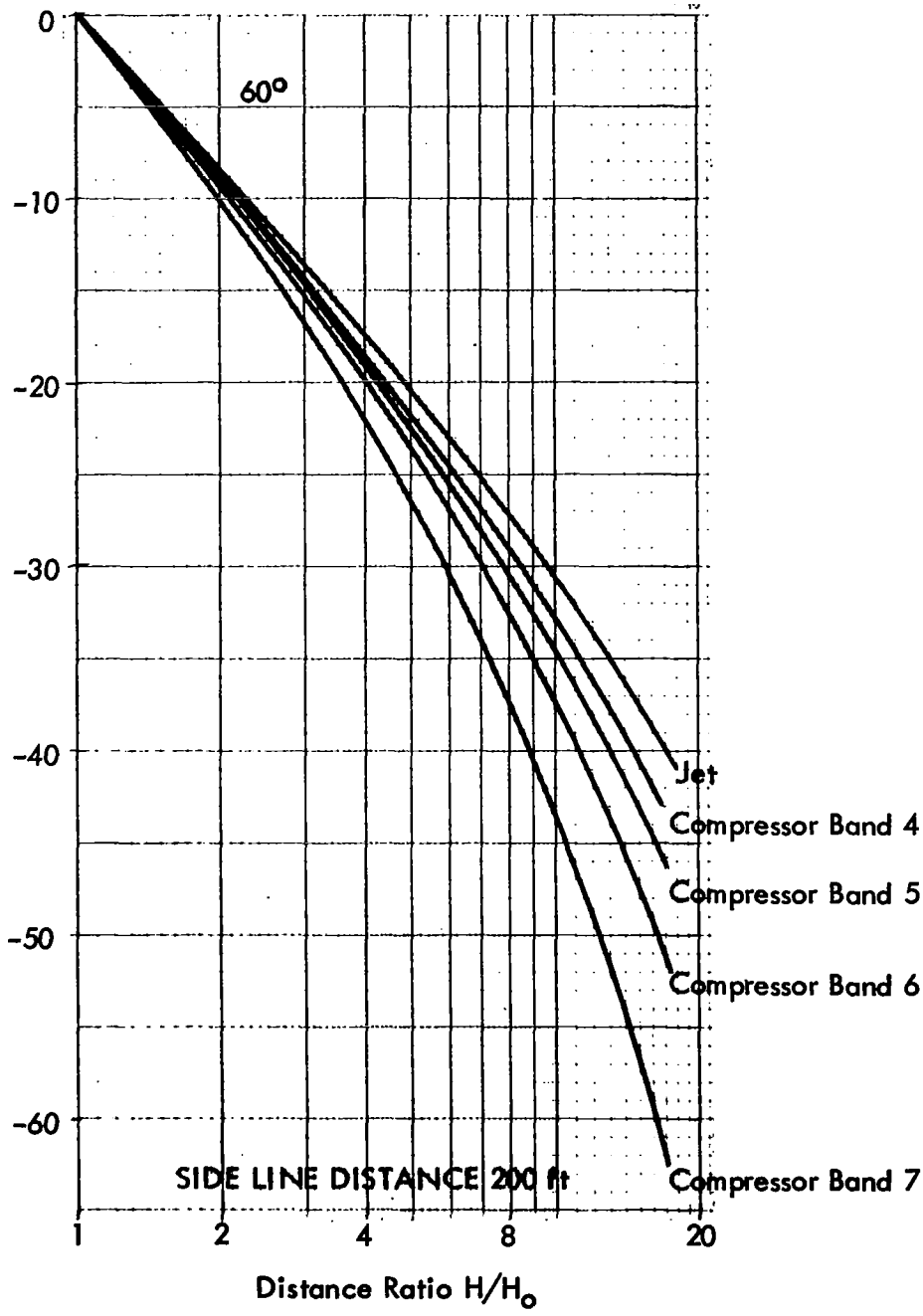

Fig. 33 - ON-Ground Combined Jet and Compressor △PNdb

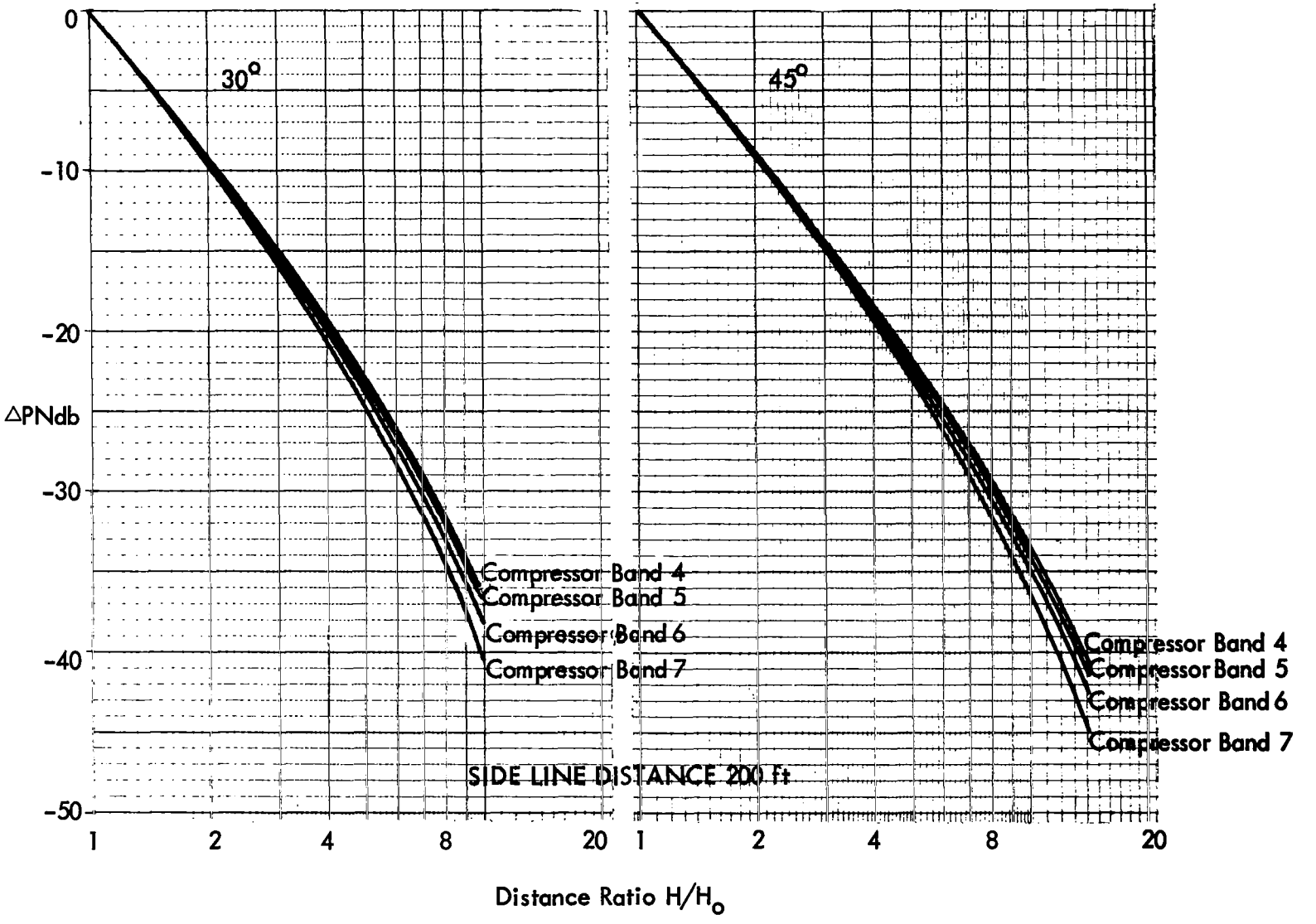

Fig. 34 - On-Ground Combined Jet and Compressor △PNdb

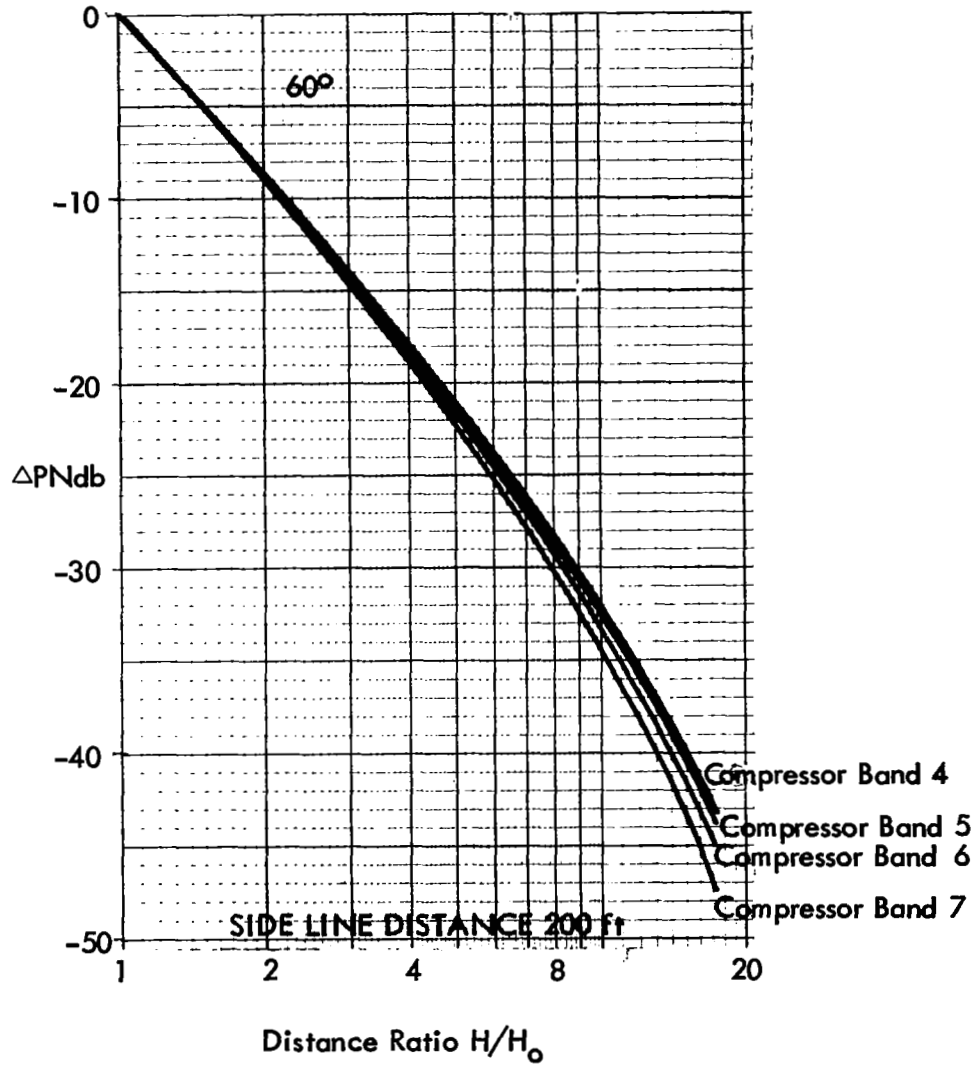

Fig. 35- In-Flight Jet Noise △PNdb

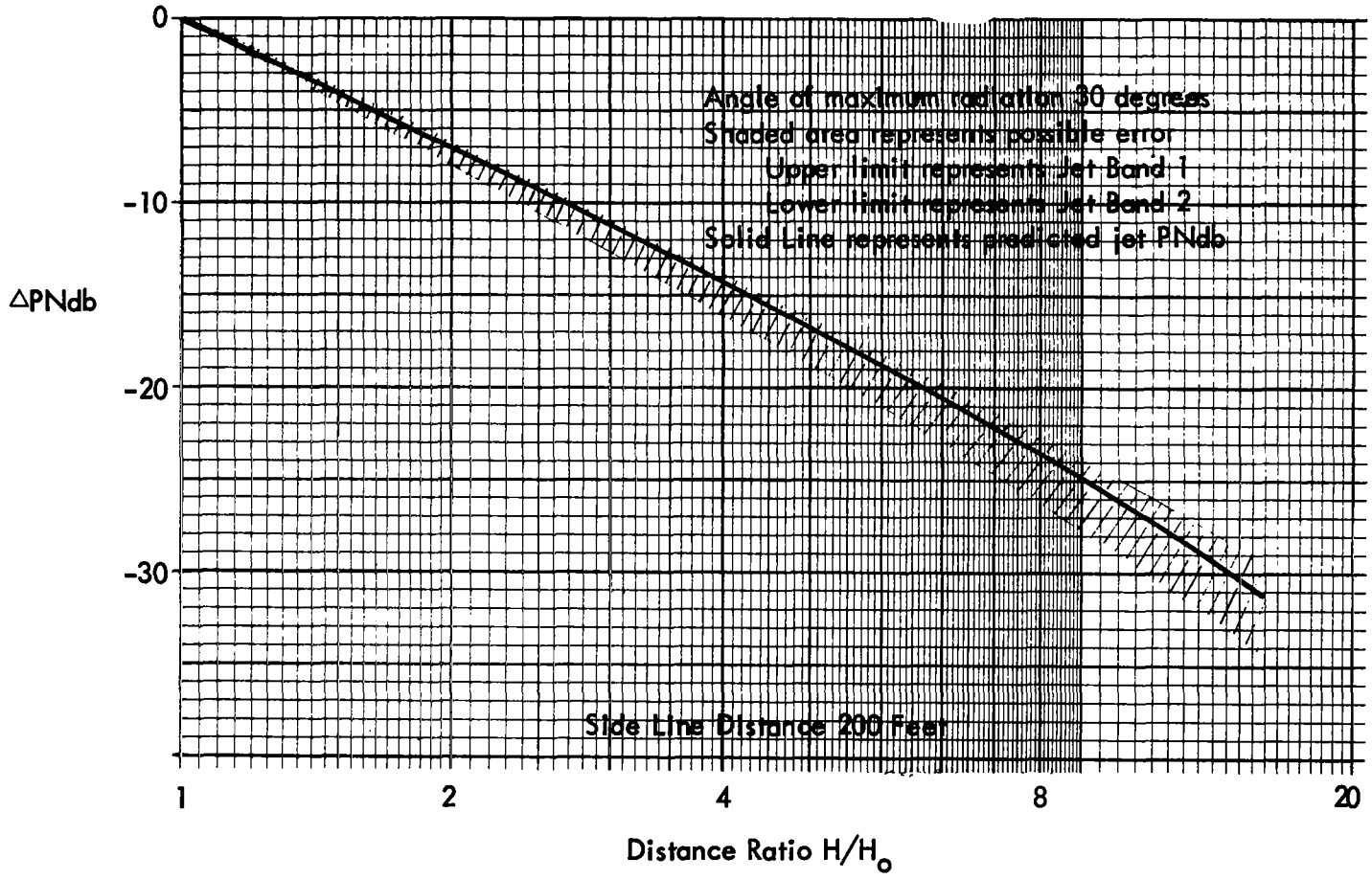

Fig. 36 - In-Flight Compressor ΔPNdb Accuracy

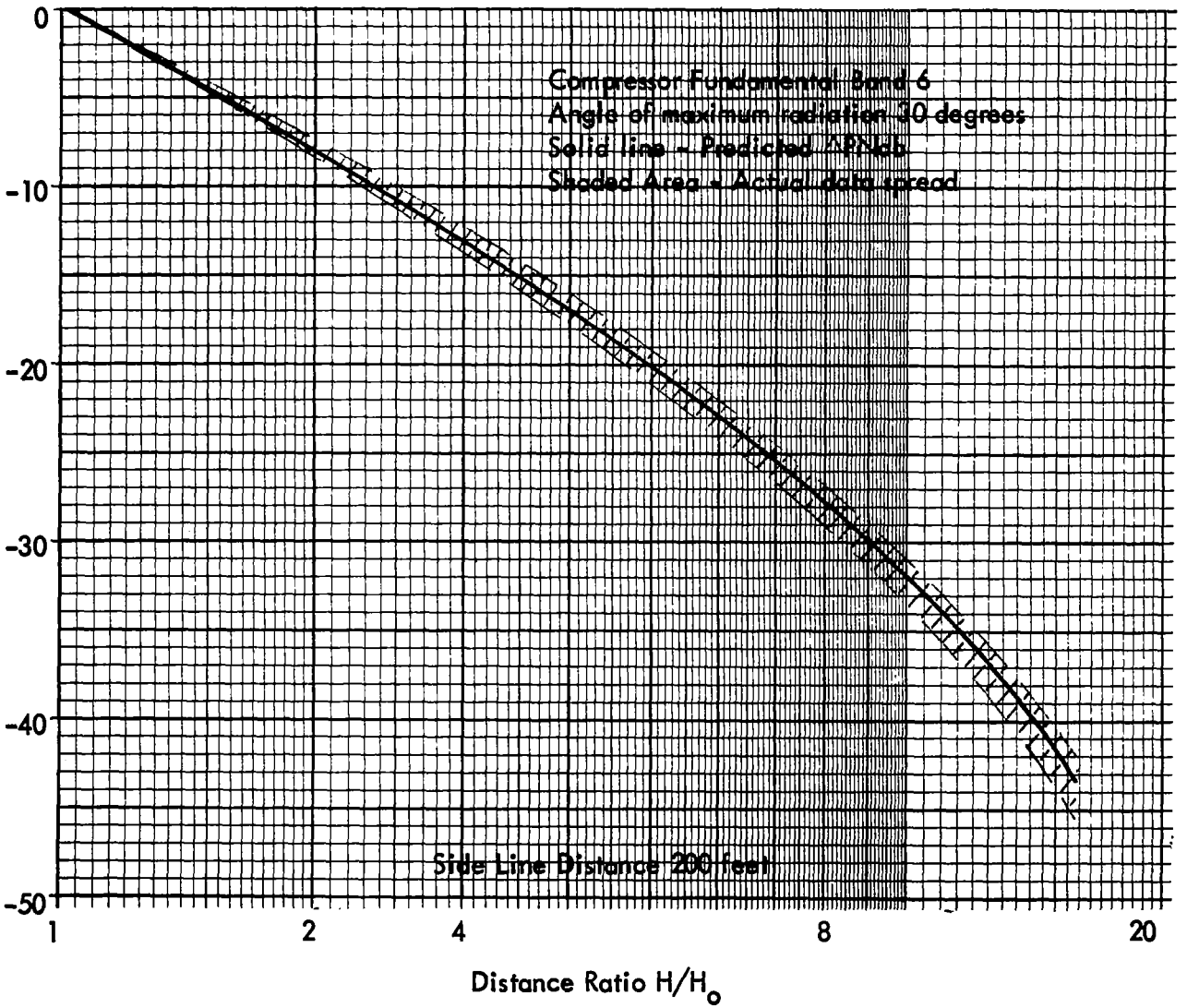

Fig. 37 - In-Flight Combined Jet and Compressor ΔPNdb Accuracy

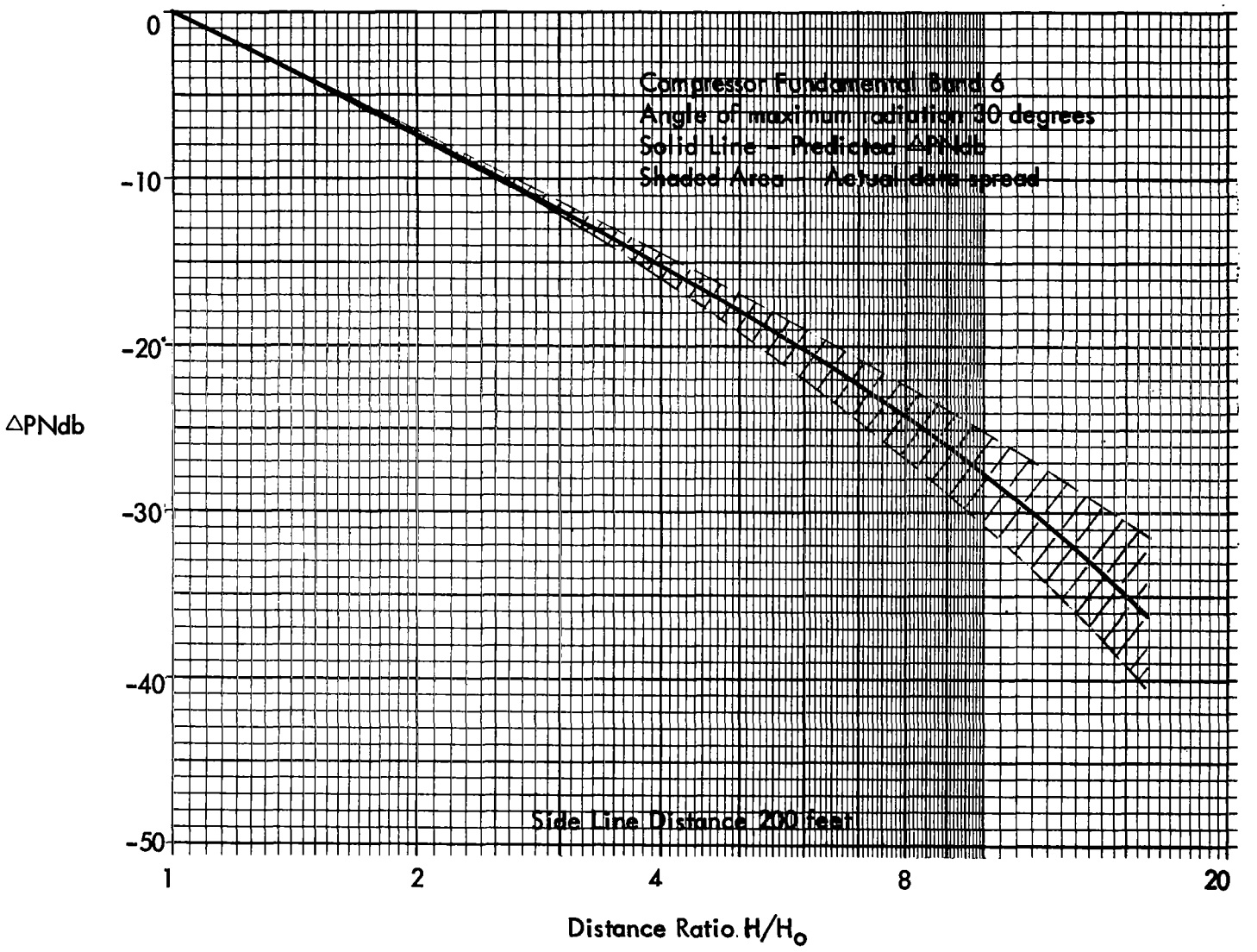

Fig. 38 - On-Ground Jet Noise ΔPNdb

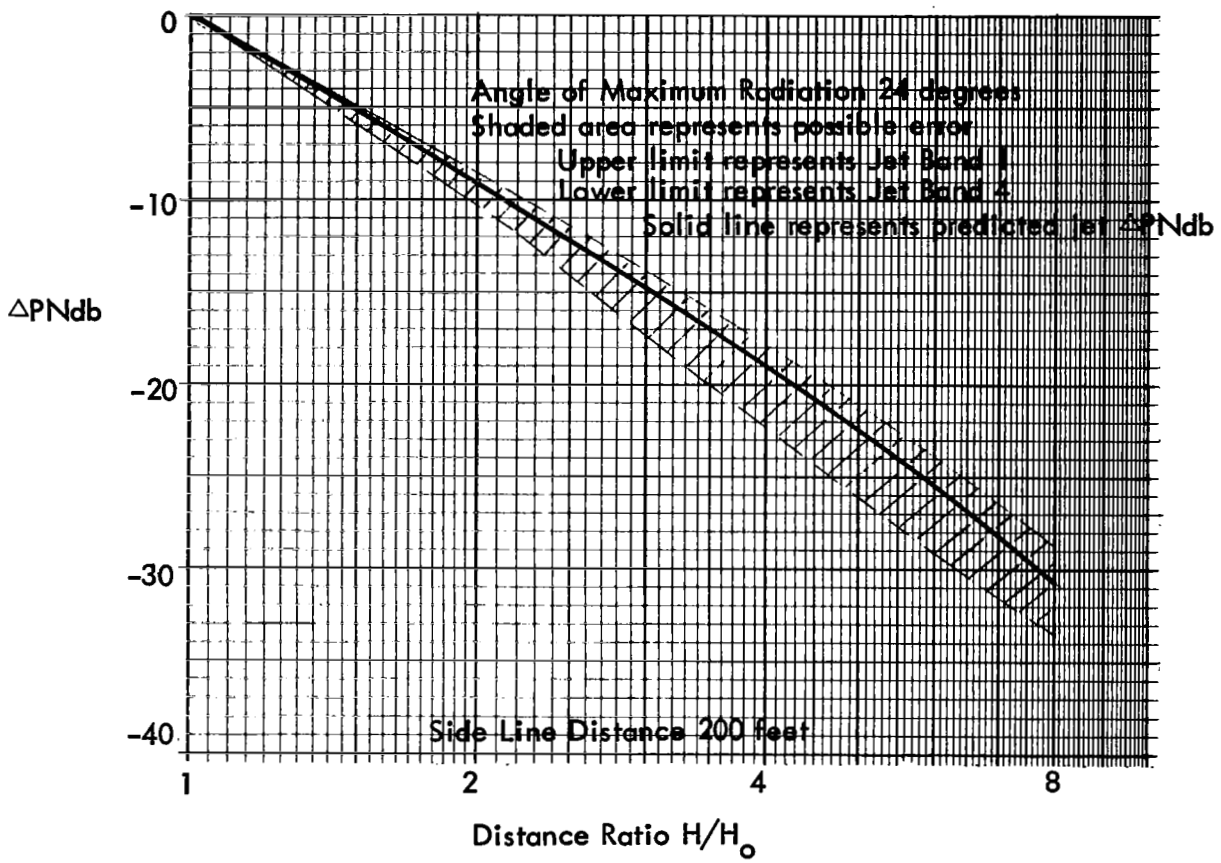

Fig. 39 - On-Ground Compressor △PNdb Accuracy

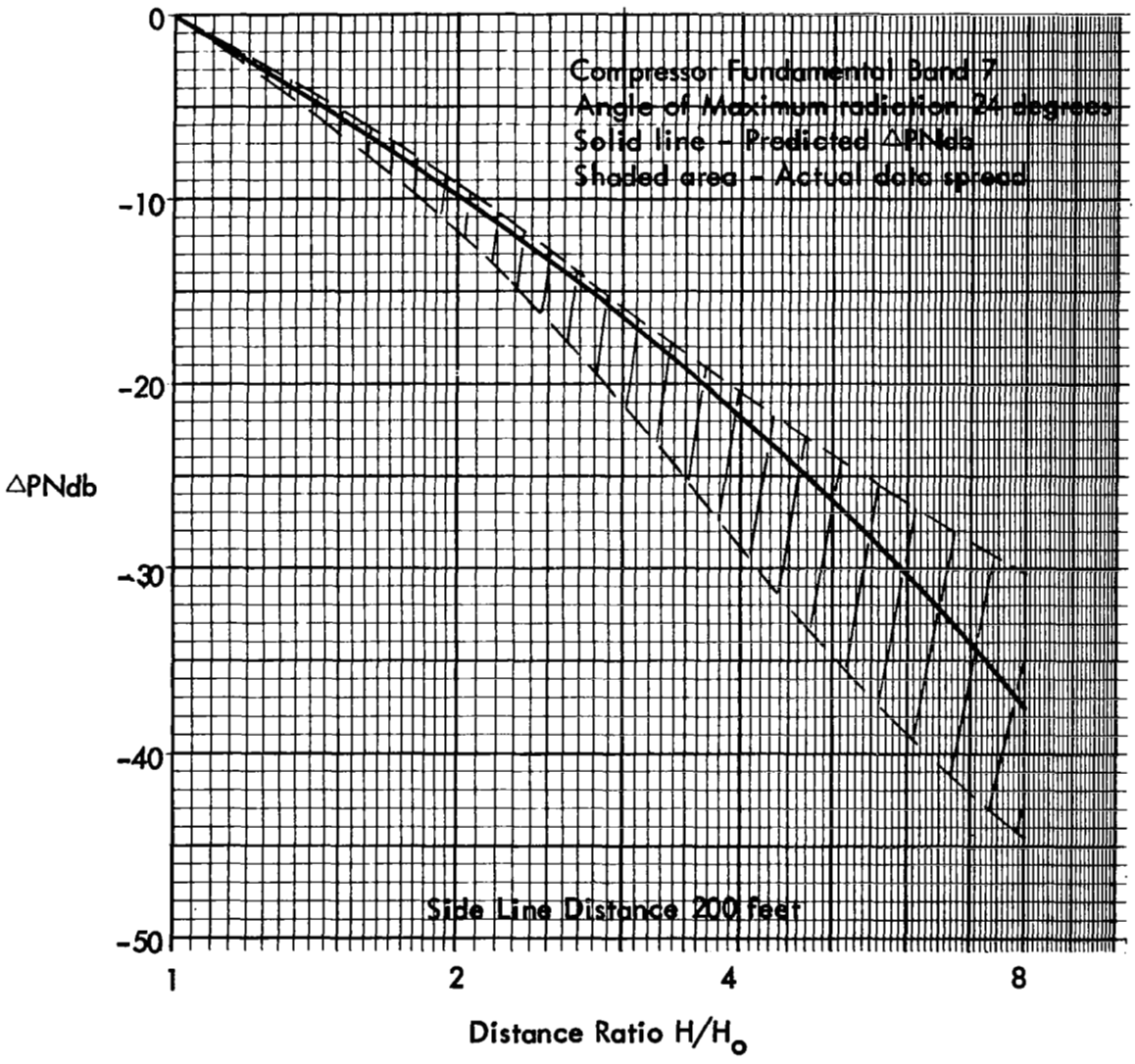

Fig. 40 - On-Ground Combined Jet and Compressor ΔPNdb Accuracy

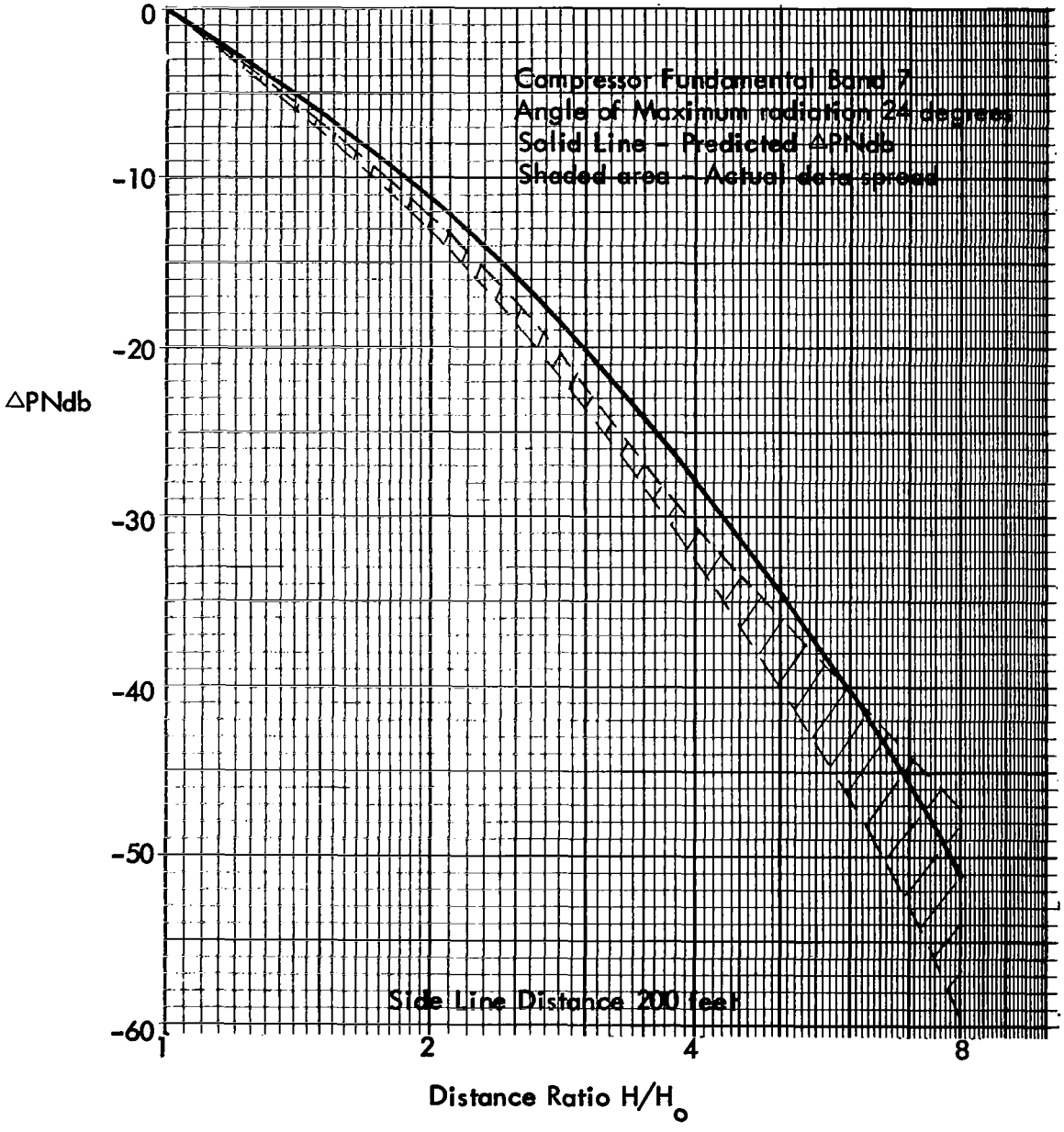

Fig. 41 - In-Flight Maximum Error Versus Angle of Radiation

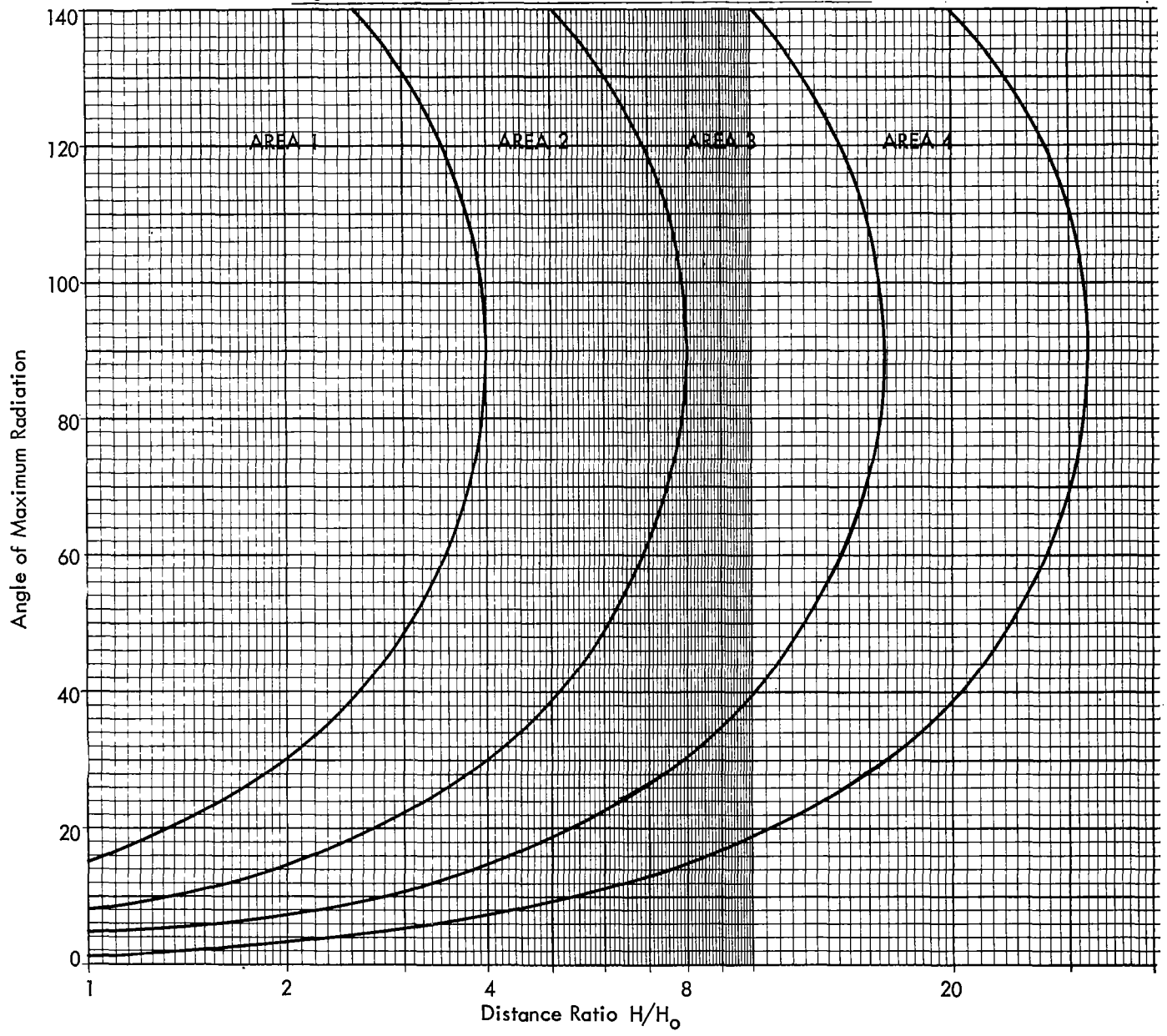

Fig. 42 - On-Ground Maximum Error Versus Angle of Radiation

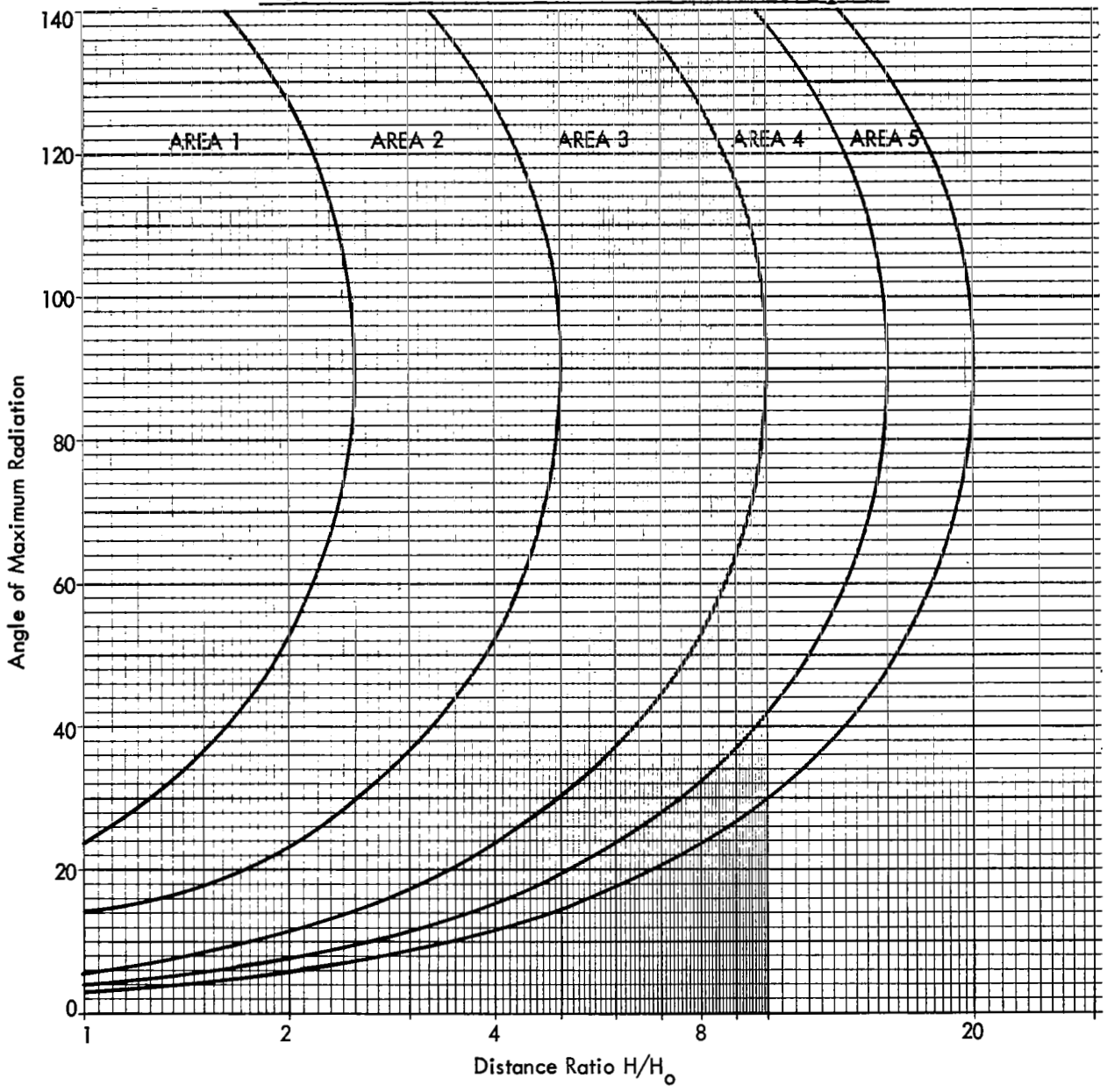

through 40 show the error plots for compressor and combined jet and compressor noise for a compressor fundamental in band 6. This octave band was selected as being typical. As can be seen, the spread of the combined jet and compressor noise is quite large. This is a result of the spread in levels between the jet noise and the compressor noise forming the combinations. The combinations varied from almost complete jet noise to almost complete compressor noise. For greater accuracy, it would be better to predict the jet and compressor noise separately, and combine their final values at the desired distance.

Figures 41 and 42 show the limits of accuracy. Table Number 4 gives the accuracy for the sideline distances indicated by the curves. Note that the accuracies given are for the worst cases, and ordinary use of the equations should give the PNdb to well within these accuracies. As can be seen, as the angle changes from 90 degrees, the error at a given sideline distance increases.

The maximum distances covered by the equations are 6400 feet in flight and 4000 feet on ground. This is absolute, or slant, distance (d on Page 59). The equations can be used to predict PNdb beyond this distance; however, as can be seen in Figures 37 through 40, the error will become progressively worse. These distance limits were picked as the distances at which the PNdb would probably drop below 70 PNdb. Studies such as Reference 5 show that noise of 70 PNdb or less is not annoying. All data was limited to 70PNdb or more, except for on-ground data. (This is another limitation, in that the equations are valid only for 70 PNdb noise and higher). The α and β were derived by averaging the available data and fitting the equation to the average by the method of least squares.

3.5 Jet and Compressor Spectra

The jet noise spectra used in the development of the foregoing techniques have been described in Section 2, and this section will describe the compressor spectra model selected for the development of the computer program.

A literature search showed that the spectrum shown in Reference 2 incorporates all the features found in other literature, and also fits the experimental data that is available. This has been used in the absence of a standard spectrum. A sample spectrum is shown in Figure 43 as a function of the ratio of frequency to the fundamental blade-passing frequency. The compressor spectrum has two features; blade whine and broad-band noise. The blade whine consists of the tone generated by the fundamental blade-passing frequency and its harmonics. The fundamental tone is the highest in level, with the harmonics declining in level by 20 log N (where N is the harmonic number). Only the tones generated by the first stage were used in preparing the spectra, since the tones from subsequent stages are attenuated by their passage through the various stages. Fundamental blade-passing frequencies of 500 to 4000 cps were used in establishing the range of the spectra, since an examination of engine parameters showed that these were the probable frequency limits.

The second component of compressor noise is the broad-band noise associated with random vortex fluctuations around the various blades and vanes. The general 1/3-octave

TABLE 4

In-Flight Maximum Error - PNdb

	Area			
	1	2	3	4
Jet Error	1	2	2.5	3
	Compressor Band 7			
Compressor	1	3	5.4	5.4
Combined	1	4	6.5	10
	Compressor Band 6			
Compressor	0.6	0.7	1	1.8
Combined	0.2	0.6	2.4	4.8
	Compressor Band 5			
Compressor	0.4	1.2	1.8	1.9
Combined	0.5	1.3	2.4	3.3
	Compressor Band 4			
Compressor	0.4	0.5	1.2	3.5
Combined	0.5	0.5	1.0	1.7

On-Ground Maximum Error - PNdb

	Area				
	1	2	3	4	5
Jet	1.0	2.4	3.3	3.3	3.3
	Compressor Band 7				
Compressor	1.5	1.5	3.7	5.2	7.6
Combined	0.9	2.3	7.6	9.0	9.0
	Compressor Band 6				
Compressor	1.4	1.4	2.3	2.3	2.3
Combined	1	1.7	4.5	5.2	6.3
	Compressor Band 5				
Compressor	1.1	1.1	3.8	3.9	3.9
Combined	1.1	1.8	4.6	4.6	5.9
	Compressor Band 4				
Compressor	0.8	0.8	2.1	2.1	2.1
Combined	1.2	1.8	2.3	3.3	5.4

Fig. 43 - Typical Compressor Spectrum

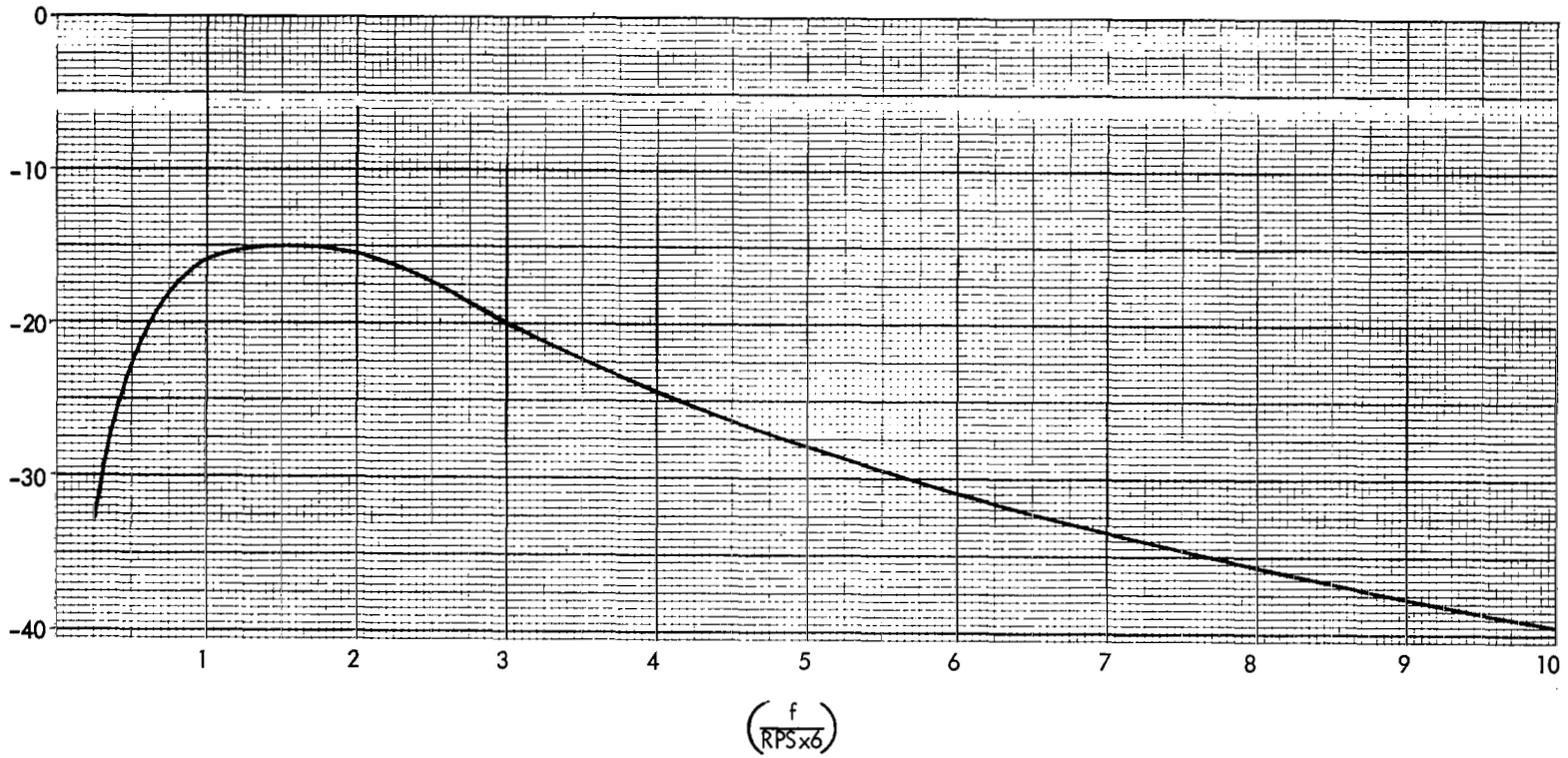

spectrum of this noise, taken from Reference 2, is given in Figure 44. The peak frequency of this noise is given approximately by $f = 2U/L$ (Reference), where U is the axial duct air velocity and L is a typical cord length such as the inlet guide vane or rotor blade. Examination of engine parameters showed that the ratio of the broad-band noise peak frequency to the fundamental blade-passing frequency was on the order of 1 to 2. Ratios of 1 to 2.5 were used in the computer program to cover the possible variations and ratios of 5, 10, 15, and 20db between the peak broad-band level and the fundamental blade tone were used to cover the various possibilities of pure tone to broad-band noise. With these options in the computer program, a specific spectra can be constructed for each engine being considered.

3.6 Computer Program

This section describes the inputs and outputs of the computer programs that were used to develop the data presented in Sections 3.1 through 3.4.

The goal in these sections was to develop suitable approximations to the usual method of calculating PNdb so that hand calculations or economical computer calculations could be carried out. To this end, it was necessary to develop sufficient data to cover most of the situations that would be encountered. Two programs were developed to handle the separate cases of in-flight and on-ground operation. The first program developed was for in-flight spectra, and used Eq. (75) where the values of the humidity absorption was taken from Reference 6. The coefficients as a function of frequency are plotted in Figure 45. The second program had an additional term due to ground absorption, and the ground-absorption coefficients were again taken from Reference 1.

The input to the programs consisted of PNdb NOYS value tables, generalized jet and compressor spectra, tables of the distances at which the PNdb was to be calculated, and indexing cards giving the range of parameter variation. The parameters and their range of variation were:

Jet peak frequency	63 to 500 cps
Compressor fundamental SPL level	+20db to -20db relative to jet level
Compressor white noise SPL level	5 to -20db relative to fundamental level
Compressor fundamental frequency	500 to 4000 cps
Compressor white noise frequency	1 to 2.5 times fundamental frequency

The computer programs basically calculated the SPL spectra, OA SPL, and PNdb of the jet, compressor, and combination at each distance for a given compressor fundamental level and frequency, fixed compressor white noise frequency, and the specified levels of compres-

Fig. 44 - Compressor White Noise Mean Spectrum

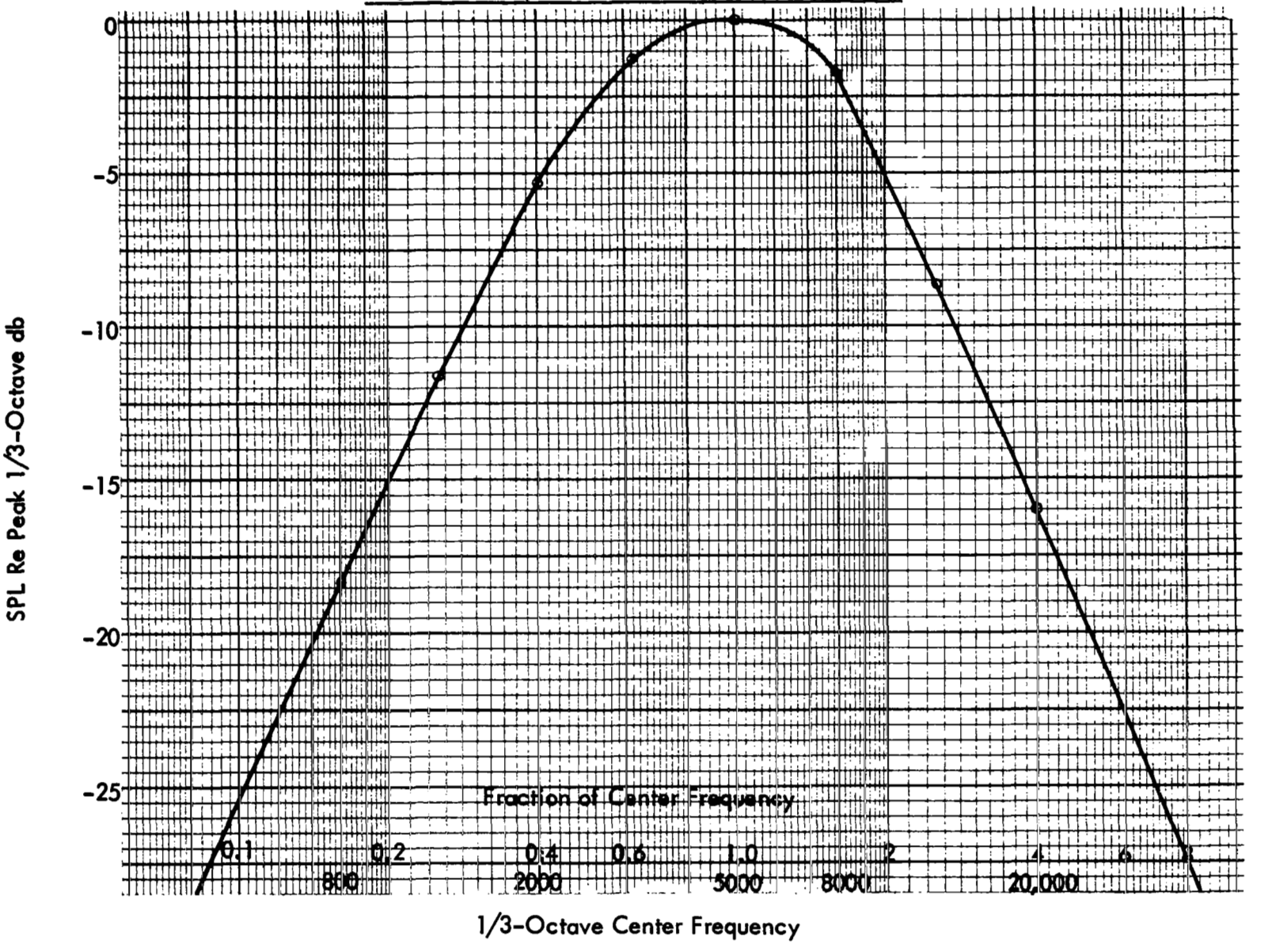

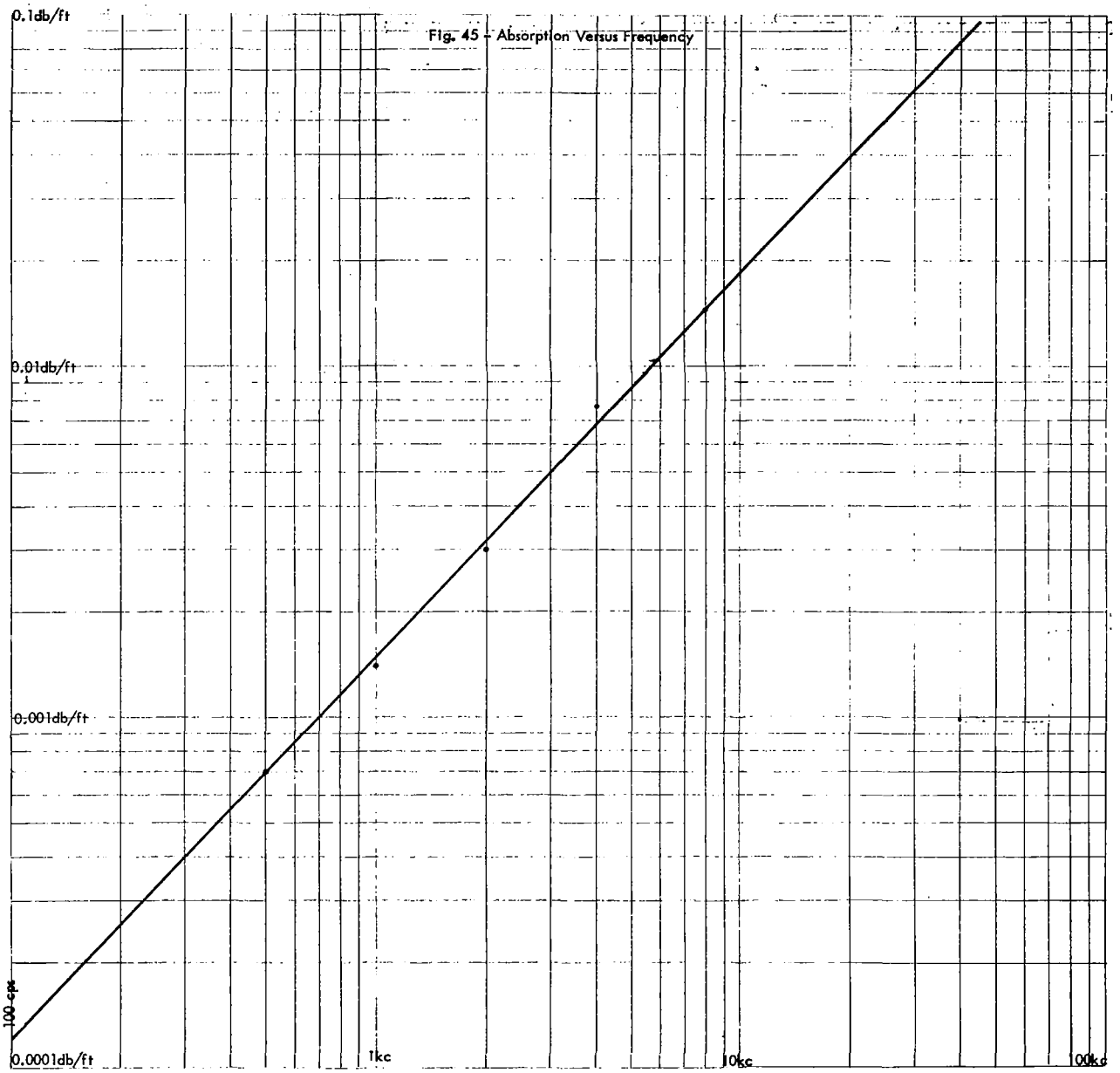

Fig. 45 – Absorption Versus Frequency

sor white noise. The difference between OA SPL and PNdb was calculated, and then the PNdb difference between the jet and compressor noise and the noise due to the combination was calculated. This process was repeated until all of the parameters were covered.

It was found subsequently that compressor white noise levels of -20db below the compressor fundamental were unrealistic, as well as the case where the compressor PNdb fell below 70 PNdb. This limited the cases to approximately 600 combinations of parameters for each condition of in-flight and on-ground analysis. In all, approximately 12,000 data points were used in developing the various curves and formulas presented in Sections 3.1 through 3.4.

4.0 AIRFRAME DESIGN AND NOISE

4.1 Introduction

Design of an air frame can indirectly influence the amount of noise received on the ground in several ways: by affectin the flight path relative to the observer, and hence the distance between the observer and the noise source, (2) by affecting the engine power requirement at various modes of take-off and landing operations, and hence the noise-source intensity, and (3) by affecting the aircraft speed characteristics which, in turn, affect both the noise source characteristics and the exposure time of the observer to the noise.

Airframe design parameters that are of special importance in noise studies include the gross weight, W, wing reference area, S, coefficients of lift (C_L) and drag (C_D) at various airplane flap configurations, and the thrust, T. Once these parameters or their limiting values are adequately defined, it is generally possible to establish the limits in flight path, power setting, and speed within which the airplane can operate.

This section of the report outlines methods by which airframe design may be evaluated in terms of noise. Relations between PNdb and airframe design factors are developed and appropriate design charts presented. Conventional take-off, take-off with power cutback, and landing operations are included in this study. Variation in operational procedures and their effects on noise will be discussed in Section 5.

In developing these methods the following simplifications have been adopted: (1) aircraft performance is based on quasi-steady flight in a vertical plane with the airplane on a straight course, (2) altitudes are limited to those below 4000 feet and a constant air density (standard sea level) is assumed, (3) the thrust axis of the engines is assumed to coincide with the flight path at all times, (4) the drag polar of the aircraft is assumed parabolic with constant coefficients, and (5) the accuracy requirements in the use of aircraft performance relations are based solely on noise considerations; thus, considerable latitude in using approximate performance equations is allowable. For example, for small climb and descent angles, aircraft lift and gross weight can be assumed equal.

4.2 Short Review of Flight Mechanics

Quasi-steady flight in a vertical plane is represented by the equations,

$$\begin{aligned} T - D - W \sin\gamma &= 0 \\ L - W \cos\gamma &= 0 \end{aligned} \tag{76}$$

where T denotes the total thrust, W the weight, D the drag, L the lift, and γ the path inclination. The force diagram is shown in Figure 46. The aerodynamic forces acting on the airplane are defined as

Thrust = Drag + W sin γ

Lift = W cos γ

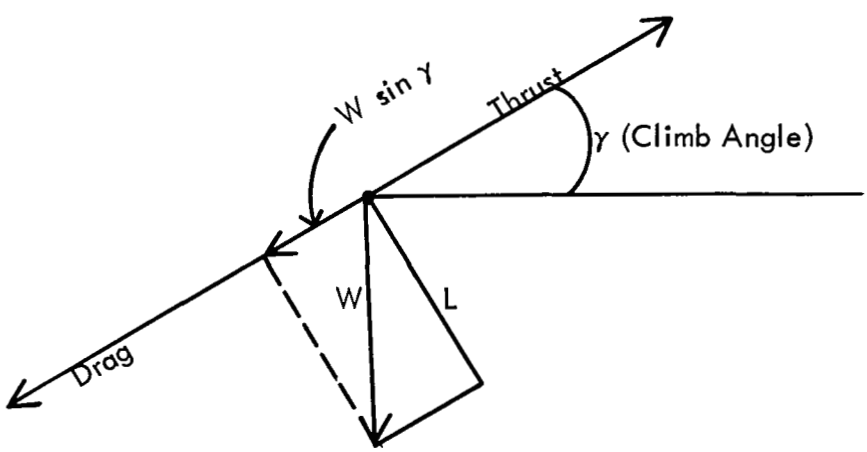

Figure 46

Force Diagram of Aircraft Flight on a Vertical Plane

$$D = 0.5 \frac{\rho}{g} C_D S v^2 \tag{77}$$

$$L = 0.5 \frac{\rho}{g} C_L S v^2 \tag{78}$$

where ρ is the air density (.075 lbs per ft^3), S the wing reference area, v the aircraft velocity, C_D the drag coefficient, and C_L the lift coefficient.

The overall drag is customarily separated into two components: the zero-lift drag, C_{do}, and the induced drag, C_{Di}, the latter term indicating drag associated with lift. Thus,

$$C_D = C_{Do} + C_{Di} \tag{79}$$

For low-speed operation, the total drag coefficient is due mainly to the induced drag coefficient, C_{Di}, although the zero-lift drag coefficient, C_{Do}, cannot be completely neglected.

Since typical airfoils and airplane configuration have induced-drag coefficients that are quadratic functions of the lift coefficients for subsonic speed and for some intervals of values of the lift coefficients, the various coefficients satisfy the relationship,

$$C_D = C_{Do} + K C_L^2 \tag{80}$$

where K is the induced-drag factor and is related to the airplane wing aspect ratio $\overline{AR}$ by the relation,

$$K = \frac{1}{\pi \overline{AR}\, e} \tag{81}$$

where e is the Oswald coefficient of the airplane and generally assumes the value between 0.75 to 0.90, and $\overline{AR}$ may be calculated in terms of wing span b and platform area S,

$$\overline{AR} = b^2/S \tag{82}$$

When Eqs. (77), (78), and (80) are combined, and the lift coefficient is eliminated, the following drag-to-weight ratio is obtained,

$$\frac{D}{W} = \frac{0.0012\, C_{Do}\, v^2}{W/S} + \frac{K\ W/S}{.0012\, v^2} \tag{83}$$

where W/S is referred to as the wing loading, and the factor 0.0012 comes from 0.5 x ρ/g= 0.075. The gross design parameter D/W (the reciprocal of L/D for level flights) is not a fixed quantity for any given airplane. It will vary depending on the aircraft speed v, the actual gross weight W, and the airplane flap setting which effects C_{Do}. The effects of K, C_{Do}, W/S, and v on D/W as given by Eq. (83) are shown in Figure 47.

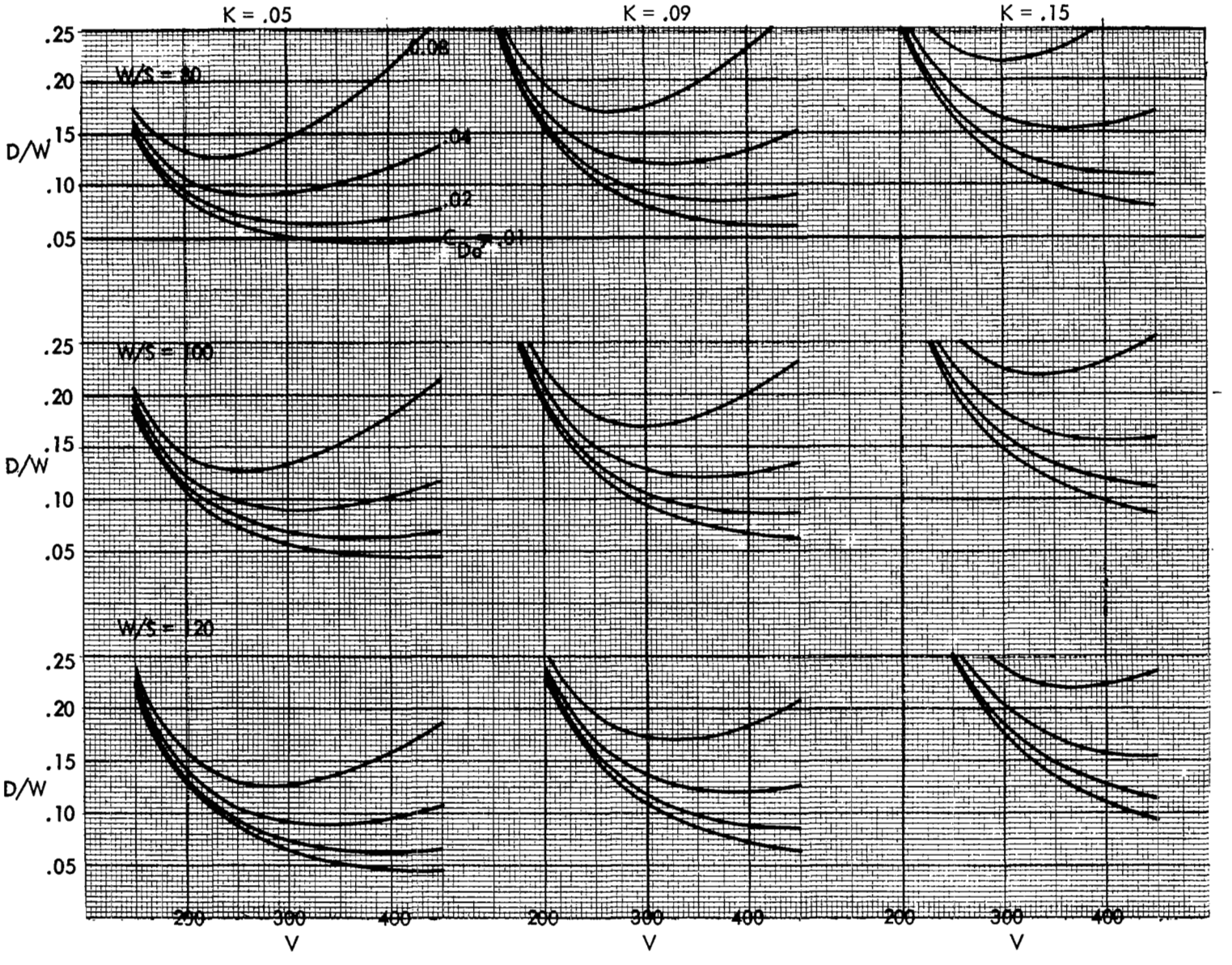

Figure 47 - D/W as a Function of K, C_{Do}, W/S, and V

The drag-to-weight ratio may be also expressed in terms of certain dimensionless parameters: E_{max}, the maximum aerodynamic efficiency of the airplane (maximum L/D); and u, the ratio of flight speed v and a reference speed v_r. These are defined below:

$$E_{max} = \frac{1}{2\sqrt{K\,C_{Do}}} \tag{84}$$

$$u = v/v_r \tag{85}$$

$$v_r = \sqrt{.0012\,W/S}\left[K/C_{Do}\right]^{1/4} \tag{86}$$

and,

$$D/W = \frac{1}{2E_{max}}\left[u^2 + \frac{1}{u^2}\right] \tag{87}$$

Eq. (87) is plotted in Figure 48 for $\frac{D}{W}E_{max}$ versus u. It can be seen that a minimum drag condition exists when the actual flight speed is equal to the reference speed v_r. This is also the condition at which the induced drag is equal to the zero-lift drag.

The importance of the D/W ratio in an acoustic analysis is that this parameter directly influences the climb-out angle of the airplane during the take-off operation and it therefore affects the separation distance between the observer and the airplane noise source. For a landing operation along a prescribed glide slope the D/W of the airplane determines the thrust requirement of the engines and, hence, it indirectly affects the noise-source intensity. Important relations in take-off and landing are,

$$\sin\gamma = \frac{R/C}{v} = \left[\frac{T}{W} - \frac{D}{W}\right] \tag{88}$$

where γ is the climb angle and R/C is the rate of climb and

$$\frac{R/D}{v} = \left[\frac{D}{W} + \frac{T}{W}\right] \tag{89}$$

where R/D is the rate of descent.

An airplane flight path, referenced to some fixed point on the ground, is dependent on six independent variables that have been discussed; thus,

$$\gamma + f\ (T, W, S, K, C_{Do}, v) \tag{90}$$

The design selection of these variables is largely determined by the airplane mission, the state-of-the-art of engine and aircraft design, and certain Government regulatory requirements. Once the design or operating limits of these variables are defined and the cycle design of the engines has been made, the noise limits are defined, and the noise on the

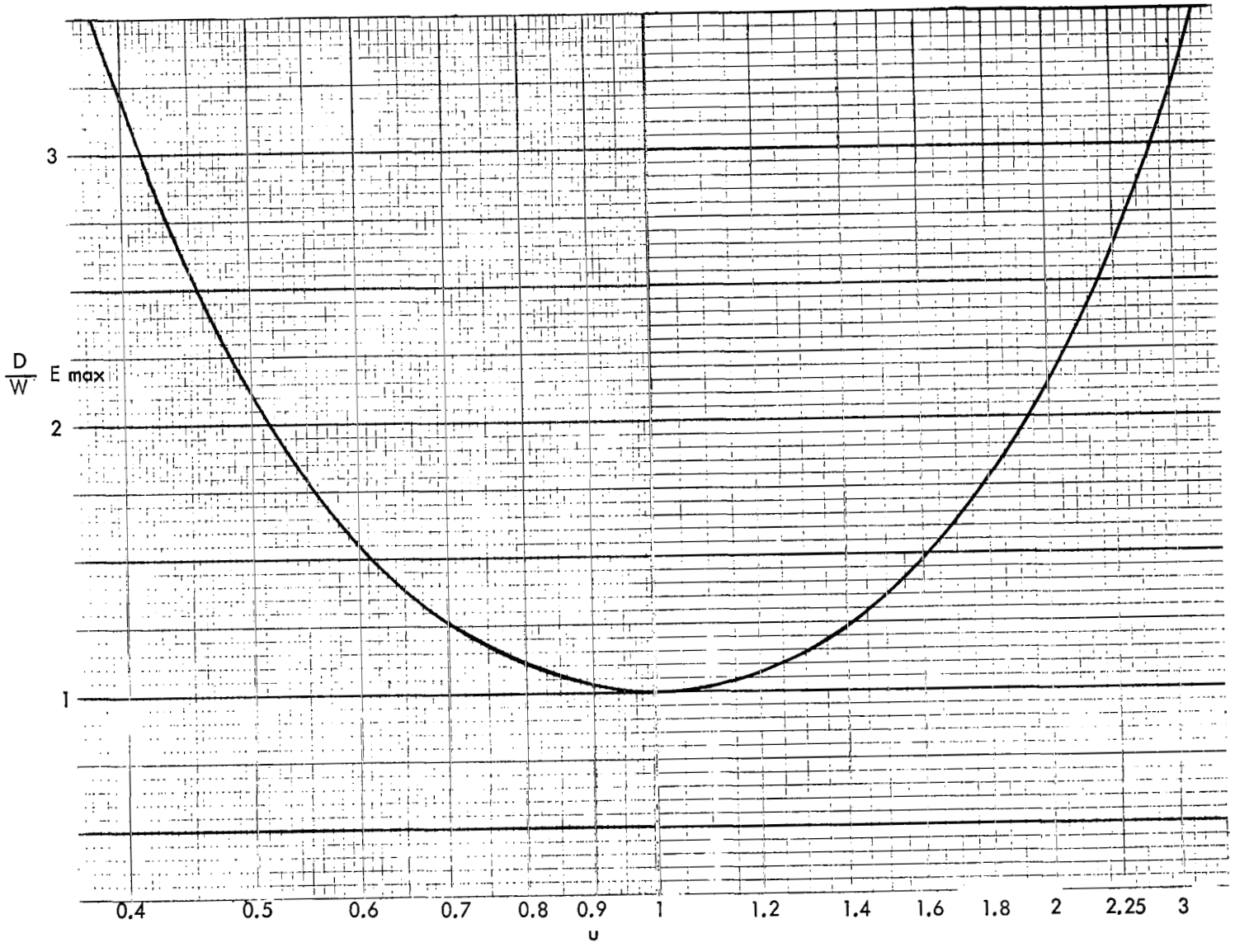

Figure 48 - D/W E max Versus υ

ground will be a function of the precise operating mode of the airplane (which is determined by how the pilot varies the thrust, speed and flap setting).

4.3 Aircraft Flight Paths and Noise During Take-Off

4.3.1 Estimating ground-roll distance and minimum separation distance.- For a power plant operating at a specific power setting during take-off, the most important variable which determines the noise level experienced by an observer on the ground is the minimum separation distance between the observer and the flight path. This minimum separation distance will be denoted by the sumbol H. If the observer is directly under the flight path and the climb angle of the aircraft is not very steep, the minimum separation distance is almost exactly equal to the altitude of the aircraft when directly overhead.

In this chapter airplane performance and noise will be related in terms of H. The choice of H for relating the flight path characteristics of an airplane to the observer is consistent with the manner in which the engine's reference noise level is defined (see Section 2).

In analyzing airport noise problems, it is customary to reference ground positions to the starting roll position of the aircraft on the runway. Often the ground positions at which noise levels are calculated or measured are selected along a line which is an extension of the runway, and the distance between the ground position along this line and the starting roll position is defined as S_o. The minimum separation distance H as a function of S_o is determined by the climb angle of the aircraft γ, and by the ground roll distance S', as shown in Figure 49. The relation is

$$H = (S_o - S') \sin \gamma \tag{91}$$

or

$$H = (S_o - S') \left(\frac{T}{W} - \frac{D}{W}\right) \tag{92}$$

Distance S', as defined in Figure 49, is not the precise ground roll distance, which is normally defined as the distance between the starting roll and the point of aircraft lift-off, and in order to maintain a simple relationship between H and S_o, S' has been defined as the distance along the runway between the starting roll and the point at which the straight-line flight path intercepts the ground. To avoid confusion, S' will be called the equivalent ground roll distance. To arrive at the initial point of the straightline flight path (see Figure 49) from the liftoff, the aircraft is assumed to have accelerated from liftoff speed to a stabilized safe climbout speed of $V_2 + 10$ knots, with gears retracted. Flap configuration is the same as that at take-off, and will remain the same during the straightline climbout. As will be seen later, maintaining the near-maximum climb gradient at the constant speed at the constant speed of $V_2 + 10$ until a certain ground point S_o is reached before performing such operations as power cutback, flap retraction, and speed acceleration is, on the whole, the most advantageous for noise abatement. This take-off procedure will be called the "Noise-Abatement Climbout".

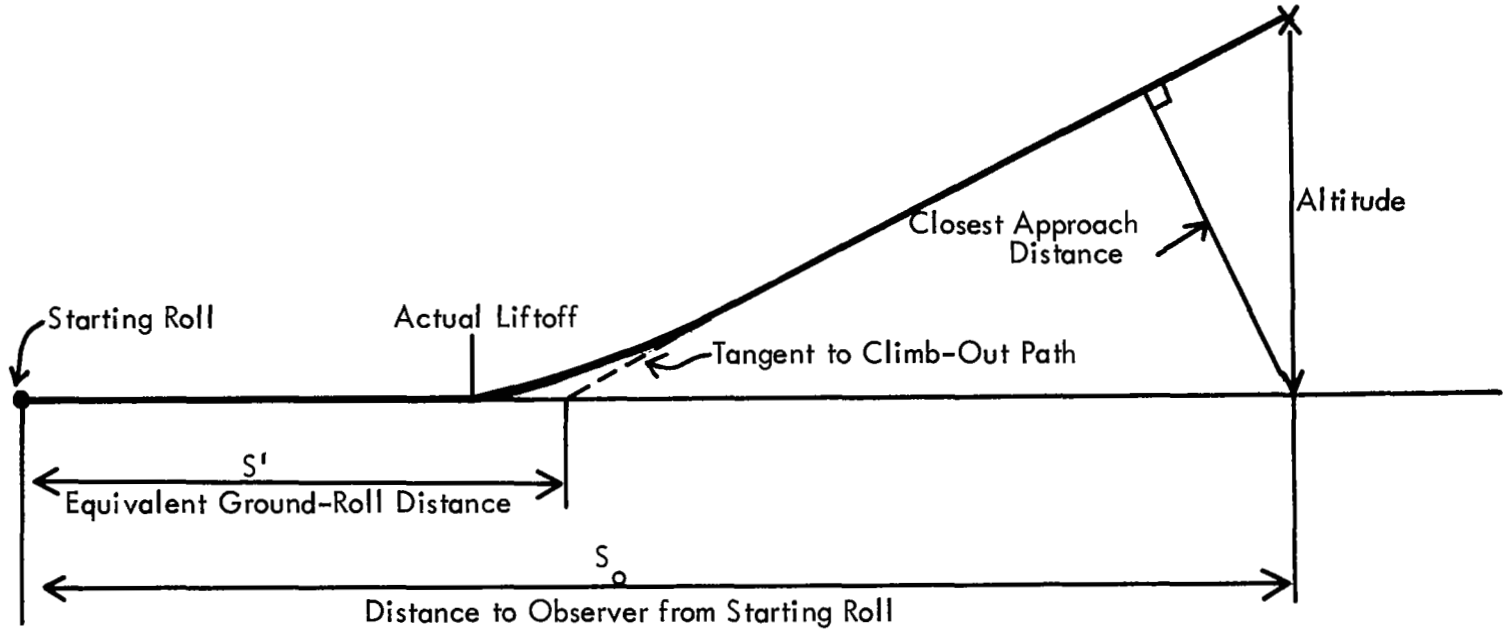

Figure 49

Take-Off Schematic

Exact calculation of the ground roll distance is complicated and involves ground-effect parameters not generally well known. Fortunately, in noise calculations a considerable inexactitude in ground roll distance estimation is acceptable. For example, an error of ten percent in estimating a typical equivalent ground roll distance introduces a maximum error of only 1db at $S_o = 3$ miles when Eq. (92) is used. At distances greater than 3 miles, the acoustical error diminishes.

With data available from Reference 7 to 11, for typical commercial jet transports the following empirical relation for estimating the equivalent ground roll distance S' has been developed,

$$S' = 39 \times \frac{W/S}{\frac{T}{W} C_L^{\wedge}} \tag{93}$$

where W/S and $\frac{T}{W}$ have already been defined and $C_L^{\wedge}$ is the maximum lift coefficient. All the data that supports Eq. (93) is for the constant climbout speed of $V_2 + 10$ knots. Figure 50 shows the data scatter in relation to the best-fit empirical curve of Eq. (93). This equation is similar in form to the one generally used by designers for approximating the ground roll distance (see Reference 12 for example).

Combining Eqs. (92) and (93) will give the important relation that directly links the airplane characteristics to the minimum separation distance H in terms of the observer position S_o

$$H = \left[S_o - 39 \frac{W/S}{\frac{T}{W} C_L^{\wedge}} \right] \left[\frac{T}{W} - \frac{D}{W} \right] \tag{94}$$

Eq. (94) is plotted in Figure 51 with $S_o = 15{,}840$ feet (3 miles). From this figure, it is easy to see how the various airframe characteristics determine the minimum separation distance H between the observer stationed at the 3-mile point and the specified flight path. Changes in H for observer positions other than the 3-mile point may be approximated by the following:

$$\Delta H \approx (S_o - 15{,}840) \left(\frac{T}{W} - \frac{D}{W} \right) \tag{95}$$

In developing Eq. (94) it was stipulated that the flight climb gradient be constant and that the aircraft be at a constant flight speed of 10 knots above the reference V_2 speed. For most aircraft, this $V_2 + 10$ (knots) may be approximated by the relationship,

$$V \approx 1.32\, V_s \quad \text{(speed in ft/sec corresponding to } V_2 + 10 \text{ knots)} \tag{96}$$

where V_s is the stall speed and is related to W/S and $C_L^{\wedge}$ by

$$V_s = \sqrt{\frac{835\, W/S}{C_L^{\wedge}}} \tag{97}$$

Figure 50 - S Versus $\frac{W/S}{F/W \times C_L}$

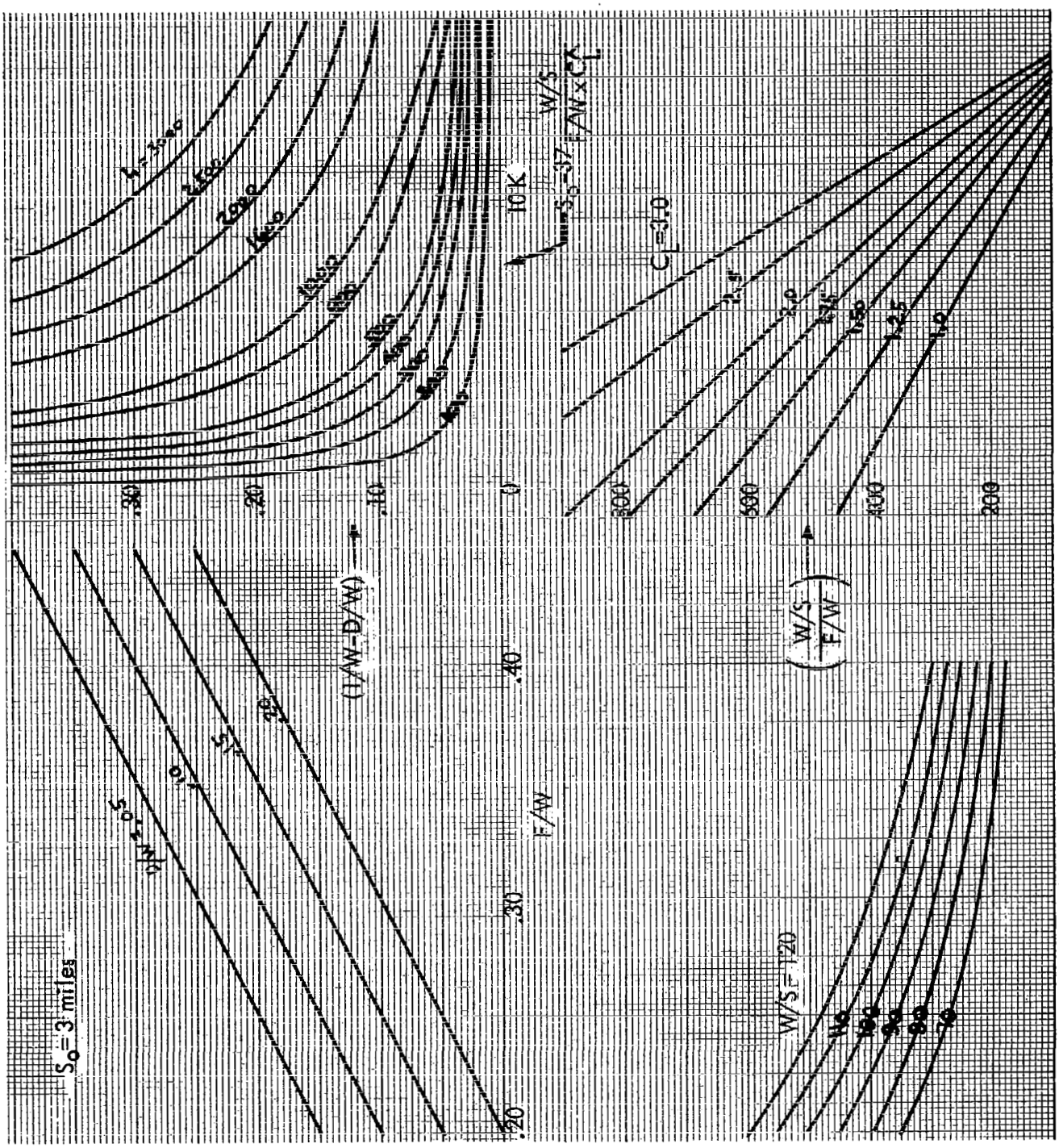

Figure 51

Minimum Separation Distance Nomograph

For any given airplane design, the maximum lift coefficient C_L varies with flap extension. In fact, the purpose of using flaps is to raise the maximum lift coefficient and thereby lower the stall speed of the aircraft and permit desirable low-speed operation during take-off and landing of the airplane. C_L generally varies from about 1.2 to 2.6 when the flap moves from a fully-retracted to a fully-extended position. For advanced flap and high-lift device designs, the maximum C_L may exceed 3.0. It should be recognized that while flap extension (higher C_L) reduces ground-run distance (Eq. (93)), it increases the drag (by increasing the zero-lift drag coefficient C_{D_o}) and, therefore, tends to reduce the climb gradient. Figure 52 shows values of C_L and C_{D_o} as functions of flap-setting angle for a typical jet transport.

4.3.2 Procedure for calculating the maximum noise level at the three-mile point.- In this section, it will be assumed that the aircraft performs a "noise-abatement climbout". The climbout path, essentially a straight line, is described by Figure 49 and is defined by Eq. (92). Assuming that there is no power cutback, a general procedure will be outlined which will permit calculation of the maximum PNdb at the three-mile point in terms of engine and airplane design parameters.

Section 2 has shown the relationship between the engine's reference level $PNdb_o$ in terms of engine component or cycle variables; thus

$$\begin{aligned} PNdb_o \text{ (jet)} &= 10 \log Fn + Q \text{ (engine design, } v \text{)} \\ PNdb_o \text{ (compressor} &= f \text{ (fan design)} \end{aligned} \tag{98}$$

Section 3 has shown that with a given $PNdb_o$ referenced to 200 feet, the maximum PNdb associated with a passby distance of H may be obtained by the following relations;

$$PNdb\ (H) = PNdb_o - \triangle PNdb(H) + 10 \log (n) \tag{99}$$

and

$$\triangle PNdb\ (H) = \alpha 10 \log \left(\frac{H}{200}\right) + \beta \frac{200}{\sin} \left(\frac{H}{200} - 1\right) \tag{100}$$

where n is the number of engines on the airplane, constants α and β are functions of the noise spectrum as defined by Table 2, θ is the angle of maximum level as observed along the 200-foot sideline. A correction factor somewhere between -1 to -3db must be added to Eq. (99) if $PNdb_o$ is defined or measured using a hemispherical radiation model.

The relationship between H and airplane design variables for a specified take-off flight path has been given by Eqs. (83), (94), (96), and (97).

The procedure for using the above equations to determine the maximum PNdb at the 3-mile point may be summarized as follows,

Figure 52

Typical $C_{L^\wedge}$ and C_{D_o} Versus δ

Commercial Aircraft

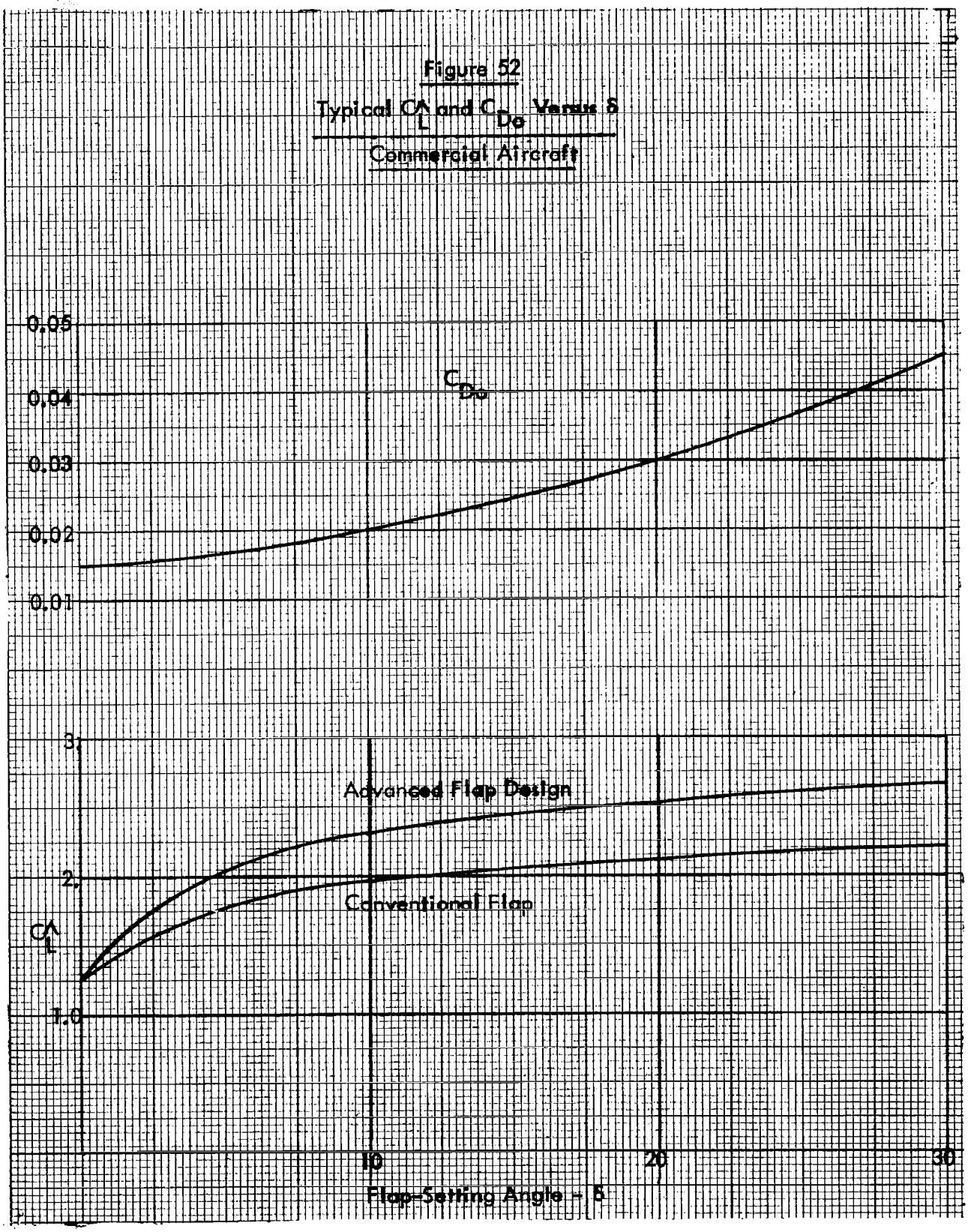

1. Calculate the minimum separation distance H based on inputs of W/S, $\frac{T}{W}$, C_{D_o}, K, and $C_{L^\wedge}$ (under take-off conditions) by the use of Eqs. (83) and (94).

2. Calculate climb-out speed v (corresponding to V_2+10), based on W/S, $C_{L^\wedge}$ by the use of Eqs. (96) and (97).

3. Refer to relevant equations in Section 2, and obtain the engine reference $PNdb_o$ (jet), based on v and engine design parameters, and $PNdb_o$ (fan), based on the fan design (compressor noise of turbojet-type engines may be ignored.

4. Calculate $\triangle$PNdb for jet and compressor sources for the appropriate H (Step 1) and powerplant related coefficients α, β, and θ max by means of Eq. (100).

5. Obtain PNdb max at the 3-mile point for both the jet and compressor sources with Eqs. (98) and (99).

6. PNdb max (jet) and PNdb (fan), determined separately in Step 5, may be combined using Figure 21 of Section 3 if the angles of maximum radiation (sideline basis) from the two sources are known or assumed to be nearly the same.

If the directional characteristics of the two sources are significantly different, the PNdb values at various θ positions along the 200-foot sideline must be established for both sources, combined according to the rules of Figure 21, and then the combined maximum PNdb and the associated angle θ must be selected. This selected PNdb may be termed the engine's reference $PNdb_o$ for combined sources. The procedure for determining the PNdb (H) on the ground will be the same as before, except that the values of α and β in Eq. (100) are for the case of combined sources.

An alternative to the above procedure for calculating noise sources with different directional characteristics is the following: establish the 200-foot sideline PNdb as a function of θ for each source (denoting them as PNdb (θ, 200' S.L., jet) and PNdb (θ, 200' S.L. fan), obtain $\triangle$PNdb functions for various angles for the two sources (denoting them as $\triangle$PNdb (θ, jet) and PNdb (θ, fan), use Eqs. (98) and (99) to obtain values of PNdb (h_o, θ, jet) and PNdb (H, θ, fan), and finally combine the two levels at the observer's position according to Figure 21 to obtain PNdb (h_o, θ, combined sources) for the various angles.

It is also interesting to note that the combined PNdb versus θ may be expressed in terms of combined PNdb versus time "t" by means of the relationship,

$$\Delta t = \frac{H}{v \tan \theta} \tag{101}$$

where the reference time $\Delta t = 0$ is when the airplane is at the minimum separation distance H ($\theta = 90^{\circ}$).

The procedures outlined above for calculating the maximum PNdb at $S_o = 3$ miles in terms of various airplane and engine variables can best be carried out on a digital computer. With a computer, the effect of design variation involving one or more independent variables may be tested very quickly. In using a computer, it is well to remember that S_o need not be fixed at the 3-mile point, since Eq. (93) contains S_o as a variable. In addition, since $PNdb_o$ (jet) and $PNdb_o$ (fan) - as developed in Section 2 - do not represent engine designs that contain noise-suppression features, a modified engine reference level could be introduced,

$$\left.\begin{aligned} PNdb_o' \text{ (jet)} &= PNdb_o \text{ (jet)} - DF \text{ (jet)} \\ PNdb' \text{ (fan)} &= PNdb_o \text{ (fan)} - DF \text{ (fan)} \end{aligned}\right\} \tag{102}$$

where DF (jet) and DF (fan) are design factors in db for the jet and fan noise that are used as input variables in the computer program. In this way, as improvements are made in engine designs to incorporate noise-reduction features, the basic methods that have been developed can still be used if a DF can be selected to account for the design change.

4.3.3 Effects of airplane design parameters on noise at the three-mile-point.- It will be assumed that the climb-out path of the airplane follows the constant angle of attack, a constant speed (V2+10) procedure, and that the power-plant design and the aircraft velocity are fixed. Under these conditions, the effect of airframe design parameters on noise is simply due to their effect on separation distance and can best be shown on a relative PNdb basis by the relations described in Eqs. (94) and (100).

The parameters of interest are power loading ($\frac{T}{W}$), wing load (W/S), maximum lift coefficient ($C_L^{\wedge}$) and drag-to-lift coefficient ratio $\frac{D}{W}$. The noise sources are jet noise, compressor noise, and jet and compressor noise combined. For the latter two sources, the peak frequency of the compressor noise is assumed to be located at $f_p = 1500$ cps, and angles of maximum noise radiation θ max for the three sources are assumed to be 45°, 70°, and 60° from the exhaust axis, respectively. It should be emphasized that the results presented in the graphs could be in error (particularly at large values of H) if the actual θ max and f_p are different from the assumed values.

Inspection of Eq. (94) indicates that wing loading (W/S) and maximum lift coefficient ($C_L^{\wedge}$) affect the separation distance H by changing the ground-roll distance,

$$S' = 39 \frac{W/S}{\frac{T}{W} C_L^{\wedge}} \tag{93}$$

It can be seen from Eq. (94) that as S_o increases the influence of W/S and $C_{L_{\uparrow}}$ on the noise diminishes. Drag-to-weight ratio ($\frac{D}{W}$) affects H by influencing the climb gradient,

$$\text{Sin } \alpha = \left(\frac{T}{W} - \frac{D}{W} \right) \approx \tan \alpha \text{ for } \alpha < 15^{o} \tag{88}$$

Its affect on noise, therefore, increases with an increase in S_o.

Power loading, T/W, affects both the climb gradient and the ground-roll distance and appears to have a very significant influence on noise somewhat independent of S_o.

The effect of power loading ($\frac{T}{W}$) on $\triangle$PNdb is shown in Figure 53 for several values of wing loading. This effect is quite strong and increasing T/W from 0.25 to 0.35, for example, can mean a noise reduction of approximately 5 to 7 PNdb for both jet and compressor noise. In the range of T/W between 0.2 to 0.4, the perceived noise change of Figure 53 may be approximated by

$$\overline{PN} \quad \alpha \left(\frac{T}{W} \right)^{\alpha} \tag{103}$$

where α varies from about -6.5 to -7.5. These values of α do not take into account the increase in noise source intensity if the change in T/W is due only to change in powerplant size. With the approximate relations shown in Section 2 that the perceived noise intensity is directly proportional to engine thrust, the change in perceived noise due to combined effects of changing separation distance and source intensity can be shown to be approximately,

$$\overline{PN} \text{ (net)} \quad \alpha \left(\frac{T}{W} \right)^{\alpha} \quad \text{for constant W} \tag{104}$$

with α being between -5.5 to -6.5. It can be also seen from Figure 53 that the relative effects on $\triangle$PNdb due to T/W variation is not strongly influenced by the $C_{L_{\uparrow}}$ and W/S of the airplane.

For constant values of $C_{L_{\uparrow}}$, $\frac{T}{W}$, and $\frac{D}{W}$, design changes in the wing loading (by altering wing reference areas) from a value of 80 to 110 have relatively minor effects on the PNdb. Generally speaking, a low wing loading is advantageous, since it tends to reduce ground-roll distance and, consequently, increase separation distance. The relative effect of W/S is stronger when $C_{L_{\uparrow}}$ and $\frac{T}{W}$ are low.

The effects of $C_{L_{\uparrow}}$ and D/W on $\triangle$PNdb at the 3-mile point are shown in parametric plots in Figure 54, and appear to be very strong. Increasing $C_{L_{\uparrow}}$ and decreasing D/W, if possible, would give extremely large noise reductions. Of course, $C_{L_{\uparrow}}$ and D/W are dictated by the flap setting. High flaps increase $C_{L_{\uparrow}}$ tending to shorten the ground roll, but induce higher drag, tending to reduce climb gradient. The net effect on H and noise appears to depend on the power loading and the observer's position. At the 3-mile point it is slightly more advantageous for aircraft of current design to always take off with extended flaps (providing that it also meets second-segment, one-engine-out FAR requirements). From the stand-

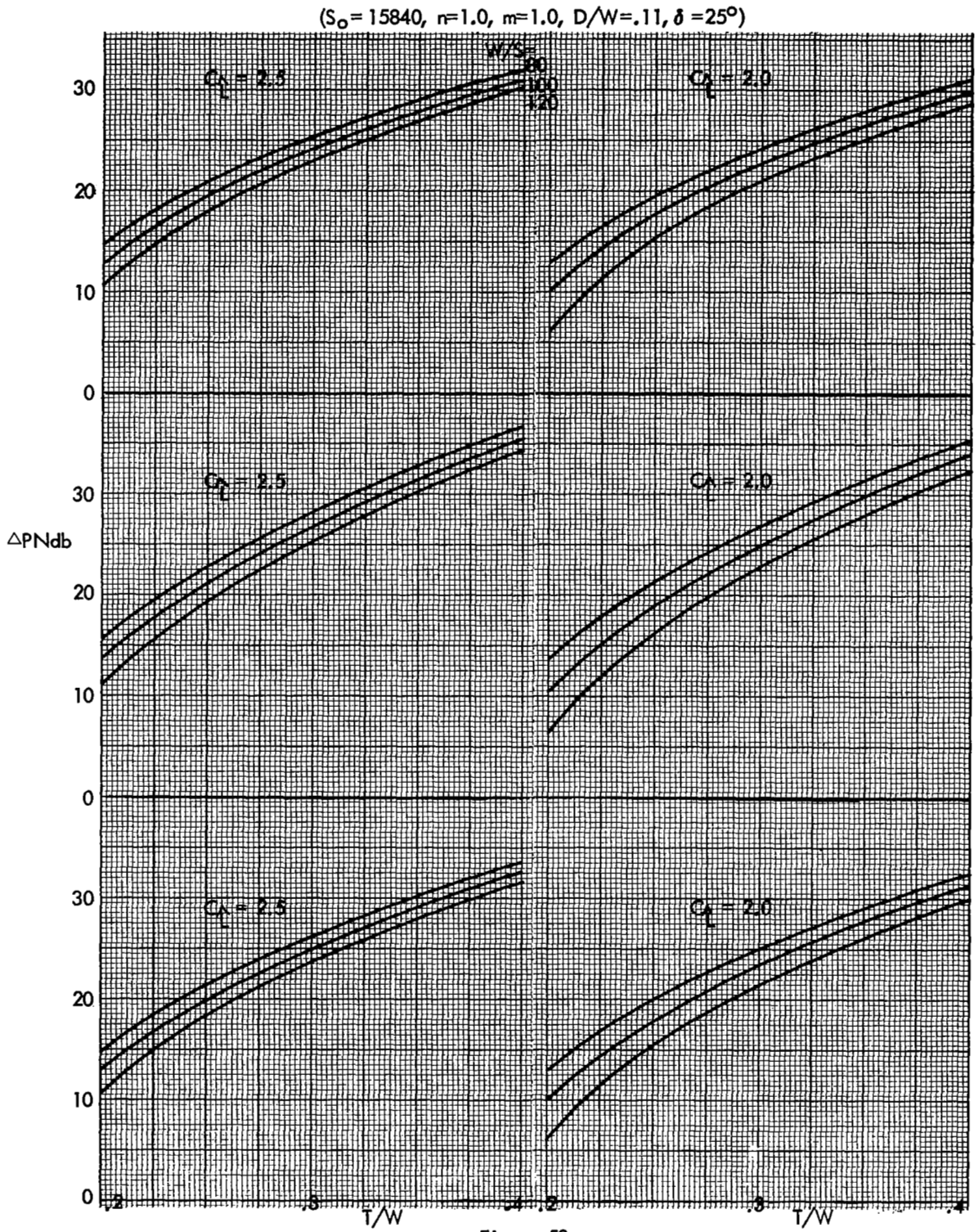

Figure 53

△PNdb Versus Power Loading

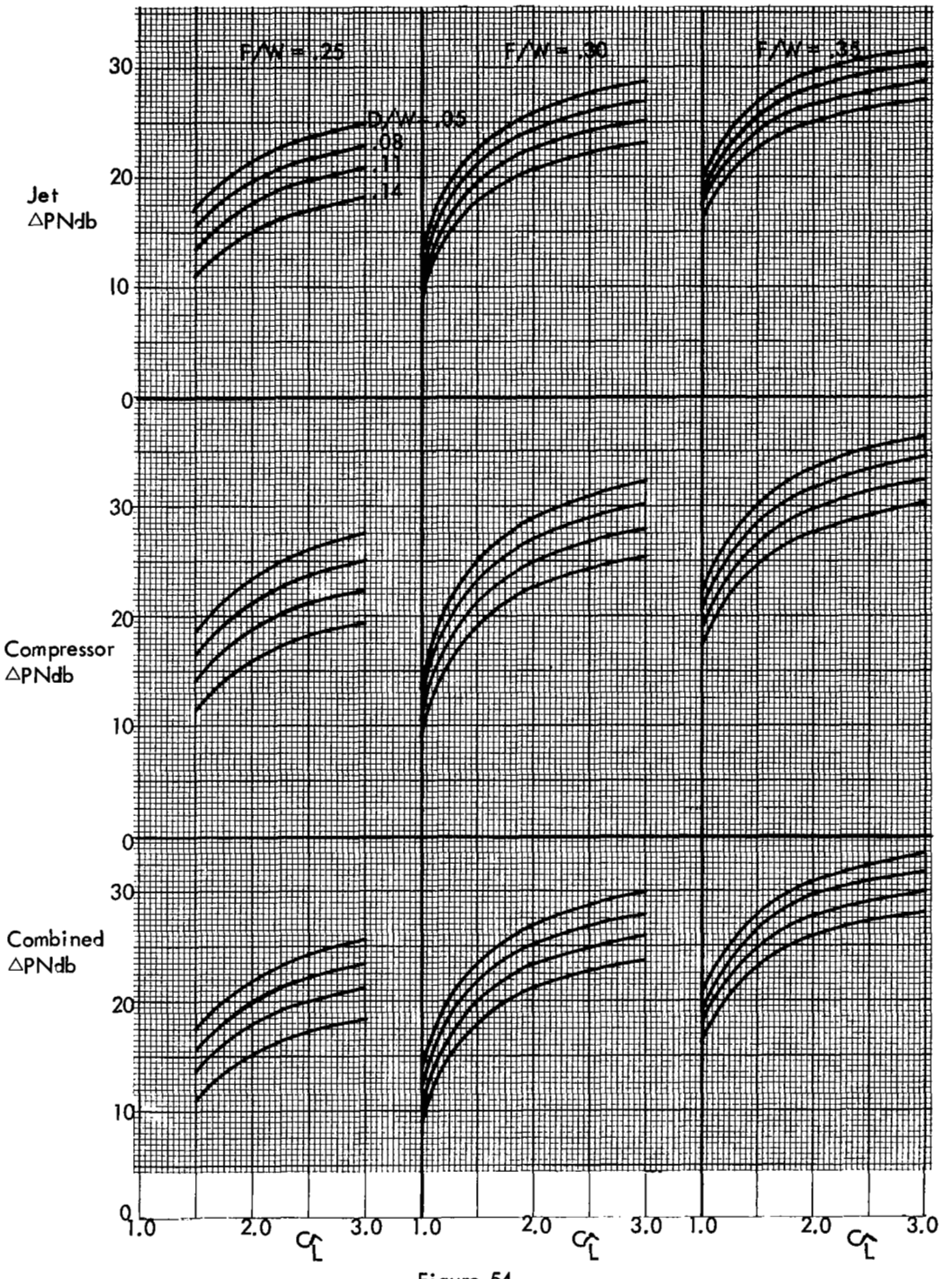

Figure 54

Three-Mile Point ΔPNdb Versus C_L and D/W

(For m=1, n=1, W_o/S=100)

point of future designs the air is clear; namely, to strive for high C_L without significant attendant increase in drag. Plots shown in Figure 54 may be used for trade-off studies relating C_L, D/W, and noise.

The noise advantage of using extended flap for the climb-out procedure is demonstrated in Figure 55, which shows ΔPNdb as a function of flap-setting angle for those flap designs that have the characteristics shown in Figure 52.

4.3.4 Effect of engine power cutback at the three-mile point.- By performing a power cutback when the airplane is over a noise-sensitive area, the level of noise exposure in that area can be significantly reduced. The noise reduction obtained depends on the amount of the power cutback which, in turn, depends on the airplane characteristics and the rate of climb desired after cutback. The ratio of post-cutback thrust to maximum take-off thrust is

$$\frac{T}{T_o} = \left[\frac{1}{T_o/W}\right]\left[\frac{D}{W} + \frac{R/C}{v}\right] \tag{105}$$

where T_o/W is the take-off power loading, R/C is the rate of climb desired after cutback, and v is the aircraft velocity. For safety reasons, it is generally required that a rate-of-climb of 500 feet per minute be maintained and that the aircraft velocity v not be reduced.

The term $\frac{R/C}{v}$ in Eq. (105) may be replaced by $\frac{0.01\ R/C'}{v'}$ if R/C is given in feet per minute and v' is given in knots.

It has already been shown in Section 2 how to obtain the amount of noise reduction associated with part-power engine operation (Eqs. (60) and (67)), and if Eqs. (60), (67), are combined with Eq. (105), the ΔPNdb function associated with power reduction in terms of airplane characteristics is obtained,

$$\Delta\text{PNdb (jet, } C\overline{B}) = -50 \log \left[\frac{1}{T_o/W}\right]\left[\frac{D}{W} + \frac{R/C}{v}\right] \tag{106}$$

$$\Delta\text{PNdb (fan, } C\overline{B}) = -25 \log \left[\frac{1}{T_o/W}\right]\left[\frac{D}{W} + \frac{R/C}{v}\right] \tag{107}$$

Figure 56 is a plot of T/T_o as a function of D/W, R/C, and v according to Eq. (105). The noise reduction due to power cutback for both the jet and compressor sources is also shown. It can be seen that for a typical jet transport with a power loading of about 0.30, a drag-to-ratio (D/W) of 0.12, and a speed of 200 knots, a noise reduction somewhere between 10 to 15db may be expected. With an increase in initial power loading the noise advantage of power cutback can be significantly improved. A more generalized presentation of T/T_o and ΔPNdb in terms of R/C, D/W, and F_o/W is shown in nomograph form in Figure 57.

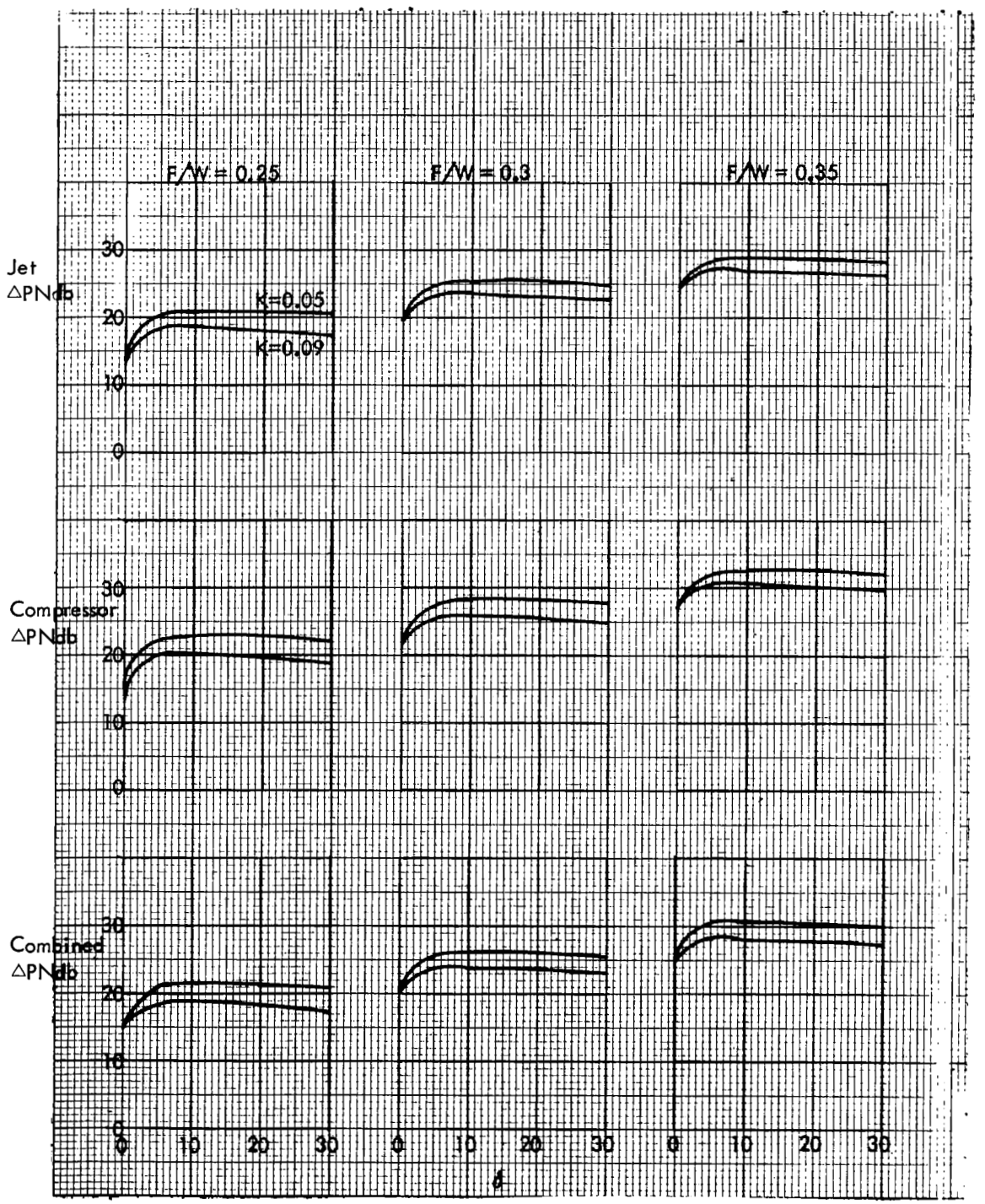

Figure 55

ΔPNdb Versus Flap Angle

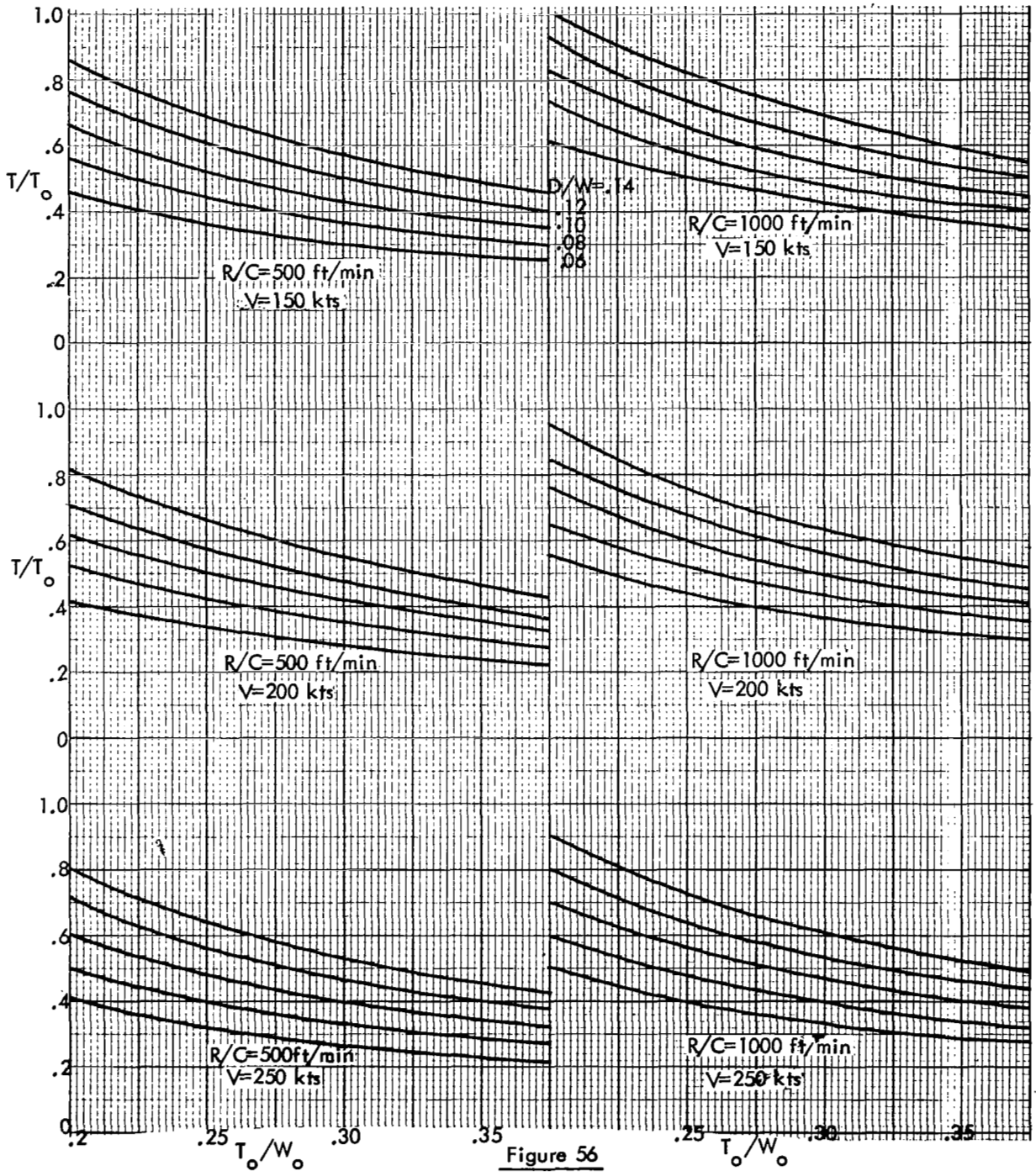

Figure 56

Thrust Cutback as a Function of D/W, R/C, and V

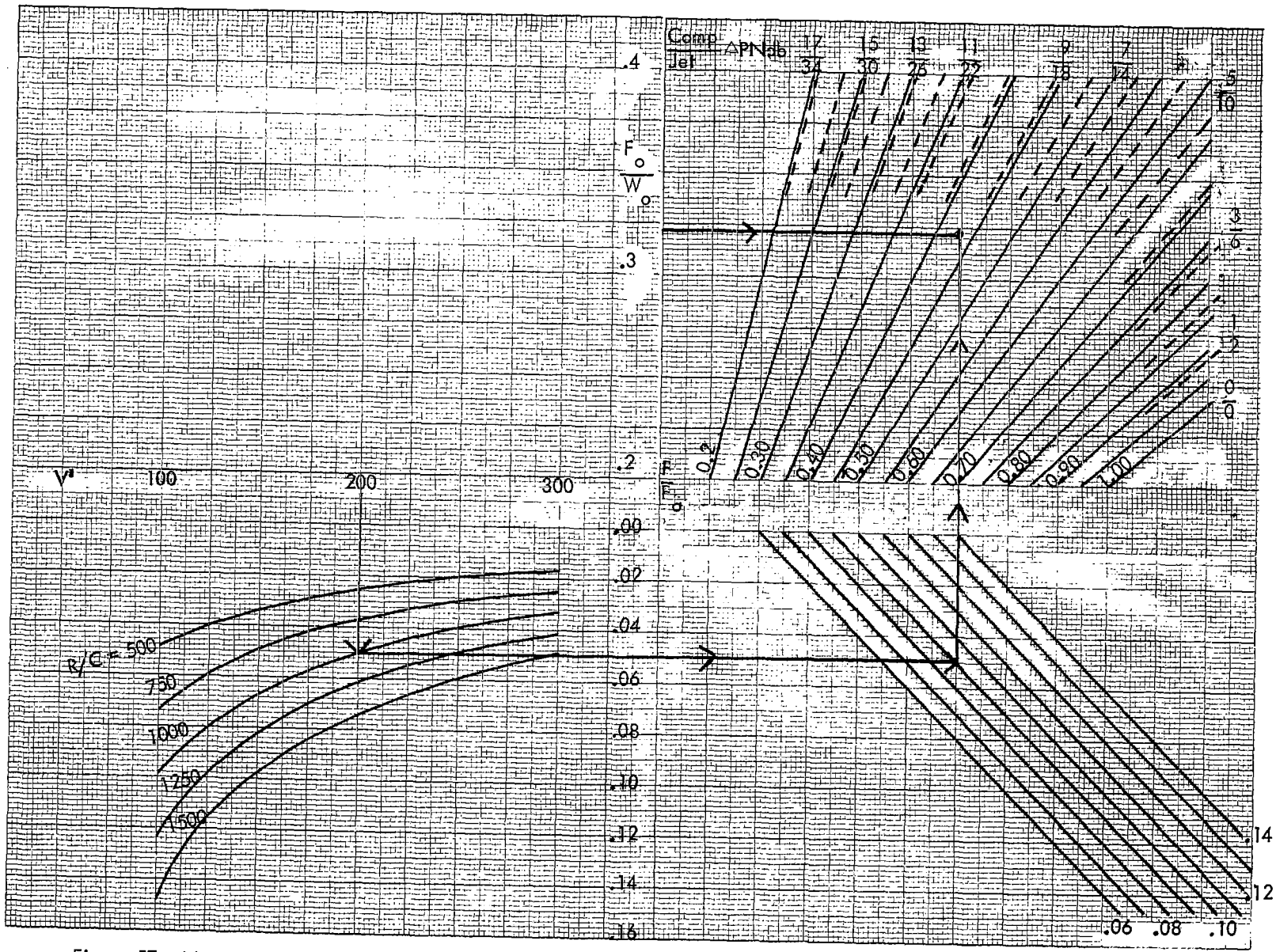

Figure 57 - Nomograph for Determining Power Cutback Capability and the Related PNdb Reduction for Jet and Fan Noise

Inspection of Eqs. (106) and (107) show that one can expect approximately a 2 PNdb and 1 PNdb reduction per ten-percent increase in initial power loading for jet noise and compressor noise, respectively.

In order to determine the noise level at the 3-mile point with the airplane performing a power cutback, the amount of $\triangle$PNdb associated with distance attenuation and power cutback is simply subtracted from the reference noise level. If the aircraft velocity v in Eq. (105) is considered to be equal to the V_2+10 climb-out velocity which is a function of W/S and $C_L^{\wedge}$ (Eqs. (96) and (97)), the total $\triangle$PNdb can be expressed in the general form,

$$\triangle\text{PNdb (total)} = \triangle\text{PNdb(H)} + \triangle\text{PNdb(CB)} = f\left[\frac{T}{W}, \frac{D}{W}, W/S, C_L, R/C\right] \qquad (108)$$

By the combined use of Eqs. (105), (106), (107), and (100), the $\triangle$PNdb (total) for various combinations of the four variables has been calculated and the results are plotted in Figure 58 for the special case of W/S = 100, and a post-cutback R/C = 500.

4.4 Landing Noise

The flight path of a typical aircraft landing approach is shown in Figure 59. The glide slope for a proper descent gradient is about three degrees and is intercepted by the straight and level flight path. The point of interception may vary from two and one-half to six miles from the runway threshold, depending on the particular airport or runway. Before intercepting the glide slope the aircraft is stabilized; that is, the landing gear is down, the flaps are in an approach configuration, and the power is set. At interception, flap extension is increased and the aircraft assumes the path coinciding with the glide slope. No appreciable thrust change is made and speed remains constant. This speed is about 1.3 stall speed in landing configuration, plus 10 knots.

The ground point for noise calculations is generally taken to be one mile from the runway threshold, and the altitude of the aircraft at this point when it is following the three-degree glide path is approximately 280 feet. For a given landing glide slope the noise level at the one-mile point depends primarily on the engine power setting, and the amount of power required for the airplane to stay at constant speed along the glide path depends on the drag-to-weight ratio, D/W, of the airplane at landing configuration and the aircraft speed. It may be written as

$$T = \left[\frac{D}{W} - \sin\gamma\right] W \qquad (109)$$

where W is the landing gross weight, and T is the total net thrust of the engines.

The ratio of landing thrust to take-off maximum thrust may be related to the take-off power loading, the ratio of landing to take-off weight, and the term $\left[D/W - \sin\gamma\right]$ in the following manner,

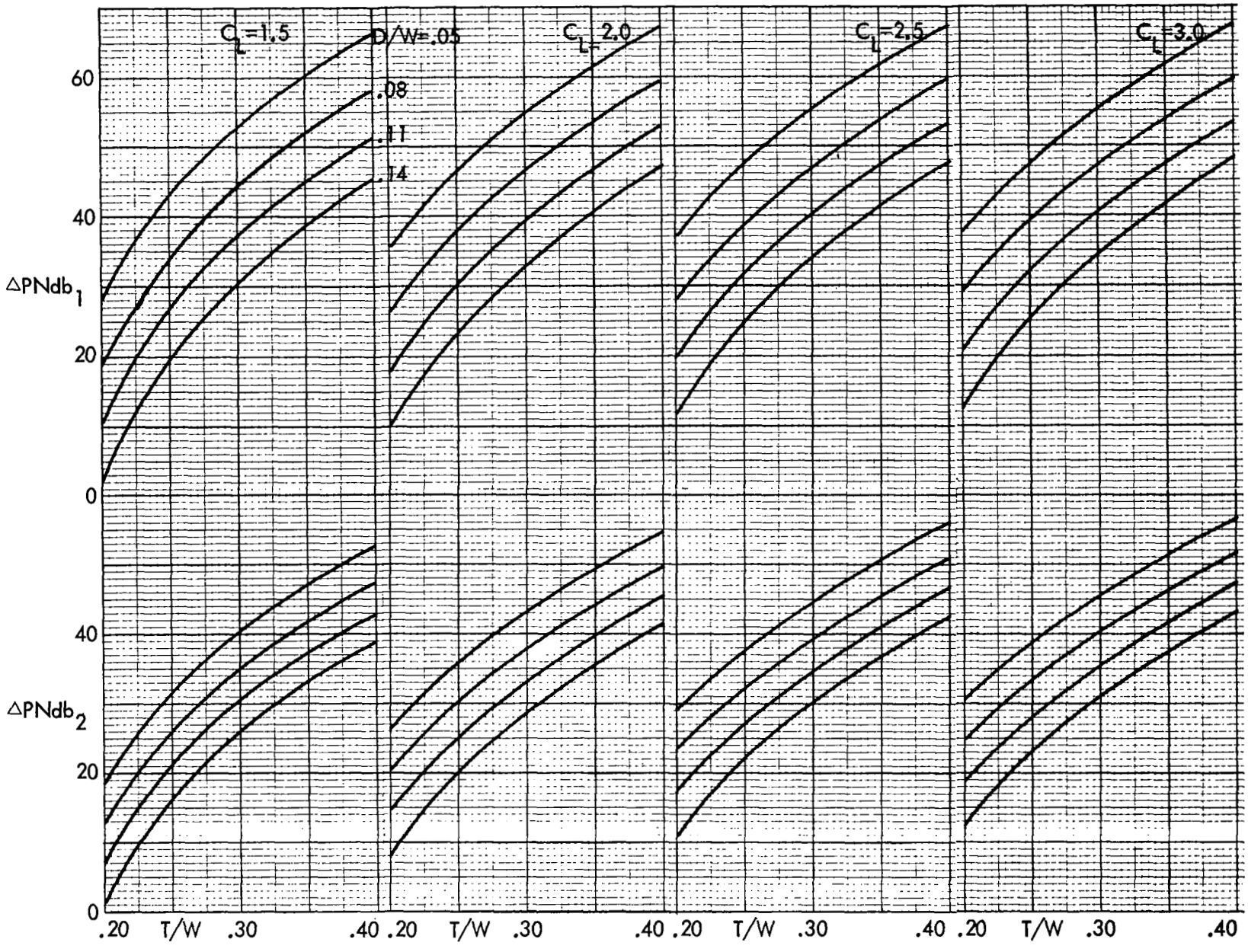

Figure 58 - $\Delta PNdb$ as a Function of T/W, D/W, and C_L ($\overline{RC}$=500, W/S=100)

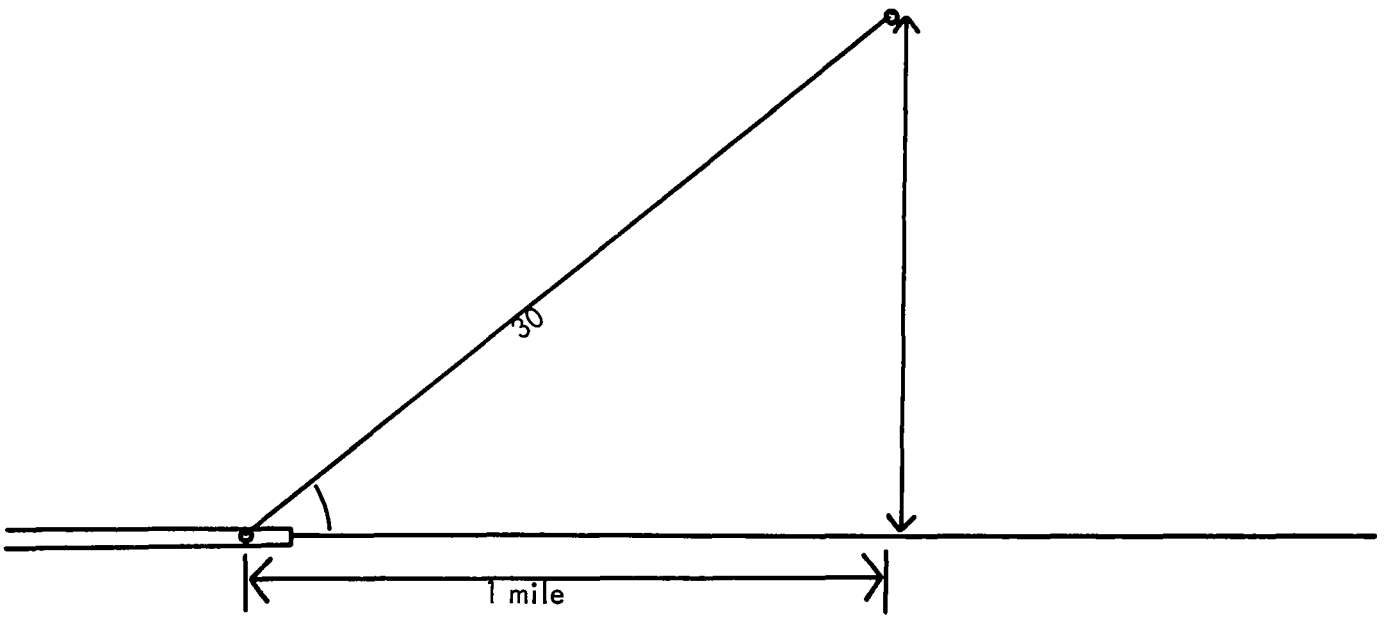

Figure 59

Landing Approach Schematic

$$\frac{T}{\bar{T}} = \frac{W}{W} \times \frac{1}{T_o/W_o} \left[\frac{D}{W} - \sin\gamma\right] \qquad (110)$$

where W/W_o is the ratio of landing to take-off gross weight and T_o/W_o is the take-off maximum power loading. The amount of thrust required during landing is generally on the order of 0.2 to 0.35 of the maximum take-off thrust, depending on the drag-to-weight ratio of the landing configuration and the low speed and landing-field requirements, and the landing weight of the aircraft.

The noise level under landing conditions may be determined by taking the engine reference noise level at the landing condition and subtracting a distance attenuation to allow for the distance between the reference distance of 200 feet and the minimum separation between the landing flight path and the observer.

If engine cycle or component design data for landing conditions are not available, the approximate relations developed in Section 2 for estimating the noise change due to part-power operation may be used together with Eq. (100) for making calculations. For minimum separation distance of less than a thousand feet, the $\triangle$PNdb(H) relations may be simplified by neglecting the term associated with $\frac{\beta H_o}{\sin\epsilon}\left(\frac{H}{H_o} - 1\right)$. The following general relations may be written for calculating the maximum noise level at the one-mile point.

$$\text{Jet:} \quad \text{PNdb (1-mile landing)} = \text{PNdb}_o \text{ (max take-off)} - 50 \log\left(\frac{W}{W_o}\right) \times \left(\frac{1}{T_o/W_o}\right)\left[\frac{D}{W} - \sin\gamma\right] - \alpha \log\left[\frac{5280 \times \sin\epsilon}{200}\right] \qquad (111)$$

$$\text{Compressor:} \quad \text{PNdb (1-mile landing)} = \text{PNdb}_o \text{(max T.O.)} - 50 \log\left(\frac{W}{W_o}\right)\left(\frac{W_o}{T_o}\right)\left[\frac{D}{W} - \sin\gamma\right] - \alpha \log\left[\frac{5280 \times \sin\epsilon}{200}\right] \qquad (112)$$

where γ is the glide slope, and the α for jets and compressors are found in Table 2 of Section 3.

The effects of W/W_o, T_o/W_o, and D/W on the total $\triangle$PNdb (last two terms of the two equations above) associated with partial power conditions and distance attenuation are shown in Figure 60 for both the jet and for compressor noise cases. Several observations may be made: (1) the effects of the design variables are much smaller on the fan compressor sound than on the jet noise; (2) the magnitude of the $\triangle$PNdb (total) is also relatively small for the compressor sound; and (3) because the distance between the aircraft and the observer during landing is not dictated by the airplane design, the noise reduction that is obtained from airplane aerodynamic improvements is much smaller for the landing condition than can be obtained for the take-off condition.

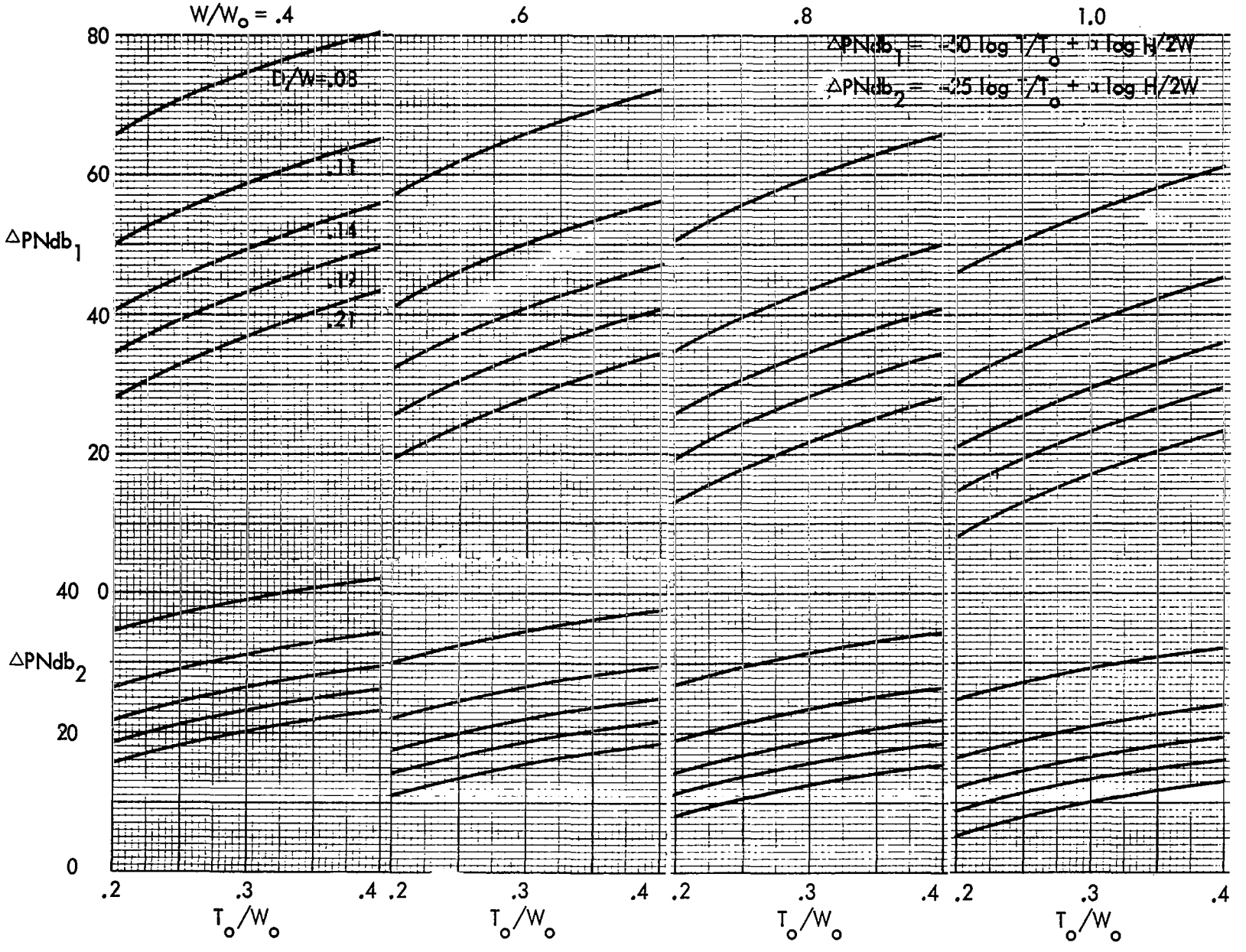

Figure 60 - ΔPNdb Versus W/W$_o$, T$_o$/W$_o$, and D/W

5. ANALYSIS OF AIRCRAFT FLY-OVER NOISE

5.1 Introduction

The following section describes two methods of determining the PNdb of an aircraft at selected positions on the ground. The first method is graphical, and gives a quick and simple procedure for determining the time, history, and magnitude of PNdb levels at selected ground points. The second method is an analytical method giving the same answers, but in a form suitable for computer applications. Of central importance in the graphical method is the concept that the aircraft noise field may be considered as fixed, and that the ground observer can be considered as moving relative to the stationary aircraft and its noise field. Thus, different observer points and flight paths may be represented by properly oriented flight paths drawn onto noise-contour maps of the aircraft. The analytic method utilizes the concept of the angle of maximum radiation and distance of closest approach to determine the maximum PNdb that a ground point experiences. By means of these concepts, a computer program has been written and used to determine the contours of constant PNdb produced by various take-off procedures. Also, by use of generalized vector equations, the time history of specified observation points was programmed.

5.2 Graphical Method

Consider a plot of the noise fields of an aircraft consisting of a series of constant-level profiles drawn around the origin in three-dimensional space. Since the noise field is axially symmetric, surfaces of constant level are surfaces of revolution about the roll axis of the aircraft, and the noise field can be described completely by a plane through the aircraft roll axis on which are shown the contours of constant level. The level at a particular ground point in the noise field can be obtained by locating it on the plot by means of its coordinates of slant range and bearing angle relative to the aircraft axis, and the track or apparent movement of the ground point through the noise field can be drawn on a two-dimensional plot as a function of range and bearing of the point. By placing time marking on the track the time history can be developed.

Figure 61 illustrates a typical take-off flight path. To visualize the development of the two-dimensional track plot, it is necessary to imagine how a fixed point on the ground appears to an observer in the aircraft. In Figure 61 at the start, the ground-observation point will be in line with the runway and several miles from the start of the ground roll. Thus, the ground point appears to the observer to be approaching along the aircraft axis. At rotation, the aircraft pitches upward, which causes the ground point to rotate down, as seen by the observer. Thus, the pitch maneuver, if negotiated quickly, can be projected on the plot as an instantaneous rotation of the ground point at constant range. The aircraft then continues to climb at a constant rate and this is a straight line parallel to the axis of the aircraft on the noise plot. In this case, with now yaw and the observer on the flight path, the closest approach of the aircraft and observer is given by

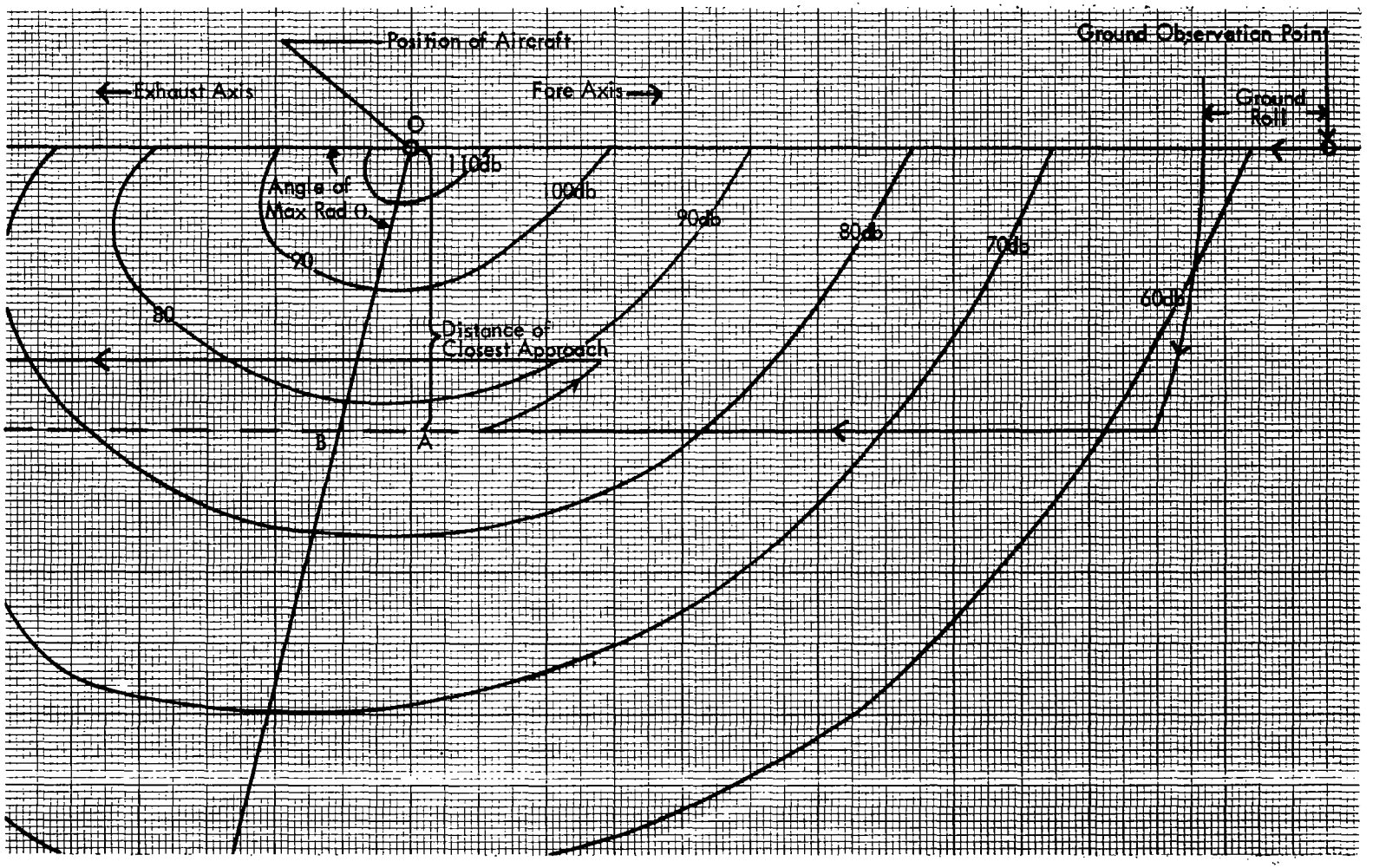

Figure 61 - Ground-Track Plot of Aircraft Take-Off

$$H = (S - Y) \sin \gamma \tag{113}$$

where S is the initial distance between the aircraft and observer
Y is the ground-roll distance
γ is the pitch angle.

As can readily be visualized, due to the axial symmetry of the noise field around the aircraft, any straight-line flight path will resolve itself into a straight line parallel to the aircraft axis on the noise plot, and each such segment of straight-line flight will have a corresponding distance of closest approach. This fact has been used to simplify the noise analysis, and its use is outlined in the following section and in Section 3.4.

The effects of a power cutback are also shown in Figure 61. As can be seen, before the track reached the point of closest approach and the point of maximum PNdb, a rotation at constant slant range has been shown. This corresponds to the downward pitch of the aircraft at power cutback. In this illustration it has been assumed the power cutback would lower the PNdb values of the contour by 10 PNdb; this is indicated by the dotted sections showing the after-cutback values of the PNdb contours. From such a diagram, if the flight velocity is known, the complete time history of the observation point can be constructed. The main difficulties in using this method are in calculating the exact angle of rotation to use on the graph when the aircraft is airborne, when yaw is involved, or when the observation point is off the flight path.

Calculation of the angle of rotation to be used on the graph or alternately the calculation of the distance of closest approach can be done with the following formulas and referring to Figure 62.

$$\cos B = \frac{(X_o - X) \cos \alpha \cos \gamma + (Y_o - Y) \sin \alpha \cos \gamma - h \sin \gamma}{\sqrt{(X_o - X)^2 + (Y_o - Y)^2 + h^2}} \tag{114}$$

$$|\bar{R}| = \sqrt{(X_o - X)^2 + (Y_o - Y)^2 + h^2} \tag{115}$$

$$H^2 = (X_o - X)^2 + (Y_o - Y)^2 + h^2 \left[(X_o - X) \cos \alpha \cos \gamma + (Y_o - Y) \sin \alpha \cos \gamma - h \sin \right]^2 \tag{116}$$

where X_o, Y_o is the observer position

X, Y, h is the aircraft position

α is the yaw angle

γ is the pitch angle

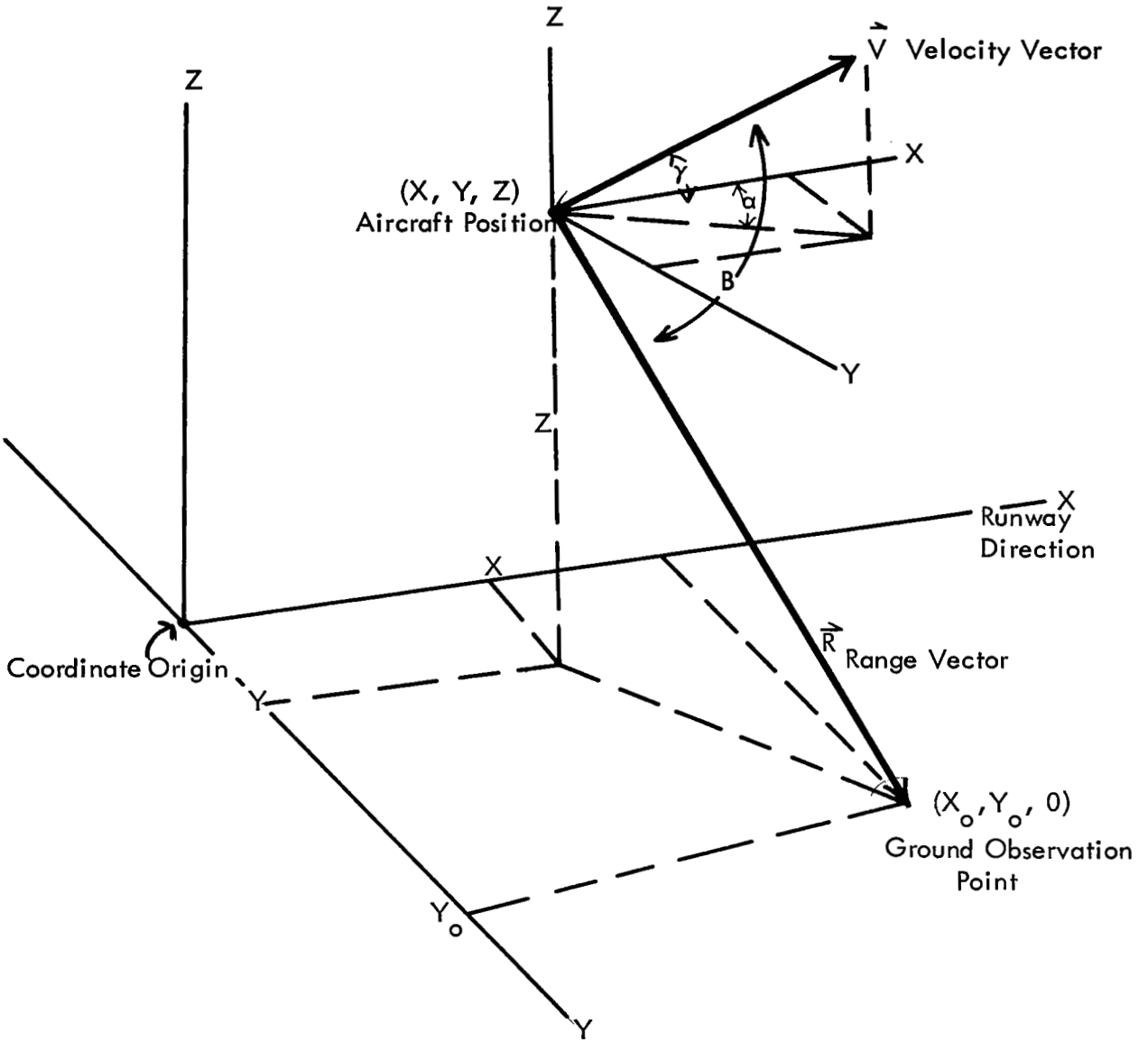

Figure 62

PNdb Contour Geometry

B is the angle between the line connecting the observer to the aircraft and the aircraft flight axis

R is the slant range to the aircraft

H is the distance of closest approach.

Note: As a general point of convenience, pick the coordinate origin at the start of the ground roll and the X axis in line with the runway direction. Any point may be used, but unnecessary complexity results.

As a guide to the construction, the following sheet has been prepared (Figure 63). With this form, it is only necessary to note the coordinate at the end of a flight segment, calculation of which is simple. As an illustration, several commonly-occurring cases will be considered. In all these cases, the following conditions are assumed: that the runway is 10,000 feet long, that the ground roll is 8,000 feet long (starting at the beginning of the runway), that the beginning of the runway is the coordinate starting point with the X axis along the runway, that the aircraft velocity is 234 ft/sec (including any power cutback sections), and that the observation point is three miles from the end of the runway on the X axis.

Case 1: Simple Take-Off

Rotation 10°

$\cos B = \cos \gamma$

This would be plotted as a simple rotation of 10 degrees occurring at the end of the take-off roll and a straight line plotted at a distance of

$H = (X_o - X) \sin \gamma$, where $X_o = 25840$ feet

$X = 8000$ feet, $\gamma = 10^{\circ}$

$H = 3100$ feet

Case 2: Simple Take-Off with Cutback

Rotation on take-off: 10°

Cutback at two miles from end of runway

Rotation on cutback: 5°

Again on take-off, the first segment of the flight would have a rotation of 10 degrees and an H of 3100 feet at the cutback point, the aircraft would have a height given by $h = \ell \tan \gamma$, where ℓ is the distance between the take-off point and the cutback point; thus, the height at the cutback point would be

SEGMENT						
α , DEG						
γ , DEG						
X , FT						
Y , FT						
H , FT						
$\lvert\vec{V}\rvert$, FPS						
SIN α						
COS α						
SIN γ						
COS γ						
X_o						
Y_o						
X_o - X, FT						
Y_o - Y, FT						
COS β						
β , DEG						
$\lvert\vec{R}\rvert$						
TIME IN SEGMENT, SEC						
$\Delta \lvert\vec{V}\rvert$, FPS						
DISTANCE ON SEG, FT						
Δ X, FT						
Δ Y, FT						
Δ H, FT						

Figure 63

Flight Path Calculation Form

$$h = (X_o - X) \tan 10$$

$$h = \left[20{,}560 - 8000\right] \tan 10 = 2180 \text{ feet}$$

Before rotation, the bearing angle of the aircraft would be

$$\cos B = \frac{(X_o - X)\cos\gamma - h \sin\gamma}{\sqrt{(X_o - X)^2 + h^2}}$$

or

$$\cos B = \frac{\left[25840 - 20560\right] \cos 10^\circ - 2180 \sin 10^\circ}{\sqrt{(25840 - 20560)^2 + (2180)^2}} = 0.844 \qquad (114A)$$

$$B = 32.5^\circ$$

This calculation is made so that with the sideline DI (Section 3.5) and H, the PNdb can be calculated if the plot is not considered sufficiently accurate.

After the cutback rotation, the same formula is used, with the result that the aspect angle is changed to

$$\cos B = 0.887$$

$$B = 27.5^\circ$$

At the same time, the slant range would be given by Eq. (115) as

$$R = \sqrt{(25840 - 20560)^2 + (2180)^2} = 5710 \text{ feet}$$

The distance that the aircraft covered to the cutback point would be

$$\text{Distance on flight segment} = 12560/\cos 10^\circ = 12750 \text{ feet}$$

Thus, to plot the rotation upon cutback, either measure 12750 scale feet along the flight track and make a five-degree rotation around and at a constant distance from the aircraft position (which is stationary). An alternative method is to set a compass at a scale distance equal to the slant range and draw a circle centered on the aircraft position. Where the circle intersects the line-of-flight (as traveled by the observer) is the point of rotation. Note that the angle to the stationary aircraft axis is equal to the angle calculated for the end of the segment as given by Eq. (114). On the graphical track, rotate five degrees toward the stationary aircraft axis. Then draw a line parallel to the aircraft axis completing the flight track. At the same time, the PNdb contours would be relabeled to reflect the lowering of the source PNdb due to the power cutback. This rotation would bring the closest approach distance to

$$H^2 = \left[X_o - X\right]^2 + h^2 - \left[(X_o - X)\cos\gamma - h\sin\gamma\right]^2$$

$$H^2 = \left[X_o - X\right]^2 \sin^2\gamma + h^2\cos^2\gamma + (X_o - X)\, h\cos\gamma\sin\gamma \qquad (116A)$$

$$H = \left[X_o - X\right]\sin\gamma + h\cos\gamma$$

$$H = 2631 \text{ feet}$$

In both of the above cases, the distance on the track is the total distance covered by the aircraft. Thus, the time history of the noise as seen by the observer can be marked on the track by simply calculating the time with

$$t = \frac{d}{v}$$

Case 3: Simple Take-Off with Yaw

Rotation on Take-Off: 10°

Yaw: 25°

On take-off, the rotation and yaw give a total bearing angle of

$$\cos B = \cos\alpha\cos\gamma$$

$$\cos B = 0.893 \qquad (117)$$

$$B = 26.8^\circ$$

Thus, at the take-off point of 8000 feet, the rotation on the plot should be 26.8 degrees. In this case, H is given by

$$H = \left[X_o - X\right]\left[1 - \cos^2\alpha\cos^2\gamma\right]^{1/2} \qquad (116B)$$

or $H = 8050$ feet

Case 4: Take-Off with Yaw and Rotation, Followed by Cutback with Yaw and Rotation

Rotation on Take-Off: 10°

Yaw: 25°

Cutback at two miles from lift-off

Rotation at cutback: 5°

Yaw: 35°

Since this is the most complex of the cases, we will fill out the form given in Figure 63. The completed form is shown in Figure 64.

At lift-off, the rotation is the same as Case 3, and the rotation on the plot is 26.8 degrees. A somewhat lengthy calculation is needed to determine the point on the graph at which to draw the next rotation. First, note that the cutback point is located at a distance of two miles from the lift-off; thus, the increment in X is given by

$$\Delta X = 10560 \cos\alpha = 10560 \cos 25 = 9560 \text{ ft}$$

$$\Delta Y = 10560 \sin\alpha = 4460 \text{ ft}$$

The actual distance covered on the graphical track is

$$\text{Distance on segment} = 10560/\cos\gamma = 10720 \text{ ft}$$

The height at the cutback point is

$$h = 10560 \tan\gamma = 1860 \text{ ft}$$

The slant range is

$$|R| = \sqrt{(8280)^2 + (4460)^2 + (1860)^2} = 9580 \text{ ft} \qquad (115)$$

and the bearing angle is given by

$$\cos B = \frac{(X_o - X)\cos\alpha\cos\gamma + (Y_o - Y)\sin\alpha\cos\gamma - h\sin\gamma}{\sqrt{(X_o - X)^2 + (Y_o - Y)^2 + h^2}} \qquad (114)$$

$$\cos B = \frac{8280.0.906.0.958 - 44600.4225.0.985 - 1860.0.1738}{\sqrt{(8280)^2 + (4460)^2 + (1860)^2}}$$

$$\cos B = 0.544$$

$$B = 57.1^\circ$$

Note that since Y_o is zero, the $Y_o - Y$ term is negative. After rotation and yaw due to cutback,

$$\cos B = \frac{8280 \cos 35 \cos 5 - 4460 \sin 35 \cos 5 - 1860 \sin 5}{\sqrt{(8280)^2 + (4460)^2 + (1860)^2}}$$

$$\cos B = 0.422$$

$$B = 65^\circ$$

and $H = 8680$ ft

A graph can now be constructed. First, at the 8000-ft point, a 26.8-degree rotation is made and a line parallel to the aircraft axis is drawn. This line should be 8050 scale feet

SEGMENT	Start of 1	End of 1	Start of 2			
α , DEG	25	25	35			
γ , DEG	10	10	5			
X , FT	8000	17560	17560			
Y , FT	0	4460	4460			
H , FT	0	1860	1860			
$\lvert\vec{V}\rvert$, FPS	234	234	234			
SIN α	0.4225	0.4225	0.874			
COS α	0.906	0.906	0.82			
SIN γ	0.1738	0.1738	0.0873			
COS γ	0.985	0.985	0.996			
X_o	25840	25840	25840			
Y_o	0	0	0			
X_o - X, FT	17840	8280	8280			
Y_o - Y, FT	0	-4460	-4460			
COS β	0.893	0.544	0.422			
β , DEG	26.8	57.1	65			
$\lvert\vec{R}\rvert$	17840	9580	9580			
TIME IN SEGMENT, SEC	0	45.9	0			
$\Delta \lvert\vec{V}\rvert$, FPS	0	0	0			
DISTANCE ON SEG, FT	0	10720	0			
Δ X, FT	0	9560	9560			
Δ Y, FT	0	4460	4460			
Δ H, FT	0	1860	1860			

Figure 64

Sample Flight Path Calculation Form

from the aircraft axis. To locate the end of the first flight segment, two methods can be used. The first and most desirable is to measure 10720 scale feet along the track on the graph. This is the distance on the segment section of Figure 64, and marks the point at which the power cutback rotation should be made. The second method is to place a compass at the stationary aircraft position on the graph and measure 9580 scale feet on a circle around the aircraft. This is the slant range R calculated in Figure 64. Where this circle intersects the flight track marks the position of the cutback rotation. At this slant range a rotation of 7.9 degrees away from the aircraft axis is made, and another line parallel to the aircraft axis is drawn, finishing the flight. The second flight segment is at a scale distance of 8680 feet from the flight axis. This can be used to check the accuracy of the graphing. Next, reduce the PNdb contour to reflect the power cutback.

The above four cases illustrate the techniques necessary to use the graphical methods. In summary, if there are multiple segments to the flight pattern, then it is necessary to calculate B, R, H, and the distance along each segment of the flight to construct the graph. For this purpose, it is necessary to use the form shown in Figure 63 and the Eqs. (114), (115) and (116). In special cases, the shorter equations developed in the examples can be used.

To summarize the properties of the graphical method:

A. The two-dimensional noise field is drawn as an overlay for the appropriate powerplant and power setting. This expresses the directivity pattern, as well as the sound level (SPL or PNdb) as a function of range and bearing from the aircraft.

B. Ground-roll is represented as a straight line along or parallel to the aircraft axis starting from the initial location of the ground observation point.

C. The take-off flight program is set up in terms of constant gradient climb or acceleration segments. Where necessary, these segments are bounded by instantaneous pitch or yaw maneuvers.

D. A constant climb angle flight segment is represented as a straight line which is parallel to the axis of the noise field and offset by the minimum closing distance between the ground point and the aircraft.

E. A pitch maneuver or yaw turn is represented as a change in bearing at constant range.

F. Distance along a flight segment is represented as displacement parallel to the axis of the noise field. By use of the flight velocity, the time history of the PNdb can be determined by placing time marks on the flight path.

Figure 65a represents the fixed space paths of an aircraft for climb angles of 5, 10, and 15 degrees. The time marks are derived from the velocity for each climb angle.

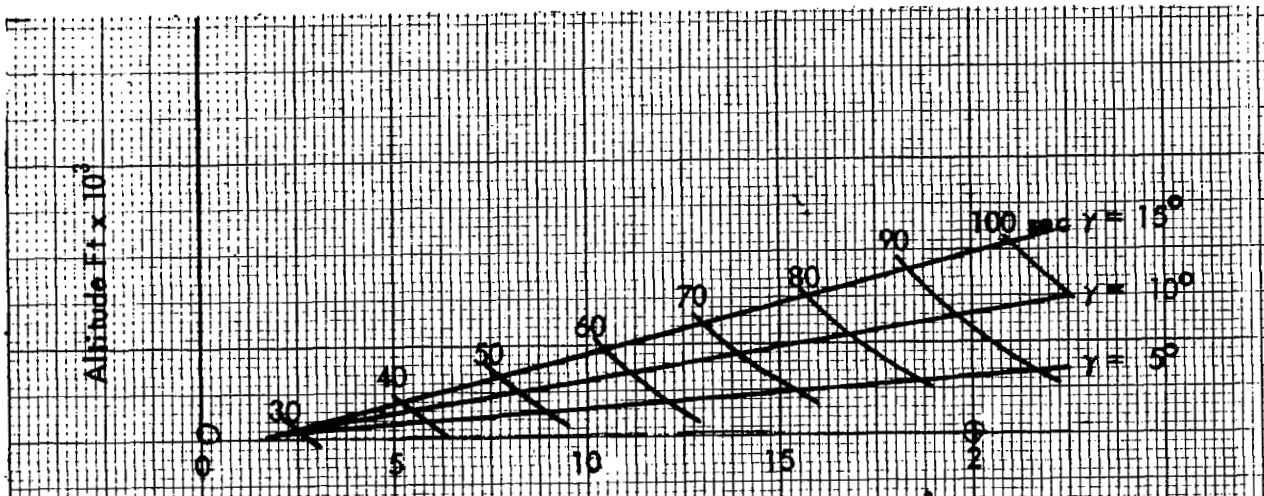

Figure 65a

Flight Paths

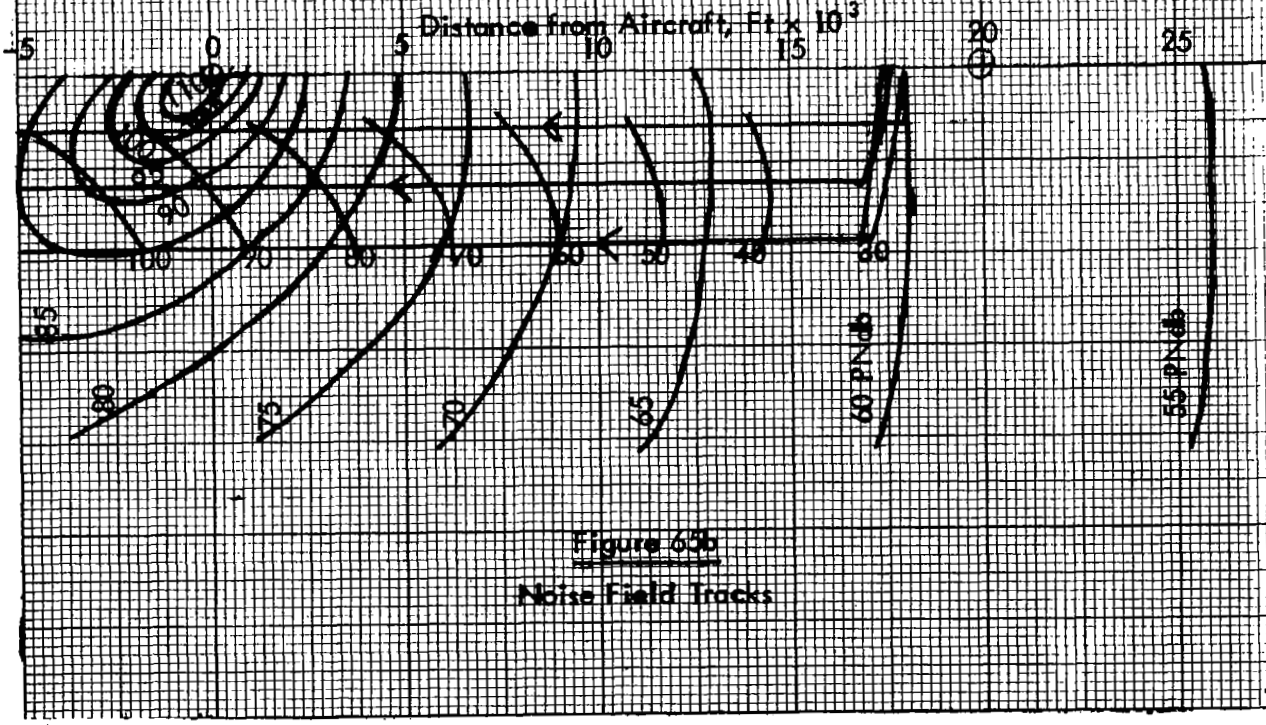

Figure 65b

Noise Field Tracks

Figure 65b shows the equivalent noise plot. By inspection it can be immediately seen that the maximum PNdb experienced at the ground point drops by 10 PNdb when the climb angle is changed to 10 degrees from 5 degrees. From the time markings the time history can be developed as shown in Figure 66. Figure 66 shows that the PNdb drops radically with the increase in climb angle, but that the time of exposure increases. By definition,

$$\text{Effective PNdb} = \text{PNdb max} + 10 \log \frac{\Delta T}{15} \tag{118}$$

and the effective PNdb is found to be,

Climb Angle	Effective PNdb
5°	106 PNdb
10°	102 PNdb
15°	101 PNdb

Thus, as the climb angle is changed from 5° to 15°, the maximum decrease in effective PNdb is 5 PNdb.

It can be seen from examining Figure 61 that all points experiencing the same maximum PNdb must follow the same time history. This follows from the nature of the flight paths. As can be seen, under constant climb angles all ground points will appear to describe lines parallel to the aircraft axis. Thus, if two separated points experience the same maximum PNdb, they all must lie on the same line and their noise level-versus-time plots must be the same. It follows, therefore, that all the points on a given constant PNdb ground contour will have the same level history. This simplifies the analysis considerably, as will be shown in the following section.

5.3 Analytic Method

This section will show the development of the equations used to predict the PNdb at any ground point and to determine the ground contours of constant PNdb. To do this, two central concepts must first be introduced; the distances of closest approach of an aircraft to an observation point, and the angle of maximum radiation. Both concepts are illustrated in Figure 61. The first concept refers to the offset distance of the flight path axis to the observation point, and is illustrated by the line Oa. Note that any flight path will have a segment parallel to the aircraft axis, and that a corresponding closest approach distance can be found. This closest approach distance has been and will be referred to as H.

The second concept of the angle of maximum radiation is illustrated by line OB in Figure 61. Note that this line passes through the points on the PNdb contours that are tangent to the parallel lines formed by the ground tracks. At this angle, the PNdb is a maximum for a given ground track, and is, thus, the angle of maximum radiation. With these two concepts, it will be shown that it is possible to completely specify the PNdb of an aircraft with two parameters; the angle of maximum radiation and the PNdb experienced at a given sideline distance, H.

Figure 66

PNdb Levels Versus Time

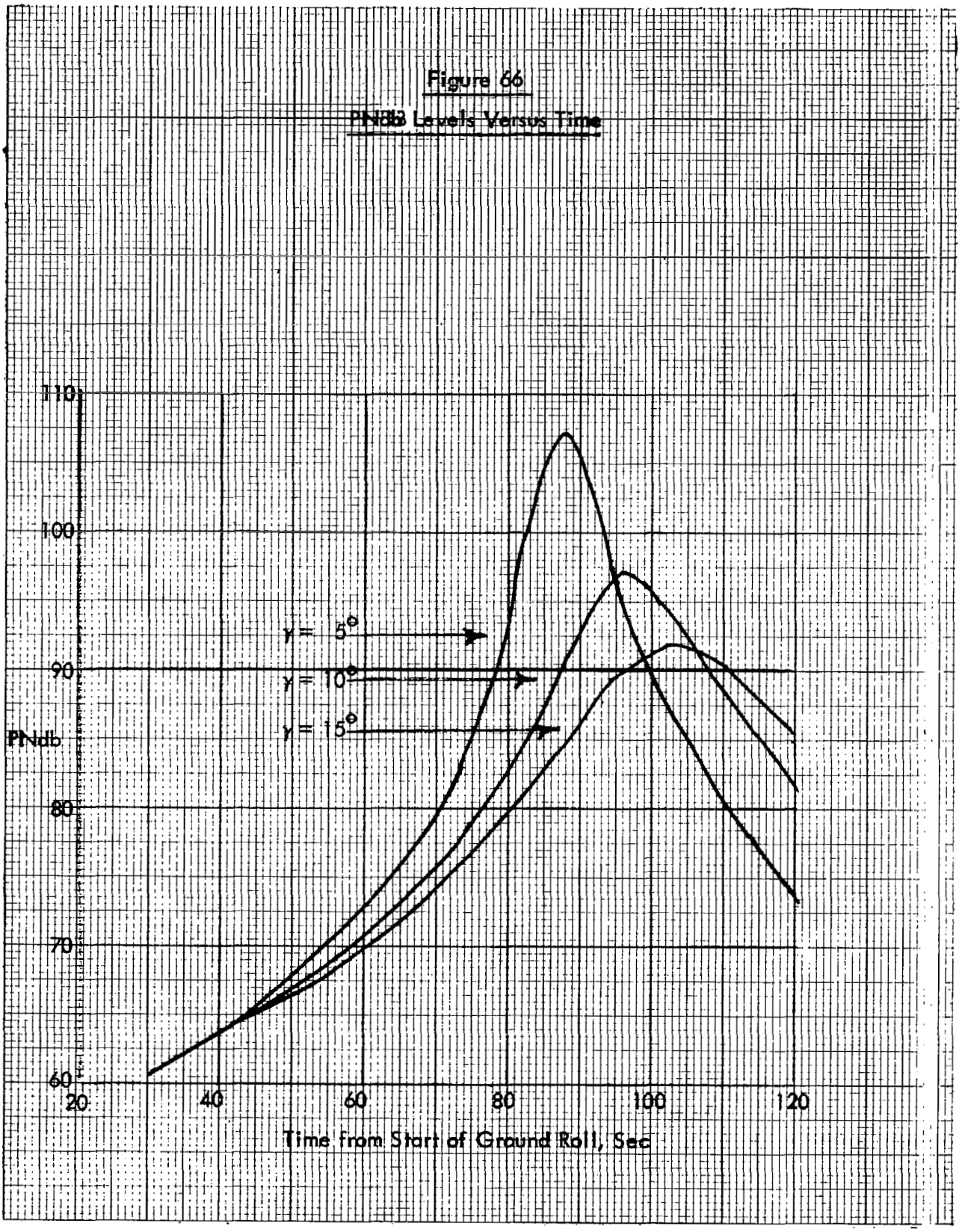

Due to the axial symmetry of the noise field, it is possible to define a cone of maximum sound intensity, as illustrated in Figure 67.

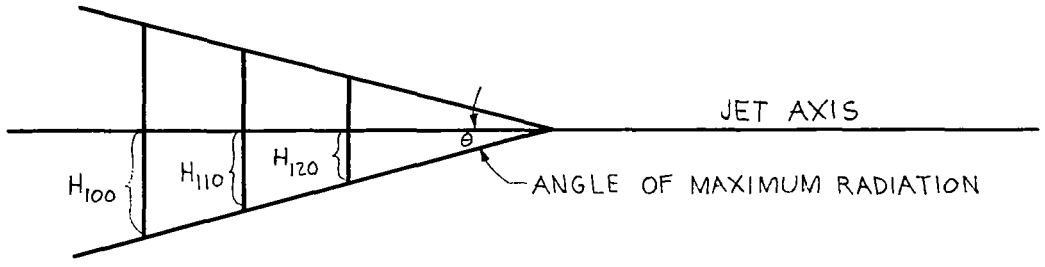

Angle of Maximum Radiation

Figure 67

θ is the angle of maximum radiation and the various H's are the closest approach distances for specified maximum PNdb. The problem reduces to simply determining the coordinates of the intersection of these circles with the ground plane. First, consider an aircraft that is in line with a coordinate system centered at the point where the aircraft flight path intersects the ground, as illustrated in Figure 68. (The general case where the coordinate system is not centered at the ground intersection point is developed later).

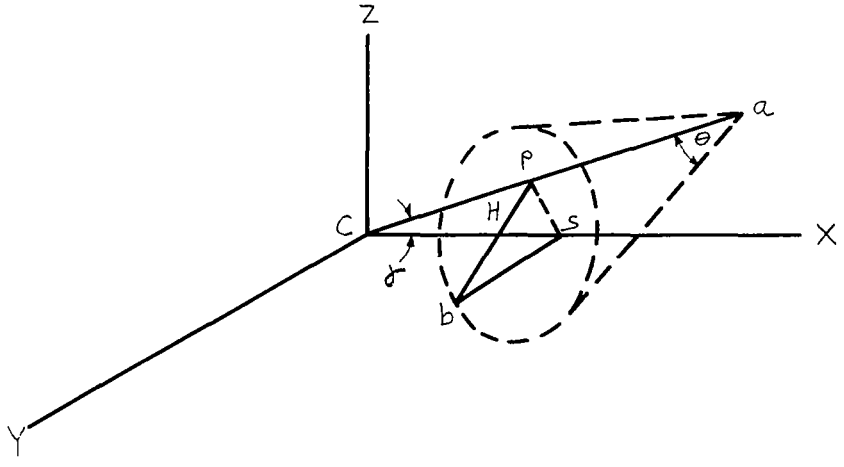

Flight Path Coordinate System

Figure 68

The X and Y coordinates of the point b are CS and Sb. The angle θ is the angle of maximum radiation, and the distance H is the distance from b to the flight path. Thus, if the distance ca is ℓ, then the distance CP is given by, $\ell - \frac{H}{\tan\theta}$, and since CS is CP/cos$\gamma$ and pS is CP tan γ,

then $$CS \text{ is } \frac{1}{\cos\gamma}\left[\ell - \frac{H}{\tan\theta}\right] \tag{119}$$

and $$pS \text{ is } \tan\gamma\left[\ell - \frac{H}{\tan\theta}\right] \tag{120}$$

As has been mentioned, CS is the X coordinate of b.

Next, consider that b lies on a circle of radius H; thus

$$H^2 = pS^2 + Sb^2 \tag{121}$$

and $$Sb = \sqrt{H^2 - \left[\tan\gamma\left(\ell - \frac{H}{\tan\theta}\right)\right]^2}\ , \tag{122}$$

which is the Y coordinate of b'. The coordinates of the point b are, thus,

$$\left.\begin{aligned} X &= \frac{1}{\cos\gamma}\left(\ell - \frac{H}{\tan\theta}\right) \\ Y &= \sqrt{H^2 - \left[\tan\gamma\left(\ell - \frac{H}{\tan\theta}\right)\right]^2} \\ Z &= 0 \end{aligned}\right\} \tag{123}$$

In these equations, ℓ is the only unknown, and is determined by the flight path of the aircraft. In this case (where the coordinate system is centered at the point where the aircraft flight path intersects the ground), it is given by

$$\ell = \frac{h}{\sin\gamma} \tag{124}$$

where h is the height of the aircraft.

To generalize these equations, that is, put them in a form so that any aircraft maneuver can be accounted for, assume a new coordinate system so that the aircraft flight path is located at an angle of α with respect to the new coordinates, as illustrated in Figure 69.

By referring to the new coordinates, it can be seen that the distance ca must be given by

$$ca = \frac{h}{\sin\gamma} \tag{125}$$

where h is the height of the aircraft.

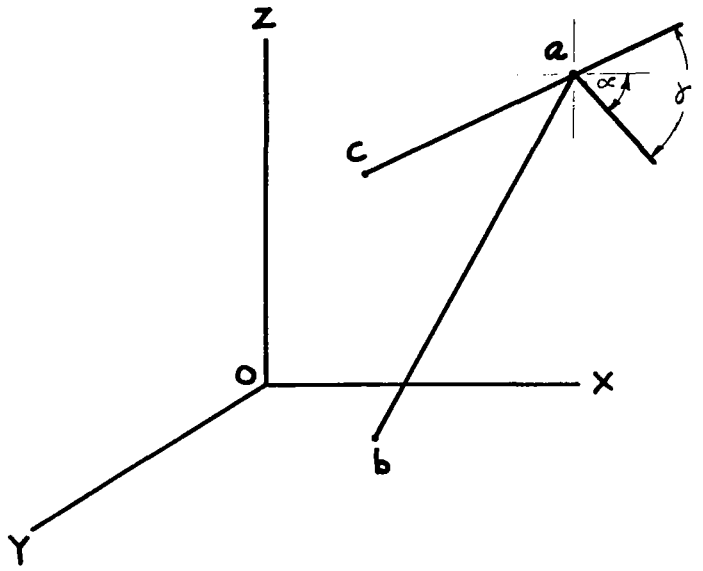

α rotation angle
γ climb angle
o, b, and c all lie in ground plane
c is the intersection of the flight path with the ground, and
b is the point where maximum noise intersects the ground.

Modified Coordinate System

Figure 69

The direction cosines of ca are cos γ cos α, cos γ sin α, sin γ , and the components joining c and a are,

$$ca = \begin{bmatrix} \frac{h}{\sin\gamma} & \cos\gamma\cos\alpha \\ \frac{h}{\sin\gamma} & \cos\gamma\sin\alpha \\ h & \end{bmatrix} \qquad (126)$$

The components of the vector joining the origin 0 to the point a are

$$\begin{vmatrix} X_1 \\ Y_1 \\ h \end{vmatrix}$$ the aircraft coordinates

Since the vector c that joins 0 and c is oa - ca,

$$c = \begin{bmatrix} X_1 - \frac{h}{\sin\gamma} \cos\gamma \cos\alpha \\ Y_1 - \frac{h}{\sin\gamma} \cos\gamma \sin\alpha \\ 0 \end{bmatrix} \tag{127}$$

It should be noted that c is the vector between the ground intersection of the flight path and the origin of the old coordinate system. In the general coordinate system, a transforming matrix giving the angle of rotation between the two coordinate systems can be formed; this transforming matrix is

$$R = \begin{vmatrix} \cos\alpha \sin\gamma & . \\ -\sin\alpha \cos\gamma & . \\ . \quad . & 1 \end{vmatrix} \tag{128}$$

The transpose of this matrix multiplied by the vector cb, and minus the vector c, gives the vector ob, or in matrix notation

$$ob = R'(cb) - c \tag{129}$$

where cb is given by

$$cb = \begin{bmatrix} \frac{1}{\cos\gamma} \left(\frac{h}{\sin\gamma} - \frac{H}{\tan\theta} \right) \\ \sqrt{H^2 - \left[\tan\gamma \left(\frac{h}{\sin\gamma} - \frac{H}{\tan\theta} \right) \right]^2} \\ 0 \end{bmatrix} \tag{130}$$

and R' (the transposed matrix of R) is given by

$$R' = \begin{vmatrix} \cos\alpha & -\sin\alpha & . \\ \sin\alpha & \cos\alpha & . \\ . & . & 1 \end{vmatrix} \tag{131}$$

This procedure breaks down when $\gamma = 0$, or in other words, when there is level flight since, in this case, the aircraft flight path does not intersect the ground.

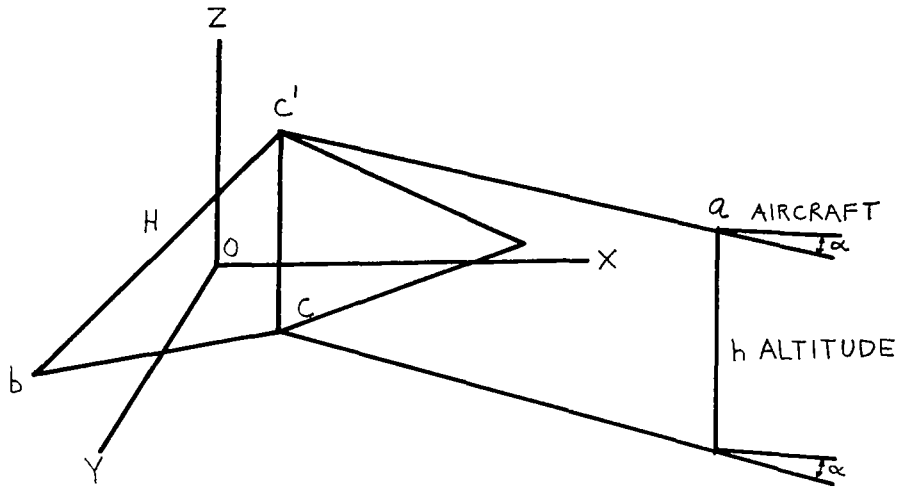

Geometry of Level Flight

Figure 70

Figure 70 illustrates the situation and the calculational procedure for considering the ground noise from level flight is developed below.

The point b is found by arranging the cone of maximum intensity so that its vertex is at the aircraft and its axis is along the flight path. The distance from the aircraft to the point c' is given by

$$c'a = H/\tan\theta \tag{132}$$

where θ is the angle of maximum radiation as defined earlier. Thus, the coordinates of the point c (in the ground plane) are

$$c = \begin{bmatrix} X_1 - \frac{H}{\tan\theta} \cos\alpha \\ Y_1 - \frac{H}{\tan\theta} \sin\alpha \\ 0 \end{bmatrix} \tag{133}$$

This is equivalent to the translation vector c defined previously. If a coordinate system is centered at the point c in the ground plane, the vector c to b is,

$$cb = \begin{bmatrix} 0 \\ \sqrt{H^2 - h^2} \\ 0 \end{bmatrix} \tag{134}$$

The translation matrix is the same as before, and the same matrix equation can be used.

$$ob = R'(cb) - c \tag{129}$$

As a result of these analyses, the form of the equal PNdb contour in the ground plane can be deduced. In the general case where there is a perceptible climb angle γ from the vector cb, the X and Y coordinates of the PNdb contour are

$$\left.\begin{aligned} X &= \frac{1}{\cos\gamma}\left(\frac{h}{\sin\gamma} - \frac{H}{\tan\theta}\right) \\ Y &= \sqrt{H^2 - \left[\tan\gamma\left(\frac{h}{\sin\gamma} - \frac{H}{\tan}\right)\right]^2} \end{aligned}\right\} \tag{135}$$

If the X equation is solved for h,

$$h = \sin\gamma\left(\cos\gamma\ X + \frac{H}{\tan\theta}\right) \tag{136}$$

and substituted into the Y equation,

$$Y^2 = H^2 - \sin^2\gamma\ X^2 \tag{137}$$

the following expression is obtained,

$$\frac{Y^2}{H^2} + \frac{X^2}{\frac{H^2}{\sin^2\gamma}} = 1 \tag{138}$$

This is the locus of the contour of equal PNdb, and is an ellipse with a minor axis of H and a major axis of $\frac{H}{\sin\alpha}$.

In the case of level flight,

$$Y^2 = H^2 - h^2 \tag{139}$$

and the X coordinates are determined by the end points of the flight.

With the above two sets of vector equations, the coordinates of points of equal PNdb can be found, and the use of these equations are illustrated in Section 6.

In the case where the PNdb time history at a given point is desired, the formulation given in Section 5.2 must be used. For convenience, the pertinent formulas are repeated. They are

$$\cos\beta = \frac{(X_o - X)\cos\alpha\cos\gamma + (Y_o - Y)\sin\alpha\cos\gamma - h\sin\gamma}{\sqrt{(X_o - X)^2 + (Y_o - Y)^2 + h^2}} \tag{114}$$

$$H^2 = (X_o - X)^2 - (Y_o - Y)^2 + h^2\left[1 - \cos^2\beta\right] \tag{116}$$

where the various quantities are as previously defined.

To use these equations, it is very important to note that β is measured from a line extending from the aircraft nose, and should be subtracted from 180 degrees to give the angle as measured with respect to the jet exhaust centerline.

The application of these equations is relatively simple. It is necessary to keep track of the aircraft coordinates, which is a matter of geometry (for examples, see Section 5.2), but once these quantities have been calculated, then the results of Section 3.4, giving PNdb as a function of sideline distance and sideline DI, can be used to calculate the PNdb at the point of interest. The aircraft position is then changed by the amount desired, and the process repeated.

As an aid to calculation, a conclusion of Section 5.2 is worth restating, and that is that for a given maximum PNdb, all points with the same maximum will have the same time history for a given flight path. The results of this section show that all points experiencing a given PNdb lie on an ellipse oriented around the aircraft. Thus, by using the results of the first part of this section to find the location of the ellipse, and the second set of equations to find the time history, it is relatively easy to draw the ellipses of effective PNdb along the flight path.

6. CALCULATION OF PNdb GROUND CONTOURS AND AREAS FOR VARIOUS FLIGHT PATHS

6.1 Introduction

This section illustrates the application of some of the tools developed in previous sections to the prediction of ground noise produced by various flight paths. The inherent complexity of possible flight operations make flight-path optimization a difficult task, and is beyond the scope of this contract. However, from the relatively simple analysis carried out in the following sections, a few generalizations are immediately evident that show the kinds of information that can be obtained from such analyses. For example, it appears that the area experiencing a given PNdb is inversely proportional to the flight angle and that the steeper the flight angle is on take-off and landing, the less area is involved. It follows, therefore, that the steepest flight angles consistent with aircraft and flight regulations should be used during operations, since the area-reduction effect is greater than the effect of power-plant noise reductions at shallower flight angles. The analysis of landing noise that has been made supports this conclusion and also shows the distinct advantages of using a two-segment approach path.

It should be mentioned that in the analyses performed in this section it has been assumed that a complete flight path consists of a landing approach, a ground roll on take-off, and the airborne portion of the take-off.

6.2 Operation Zones

The complete landing/take-off sequence can be divided into three sections or zones of airport noise. These zones are: landing approach, ground roll for take-off, and the airborne portion of the take-off, and they have been selected because of the different acoustical characteristics associated with each zone. The landing portion of the flight sequence is made with the engines throttled back considerably; thus, the source level of the noise is lower than in the other zones. However, since the angle of approach is lower than the climb angle on take-off, the area affected by the noise is proportionally higher. The ground-roll portion of the flight, used to accelerate the aircraft to lift-off speed, is made at full power. However, since the aircraft is on the ground, there is additional ground-effect attenuation, so that the noise diminishes quite rapidly at increasing distances from the aircraft. The airborne portion of the take-off segment may consist of several parts. Usually it consists of a full-power, high-climb-angle segment followed by a lower power, lower climb angle, cutback segment, followed by an eventual resumption of full power. In this type of take-off, there is the highest noise source level, the engines are at full power, and there is the lowest attenuation and, thus, for the early portion of the flight, the area experiencing high sound levels is quite extensive. This is balanced by the high rate of climb which reduces the area rapidly. During the cutback portion of the flight, the source level is reduced. However, the climb angle also is reduced, thereby expanding the area experiencing a specific PNdb level. When full power is restored, the width of the area experiencing noise

rises, but since the aircraft has appreciable height and the climb angle is high, the total area is less than that produced during the original take-off portion of the flight.

These zones are illustrated in Figure 71, where the PNdb level contours have been plotted for several flight sequences. Figure 71 shows the simple case where the aircraft lands with a three-degree approach angle and takes off at full power with the maximum climb angle. The three zones can be clearly seen; the contours of the landing zone on the left are long in proportion to their width and their widths are smaller than the other zones. The short ground-roll zone consists of a series of parallel contours that are equivalent in length to the ground covered by the aircraft, while the take-off portion has the widest contours but, due to the climb angle, they are shorter in proportion to their length. Reasons for the shapes of these contours will be discussed in the following section.

6.3 PNdb Level Contours

This section illustrates the method by which PNdb level contours and PNdb at specific points are calculated. Calculations were made for a CV 880 aircraft, and contours were developed for a simple take-off sequency, a sequence involving a cutback in power carried out at three miles from the runway and continued till the sound is below the PNdb contour level, and a sequence involving a cutback in power at the three-mile point and a resumption of power at the ten-mile point.

In the analysis, it is assumed that there is a 10,000-foot runway with the aircraft landing point at the start of the runway and the ground roll beginning at the start of the runway. For ease of calculation, it is assumed that the flight path is in line with the runway. The maximum PNdb will be calculated at the 1500-foot sideline for the ground-roll segment, three miles from the end of the runway for the take-off segment, and one mile from the end of the runway for the landing segment.

The important aircraft parameters are:

CV 880

Thrust per engine	$F = 10,500$ lbs
Number of engines	$n = 4$
Weight with full fuel load	$W = 185,000$ lbs
Full thrust-to-weight ratio	$T_o/W_o = 0.23$
Drag-to-weight ratio	$D/W = 0.11$
Lift coefficient	$C_L = 2.5$
Wing loading	$W/S = 95$
Fundamental blade-passing frequency	$f_o = 2500$ cps
Jet $PNdb_o$ at 200-ft sideline	$PNdb_{oj} = 128.3$ PNdb
Compressor $PNdb_o$ (both of the above at full thrust)	$PNdb_{of} = 108.3$ PNdb

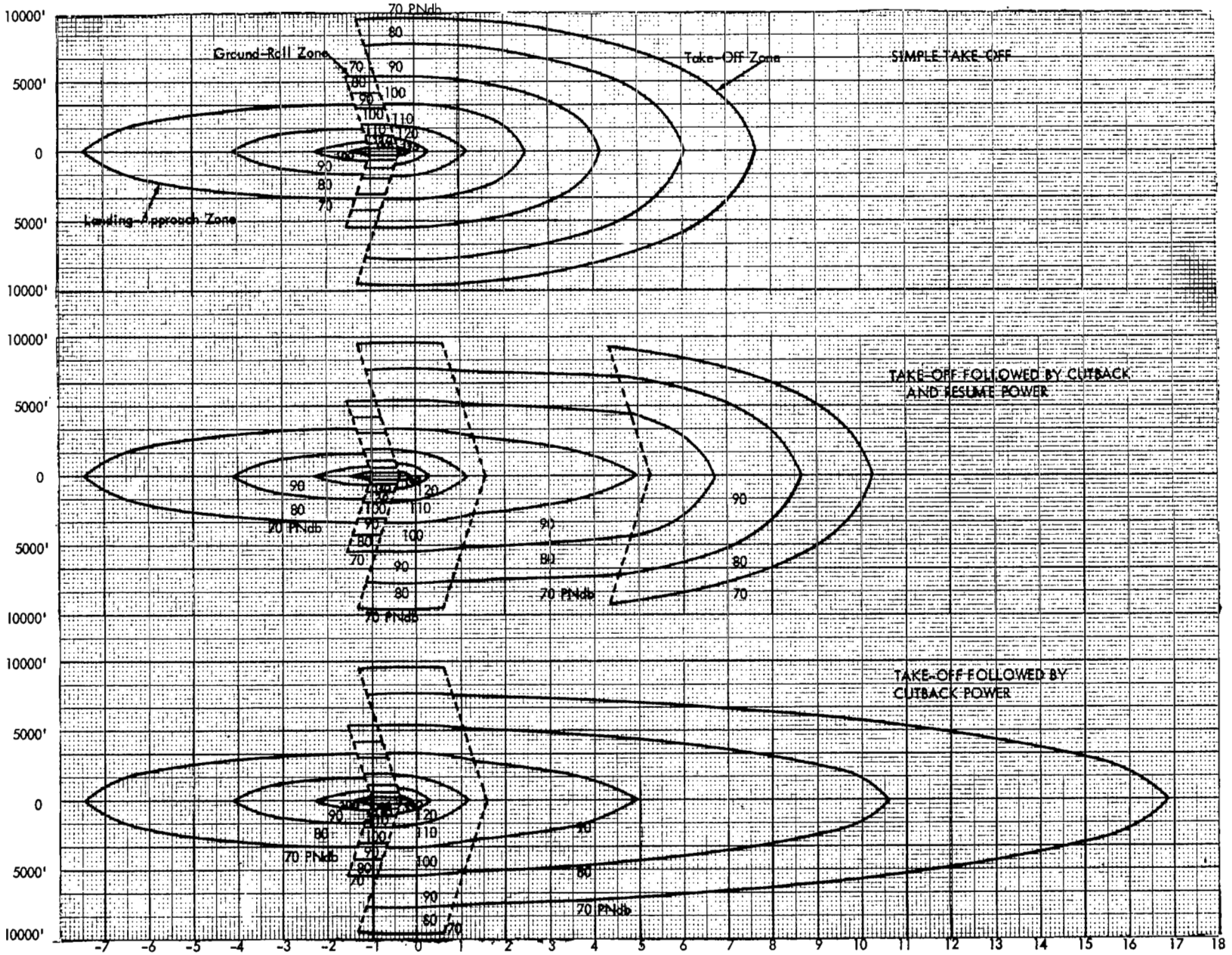

Figure 71 - PNdb Contours for Various Flight Patterns

For the combination of jet and compressor noise, the angle of maximum radiation is assumed to be at 45 degrees from the exhaust axis.

Weight ratio upon landing $W/W_o = 0.65$

The equations to be used to calculate the flight path and noise-source levels are:

Ground roll $S = 39 \left[W/S/T_o/W_o\right] C_{L\uparrow}$ (93)

Take-off climb angle $\gamma_o = \text{ARC SINE}\left[\frac{T_o}{W_o} - \frac{D}{W}\right]$ (88) (modified)

Thrust cutback during take-off $\frac{T}{T_o} = \frac{1}{T_o/W_o}\left[D/W + \frac{R/C}{60\ V}\right]$ (105) (modified)

where R/C is the minimum specified rate of climb after cutback, in our case, 500 feet per minute.

V is the minimum aircraft velocity given by $V = 1.31\sqrt{\frac{835\ W/S}{C_{L\uparrow}}}$ (97)

Cutback climb angle $\gamma_2 = \text{ARC SINE}\ \gamma\left[\frac{R/C}{60\ V}\right]$ (88) (modified)

Total thrust $T_o = nF$ (140)

Total full-power jet noise at 200-ft sideline $PNdb_{To} = PNdb_{oj} + 10 \log n$ (141)

Total full-power fan noise where n is the number of engines $PNdb_{TF} = PNdb_{of} + \log n$ (142)

Jet noise reduction due to cutback alone $\triangle PNdb_j = 52 \log \left[T/T_o\right]$ (60)

Fan noise reduction due to cutback alone $\triangle PNdb_f = 25 \log \left[T/T_o\right]$ (67)

Fan frequency after cutback $f = f_o \sqrt[3]{T/T_o}$ (143)

On landing, the thrust cutback is given by:

$$\text{Landing thrust cutback} \qquad T/T_o = \frac{1}{\frac{T_o}{W_o}} \left(\frac{W}{W_o}\right)\left[D/W - \sin \gamma 3\right] \tag{110}$$

where $\gamma 3$ is the landing approach angle and in the example, it is 3 degrees.

From Section 5.3 the coordinates of the points on the ground experiencing a given maximum PNdb for this case are given by

$$X = \frac{1}{\cos \gamma}\left[\frac{X_o}{\cos \gamma} - \frac{H}{\tan \theta}\right]$$

$$Y = \sqrt{H^2 - X^2 \sin \gamma} \tag{135 (modified)}$$

where X_o is the aircraft position measured from the point at which the line of the flight path touches the ground.

X is the X coordinate of the PNdb contours in the same coordinate system

γ is the climb or approach angle

θ is the angle of maximum radiation

H is the sideline distance to the PNdb level of interest

Y is the Y coordinate of the PNdb contour measured from the line of flight.

6.3.1 Ground roll.- The first contour calculations made are on the ground-roll segment of the flight. As the first step, the PNdb of the fan and jet are calculated using Eq. (98), and the combined value of the noise is determined from Figure 21. This value was found to be 134 PNdb. Since the aircraft is on the ground, the on-ground values of α and β are used for the $\triangle$PNdb calculation. Also, since the fundamental blade-passing frequency is 2500 cps (with little error), the 45-degree angle plot of band 6 noise showin in Figure 33 can be used. To use this plot, first the $\triangle$PNdb between the contour level of interest and the source level is calculated. By following the curve for the appropriate band of noise, the sideline distance ratio for the contour can be found. From this, the actual sideline distance can be calculated. The X and Y coordinates of the start of the PNdb contours are then calculated using a modified form of Eq. (135); the length of the ground roll is calculated from Eq. (93), and the X and Y coordinates of the ends of the contours are determined. These two sets of points are sufficient to draw the contours since γ is 0 and the Y coordinates are constant. These points are plotted on the graph and connected by straight lines. By using Eq. (100), the $\triangle$PNdb to the 1500-foot sideline is calculated and subtracted from

the source level PNdb. This gives 101.6 PNdb at the 1500-foot sideline and completes the calculations necessary for the ground-roll segment.

6.3.2 Simple take-off.- The simple take-off pattern is one in which the aircraft takes off at the maximum possible climb angle and maintains this climb until the sound is below the PNdb contour level being calculated. The flight path intersects the ground at the end point of the ground roll. In the calculation of the contours, this point is specified as the zero of the coordinates, and this coordinate system is called the flight path coordinate system. Since the engines are still at full power, the source level used for the ground roll can be used. However, the aircraft is now airborne, so that it is necessary to use the in-flight $\triangle$PNdb curves to calculate the contour sideline distances. Following the same procedure as for the ground roll, but using Figure 29 , the new set of sideline distances are calculated. Using Eq. (135, modified), the new X and Y corrdinates are calculated with the aircraft at its zero coordinate position. Then the extreme point of the ellipse is calculated using

$$X = H/\sin\gamma \tag{144}$$

This follows from the nature of Eq. (138). The furthest extent of the ellipse occurs when Y is zero. Solving for X (H and γ known) gives two points on the ellipses. It then is necessary to calculate several other points between these to give the shape of the ellipses. One convenient point is the one where X equals zero. At this point, the ellipse is widest and equal to the sideline distance. Once this is done, the ground-roll distance is added to the calculated X's. This returns the contour coordinates to the original coordinate system and they can then be plotted on the graph. To calculate the maximum PNdb at the three-mile point, it is necessary to note that the maximum PNdb experienced would be given by the contour ellipse that ends at the three-mile point. Thus, the sideline distance would be given by

$$H = \sin\gamma\, X \tag{145}$$

where the X is in the flight path coordinate system. In the present case, the X at the three-mile point is given by

$$25{,}840 - 6443.5 = 19{,}396 \text{ ft}$$

The sideline distance of the ellipse is 2328 feet.

Using Eq. (100) with the appropriate values of α and β, the $\triangle$PNdb is 28 and the maximum PNdb at the three-mile point is found to be 106.3.

6.3.3 Take-off with power cutback.- The second maneuver considered is the one where the power is cut back at the three-mile point and the resultant climb angle maintained until the sound is below the PNdb level being calculated. Two sets of contours must be calculated, one for the full-power climb segment and the other for the cutback. Following the procedure of the preceding section, the contours are calculated for the lift-off point, cutback point, and as many points in between as necessary. It should be noted that if the

ellipse is terminated before the three-mile point, Eq. (144) must be used to determine the ellipse end point. Again, following the procedure of the preceding paragraph, these contours are plotted on the graph. The aircraft is now at the three-mile point and its height is given by

$$h = X \tan \gamma \tag{146}$$

where X is the three-mile point in the flight path coordinate system.

The power cutback is calculated with Eq. (105), and a new source level using Eqs. (60) and (67), and Figure 21. The compressor frequency is calculated by Eq. (143) and the new climb angle by Eq. (88 modified). Using

$$X = h/\tan \gamma_2 \tag{147}$$

the distance from the three-mile point to the point of intersection of the flight path with the ground is calculated. The three-mile point is now at 65,196 feet in the new flight path coordinate system. This is the first point to be used as the aircraft position in calculating the contour positions. Following the same procedure as the previous section, the sideline distances to the contours are calculated after noting that the new source level is 125. Because of the aircraft height, it is necessary to determine whether there are any ground points corresponding to the PNdb contour. The smallest sideline distance that touches the ground is given by

$$H = \frac{X_o \tan \gamma \tan \theta}{\cos \gamma (\tan \gamma + \tan \theta)} \tag{148}$$

Thus, the only contours to be considered are those with sideline distances equal to or greater than this value, which in this case is 2270 feet.

With this in mind, the contour coordinates are calculated with X_o equal to 65,196 feet. The end points of the contours are determined by using Eq. (144) and as many points as are needed are calculated between these points. The X coordinates in the flight path coordinate system* are converted to the original coordinate system by subtracting

$$65,196 - 25,840 = 39,356 \text{ ft}$$

from each X. These contours are then plotted on the graph. To determine the maximum

*For ease in calculation, several coordinate systems are used. Eq. (135) is used to calculate the contour points; however, the use of Eq. (135) assumes that the coordinate origin occurs at the intersection of the flight path with the ground. Since each flight path has a different intersection point on the ground, there is a new coordinate system for each flight path or change in flight path. The difference in origin between the flight path coordinate system and the original coordinate system (in this case, the start of the ground roll) is added or subtracted from the calculated contour points to bring them back to he original coordinate system. This is the mechanical description of the application of Eq. (129), the general relation for the contour coordinates.

PNdb at the three-mile point, it is noted that the maximum sound reaches the ground behind the aircraft position (this is because of directionality). Therefore, the PNdb contours of the full-power segment of the flight do not extend to the three-mile point since cutback occurs at this point. This means that the sound at the three-mile point is generated during the cutback portion of the flight. Thus, using Eq. (145) and the X of the three-mile point in the new cutback flight segment coordinate system, the sideline distance to the three-mile point can be calculated and the maximum PNdb determined. In this case it is 97.2 PNdb.

6.3.4 Cutback with power resumption.- The third case considered is one where the aircraft lifts off at full power, cuts back at the three-mile point, and resumes power at the ten-mile point. It then continues at full power until the sound is below the PNdb level being calculated. The contours for the lift-off and cutback portion are calculated in the same manner as in the previous section with the difference that the resume-power point serves as the end point for the cutback section. To deal with the resume-power section, it is necessary to first calculate the aircraft height. This is done with

$$h' = h + 52{,}800 \tan \gamma_2 \qquad (149)$$

where h is the aircraft height at the start of the cutback portion and γ_2 is the climb angle of the cutback portion of the flight. This gives the total height of the aircraft at the resume-power point. Using Eq. (146) with the resume-power climb angle, the new flight path zero coordinate is determined, and using Eq. (135 modified) the contours are calculated using the sideline distances calculated from the lift-off segment. Note, as in the cutback segment (Section 6.3.3), Eq. (148) should be used to check that a given PNdb contour actually has corresponding ground coordinates. The maximum PNdb at the three-mile point is the same as in th4 cutback case. This follows, since only the maximum PNdb contours from the cutback segment actually extend to the three-mile point.* Again, the X's must be adjusted to conform to the original coordinate system. In this case, it is necessary to add

$$62{,}800 - 30{,}393 = 32{,}407 \text{ ft}$$

to the X's in the flight path coordinate system.

6.3.5 Landing approach.- The landing zone will now be considered. First, the cutback level is calculated with Eq. (110), and with Eqs. (60) and (67), the new source level of 102 PNdb is calculated. Following the same procedure as in Section 6.3.2, the sideline distances are determined using the in-flight $\triangle$PNdb curves in Figure 29. In calculating the contours, it is easiest to reverse the coordinates and consider the flight as a take-off with the angle of maximum radiation equal to $180 - \theta$. When this is done, the procedure is the same as in the case of simple takeoff. As in the case of simple take-off, the sideline distance at the one-mile point is given by Eq. (145), and the maximum PNdb at the one-mile point is then 99 PNdb. The contour X's are then made negative and the contours plotted on the three graphs.

*This assumes that the contours at the three-mile point that are generated by the cutback portion of the flight are of higher level than the contours generated by the full-power segment of the flight.

6.3.6 Contours.- The results of these calculations are shown in Figure 71. As can be seen, the area of the on-ground portion of the contours is small. The only variation in the contours is due to the take-off portion of the flight. It is to be noted that the smallest area covered by the contours is the simple take-off case. The maximum PNdb at the three-mile point is 106.3, which is the highest of the maximums experienced. However, this is somewhat offset by the decreased area bothered by noise. This relationship of noise and area will be examined in Section 6.5.

In Figure 72, the PNdb contours for a 3-degree, 6-degree, and 6-degree followed by a 3-degree landing approach angle are compared. As can be seen, the 6-degree landing approach gives the least area annoyed by noise. Additionally, the maximum PNdb at the one-mile point is 68.6, which is considerably lower than the 99 PNdb of the 3-degree approach. However, a 6-degree approach would probably not be acceptable from a safety standpoint. With safety in mind, a calculation was, therefore, made for a two-segment approach consisting of a 6-degree approach to the three-mile point followed by a 3-degree approach to the touchdown. The maximum PNdb at the one-mile point is not reduced from that of the conventional constant 3-degree approach. However, as can be seen, the total area annoyed by noise is reduced considerably from the conventional approach.

It should be noted that the procedures demonstrated in this section can only be used for flights that are in line with the runway axis. For more complex cases, the geometric methods of Section 5.3 would have to be used (the equations dealing with source level and cutback power are still applicable).

6.4 Effective PNdb

This section deals with the effects of the time duration upon the perceived PNdb on the ground. Since directivity index (DI) information was not available, the analyses in Sections 6.3 and 6.5 do not include effective PNdb calculations. However, procedures are derived in this section so that contours of effective PNdb can be calculated whenever DI information is available.

To calculate the effective PNdb, the following relation is used:

$$\text{Effective PNdb} = \text{PNdb max} + 10 \log \frac{\Delta T}{15} \qquad (150)$$

where ΔT is the time in seconds at a specific point during which the noise level is within 10 PNdb of the maximum PNdb. To relate this to the sideline distance, the following figure representing the flight path of an aircraft can be used. In this figure (Figure 73),

θ is the angle of maximum radiation
θ_1 is the angle of -10 PNdb before θ
θ_2 is the angle of -10 PNdb after θ
H is the sideline distance
d is the distance traveled by the aircraft between θ_2 and θ_1

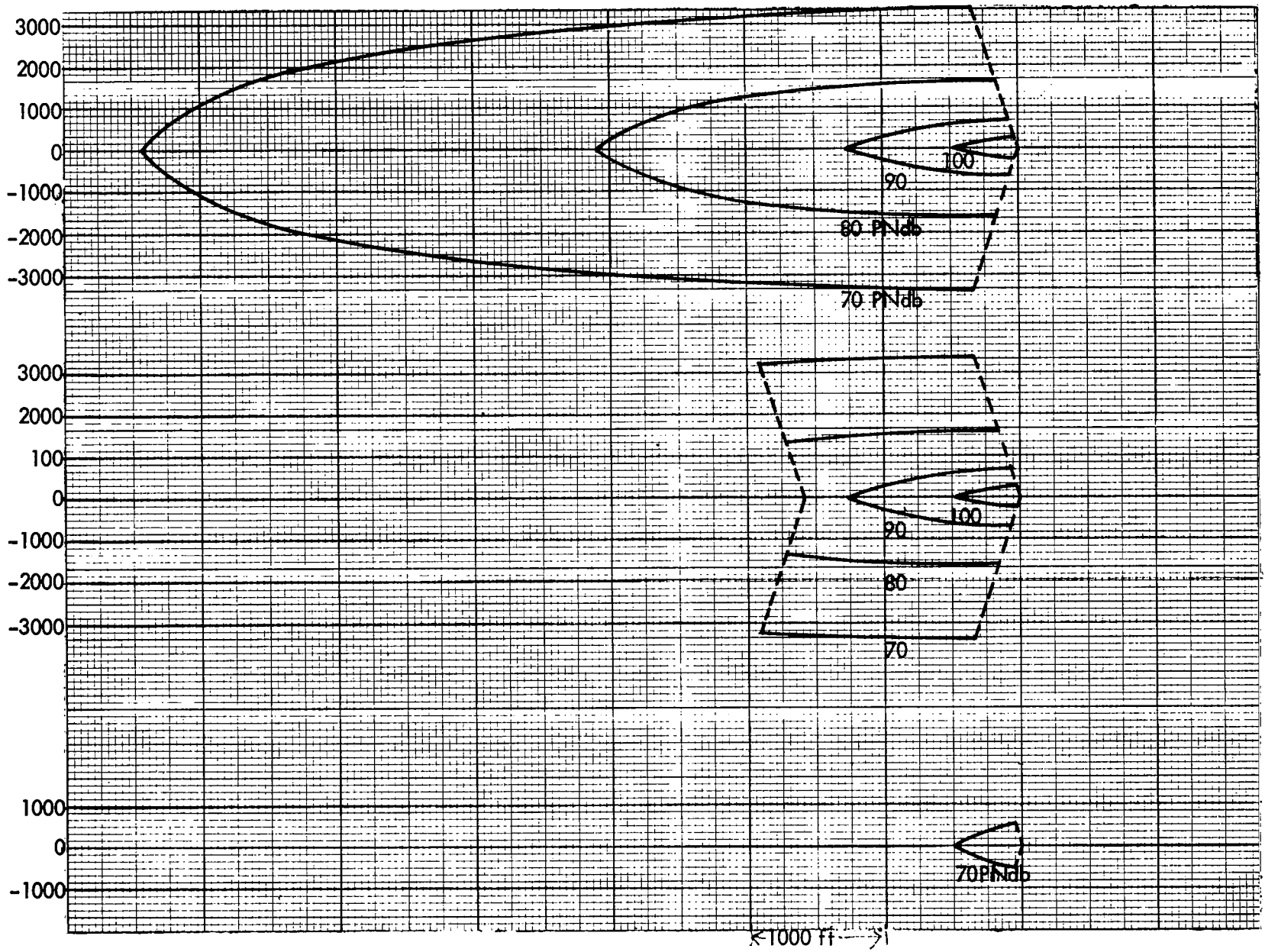

Figure 72 - The Effect of Landing Approach Angle on PNdb Contours

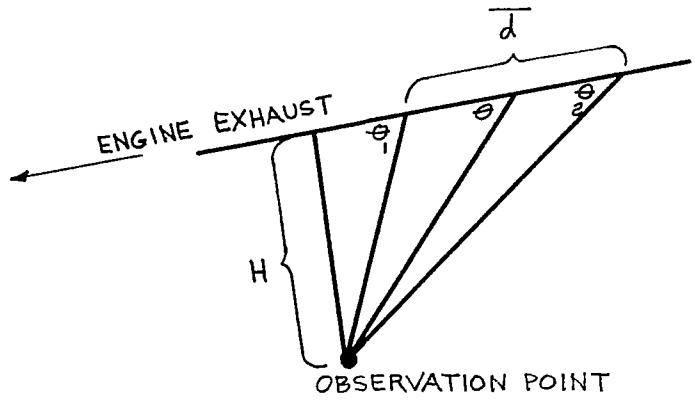

Radiation Angles for Effective PNdb Calculation

Figure 73

The distance d is given by

$$d = H \left[\frac{1}{\tan \theta_2} - \frac{1}{\tan \theta_1} \right] \tag{151}$$

Therefore, the time taken by the aircraft to traverse this distance is given by

$$\Delta t = \frac{d}{V} = \frac{H}{V} \left[\frac{1}{\tan \theta_2} - \frac{1}{\tan \theta_1} \right] \tag{152}$$

where V is the aircraft velocity. Thus, the effective PNdb equation can be written as

$$\text{Effective PNdb} = \text{PNdb max} + 10 \log \frac{H}{15V} \left[\frac{1}{\tan \theta_2} - \frac{1}{\tan \theta_1} \right] \tag{153}$$

or, separating the constants,

$$\text{Effective PNdb} = \text{PNdb max} + 10 \log H + 10 \log \frac{1}{15V} \left[\frac{1}{\tan \theta_2} + \frac{1}{\tan \theta_1} \right] \tag{154}$$

If the expression in Eq. (100) for the maximum PNdb is included, the equation becomes

$$\text{Effective PNdb} = \text{PNdb}_o - \alpha \log \frac{H}{H_o} - \frac{BH_o}{\sin\theta}\left[\frac{H}{H_o} - 1\right] + 10 \log H + 10 \log \left[\frac{1}{15V}\left(\frac{1}{\tan\theta_2} + \frac{1}{\tan\theta_1}\right)\right] \quad (155)$$

It would be very difficult to evaluate this equation to find the sideline distances for contour levels. However, if the increase in sideline distance is considered, the procedure can be simplified. Eq. (155) is differentiated to get

$$\triangle \text{ Effective PNdb} = \frac{-\alpha \log e}{H} \triangle H - \frac{B \triangle H}{\sin\theta} + \frac{10 \log e}{H} \triangle H \quad (156)$$

$$\text{or} \quad \triangle \text{ Effective PNdb} = \triangle H \left[\frac{4.3429}{H} - \frac{0.43429\,\alpha}{H} - \frac{B}{\sin\theta}\right] \quad (157)$$

Since Eq. (157) is an approximate differential, its use will give a slight over-estimation of the increase in $\triangle H$. However, the error will be small.

By use of Eq. (145) the sideline distances to the PNdb contours can be calculated. The procedure would be to first calculate the $\triangle$ effective PNdb at the 200-foot sideline using Eq. (155). Note that the angles used are for sideline DI's, not the usual DI. Once the $\triangle$ effective PNdb to the first contour is calculated, the $\triangle H$ is then added to the 200 feet, giving the first sideline distance. Using the new H and the $\triangle$ effective PNdb, the next increase in H is calculated by solving Eq. (157) for $\triangle H$. This process is repeated until all of the sideline distances are established. Once this is completed, the techniques of Sections 6.3 and 6.5 can be used in their normal manner.

6.5 PNdb Versus Area

In this section are derived approximate relations for calculating the area covered by a given average PNdb level; these area summations are applied to the flight patterns discussed in Section 6.3 and a method of estimating the cumulative effect of noise over the area is developed and discussed.

Since the maximum PNdb or effective PNdb experienced over an area is a continuously-varying function of position, it is necessary to divide the area into sections having an average PNdb level. PNdb contours were drawn for each 10 PNdb level, such as 110 PNdb, 100 PNdb, etc., and it was assumed that the average PNdb over the area was the average of the two adjacent contour values; for example, the area having average value of 105 PN db would lie between the 100 and 110 PNdb contours. In the derivations of area that follow it is assumed that the sideline distances used are associated with the contours that enclose the areas of interest.

6.5.1 Ground-roll area.- The area experiencing some average PNdb level during ground roll is shown as the shaded area in Figure 74.

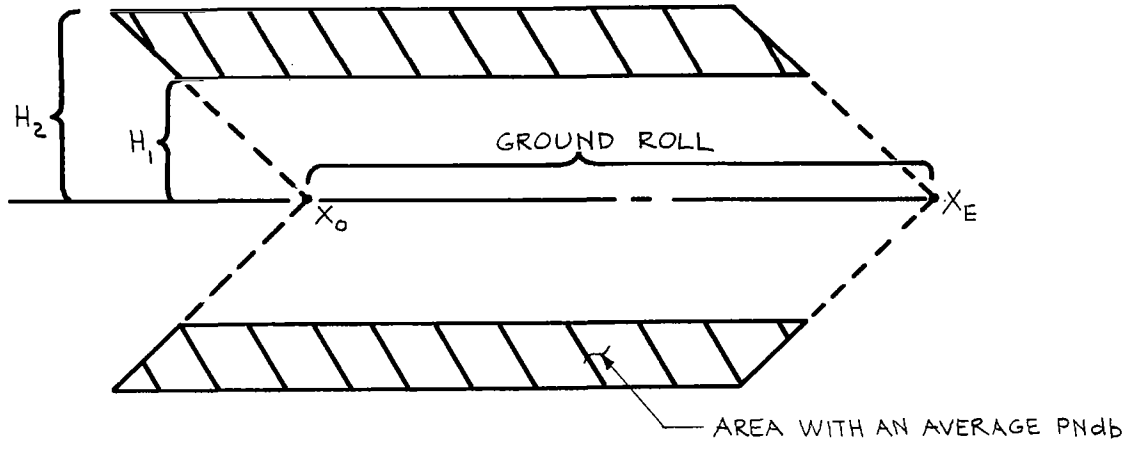

Figure 74
Ground-Roll Area

The exact equation for the area is

$$\text{Area} = 2\left[H_2 - H_1\right]\left[X_E - X_o\right] \tag{158}$$

where H2 and H1 are the sideline distances to the outer and inner contours, respectively, and

X_E is the end point of the ground roll

X_o is the starting point

6.5.2 Simple take-off area.- The area experiencing some average PNdb level during a take-off involving no cutback or changes in flight direction is shown as the shaded area in Figure 75.

Since the aircraft starts on the ground, the middle of the contour ellipses start at the point of lift-off, X_o. If a division is made at this point and the areas 1 and 2 are integrated the total area is found to be

$$\text{Area} = \left[H_2^2 - H_1^2\right]\left[\frac{1}{\cos\gamma \tan\theta} + \frac{\pi}{2\sin\gamma}\right] \tag{159}$$

where γ is the climb angle and θ is the angle of maximum radiation.

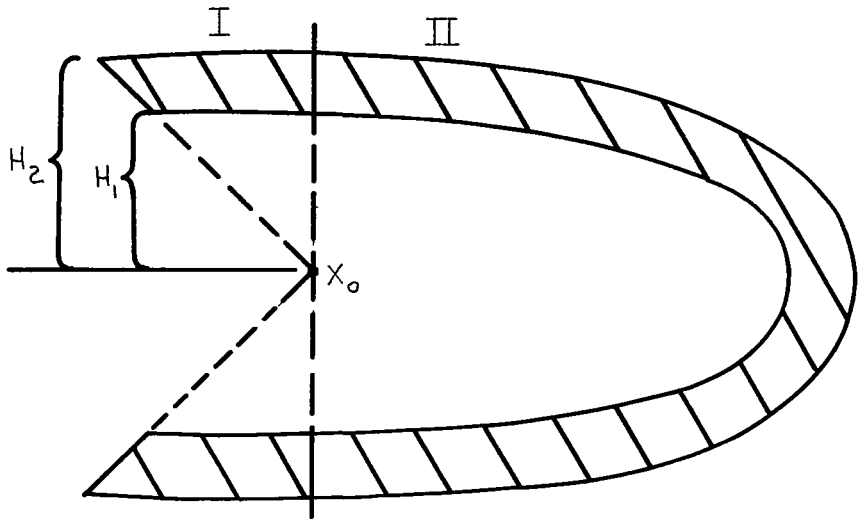

Take-Off Area

Figure 75

Since the area to the left of the lift-off point, indicated by 1 in the figure, is, in fact, small, its contribution can be ignored, and the area will be

$$\text{Area} = \left[H_2^2 - H_1^1\right]\left[\frac{\pi}{2 \sin \gamma}\right] \tag{160}$$

From a comparison of results using this approximate area equation (Eq. (160)), and results using Eq. (159), it appears that the percent error involved in using Eq. (160) is equal to the number of degrees of climb angle, i.e., 7-degree climb angle would have a 7-percent error. Thus, this equation is a good approximation to the area.

It is evident from Eq. (160) that the area is a function of the climb angle and that the higher the climb angle the smaller the area. This can also be deduced from the contours in Figure 72, where it is evident that the higher climb and approach angles minimize the high noise areas.

6.5.3 Area due to simple power cutback or resumption.- The area affected is illustrated by Figure 75, with the difference that X_o is now the point at which cutback or resumption of power occurs. Making the same approximation as before, i.e., integrating only over the area to the right of the cutback point, the equation for area is

$$\text{Area} = \left[H_2^2 - H_1^2\right]\left[\frac{\pi}{2 \sin \gamma}\right] - X_o\left[\sqrt{H_2^2 - X_o^2 \sin^2 \gamma} - \sqrt{H_1^2 - X^2 \sin^2 \gamma} + H_2 - H_1\right] \tag{161}$$

where X_o is the cutback or resume-power point.

From this equation it can be seen that the area decreases with increasing climb angle and increasing distance of cutback or power-resumption point.

In the special case where a contour ellipse has terminated before the cutback or power-resumption point, the area is the area under one ellipse and in this case the following equation should be used

$$\text{Area} = \frac{H_2^2 \pi}{2 \sin\gamma} - X_o \left[\sqrt{H_2^2 - X_o^2 \sin^2\gamma} + H_2 \right] \qquad (162)$$

6.5.4 Area due to power cutback followed by power resumption.- The affected area is shown in Figure 76; in this figure X_o is the point at which cutback is initiated and X_E is the point at which power is resumed.

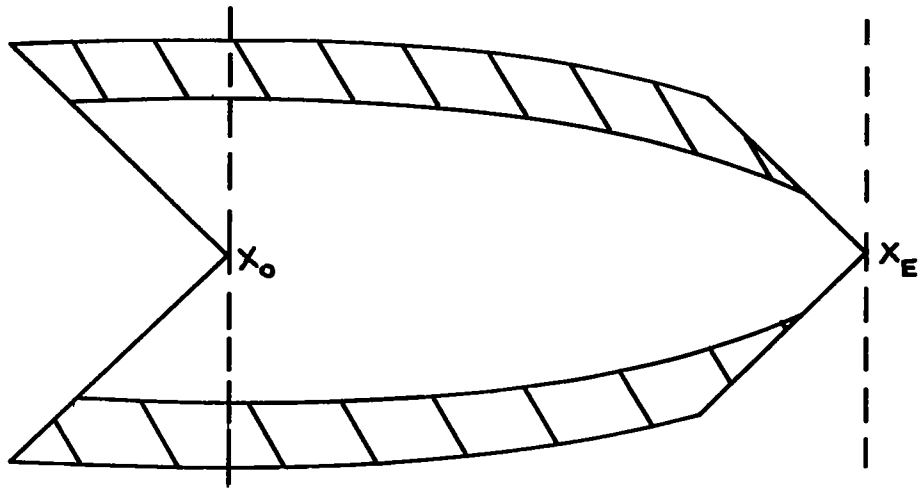

Cutback Followed By Power-Resumption Area

Figure 76

To calculate this area the approximation was made that the area would extend from X_o to X_E. The area lost to the left of X_o would be compensated for by the area gained by extending the ellipses to X_E. The area is given by

$$\text{Area} = X_E \left[\sqrt{H_2^2 - X_E^2 \sin^2\gamma} - \sqrt{H_1^2 - X_E^2 \sin^2\gamma} + H_2 - H_1 \right] - X_o \left[\sqrt{H_2^2 - X_o^2 \sin^2\gamma} + H_2 - H_1 \right] \qquad (163)$$

Again it can be seen that by extending X_E the area will increase, and by extending X_o the area will decrease. The dependance upon the climb angle is not as evident; however, an increase in climb angle will reduce the size of the square root terms and thus the area will shrink.

In that instance where the inner ellipse terminates before X_o is reached (moving from the left on the diagram), the area is given by

$$\text{Area} = X_E\left[\sqrt{H_2^2 - X_E^2 \sin^2\gamma} + H_2\right] - X_o\left[\sqrt{H_2^2 - X_o^2 \sin^2\gamma} + H_2\right] \qquad (164)$$

In the case where the inner ellipse terminates between X_E and X_o, the following equation should be used,

$$\text{Area} = X_E\left[\sqrt{H_2^2 - X_E^2 \sin^2\gamma} + H_2\right] - X_o\left[\sqrt{H_2^2 - X_o^2 \sin^2\gamma} + H_2\right] - \frac{H_1^2\pi}{2\sin\gamma} + X_o\left[\sqrt{H_1^2 - X^2 \sin^2\gamma} + H_1\right] \qquad (165)$$

If it happens that the outer ellipse terminates before X_E, the equations of Section 6.5.3 should be used.

6.5.5 Area due to take-off followed by cutback.- The area is illustrated by Figure 76, with the difference that X_o is zero and the area is given by the equation,

$$\text{Area} = X_E\left[\sqrt{H_2^2 - X_E^2 \sin^2\gamma} - \sqrt{H_1^2 - X_E^2 \sin^2\gamma} + H_2 + H_1\right] \qquad (166)$$

It can be seen that as X_E is extended the area increases also; as the climb angle increases the area decreases.

If the inner ellipse terminates before X_E is reached, the following equation should be used.

$$\text{Area} = X_E\left[\sqrt{H_2^2 - X_E^2 \sin^2\gamma} + H_2\right] - \frac{H_1^2\pi}{2\sin\gamma} \qquad (167)$$

In the instance that both ellipses terminate before X_E is reached, the equations of Section 6.5.2 should be used.

6.5.6 Area due to a simple landing or a two-segment landing.- In these cases the same approximations are made as before; i.e., area integration is carried to the end points of the flight segment. For a simple landing approach involving no changes in direction or approach angle before touchdown, the equations of Section 6.5.3 are used for the initial approach angle and the equations of Section 6.5.5 are used for the touchdown segment.

6.5.7 Calculated areas of Section 6.3 flight paths.- With the formulas of Section 6.5.1 through 6.5.6 the area for various average PNdb was calculated and the size of area as a function of PNdb level was established for the cases of simple take-off, take-off with cutback, and take-off with cutback followed by resumption of power. All of these cases were considered with a 3-degree landing approach, 6-degree landing approach, and a

6-degree approach followed by a 3-degree touchdown. The histograms of the area versus PNdb for all nine cases are shown in Figure 77. As can be seen, the least area is affected when a 6-degree approach is used with a simple take-off, and the worst case is the 3-degree approach followed by simple cutback. The shapes of the histograms are significant in that the cutback followed by power resumption has a high level PNdb covering the greatest area.

From the histograms it appears that the best flight path would be a two-segment landing approach followed by a simple take-off. This result is based on a rather simple analysis and to verify it and to establish optimum paths would require analyzing many combinations and, probably, some refinement of the analytical procedures. For example, because of the calculational difficulties of trying to separate out the airport area, it was considered as part of the noise-affected area. Now in fact, people in the airport area may not be greatly annoyed by the noise, so that this particular area probably should not be considered. Neglecting the airport portion of the area would reduce the high-level-PNdb area and, consequently, would change the area effect of the various flight paths. As will be discussed in Section 6.5.8, there are also other factors that can influence the choice of a flight path.

6.5.8 Weighted areas.- The historgrams of Figure 77 or the total area figures do not give an accurate picture of the effect of a flight pattern. This can be seen by looking at the histograms. The total area of the simple cutback pattern is the largest of the three take-off patterns; however, by the histograms it can be seen that most of this area is subjected to low-intensity noise. In an actual airport situation it could be expected that the greatest complaints would be generated by the higher-intensity noise. Thus, a flight pattern subjecting a large area to low-intensity noise might well be less objectionable than a small area of high-intensity sound.

To show how this might be taken into account, a calculation was made in which the PNdb areas were weighted by a factor expressing the degree of annoyance the noise would cause. Data on noise-annoyance effects is scarce and not in any way precise, but Reference 5, Part II, Page 32, gives a curve relating PNdb to a degree of unacceptability rated on a scale of 10. With this graph, the following table of PNdb versus percent of unacceptability was derived.

TABLE 5

PNdb	Percent Unacceptability
70	3
80	18
90	40
100	63
110	86
120 and higher	100 percent unacceptable

With this table and an assumed density of population around an airport, a calculation can be made of the number of complaints that a given flight path would develop. Applying

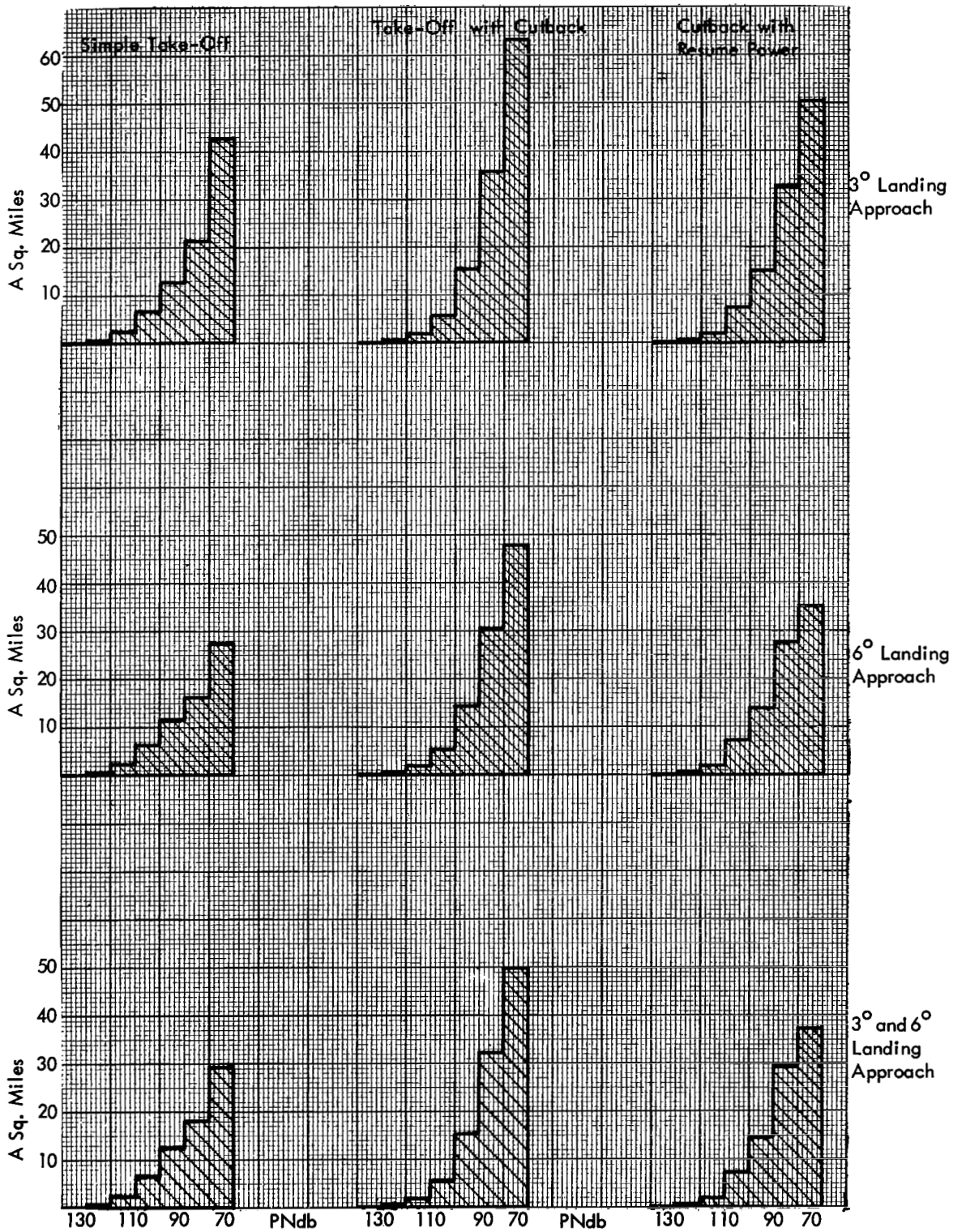

Figure 77 - Area Versus PNdb

these unacceptability figures to the area of Section 6.5.7, the following table was developed:

TABLE 6

Flight Path	Annoyed Square Miles
3-degree approach with cutback and resume	20.9
3-degree approach with cutback	21.0
3-degree approach with simple take-off	17.8
6-degree and 3-degree approach with cutback and resume	19.8
6-degree and 3-degree approach with cutback	19.9
6-degree and 3-degree approach with simple take-off	16.7
6-degree approach with cutback and resume	19.0
6-degree approach with cutback	19.2
6-degree approach with simple take-off	16.0

By this method of rating the cutback after take-off would annoy more people if a uniform population density is assumed. Although both cutback and cutback-and-resume-flight patterns reduce the noise at the standard three-mile point, as can be seen by this method, the simple take-off is preferable since less people would be annoyed. This method of weighting areas according to the PNdb experienced is only to illustrate the possibilities of flight-noise analysis, and much work would have to be done before reliable results could be obtained.

This section has illustrated how to produce contours of PNdb and to calculate the area experiencing PNdb levels. These methods were only applied to simple cases of flight paths in line with the runway; however, by use of the results of Section 5 and further work on the area calculation, these methods can be made quite general.

7. CONCLUSIONS AND RECOMMENDATIONS

7.1 Conclusions

The purpose of the program was to develop procedures for estimating the effects of design and operational characteristics of jet aircraft on ground noise; this has been done for various engine-cycle parameters, aircraft-design characteristics, and aircraft-flight characteristics; parametric plots have been prepared to show how these different inter-related factors influence noise; and, when possible, assessments have been made of the accuracies and limitations of the graphs, nomographs, and equations that have been developed. One important general conclusion that can be drawn from all this effort is that it is feasible to develop simplified analytic procedures for relating aircraft design and flight characteristics to ground noise, and that such techniques can be extremely useful for providing design guidance and for showing how various flight paths influence ground noise. Many of the procedures or results that have been developed have not been experimentally verified as to the accuracy of the ground-noise predictions; however, the techniques are still extremely useful in that they provide a rational framework within which aircraft designs and flight characteristics can be assessed as to their relative effects.

During the development of the techniques and the parametric plots, and from the analysis of flight-path noise effects, data was generated that permitted several conclusions to be drawn. These illustrate the kinds of information that can be obtained from the different analyses.

1. For a constant climb gradient, the ground contours of constant PNdb and effective PNdb will be in the form of ellipses.

2. The area experiencing a given PNdb level will be reduced by increasing the climb-out or landing-approach angle.

3. To minimize the peak noise experienced at a ground point, power cutback should be performed just before the point is reached.

4. In high by-pass ratio designs of turbofan engines, both the compressor noise per unit flow and the jet noise Q, tend to be minimized; thus, on an "equal thrust" basis, high by-pass designs are desirable for minimum noise.

5. Ground noise levels under the aircraft during second segment climbout may be reduced markedly as a result of increased power loading of the aircraft. Increased power loading may result in a shortened take-off roll, a steep initial climb angle, and a greater power reduction during cutback. For example, increasing the power loading from .25 to .35 can result in a noise reduction of from 5 to 7 PNdb for both jet and compressor noise under the second segment.

7.2 Recommendations

The following recommendations are made regarding the future work that could be done to improve the techniques or regarding how the techniques could be used.

7.2.1 Experimental verification.- An essentially analytical project has been performed and it would be valuable to verify the work by checking agains experimental data. Much noise data has been gathered on flight tests (e.g., NASA Wallop Island tests) that could be analyzed and compared with values calculated by the techniques that have been developed. Such comparisons would provide the basis for modifying, simplifying, or extending the techniques.

7.2.2 Noise study of specific aircraft/airport combinations.- The work accomplished on this program has mostly involved the development of methods and techniques for investigating the ground noise produced by various combinations of engine, airframe, and operations parameters. It was not within the scope of the present program to apply these techniques to existing aircraft under various operational conditions to see what could be gained by modifying various parameters. Such a study involving specific aircraft, specific airports, and specific operational procedures would be of great interest, not only because of the direct information that would ensue, but because it would be the first step toward a complete study of noise at airports.

7.2.3 Extension of procedures to complex situations.- It should be emphasized that the procedures developed are only the beginning of what might be done. Many simplifications and approximations had to be made and considerable refinement is possible. For example, simplified equations for ground area were used in computing area as a function of PNdb and annoyance levels. Precise area equations could be used, the procedure could be programmed, annoyance factors and population densities could be included, and the program could optimize a flight path in terms of minimum annoyance at various airports.

APPENDIX A

SYMBOLS

A	Exhaust nozzle area, compressor flow area, humidity-absorption coefficient
AB	Afterburning
$A_R = \frac{A_2}{A_1}$	Area ratio
AR	Compressor blade aspect ratio
B	Angle between the line connecting the observer to the aircraft and the aircraft flight axis
C_D	Drag coefficient
C_{Di}	Induced drag coefficient
C_{Do}	Zero-lift drag coefficient
C_L	Lift coefficient
$C_L^\wedge$	Maximum lift coefficient
D	Drag of aircraft, tip diameter
D_h	Hub diameter
D_t	Tip diameter
d_o	Slant range to sideline
E	Energy flux
E_{max}	Maximum aerodynamic efficiency
e	Hub-tip ratio = $\frac{D_h}{D_t}$
F_n	Net thrust of aircraft
f	Frequency
g	Gravitation constant

SYMBOLS
(Continued)

H	Distance of closest approach
H_o	Standard sideline distance
K	Induced drag factor (see Eq. 81)
L	Lift of aircraft
M	$1 - \frac{V_o}{V_i}$
N	Fan rpm
N_R	Number of rotor blades
n	Compressor rpm
OA	Overall
PNdb	Unit of perceived noise level (PNL)
P_r	Nozzle pressure ratio
PWL	Sound power level
Q	$PNdb_o - 10 \log F_n$ = log of ratio of perceived noise to thrust
R	Ratio of passby distance to standard sideline distance, slant range to the aircraft
S	Wing reference area, initial distance between observer and aircraft
S'	Ground-roll distance
S_o	Starting roll position
SFC	Specific fuel consumption
SPL	Sound pressure level
SPL_o	Sound pressure level at reference sideline distance
T	Net thrust of aircraft
T_t	Nozzle total temperature

SYMBOLS
(Continued)

T_4	Turbine inlet temperature
t	Time
U_t	Tangential compressor speed
U_z	Compressor axial speed
u	Ratio of flight speed to a reference speed
u_r	$\frac{V_{i2}}{V_{i1}}$, exit velocity ratio
u_{rel}	Relative blade tip velocity
V_i	Jet exit exhaust velocity
V_R	Relative velocity between jet exit exhaust velocity and aircraft velocity
V_s	Stall speed
v_f	Fan stream exhaust velocity
v or v_o	Aircraft velocity
W	Weight of aircraft
w	Weight flow
w_r	$\frac{P_2 A_2 V_{i2}}{P_1 A_1 V_{i2}}$, bypass ratio
X_o, Y_o	Coordinates of observer position
X, Y, h	Coordinates of aircraft position
Y	Ground-roll distance
$\overline{CPR}$	Overall cycle pressure ratio
$\overline{FPR}$	Fan pressure ratio

SYMBOLS
(Continued)

$\overline{PN_o}$	$\log^{-1} \frac{PNdb_o}{10}$ (this is an operational definition and $\overline{PN_o}$ is called the perceived noise)
$\left(\frac{s}{c}\right)$	Ratio of rotor-stator spacing to rotor chord
α	Climb angle, yaw angle
α, β	Attenuation constants in Tables 2 and 3
β	By-pass ratio
γ	Angle of maximum noise at sideline, flight-path inclination, pitch angle
ΔF	Flow correction factor for forward arc radiation
δ	Flap set angle
n_c, n_{fc}, n_b, n_t, n_n	Component efficiences for the main compressor, fan, burner, turbine, and nozzle, respectively
θ	Angle of maximum noise at 200-ft sideline distance
λ	Exponent for density function (Eq. 55)
ρ	Exhaust jet density
ρ_f	Density of fan exhaust
ρ_r	$\frac{\rho_2}{\rho_1}$, density ratio
σ	Compressor solidarity
ϕ	Compressor flow coefficient
ψ	Compressor temperature rise coefficient (Eq. 48)

REFERENCES

Reference 1 — Anon., Aircraft Turbo Jet or Turbofan Noise Prediction, AIR 876, Society of Automotive Engineers.

Reference 2 — M. J.T. Smith and M.E. House: Internally-Generated Noise from Gas Turbine Engines, Measurement and Prediction. Transactions of ASME, April 1967.

Reference 3 — R.J. Wells and J.M. McGrew: Model Freon Compressor for Acoustic Investigation. FAA-ADS-47, Report prepared by GE for FAA, June 1965

Reference 4 — Anon., Aircraft Compressor Noise Prediction. Privately-circulated paper prepared by a Standards Committee of the Society of Automotive Engineers, Not Adopted.

Reference 5 — Anon., Analysis of Community and Airport Relationships/Noise Abatement. SRDS Report RD-65-130, Report prepared by Bolt, Beranek and Newman, Inc., for FAA, December 1965.

Reference 6 — I.J. Sharland: Sources of Noise in Axial Flow Fans. Journal of Sound and Vibration, July 1, 1964, p. 307.

Reference 7 — Anon., Study of Noise Characteristics of the Boeing 707-120 Jet Airliner and a Large Conventional Propellor-Driven Airliner. Wallops Island Test 722, BBN-prepared Report for the Port of New York Authority, October 1958.

Reference 8 — Anon., Evaluation of Exterior Noise from Flight and Ground Operations of the Convair 880 Jet Airliner. Report No. 657, BBN Report prepared for Convair, December 8, 1959.

Reference 9 — Anon., Evaluation of Noise for Flight Operations of Douglas DC8 Jet Airliner with JT$A-9 Engines and BASY Ejector Suppressors. Report 656, BBN, Report prepared for Port of New York Authority, October 26, 1956.

Reference 10 Anon., Evaluation of Noise for Flight Operations of Douglas DC8 Jet Airliner with JTC3-6 Engines and BASY Ejector Suppressors. Report 655, BBN Report prepared for Port of New York Authority, September 18, 1959.

Reference 11 Anon., Flyover Noise During Take-Off and Landing of the Series 50 DC8 with Pratt and Whitney JT3D-1 Turbofan Engines. Douglas Report No. LB-30637, July 20, 1961.

Reference 12 C.D. Perkins and R.E. Hage: Airplane Performance, Stability, and Control. John Wiley and Sons, 1949, p. 197.